THE USE OF SILENT SUBSTITUTION IN MEASURING ISOLATED CONE- & ROD- HUMAN ERGs

D KOMMANAPALLI

MPhil

2018

THE USE OF SILENT SUBSTITUTION IN MEASURING ISOLATED CONE- & ROD- HUMAN ERGs

Deepika KOMMANAPALLI

Submitted for the

Degree of Masters of Philosophy

Faculty of Life Sciences

University of Bradford

2018

Abstract

Deepika Kommanapalli

The use of Silent Substitution in measuring isolated cone- and rod- Human ERGs.

Keywords: Electroretinograms, cone photoreceptors, rod photoreceptors, human vision

After over a decade of its discovery, the Electroretinogram (ERG) still remains the objective tool that is conventionally used in assessment of retinal function in health and disease. Although there is ongoing research in developing ERG-recording techniques, interpretation and clinical applications, there is still a limited understanding on how each photoreceptor class contribute to the ERG waveform and their role and/or susceptibilities in various retinal diseases still remains unclear. Another limitation with currently used conventional testing protocols in a clinical setting is the requirement of an adaptation period which is time-consuming. Furthermore, the ERG responses derived in this manner are recorded under different stimulus conditions, thus, making comparison of these signals difficult. To address these issues and develop a new testing method, we employed silent substitution paradigm in obtaining cone- and rod- isolating ERGs using sine- and square- wave temporal profiles. The ERGs achieved in this manner were shown to be photoreceptor-selective. Furthermore, these responses did not only provide the functional index of photoreceptors but their contributions to their successive postreceptoral pathways. We believe that the substitution stimuli used in this thesis could be a valuable tool in functional assessment of individual photoreceptor classes in normal and pathological conditions. Furthermore, we speculate that this method of cone/rod activity isolation could possibly be used in developing faster and efficient photoreceptor-selective testing protocols without the need of adaptation.

Acknowledgements

Firstly, I would like to thank Prof. Declan McKeefry and Dr Srimant Tripathy for their support through all these years and Prof Brendan Barrett for his encouragement and emotional support.

I am grateful for the scholarship support from the Bradford School of Optometry and Vision Sciences.

Special thanks to my friends Karen, Graham and Manju who made living abroad a little easier and my family who finally understood and supported me through the final stages of this degree.

A big thanks to all my friends and family across the globe for all the love and support and this would not have been possible without you.

I would like to thank all my participants for their time and patience and helping me in the successful completion of all my experiments.

To all my colleagues in the department, thank you for making BSOVS a lovely place to work. I appreciate your support and kindness through all these years and thanks for educating me on life in the UK. I would cherish those conversations for the rest of my life.

Lastly, I would like to thank all those amazing friends I made in the PGR lounge, a special shout out to Julia, Dom, Nura, Destina and Itoro, for you have been my greatest support through those difficult times and reminded me to play my strengths. I am glad to have known you all in the end.

This thesis is dedicated to everyone who had helped me along the way.

TABLE OF CONTENTS

Abstract i

Acknowledgements ii

Table of Contents iii

List of Figures viii

List of Tables xiv

Abbreviations xv

Chapter 1 General Introduction 1

1.1 Introduction 2

1.2 Overview of human trichromatic vision 3

1.3 Retina 4

1.3.1 Retinal pigment epithelium (RPE) 6

1.3.2 Photoreceptors and circuitries in the human retina 7

1.3.3 Horizontal cells (HCs) 34

1.3.4 Bipolar cells 37

1.3.5 Amacrine cells 40

1.3.6 Ganglion cells 44

1.4 Postreceptoral retinal pathways 48

1.4.1 The L-M cone (Red-Green) opponent pathway 48

1.4.2 The S/(L+M) (Blue-Yellow) Pathway 50

1.4.3 +L+M non-opponent (luminance) pathway 51

1.5 Lateral geniculate nucleus 52

1.5.1 Magnocellular pathway 53

1.5.2 Parvocellular pathway 53

1.5.3 Koniocellular pathway 56

1.6 Visual cortex 56

1.6.1 V1 and V2 cells 56

1.6.2 V4 57

1.6.3 Inferior temporal and frontal cortices 58
1.7 Research Rationale 59
Chapter 2 - Introduction to Electroretinogram 60
2.1 Introduction 61
2.2 History of ERG 61
2.3 Electrical basis of the electroretinogram 61
2.4 Granit's analysis of cat ERG 63
2.5 The Human Flash ERG 65
2.5 (i) Origins of components of ERG 66
a- wave 67
b-wave 69
c-wave 71
d-wave 72
Oscillatory potentials (OPs) 73
2.5 (ii) Amplitudes and Implicit times- measures of ERG 74
2.6 The Clinical full-field ERG 75
2.6.1 Scotopic ERG assessment 75
Dark adapted 0.01 ERG (Isolated rod response) 75
Dark adapted 3 ERG (maximal combined cone and rod response) 76
Dark adapted 10.0 ERG (combined responses to stronger flash) 76
Dark adapted 3.0 oscillatory potentials 76
2.6.2 The Photopic ERGs 77
Light-adapted 3.0 ERG (Single flash cone ERG) 78
Light-adapted 30 Hz flicker ERG 79
2.7 Factors effecting ERGs 79
2.8 Full-field Flash ERG applications 80
2.9 Methods to achieve isolated rod and cone ERGs 82
2.9.1 Coloured stimuli 82
2.9.2 Flicker ERGs 83
2.9.3 Paired-flash paradigm 84
2.9.4 Manipulation of adaptation 84
2.10 Isolation of cone isolated ERGs 85
2.10.1 Chromatic adaptation 85
2.10.2 Silent Substitution 86

Advantages of silent substitution 90
2.11 Summary 92
Chapter 3 - General Methods 93
3.1 Introduction 93
3.2 Colour matching functions and spectral sensitivities 93
3.2.1 CIE 1931 xyL colour space 96
3.3 Cone fundamentals 96
3.4 Transformation of cone fundamentals into CMFs 98
3.5 Four Primary ganzfeld stimulator 100
3.5.1 Calibration of photostimulator 104
3.6 General experimental procedures 105
Subject preparation 105
3.6.1 (A) Colour vision tests 105
3.6.2 Electrodes 109
(i) Active electrode 109
(ii) Reference and Ground electrodes 110
3.6.3 The Stimulus presentation 111
3.6.4 ERG recording and analysis 112
3.7 Repeatability of steady state cone isolated ERG 114
Chapter 4 - Incremental and decremental L- and M- cone isolated ERGs derived using square-wave pulse stimulation 119
4.1 Introduction 119
4.2 Methods 123
4.2.1 Subjects 123
4.2.2 Stimuli 124
Experiment 1 Equal mark:space ratio (250 ms: 250 ms) 125
Experiment 2 (Unequal mark:space ratio (100 ms:150 ms)) 127
4.2.3 Recording 127
4.3 Results 128
4.3.1 Experiment 1 (Equal mark:space ratio (250 ms: 250 ms)) 128
L- & M- cone onset/offset response characteristics in normal trichromats 129
4.3.2 Experiment 2 132
Unequal mark:space ratio (100 ms:150 ms) 132
(A) L- and M- cone isolating ERGs 132
(B) Dichromatic Controls 136

4.4.3 Counter-phase and in-phase L/M cone Stimulation 140
4.4.1 Validation of L- and M-cone silent substitution Stimuli 143
4.4.2 L- and M- cone isolated ERGs..... 144
4.4.3 Counter-phase and in-phase L/M cone Stimulation..... 147
4.4.4 L/M cone Ratios 147
4.5 Conclusion 149
Chapter 5 - Temporal response characteristics of L- and M- cone isolated flicker ERGs using sine wave stimuli 150
5.1 Introduction 150
5.2 Methods..... 156
5.2.1 Subjects..... 156
5.2.2 Visual stimulation 157
5.2.3 ERG recordings..... 159
5.2.4 Data analysis..... 159
5.3 Results 161
5.3.1 Experiment 1 (Non-intensively sampled data) 161
(A) Temporal response characteristics of the fundamental components of L- and M- cone ERGs in trichromats 162
(B) Temporal response characteristics of the fundamental components of L- and M- cone ERGs in dichromats..... 163
5.3.2 Experiment 2 (Intensively sampled data) 166
Apparent latency..... 170
5.3.3 Experiment 3 (S- Cone Intensively sampled data)..... 172
5.4 Discussion..... 176
(A) L- and M- cones 176
(B) L:M cone ratios..... 177
S- cone 184
5.5 Conclusion 185
Chapter 6 - The effect of temporal frequency and retinal illuminance on Rod and Cone driven Human ERGs using Silent Substitution 186
6.1 Introduction 186
6.2 Methods..... 189
6.2.1 Stimuli..... 189
6.2.2 Subjects..... 190
6.2.3 ERG recording..... 191

6.2.4 Data Analysis 192
6.3 Results 193
6.3.1 Experiment 1 Temporal properties of isolated rod ERGs under mesopic and photopic conditions 193
6.3.2 Experiment 2 195
Rod, L- and M- cone ERGs as a function of Temporal Frequency at different Retinal Illuminances 195
6.3.3 Experiment 3 201
8- and 30- Hz Rod isolated flicker ERGs versus Retinal Illuminance 201
6.4 Discussion 203
Chapter 7 - General discussion, Conclusions, Limitations and Future work ... 208
7.1 General Discussion 208
7.2 Conclusions 211
7.3 Limitations 211
7.4 Future work 212
References 213
Presentations and Publications 250

LIST OF FIGURES

Figure 1-1 Cross section of human eye showing object forming an image on the retina (left) and cross section of human retina showing basic retinal circuitry and associated neurons (right). 5

Figure 1-2 illustrates anatomy of human rod and cone photoreceptors 8

Figure 1-3 : Schematic representations of stages of phototransduction in rod and cone-photoreceptors 9

Figure 1-4 Stages of phototransduction cascade in human rod photoreceptor under dark (scotopic) and light (photopic) conditions respectively. 11

Figure 1-5 Schematic representations of five stages of phototransduction cascade. 14

Figure 1-6 Visual cycle in rod and cone photoreceptors 17

Figure 1-7 Graph demonstrates the distribution of rods and cones along the horizontal meridian of the human retina. 23

Figure 1-8 Normalised spectral sensitivities of rods, S-, L- and M- cones (Bowmaker and Dartnall, 1980). 25

Figure 1-9 Spectral sensitivities of S-, M-, and L-cones as observed in two different studies 27

Figure 1-10 Graph showing changes in macular pigment and optical density of the crystalline lens as a function of wavelength (Foster, 2010). 28

Figure 1-11 Spectral coding of human L- and M- cone pigments. 31

Figure 1-12 showing light micrograph of different types of human horizontal cells from Golgi stained whole mounts (left) lateral connection of different types of horizontal cells with different types of photoreceptors (right). 36

Figure 1-13 Classification of bipolar cells based on their response of their receptive fields and stratification in the proximal (PIPL) and distal strata (DIPL) of the inner plexiform layer (adapted from Joselevitch, 2008). 38

Figure 1-14 Golgi drawings of amacrine cells in human retina 41

Figure 1-15 P and M ganglion cells that project to layers 3, 4, 5 or 6 of parvo- and layers 1 or 2 of magnocellular layers 47

Figure 1-16 L and M cone opponent pathway in the human retina 49

Figure 1-17 The blue- yellow pathway in the retina. 49

Figure 1-18 L and M cone opponent pathway in the human retina 51

Figure 1-19 showing different layers of human lateral geniculate nucleus (LGN) and innervation of LGN in the primary visual cortex. 52

Figure 1-20 Types of type 1 LGN cells. upper half of the panel show L-ON, M-OFF, M-ON, L-OFF, S-ON, M-OFF and the lower half of the panel shows M-OFF, L-ON and ; L-OFF, M-ON receptive fields respectively. 55

Figure 1-21 Type II cells of human lateral geniculate nucleus. 55

Figure 1-22 Type III cells of human lateral geniculate nucleus 55

Figure 1-23 (A) Representation of different types of lobes and vision centers in the human brain and (B) lateral view of human brain showing different cortical areas that are responsible for vision. 58

Figure 2-1 Schematic representation of electrical basis for corneal electroretinogram 63

Figure 2-2 The ERG recordings from the anesthetised cat retina with a 2 second light stimulus. 65

Figure 2-3 Theoretical flash ERG waveform showing all components when stimulated by a long pulse of light 66

Figure 2-4 Diagram showing the retinal cellular origin of major components of ERG 66

Figure 2-5 Effect of L-glutamate and APB on ERG b- wave 67

Figure 2-6 Normal macaque flash ERG showing a-, b- and d-waves (upper trace) and the demolition of photopic b-wave post application of glutamate analogue (APB) (lower trace) 70

Figure 2-7 ERG recordings from skate retina. 71

Figure 2-8 (A) Location of Oscillatory potentials on the ascending limb of the b-wave, (B) Isolation of these wavelets by using FFT and (C) Power spectrum of OPs 74

Figure 2-9 Typical ERG waveform showing signal amplitudes (aA and bA represented by black dotted lines) and onset-to-peak times (at and bt represented by red dotted lines) of a- and b- waves respectively. 75

Figure 2-10 shows six normal waveforms elicited by ISCEV standardized full-field ERG 77

Figure 2-11 (A) blue and red filters that can be used to obtain separate rod and cone components of ERG using weak flashes under scotopic conditions (B) coloured stimuli that can aid the isolation of rod and cone ERGs..... 83

Figure 2-12 An example of silent substitution paradigm using spectral distributions of L- and M-cones. 88

Figure 3-1 (A) Example of a colour matching function derived using red (700 nm), green (546.1nm) and blue (435.8 nm) primaries against yellow test light. 94

Figure 3-2 x,y,z colour matching functions plotted as a function of wavelength (nm), ... 95

Figure 3-3 (A) The relative (normalised) spectral sensitivities of rods, S-, M-, and L cones plotted as a function of wavelength, (B) LED spectral distributions of our equipment and (C) LED chromaticities in 1964 CIE 10^0 space. 103

Figure 3-4 shows circuit board comprising of LEDs located on either side of the front hole (left). 104

Figure 3-5 a participant performing all three Colour vision tests (left to right) Ishihara pseudoisochromatic plates, Farnsworth-Munsell 100 Hue test and Anomaloscope prior to the recording session..... 108

Figure 3-6 Electrode placement for monocular ERG recording with left eye occluded (left). Observer presented with stimulus on ColorDome ganzfeld stimulator (right). 110

Figure 3-7 showing experimental set-up with patient positioned facing the front of the ganzfeld stimulator. 112

Figure 3-8 showing L cone driven ERG signal as a function of time 113

Figure 3-9 showing test vs retest 30 Hz flicker L- and M- cone driven ERG signal amplitudes (top row) and phase (bottom row) with the straight line showing perfect correlation. 117

Figure 4-1 Hypothetical Human ERG waveform elicited using long duration flash stimuli. a-, b- and c- waves as observed in response to ON- stimuli and d- wave elicited in response to OFF- stimuli. 120

Figure 4-2 Luminance profiles of red, green, blue and amber LEDs to generate L and M cone excitations. 125

Figure 4-3 shows luminance outputs of different classes of LEDs required to generate incremental luminance flash (LUM-On) stimulation 126

Figure 4-4 Temporal profiles of compound L- and M- cone isolating square wave pulse stimuli created using different luminance outputs of four LED classes.. 126

Figure 4-5 Group averaged ERGs (n=11) elicited in response to L-On/Off, M-On/Off and Luminance-On/Off equal spaced square-wave pulse stimuli with a stimulus duration of 250 ms onset and 250 ms offset. 130

Figure 4-6 On-Off response inversion of the M- cone ERG in normal trichromats. 133

Figure 4-7 Individual L-On and M-On driven ERGs obtained in response to 100:250 ms on/off transient, square- wave pulse stimuli. 134

Figure 4-8 Individual L-Off and M-Off driven ERGs obtained in response to L- and M- cone isolating decrement/increment transient, square- wave pulse stimuli. 135

Figure 4-9 L- (upper traces) and M- cone (lower traces) driven ERGs of two Protanopic observers (IP and SH) elicited in response to L- and M- cone isolating increment flash followed by a decrement transient flash stimulation. 138

Figure 4-10 L- (upper traces) and M- cone (lower traces) driven ERGs of 2 deuteranopes (IB and MAW) elicited in response to L- and M- cone isolating increment flash followed by a decrement transient flash. 139

Figure 4-11 illustrates group averaged Luminance, actual +L+M response and computed +L+M responses obtained by linear addition of L- and M- cone ERGs using brief on/off pulse stimulation. 141

Figure 4-12 Group averaged ERGs elicited in response to counterphase (left panel) and in-phase (right panel) stimulation in normal trichromats (n=6) using 100 ms onset followed by a 150 ms offset square wave profile. 142

Figure 4-13 ERGs recorded in a protanopic observer (IP) to inphase (+L+M and –L-M), counterphase (+L-M and –L+M) and luminance (LUM) stimulation. ... 143

Figure 5-1 Fundamental harmonic flicker ERG responses plotted as a function of temporal frequency in (A) Macaque (Kondo & Sieving, 2001); (B) Rabbit (Qian et al., 2010); (C) Mouse and (D) Human (Krishna et al., 2002) retina. 152

Figure 5-2 showing combination of four LED outputs used in the generation of L and M cone isolating stimuli at 5- (top row) and 30- (bottom row) Hz using modified Stockman fundamentals. 158

Figure 5-3 Examples of original ERG waveforms elicited from one observer by sinusoidally modulated L- (top row, red coloured traces) and M- (bottom row, green coloured traces) cone isolating stimuli at 11% cone contrast, presented at temporal frequencies 5-, 10- and 30 Hz. Each trace represents the average of at least 16 sweeps. 160

Figure 5-4 Fundamental component amplitudes of individual L- and M- cone isolated flicker ERGs plotted as a function of temporal frequency..... 163

Figure 5-5 Temporal responsivity of the first harmonic (F) signal amplitudes of L- and M- cone steady ERGs obtained in four dichromats, protanopes (n=2) (first column), deuteranopes (n=2)(middle column) and two anomalous trichromats (last column). 165

Figure 5-6 Vector averaged fundamental and second harmonic ERG amplitudes obtained in response to L- (left) and M- cone isolating sine wave stimuli in normal trichromatic observers plotted as a function of temporal frequency. 166

Figure 5-7 Graphs showing individual L- and M- cone amplitudes plotted as a function of temporal frequencies 167

Figure 5-8 Vector averaged L- and M- cone phase data plotted as a function of temporal frequency (n=6). 168

Figure 5-9 Individual phase data obtained from six normal trichromatic observers plotted as a function of temporal frequency. 169

Figure 5-10 Apparent latencies of vector averaged L- and M- cone driven steady state ERGs plotted as a function of temporal frequency. 170

Figure 5-11 L:M cone ERG signal amplitude ratios plotted as a function of temporal frequency. 172

Figure 5-12 (A) Group average data of Fundamental component (F) amplitudes of S- and L+M cone driven ERGs plotted as a function of temporal frequency. (B) Vector averaged S- and L+M cone phase data plotted as a function of temporal frequency obtained from normal trichromats (n=5). 173

Figure 5-13 Graphs showing individual S- and L+M cone amplitudes obtained from normal trichromatic observers plotted as a function of temporal frequency (n=5). 174

Figure 5-14 Individual phase data obtained from five normal trichromatic observers plotted as a function of temporal frequency..... 175

Figure 5-15 L:M cone ERG response amplitudes measured at a temporal frequency of (A) 5 Hz and (B) 30 Hz respectively. 179

Figure 5-16 Contribution of flicker ERGs at high (left) and low (right) temporal frequencies reflecting activity of magno- and parvo-cellular pathway mechanisms of human visual system and their contribution to steady state ERGs..... 182

Figure 6-1 Vector averaged Fundamental (F) rod responses (n=5) plotted as a frequency of temporal frequency, derived at retinal illuminances 120 Td (mesopic) and 12000 Td (photopic). 194

Figure 6-2 Temporal response characteristics of rods, L- and M- cone isolated ERGs for five stimulus conditions ranging from low mesopic to photopic light levels (1 Td, 10 Td, 100 Td, 1000 Td and 10000 Td) recorded in observer MK. 196

Figure 6-3 Temporal response characteristics of rods, L- and M- cone isolated ERGs for five stimulus conditions ranging from low mesopic to photopic light levels (1 Td, 10 Td, 100 Td, 1000 Td and 10000 Td) recorded in observer DK. 197

Figure 6-4 Temporal response characteristics of rods, L- and M- cone isolated ERGs for five stimulus conditions ranging from low mesopic to photopic light levels (1 Td, 10 Td, 100 Td, and 1000 Td) recorded in observer GG. 198

Figure 6-5 Response phase characteristics of rods driven ERGs recorded at 1 Td (mesopic) & 10000 Td (photopic) retinal illuminances plotted as a function of temporal frequency for subjects MK and DK. 200

Figure 6-6 Group averaged 8- and 30- Hz rod isolated flicker ERG amplitudes (top graph) and phase (bottom graph) plotted as a function of temporal frequency. 202

LIST OF TABLES

Table 2-1 : Summary of studies that have used silent substitution..... 991

Table 3-1 R^2 and R values for 30 Hz L and M cone amplitudes and phase.... 116

Table 3-2 (A) Cone isolated ERG amplitudes for retinal illuminance of 10,000 trolands (mean luminance=198.94 cd/m^2) 1177

Table 3-2 (B) Mean Phase and Mean Test-Retest difference 30 Hz L- and M-cone isolated ERG amplitudes for retinal illuminance of 10,000 trolands (mean luminance=198.94 cd/m^2)……..…… 1178

Table 4-1 Photoreceptor contrasts (%) of the isolated L- and M- cone, luminance and compound stimuli..... 125

Table 4-2 shows components of L- and M- cone increment and decrement ERGs that have similar response characteristics as a, b and d waves of photopic flash Electroretinogram 128

Table 4-3 Measured implicit times of different components of luminance, L- and M- cone isolating ERGs in normal trichromats(n=19) ……..……. 131

Abbreviations

Frequency	Hz	Hertz (cycle per second)
Wavelength	nm	Nanometre
Voltage	V	Volt
Retinal illuminance	Td	Troland
Angle	^{0}	Degree
Electrical resistance	Ω	Ohms
Percentage	%	Percent
Illuminance	lux	one lumen per square metre
Luminance	cd/m^2	Candela per square metre

Chapter 1 General Introduction

This thesis validates the use of silent substitution technique in recording electroretinograms from individual photoreceptor classes using a commercially available four-primary stimulator in normal trichromats and dichromats using Sine- and square- wave stimulus profiles.

Chapter 1 describes three classes of cone photoreceptors, short (S)- medium (M)- and long (L)- wavelength sensitive cones and their contribution to three postreceptoral (magnocellular (MC), parvocellular (PC) and Koniocellular (KC) pathways. Furthermore, spectral sensitivities of four photoreceptor classes is explained which forms the basis for silent substitution paradigm and also the factors affecting these spectral sensitivities is discussed briefly.

In Chapter 2, typical ERG waveform and the origin of its components is discussed. In addition to ISCEV standards, ERGs recorded using paired-flash paradigm, chromatic adaptation and silent substitution has been discussed.

Chapter 3 describes general methods which include basis for the silent substitution, computations related to silent substitution stimuli used in our experiments, colour vision tests used to categorise participants with colour vision deficiency and to establish normalcy in trichromats. Furthermore, recording and analysis of ERG recordings using sine- and square wave stimuli is briefly explained.

Experiment 1 (Chapter 4) & experiment 2 (Chapter 5) describes use of silent substitution in eliciting signals from L- and M- cone classes using sine wave and square wave pulse stimuli respectively. In experiment 3 (Chapter 6) temporal

properties of rod ERGs and how they vary with change in retinal illuminances is discussed. Chapter 7 discusses how photoreceptor specific ERGs obtained using SS can be potentially used to understand the pathophysiology of specific retinal diseases.

1.1 Introduction

A world devoid of colour is dreary. Colour perception allows human to discriminate objects based on the distribution of their spectral wavelengths that they project to the eye. Although luminance and texture of a surface gives sufficient clues that helps us distinguish objects, colour adds another perceptual dimension and allows us to recognise the objects under conditions where difference in brightness is subtle or non-existent. Substantial research shows that colour plays a crucial role in visual experience. The physiological mechanisms that mediate colour vision also enable perception of a wider range of hues, object recognition, visual memory and image segmentation (Gegenfurtner and Kiper, 2003)

Colour vision begins with the absorption of photons in specialised, photo-sensitive retinal cells called cone photoreceptors. This causes a chain of reactions that result in transduction of electromagnetic energy into electrical impulses. These electrical voltages are further converted into action potentials by an intricate network of retinal cells and are transferred to area V1 (striate cortex) for further processing.

The human visual system has the ability to operate over a range of 12 log units ranging from 10^{-3} lux to 10^{5} lux which is equivalent to star light and daylight conditions respectively. Under dim-light scotopic conditions (<0.003 cd.m^{2}), rods are sensitive, whilst the response of cones is below threshold. Therefore, rods

mediate vision under these conditions. When rods saturate under bright light, photopic conditions (>3 cd.m^2) cones involve in transmission of signals to lateral geniculate nucleus via three distinct parallel pathways producing the basis for colour vision and visual acuity. Under mesopic or twilight conditions (0.003 cd.m^2< mesopic luminance < 3 cd.m^2), both rods and cone mediate signal transmission (Osram Sylvania, 2000).

1.2 Overview of human trichromatic vision

The machinery of human vision relies on three stages:

1) Photoreception
2) Segregation of signals into parallel neural postreceptoral pathways
3) Transmission of visual information, processing & interpretation.

The initial stages of vision takes place in retina. Retina is a complex, heterocellular, multi-layered and accessible extension of the central nervous system in all primates. It comprises of several millions of closely packed neurons arranged in layers with different physiological properties. These neurons are interconnected with synapsis in between the layers. Since the initial stages of analysis of image occurs in retina, it therefore becomes necessary to understand the method of generation of the visual image in photoreceptors and transmission of signals to the succeeding neurons. These operations in the preliminary stages of vision have a considerable control over the subsequent stages of analysis in the visual centres of the visual cortex. It is an interesting locus to assess how responses of retinal elements in human relate to their synaptic relationship with other retinal neurons and to visual performance (Dowling, 1987). Is it said that retina is also a wonderful tool to document different phenotypes of genetic diseases (Francis, 2006).

1.3 Retina

The human retina is designated to capture heavy flow of photons that elicits relative excitations in different photoreceptors, sample the retinal image, segregate retinal image into neural signals produced by the photoreceptors into several sets of filtered neural images and transmission of these signals to higher order neurons via different parallel pathways (Oyster, 1999). The anatomical composition of retina in human and non-human primates involves distinct cell types with unique anatomic & physiologic characteristics which are arranged in ten layers (see figure 1.1):

1) Retinal Pigment Epithelium (RPE)
2) Photoreceptors
3) External limiting membrane (ELM)
4) Outer nuclear layer (ONL)
5) Outer plexiform layer (OPL)
6) Inner nuclear layer (INL)
7) Inner plexiform layer (IPL)
8) Ganglion cell layer (GCL)
9) Nerve fiber layer (NFL)
10) Internal limiting membrane (ILM)

These anatomical structures will be further discussed as per the classification of retina into neural (photoreceptors and other neural circuitries of the retina) and non-neural components (RPE). The five retinal layers that form a basis for neural

retina play a prominent role in processing and transmission of visual sensation, which form the basis of neuronal connectivity that defines vision include (Lee et al., 2010):

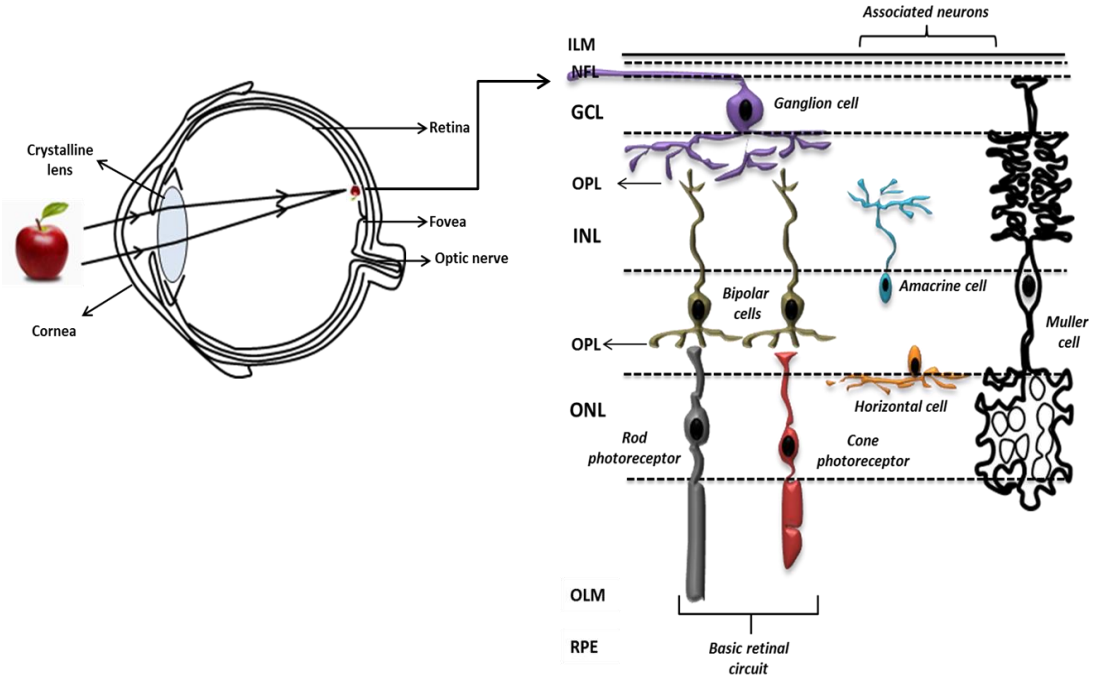

Figure 1-1 Cross section of human eye showing object forming an image on the retina (left) and cross section of human retina showing basic retinal circuitry and associated neurons (right).

1) The Outer Nuclear Layer **(ONL):** cell bodies of photoreceptors

2) The Outer Plexiform Layer **(OPL):** synaptic plexus of the photoreceptor axon terminals and dendrites of bipolar and horizontal cells.

3) The Inner Nuclear Layer **(INL):** cell bodies of the horizontal and bipolar cells, Muller cells, and most amacrine cells.

4) The Inner Plexiform Layer **(IPL):** axon terminals of the bipolar cells and a rich connective mesh of amacrine cell processes and ganglion cell dendrites.

5) The Ganglion Cell Layer (GCL): cell bodies of the ganglion cells and the cell bodies of displaced amacrine cells, which then, project to the thalamus.

1.3.1 Retinal pigment epithelium (RPE)

The single layer of polygonal cells of the RPE form a simple cuboidal epithelium with their basal membranes attached to Bruch's membrane. Bruch's membrane separates RPE from the choriocapillaries, which is the major source of blood and nutrients to the outer retina. The apical membrane of the RPE is located towards the photoreceptor outer segments. The lateral membrane of the RPE is the site for cell-cell adhesion and cell communication (Marrs et al., 1995).

The basic functions of RPE with regard to photoreceptors include: a) Photoreceptor membrane turnover, b) Maintenance of retinal homeostasis, c) Phagocytosis of toxic by-products of photoreceptors and d) Retinoid metabolism (Lamb and Pugh, 2004). The apical surface of the RPE bears numerous microvilli, which extend into the inter-photoreceptor space, therefore, facilitating the renewal of photoreceptor outer segments by process of phagocytosis and ingestion of remnants of shed photoreceptors (Borwein, 1981). The Na^+-K^+ adenosine triphosphatase (ATPase) molecules are abundantly present on the apical surface membranes of RPE cells whose chief function is the exchange of molecules in and out of the subretinal space. It also has the ability to adapt to the fast occurring changes in the ion composition in the subretinal space, which may risk the health of photoreceptors, and their function. Hence, this mechanism helps in the maintenance of retinal homeostasis (Ostwald and Steinberg, 1980 , Steinberg, 1985).

The RPE mediates the transfer of retinol from choriocapillaries to the interphotoreceptor space by utilizing numerous retinoid binding proteins as carriers and thus, play a key role in the process of phototransduction (Kefalov, 2012). Upon photon absorption by rhodopsin or iodopsin, metarhodopsin-II

dissociates to opsin and all-trans-retinal. The photoreceptors inability to reisomerize the all-trans retinal to 11-cis-retinal disturbs the maintenance of photoreceptor excitability. In the RPE cells, all-trans-retinal reisomerize to 11-cis-retinal and transported back to the photoreceptors which is an important step in the visual cycle (Steinberg, 1985 , Dornonville de la Cour, 1993).

1.3.2 Photoreceptors and circuitries in the human retina
(A) Morphology of photoreceptors

The human retina is composed of two distinct types of photoreceptors: the cones and the rods. Cones and rods subserve photopic (daylight) and scotopic (twilight) vision respectively. The retinal photoreceptors form the first sensory component of the visual system. The vitreal portion of the axonal processes of photoreceptors extends to synapse with bipolar and horizontal cells. Each photoreceptor is typically composed of (see figure 1.2):

(a) The photosensitive outer segment formed by the extension of plasma membrane which holds stacks of membranes. The geometry of the outer segment determines the type of photoreceptor.

(b) The inner segment is composed of mitochondria, ribosomes and membranes where opsin molecules assemble and migrate to the outer segment to adhere with the free-floating discs.

(c) a cell body with central nucleus and

(d) a synaptic terminal connecting to second order neurons with the help of neurotransmitters.

The length and conical angle vary throughout the outer-segment of these cone photoreceptors. Each cone photoreceptor contains a specific visual pigment,

which is composed of a protein called opsin and a chromophore, which actively participate in the process of phototransduction.

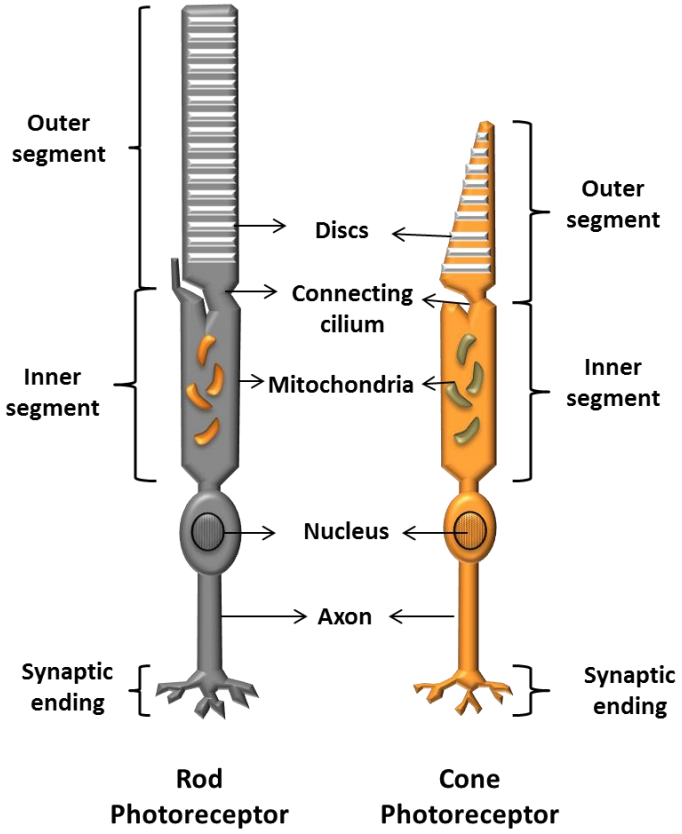

Figure 1-2 illustrates anatomy of human rod and cone photoreceptors

(B) Phototransduction

For over 40 years, G-protein coupled receptor (GPCR) based signalling have been an outstanding model system in understanding the basic principles of rapid photoactivation and inactivation, signal amplification, and gain control (Julius and Nathans, 2012). Phototransduction is the process by which a photon of light upon absorption in the photopigment of a photoreceptor generates an electrical response in the photoreceptor. It is the first event in encoding visual information followed by a photon capture in the opsin. A century after discovery of the first G-protein coupled receptor (GPCR), rhodopsin by Kuhne (1878), knowledge about molecular mechanisms underlying GPCR signalling has greatly expanded.

Since the suction electrode recording technique was introduced in the late 1970s, the understanding of rod phototransduction has become clearer in terms of how these photoreceptors react to low and high light levels under scotopic and photopic conditions respectively (Baylor et al., 1979).

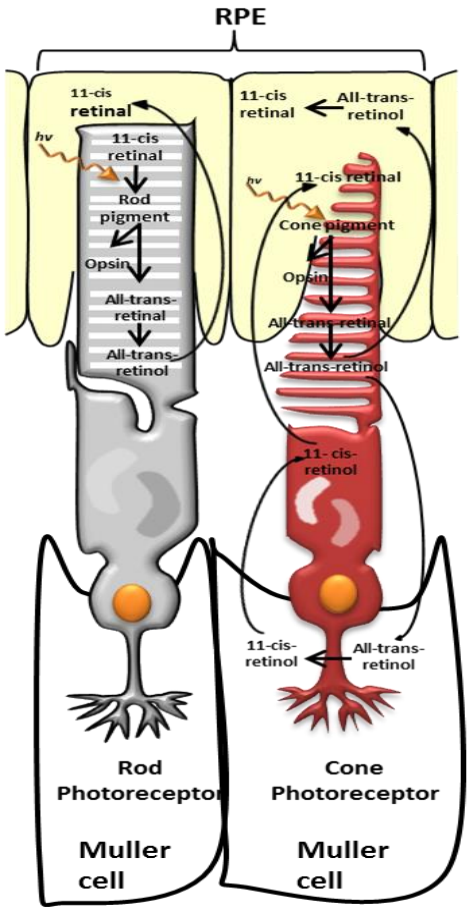

Figure 1-3 : Schematic representations of stages of phototransduction in rod and cone-photoreceptors

(I) In the Dark

Unlike other cells in the human body, photoreceptors depolarise in the absence of light stimuli (scotopic conditions) (see figure 1.3 & 1.4). Under scotopic conditions, cGMP levels are high and result in opening of cGMP- gated sodium

channels allowing inward flow of Na+ ions driven by the electrochemical gradient through the plasma membrane of the outer segment (Yau and Hardie, 2009). This causes depolarisation of the photoreceptor at about -40 mV.

In the dark when the cell is in a depolarised state (see figure 1.4), the voltage-gated calcium channels of the cell membrane open with subsequent increase in intracellular concentration of Ca2+ ions which inturn results in release of neurotransmitter, glutamate at the synaptic terminal of the photoreceptor.

Glutamate hyperpolarises ON- bipolar cells (see figure 1.4). This neurotransmitter is excitatory in nature and when released in the synaptic cleft binds with the metabotropic glutamate receptors (mGluR6) of the bipolar cells. As a consequence, closure of non-specific cation channels occurs through G-protein coupling mechanism, thus, hyperpolarising the bipolar cell.

On the other hand, Glutamate depolarise OFF- center bipolar cells by binding to ionotropic glutamate receptors causing inward flow of cations.

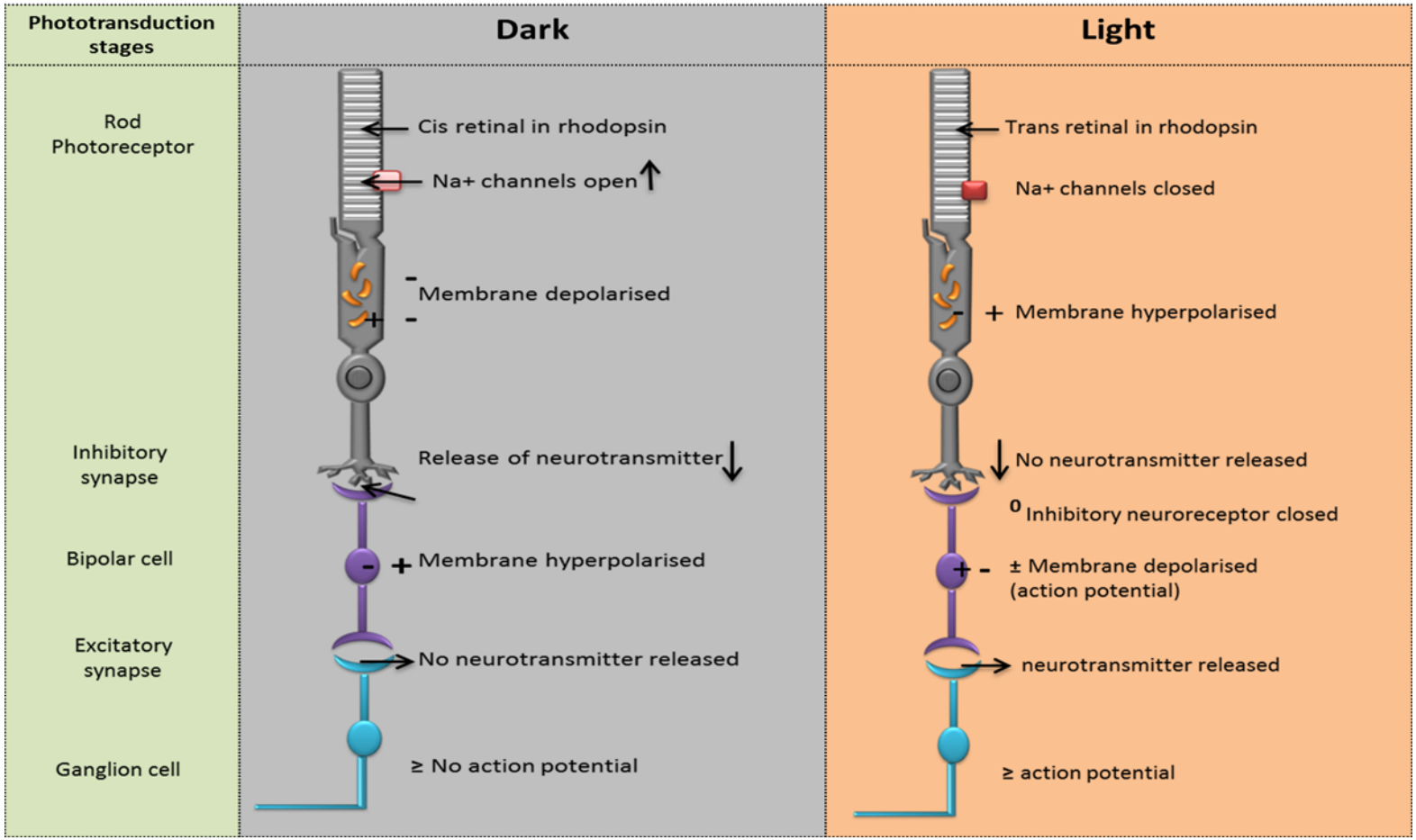

Figure 1-4 Stages of phototransduction cascade in human rod photoreceptor under dark (scotopic) and light (photopic) conditions respectively.

(II) In the Light

Activation of phototransduction cascade can be divided into five important steps with the first three involving activation of proteins associated with rhodopsin and the last two steps involving cyclic GMP (cGMP) and the transfer of electrical signal (see figure 1.4 and 1.5) (Pugh and Lamb, 2006).

Step 1 (activation of rhodopsin)

When a rod photoreceptor is struck by a photon, it interacts with retinal that isomerizes from 11-cis to all-trans configuration. Since the altered form of retinal cannot fit into the opsin binding site, opsin further transforms into an unstable metarhodopsin II which breaks down into opsin (R) and all-trans retinal (see figure 1.5).

Step 2 (activation of G- protein)

Within a millisecond of photon capture opsin (R) transforms to metarhodopsin II (R*) and activates a regulatory protein called transducin (G*). This results in transducin to dissociate from its bound GDP in exchange of cytoplasmic GTP, causing dissociation of alpha subunit from beta and gamma subunits with GTP still attached to the alpha subunit (Gα_t).

Step 3 (activation of PDE)

The alpha subunit- GTP complex (G*) binds with inhibitory gamma subunits of phosphodiesterase (PDE) and activates the alpha and beta subunits of PDE.

Step 4 (hydrolysis of cyclic GMP)

The activated PDE then hydrolyses cGMP (the second messenger in phototransduction) synthesized by Guanylyl cyclase (GC) to 5'-GMP. This leads to the drop in cGMP concentration.

Step 5 (Closure of Ion channels)

The drop in cGMP concentration then causes closure of sodium channels preventing further influx of Ca2+ and Na+ ions. As a result, concentration of Ca2+ in the photoreceptor decreases leading to drop in glutamate at the synaptic terminal as Ca2+ is required for vesicles comprising of glutamate to attach with cell membrane to release their contents. These changes result in depolarisation and hyperpolarisation of ON- and OFF- center bipolar cells respectively thereby, relaying the light signal to the successive neurons as electrical signal (Lamb and Pugh, 2000; Yau and Hardie, 2009).

It is at these steps of phototransduction cascade where signal amplification takes place when multiple tranducins are activated by a single R* (Burns and Arshavsky, 2005). Steps 3, 4 and 5 of the phototransduction cascade retinal (see figure 1.5) determine the degree of signal amplification and ensure high sensitivity of rods secondary to single photon absorption in rod photoreceptors (Pugh and Lamb, 2004 and 2006).

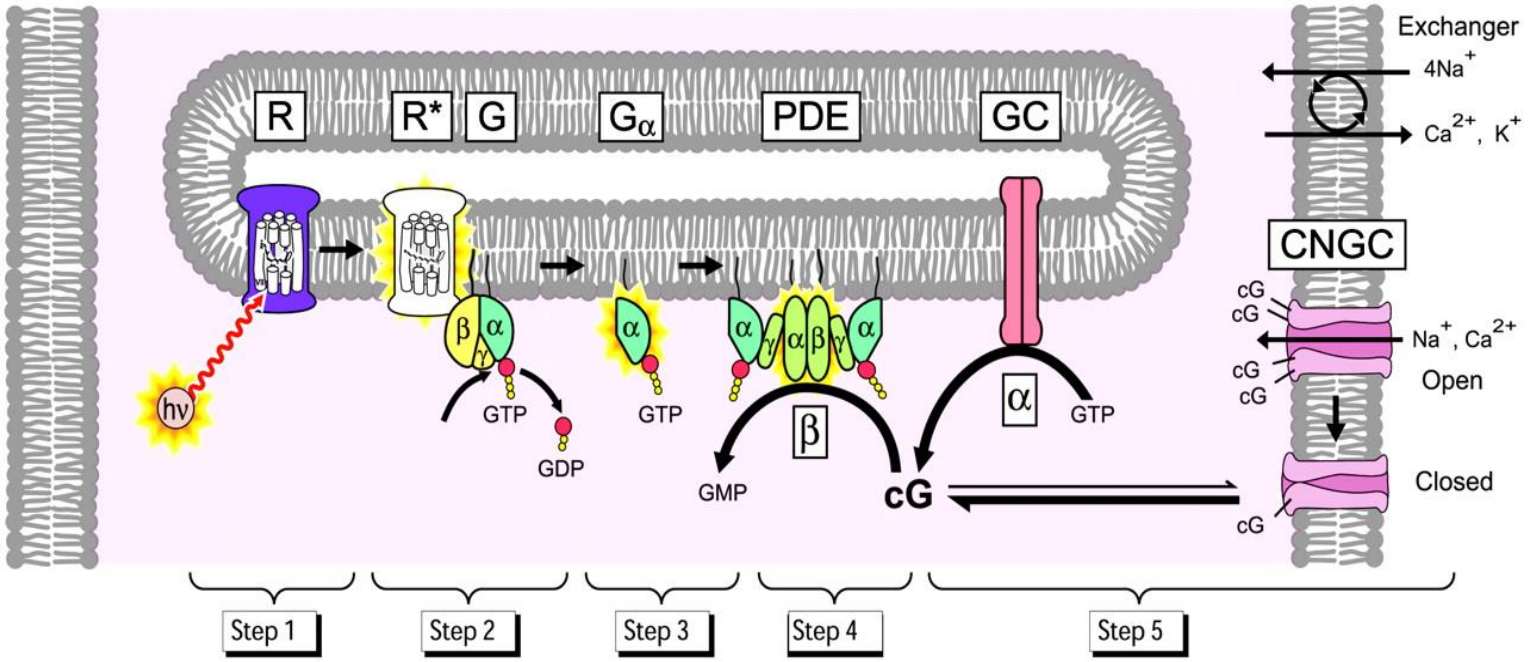

Figure 1-5 Schematic representations of five stages of phototransduction cascade.

Upon absorption of a photon (hv), the activated rhodopsin continuously interacts with the heterotrimeric G protein (G) which results in exchange of GDP for GTP generating Gα-GTP complex (G*) which further binds with γ subunits of the phosphodiesterase (PDE). This results in activation of one or both of the corresponding α and β subunits catalysing the hydrolysis of cyclic GMP (cG). As a result, concentration of cGMP decreases in the cytoplasm. This leads to the closure of ion gated channels and block influx of Na^+ and Ca^{2+} thereby minimizing the circulating current. (Source: Lamb and Pugh, 2006).

R* inactivation

Upon photoresponse reaching its peak, internal current returns to its ground state. To maintain continuous responsiveness of photoreceptors to light, timely recovery is essential and the phototransduction in the outer segment of the receptor has to be efficiently terminated. The inactivation of all the transduction components R*, G* and PDE* is required for cGMP recovery. Cyclic GMP is a key molecule in the phototransduction process as the visual signalling relies on the balance between its synthesis and hydrolysis in the cytoplasm of the photoreceptor outer segment (Lamb and Pugh, 2004; Burns and Arshavsky, 2005; Fu and Yau, 2007).

Rapid inactivation of R* during phototransduction cascade is achieved in two steps: Phosphorylation by rhodopsin kinase and subsequent arrestin capping. First the activity of R* is partially blocked through incorporation of atleast three phosphates into a molecule of R* (Kuhn and Wilden, 1987; Whitlock and Lamb, 1999; Kennedy et al, 2001). Second, the binding protein- arrestin binds to the phosphorylated R* and completely inactivates R* by intercepting its access to transducin (Xu et al, 1997 and Vishnivetskiy et al, 2000). Due to change in R* configuration, it can either decay into opsin and all- trans retinal or transform into the inactive Meta III from which eventually separates into apo-opsin and retinoid (Kolesnikov et al., 2003). The rate of R* decay is remarkably slower than the complete inactivation of R*, as a consequence, it does not affect the flash response (Imai et al., 2007).

cGMP restoration

Only inactivation of R* does not produce complete recovery of the photoresponse. When exposed to bright light, the activation and bleaching of significant fraction of the visual pigment takes place. This results in reduced sensitivity if photoreceptors by two mechanisms: 1) decline in the amount of visual pigment for subsequent light activation and 2) produces activity due to accumulated apo-opsin as the bleached pigment decays. Therefore, to accomplish complete recovery of dark adapted sensitivity of the photoreceptors requires constant restoration of the bleached visual pigment with 11-cis RAL (Pepperberg et al., 1978 and Cornwall et al., 1995).

(C) Visual cycle

As described by George Wald (1935), visual cycle is the ability to “recycle” Vitamin A through a metabolic process through which the visual pigment (opsins) is synthesised after photoactivation. The biochemical reactions involved in the process of phototransduction occur at a rapid rate. However, for photoreceptors to uninterruptedly function when exposed to light requires the continuous restoration of inactivated opsin (Burns and Arshavsky, 2005). The kinetics of visual cycle are regulated by several important enzymes and binding proteins. Defects in these chemical components can decelerate or disturb the visual cycle resulting in a lack of chromophore which as a consequence leads to various retinal diseases causing moderate visual impairment to severe blindness (Gu et al., 1997; Morimura et al., 1998; Thompson and Gal, 2003; Jacobson et al., 2005; Travis et al., 2007; Aguirre et al., 2007). In some cases, toxic byproducts released in visual cycle accumulate and has a pathological consequence (Paskowitz et al., 2006; Golczak et al., 2008). Therefore, it

becomes necessary for us to understand the visual cycle in rod and cone photoreceptors.

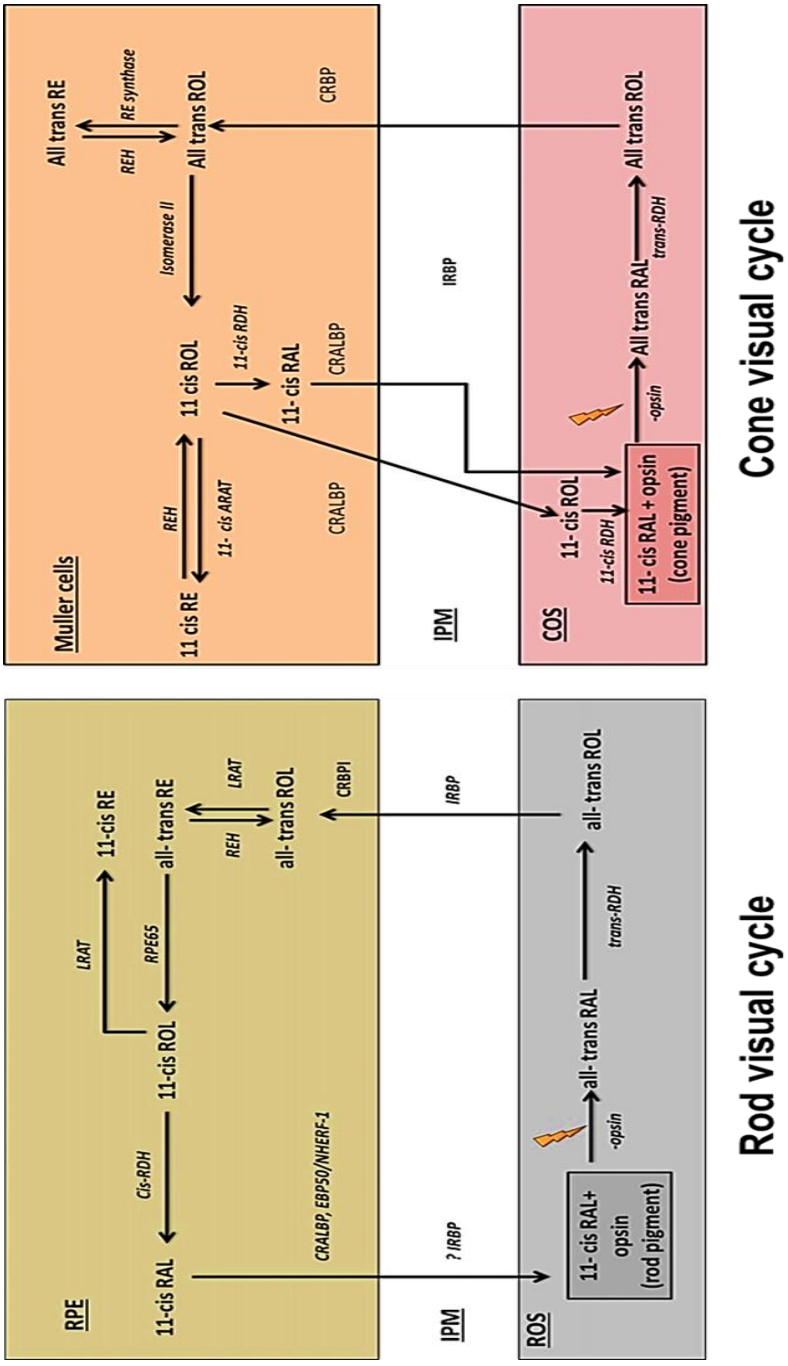

Figure 1-6 Visual cycle in rod and cone photoreceptors

The conversion of all-trans retinal back to 11-cis retinal involves a sequence of biochemical reactions many of which occur outside the photoreceptors primarily in the RPE. However there is evidence that suggest that especially for cone visual cycle, majority of these reactions occur in the muller glial cells than in the RPE (see figure 1.3) (Goldstein, E,B. and Wolf, 1973; Das et al., 1992; Muniz et al., 2006).

(I) Rod visual cycle

Over six decades later, as a result of several studies, a great deal of knowledge on rod visual cycle has now been acquired (Crouch et al, 1996; McBee et al., 2001; Lamb and Pugh, 2004; Travis et al., 2007). Typically, visual cycle involves the outer segment of photoreceptors and the RPE. Kuhne (1878) and Weinsten et al., (1967) conducted experiments on animal models with rod dominated retinas and reported that RPE plays a key role in pigment regeneration in the visual cycle (see figure 1.6).

Followed by photon absorption in the outer segment of the receptor, 11-cis retinal (11-cis RAL) isomerizes to all-trans retinal (all-trans RAL). Upon bleaching, a series of conformational changes occur, eventually decays to opsin and all-trans RAL. All-trans RAL further reduce to all-trans retinol (ROL) by NADPH-dependent retinol dehydrogenase (RDH) (Rattner et al., 2000, Jang et al., 2000, Wang and Kefalov, 2011). All-trans ROL is then transported from outer segments of photoreceptors to the apical processes of RPE assisted by a carrier protein, Interphotoreceptor Retinoid Binding Protein (IRBP) in the interphotoreceptor matrix (Lai et al., 1982 and Liou et al., 1982). In the RPE, all-trans ROL binds with a protein called Cellular Retinol Binding Protein I (CRBPI) (Noy, 2000) and diffuse

from the apical processes to the cell body of RPE cell (Saari, 2000; Huang et al., 2009).

It is at this site where all-trans ROL esterifies into all-trans retinyl ester (all-trans RE) by lecithin:retinol acyltransferase (LRAT) (Saari et al., 1993; Ruiz et al., 1999 and Mondal et al., 2000). RPE65 (Isomerohydrolase (IMH), Isomerase I) is a protein coding gene that isomerizes and hydrolyses all-trans-RE to 11-cis-ROL (Redmond et al., 1998 and Gollapalli and Rando, 2003b). 11-cis-ROL bound to CRALBP (Cellular Retinaldehyde Binding Protein) oxidizes into RAL by retinol dehydrogenase (11-cis-RDH). esterification of 11-cis-ROL to 11-cis-RE take place with the assistance of LRAT. 11-cis-RE hydrolyses to 11-cis-ROL by 11-cis-retinyl ester hydrolase (REH) to supply 11-cis-retinol for pigment regeneration (Saari et al., 2000).

Still attached to CRALBP, 11-cis-RAL diffuses from the cell body to the apical processes of the RPE cells close to the outer segments of rod photoreceptors. 11-cis-RAL, then departs RPE and navigates across interphotoreceptor matrix (IPM) probably assisted by CRALBP, EBP50/NHERF-1,ezrin and actin complex (Saari et al., 2004 and Huang et al., 2009). In the interphotoreceptor matrix, IRBP is assumed to carry 11-cis RAL and send it to the outer segments of rod receptors for pigment regeneration (Pepperberg and Clack, 1984 and Wang and Kefalov., 2011).

(II) Cone visual cycle

Despite equal pigment concentration and density in both rod and cone photoreceptors (Harosi, 1975), when exposed to bright light, cones dark adapt rapidly (3-4 min) in comparison to rods (30 min) (Hecht et al., 1937) and this is due to the rapid regeneration of their respective pigments (Lamb and Pugh, 2004).

Extensive research using biochemical and physiological approaches on animal models has led to the discovery of a novel pathway for cone-specific visual cycle (Das et al., 1992; Travis et al., 2002; Muniz et al., 2006). Based on these results, it has now been established that cone visual cycle involves transfer of retinoid necessary for cone pigment regeneration between Muller cells and cone outer segments (Goldstein, E,B. and Wolf, 1973; Okajima et al, 1989; Das et al., 1992; Muniz et al., 2006). Interestingly, these studies also found retinoid binding proteins CRBP and CRALBP that are found in RPE cells were also found in Muller cells (Bunt-Milam and Saari, 1993). Furthermore, presence of 11-cis ARAT in Muller cells (Muniz et al., 2006; Kaylor et al., 2014) also support the theory that Muller cells play a key role in cone visual cycle.

Upon photon absorption 11- cis retinal is isomerized to all- trans-RAL which is then reduced to all-trans-ROL by an unclassified and anonymous retinol dehydrogenase. This all-trans-ROL is then transferred to the Muller cells via extracellular intraphotoreceptor matrix probably with the assistance of IRBP (Okajima et al, 1989, Jin et al., 2009 and Parker et al., 2009). In the Muller cells, all-trans-ROL binds with CRBP and isomerizes to 11-cis-ROL by Isomerase II (Eisenfeld et al., 1985; Mata et al., 2002).

All-trans-ROL may also esterify into all-trans Retinyl Ester (RE) by an unidentified and unclassified retinyl ester synthase. This all-trans-RE may also be isomerohydrolyzed to 11-cis-ROL by 11-cis-retinyl ester hydrolase (REH) (Gollapalli and Rando, 2003b). Like in rod visual cycle ,11-cis-ROL in cone visual cycle, follows one of two paths: 1) esterify to 11-cis-RE by the help of 11-cis Acyl Transferase (ARAT) (Muniz et al., 2006) which later hydrolyses to 11-cis-ROL by 11-cis-retinyl ester hydrolase (REH) to supply 11-cis-retinol for pigment regeneration (Bustamante et al., 1995; Blaner et al., 1987; Mata and Tsin, 1998). 2) 11-cis-ROL oxidises to 11-cis-RAL with the help of retinol dehydrogenase which is abundant in both cones and Muller cells (Mata et al., 2002). When the resulting 11-cis-RAL is mediated by retinol dehydrogenase in Muller cells, it will then be attached to and protected by CRALBP. CRALBP is a protein found in both in RPE and Muller cells that has affinity to bind both 11-cis-ROL as well as 11-cis-RAL (Noy, 2000). The 11-cis-RAL then exits Muller cells and carried to the cone outer segments via IRBP where it binds with cone opsin to form cone pigment. Few studies suggest that it is also likely for 11-cis-ROL to directly contact cones where they are oxidised to RAL for pigment regeneration (Mata et al., 2002).

(D) Density and distribution of photoreceptors

The number and distribution of rods and cone photoreceptors throughout the surface of the retina has important consequences for vision. The average number of cones and rods in human retina measured on human donor retinas as reported by Curcio et al. (1990) was 4.6 million cones and 92 million rods respectively. The average horizontal diameter of the fovea, which is rod-free is 0.350mm (1.25 degrees). The one-to-one relationship of cones with midget bipolar cells and subsequently with midget ganglion cells in the foveal region accounts to basis for high spatial acuity. With retinal eccentricity cone density drops with increase in the convergence onto retinal bipolar cells causing significant decrease in acuity. However the advantage of this distribution is that the threshold required for detecting a light stimulus in the periphery where rods are abundant is lesser in comparison to the fovea thereby helping us to appreciate the objects under dim light conditions.

Like most vertebrates, human retina is predominantly rod- dominated with rods outnumbering cones by a ratio of 95:5. However, the central area of the retina called fovea is rich in cones and is a rod-free zone (Wang and Kefalov, 2011). The mean of highest cone densities is about 199,000 cones/ mm^2, found at the foveola and the average of highest rod densities found at along the elliptical ring at the eccentricity of the optic disc, extending into nasal retina is 176,000 rods/mm^2. The highest densities of cones and rods are highly variable between individuals (100,000-324,000 cones/mm^2 at foveola and 157,900-188,600 rods/mm^2 at rod ring). Cone and rod densities steeply fall with increase in eccentricity (see figure 1.7) (Curcio et al., 1990).

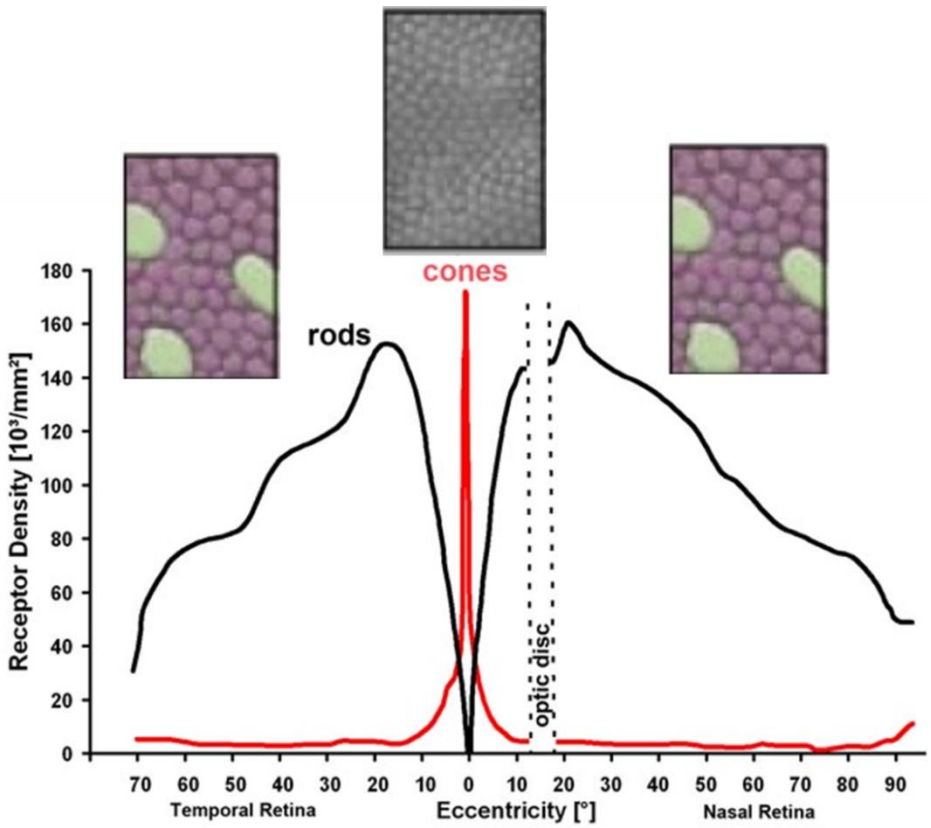

Figure 1-7 Graph demonstrates the distribution of rods and cones along the horizontal meridian of the human retina.

Central foveal region shows no rods and highest cone density. At about 10-15 degrees eccentricity, densities of cones fall rapidly to a constant level. Optic nerve is photoreceptor-free and hence called blind spot. Conversely, the density of rods reaches a maximum at 15-20 degrees from the fovea. Source: Adapted from Osterberg (1935) and Purves (2001).

The nature of colour vision in a living organism depends on (Jacobs, 1996):

(1) Number of photopigment classes

(2) The spectral separation of the photopigments and

(3) The relative representation of the different pigments among the population of photoreceptors.

(E) Classification of cone photoreceptor types

The human cone photoreceptors can be further classified based on their spectral sensitivity and absorption of photons in their corresponding photopigment opsins. The human retina comprises of a mosaic of three classes of cone photoreceptors: long (L-), middle (M-) and short (S-) wavelength sensitive cones categorized based on their peak spectral sensitivities (Bowmaker et al, 1980 and Schnapf et al, 1987).

(F) Human cone spectral sensitivities/ Cone fundamentals

Spectral sensitivities of L-, M- and S- cone photoreceptors underpin human trichromatic colour vision. A precise knowledge of spectral sensitivities or cone fundamentals of these three cone types is crucial in understanding normal and reduced forms of colour vision in which either one or more cone types are absent and/or a functional photopigment is replaced by a non-functional pigment type.

Spectral sensitivity sometimes also referred to as quantum efficiency, can be defined as the ability of human eye to detect light as a function of wavelength or frequency of the signal. This measurement describes the distinctive characteristics of the photopigments of rod and cone photoreceptors whose maximum spectral sensitivities (λ_{max}) under photopic and scotopic conditions are at 555 and 507 nm respectively (Wyszecki and Stiles 1967).

The spectral sensitivities as shown in figure 1.8 overlap across the visible spectrum. It is relatively easier to isolate S- cones 1) as their spectral sensitivities fall in the shorter wavelength region and 2) due to their temporal response properties limited upto <28 Hz (Stockman et al 1991) and isolation of rods is relatively straight forward due to their bleaching properties, saturation at high light levels, reaction times and temporal resolution of upto 28 Hz (Conner, (1981) & Conner and MacLeod (1977)). On the other hand, isolation of L- and M- cone signals is difficult due to their 1) similar biochemical and genetic composition, 2) 95% identical photopigments as a result of which they exhibit 3) highly overlapping spectral sensitivities (see figure 1.8) (Hofer et al, 2005).

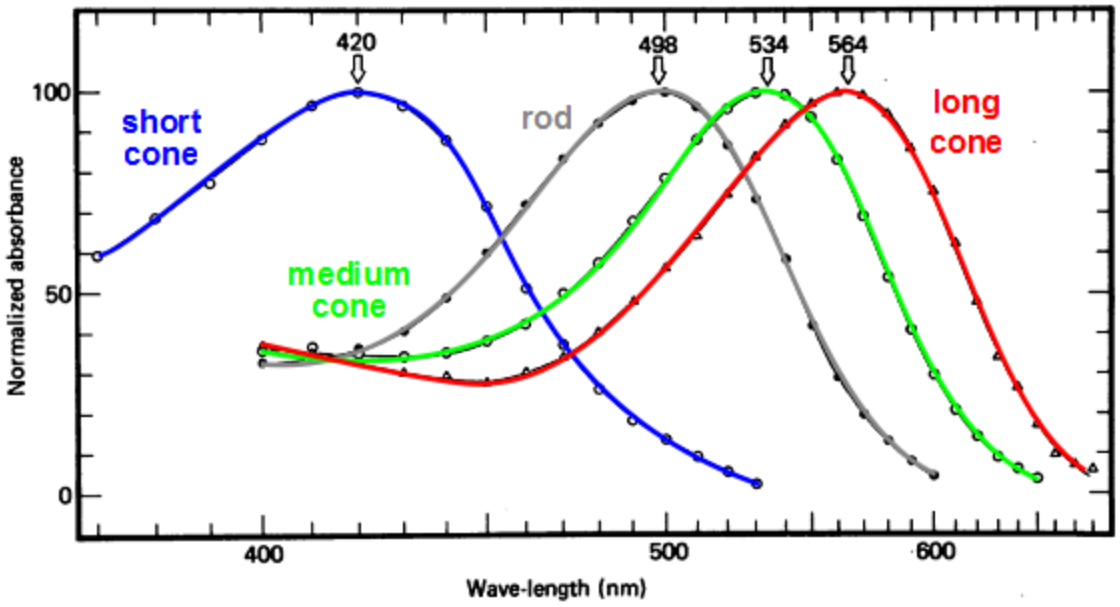

Figure 1-8 Normalised spectral sensitivities of rods, S-, L- and M- cones (Bowmaker and Dartnall, 1980).

To overcome this problem, Stockman and Sharpe (2000) conducted heterochromatic flicker photometry experiments in dichromats where one of the two cone types is absent (M- cones are absent in deuteranopes and L- cones are absent in protanopes) (see section. They used a conventional Maxwellian-view optical system to present two targets (2^0) reference light (560 nm) presented in opposite phase at 25 Hz with a superimposed test light (random presentation of wavelength ranging from 400 to 700 nm). To achieve spectral sensitivities, first, the thresholds were established for each participant and then the dichromatic observers were asked to alter the intensity of the flickering reference light in order to match with the test light. This procedure was continued for different wavelengths until the participant reported the flicker to have been disappeared. By doing so, they could achieve discrete L- and M- cone spectral sensitivities (see figure 1.9). Knowledge of these spectral sensitivities is required when working with isolation of signals from individual photoreceptor classes.

(i) Factors effecting spectral sensitivities

Although, different individuals with normal colour vision have photopigments that are similar in composition, there are factors that alter the light reaching the photopigments of the photoreceptors. These factors are lens pigment density, macular pigment density and photopigment optical density as they attenuate the spectrum of the light reaching the retinal cells and produce transmission losses especially at short wavelengths which successive could impact spectral sensitivities of cone photoreceptors (see figure 1.10).

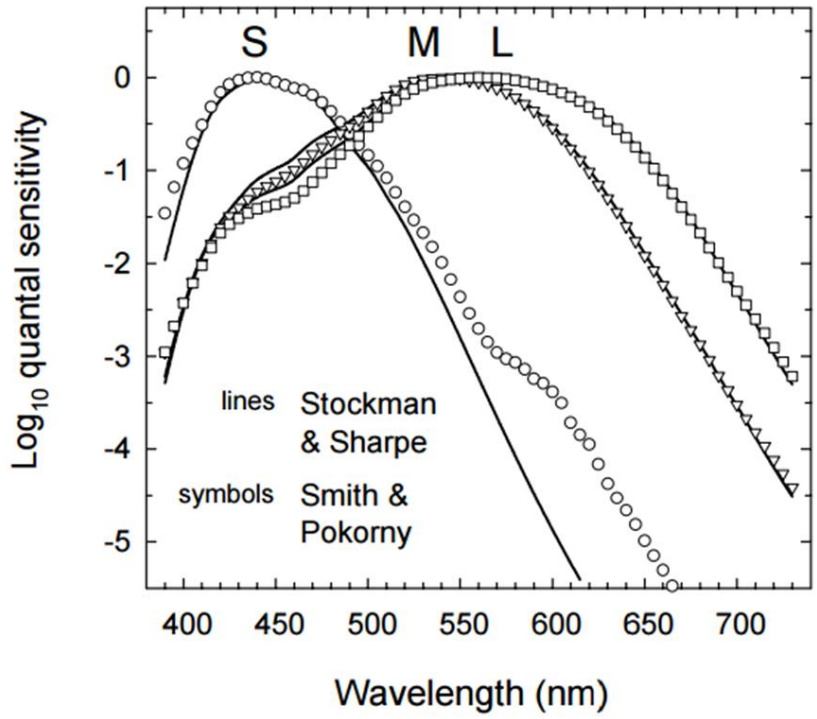

Figure 1-9 Spectral sensitivities of S-, M-, and L-cones as observed in two different studies.

S- (open circles), M- (open inverted triangles), and L- (open squares) cone spectral sensitivities of Smith and Pokorny (1975) compared with Stockman and Sharpe (2000a) spectral estimates (continuous lines) compared with the. S- cones exhibit a difference in their spectral sensitivities at higher wavelengths.

(a) Lens density spectra

There is evidence that short wavelengths of light are absorbed by the lens pigment. Previous studies (Pokorny et al 1987) report that lens density spectra changes with age. Therefore, whilst recording cone driven responses especially from young and old age cohorts of subjects, these changes should be taken into consideration.

(b) Changes in macular pigment density

The effect of macular pigment density on spectral sensitivities can be measured by comparison of spectral sensitivities at fovea and at 10 degrees eccentricity where macular pigment is largely absent (Bone et al 1988). They also reported a large inter-individual difference in macular pigment. Both photopigment optical

density and macular pigment density vary from center to periphery. These factors have different effects on the sensitivities of cone photoreceptors 1) based on their eccentricity and 2) the type of the cone photoreceptor (Pease et al 1987).

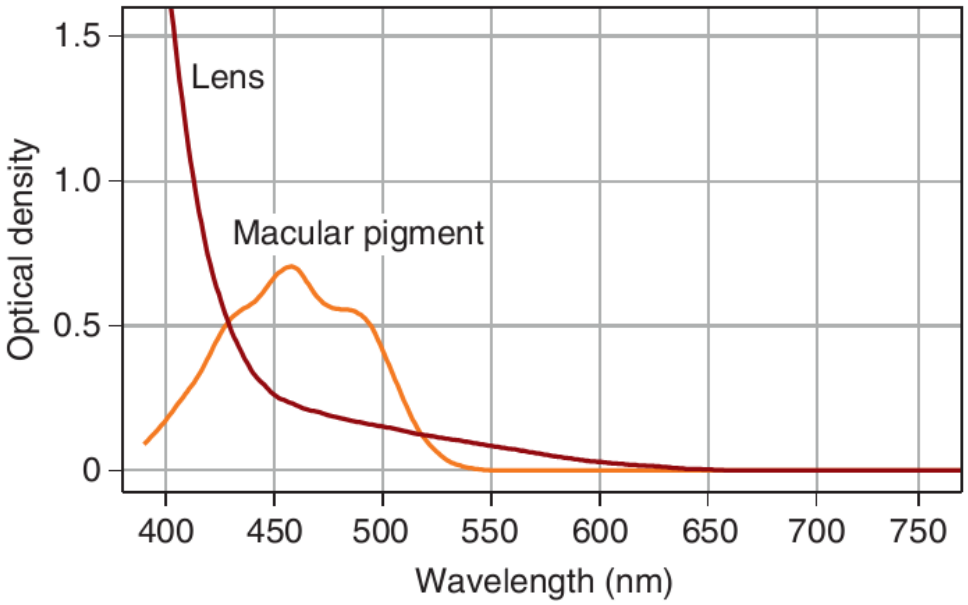

Figure 1-10 Graph showing changes in macular pigment and optical density of the crystalline lens as a function of wavelength (Foster, 2010).

(c) Photopigment optical density

Addition to macular pigment, optical density of the photopigment also had shown to affect cone spectral sensitivities. However, Stockman, Sharpe and Fach (1999) and Stockman and Sharpe (2000a) observed the mean peak photopigment optical densities for L- and M- cones for central 10^0 and 2^0 of vision to be similar (0.38 & 0.50 respectively). Since the relative photopigment optical densities for L & M cones are identical, we could rule out the possibility of this factor affecting our signals.

(G) Genetics of colour vision

Interpretation of the neural machinery that underpin both normal and defective colour vision is complicated and needs an understanding of events at the level of genes, neurons, proteins and circuits which are not readily available. Although results from electrophysiological and psychophysical studies provided information on electrical responses and perceptual aspect of colour vision, genes that cause changes in colour vision is still not completely understood.

The genetic mechanisms underlying colour vision were first studied by isolating and sequencing the genes encoding the human long (L-), middle (M-) and short (S-) wavelength sensitive cone opsins. The variation in the amino acid sequence in a cone opsin and alterations in the cone opsin gene are the major reasons behind colour vision deficiencies (Nathans et al, 1986a).

The human genes encoding L and M cone opsins were localised at Xq28 on X chromosome, the gene encoding S cone opsin was localised at 7q32 on an autosome chromosome 7 (Nathans et al., 1986a). The genes encoding L, M, and S wavelength cone opsins were designated as OPN1LW, OPN1MW, and OPN1SW respectively. OPN1LW and OPN1MW were observed to be arranged in a tandem array (Nathans et al., 1986b and Vollrath et al., 1988). The data in the tandem array infers that the most people with normal colour vision have both L- and M- cone genes (Nathans et al., 1986; Nathans et al., 1986b; Drummond-Borg et al., 1989; Neitz and Neitz., 1995; Macke and Nathans, 1997; Ueyama et al., 2001). OPN1LW and OPN1MW share 98% nucleotide sequence identity, indicating OPN1LW and OPN1MW arise via relatively recent gene duplications (Nathans, 1986b). On the contrary, OPN1SW share 40% nucleotide sequence identity with OPN1LW and OPN1MW.

The major similarity between L and M opsin genes is responsible for the unequal homologous recombination between them, which has profound implications on vision. This recombination has intermixed L and M opsin genes resulting in the variation in the amino acid sequences of both L and M opsins among individuals with normal colour vision (Neitz and Neitz, 2011). The amino acid differences shift the spectral peaks of L and M cone pigments which have consequences for colour vision (See figure 1.11).

Pigments in all eutherian mammals have the same 11-cis retinal chromophore (Wald, 1967, 1968). The chromophore binding to opsin-red shifted the absorption spectrum of the chromophore. The differences in amino acid sequence were responsible for the spectral characteristics of each of the cone pigments (see figure 1.11) (Wald, 1967; Kosower, 1988 and Chen, 1989). The advancements in the technology made it possible to measure the spectral sensitivities of individual cone classes (Dartnall et al., 1983; Baylor et al., 1987; Schnapf et al., 1987; and Kraft et al., 1998) and analyse the effects of amino acid sequence differences in spectral sensitivity (Asenjo et al, 1994; Carroll et al., 2002; Merbs and Nathans, 1992; Neitz et al., 1995b; Sharpe et al., 1998 and Stockman et al., 2000).

Both L- and M- cone opsin genes consist of 6 exons each. The majority of the spectral differences between L- and M- pigments are due to the amino acid dimorphisms at positions 277 and 285 which are encoded by exon 5 (see figure 1.11). Exons 2, 3 and 4 also encode amino acid sequences of L- and M- cone pigments which in turn produce small variability in the absorption spectra. Exons 1 and 6 are similar in L and M opsin genes (Neitz and Neitz, 2011).

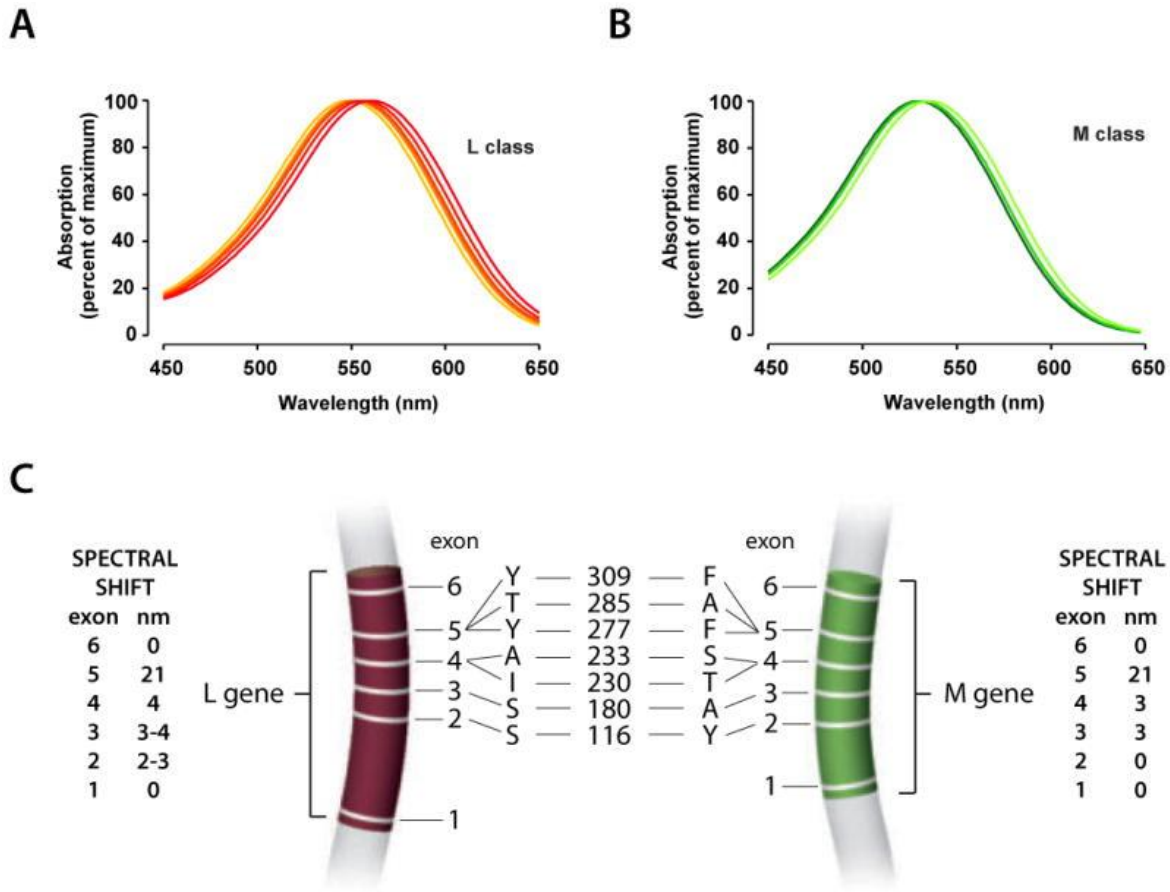

Figure 1-11 Spectral coding of human L- and M- cone pigments.

A) and B) show peak spectral sensitivities of L- and M- cone pigments at 560 and 530 nm respectively. C) Genes encoding both L and M cone opsins possess 6 exons each represented by thin white bands and numbered 1 through 6. The red and green coloured regions indicate the exons in the L and M opsin genes. The type of codons that specify amino acids that mediate spectral tuning and the amino acid position are indicated by letters and numbers in the middle of the panel respectively. (Amino acids, S=serine, I=isoleucine, A=alanine, T=threonine, Y=tyrosine, F=phenylalanine). The amino acid differences specified by each exon can cause a spectral shift and the magnitude of these shifts for each exon is shown on the far left and far right of the panel. (Source: Neitz and Neitz, 2011)

(H) Colour blindness

Normal colour vision can differ significantly among both males and females. This variation in normal colour vision could be due to individual differences in the macular pigment density, optical densities of the crystalline lens and macular pigment (see section on spectral sensitivities).

Trichromacy, however cannot be appreciated by all. Many people are either partially or completely colour vision deficient. Colour vision deficiency is prevalent in about 8% males and 0.4% females (Steward and Cole, 1989) and the percentage varies across the globe and is different in different races (Birch, 2001)

Colour vision defects can be classified into two types: congenital and acquired. Congenital or inherited colour vision defects are the most common form of colour blindness that arise from changes in the genes that encode colour.

These genetic alterations can cause three forms of colour vision defects (1) anomalous trichromacy, where when one of the three cone pigments is changed in its spectral sensitivity but trichromacy is not fully compromised (2) dichromacy where one of the three cone pigments is completely absent and (3) monochromacy, a condition where two or all the cone pigments are absent which results in a unidimensional colour or luminance vision (Sharpe et al., 1999).

Protanopia and Deuteranopia

These are the two types of colour vision defects that are common of all colour vision deficiencies. The absence of L-, M- and S- cones result in protan, deutran and tritan defects respectively. The replacement of normal M gene with the gene that encodes a L- pigment for deuteranopia and the replacement of the normal L gene with the gene which encodes an M pigment for protanopia were the responsible mechanisms behind the behind the protanopia and deuteranopia respectively (Konig and Dieterici, 1886). The L and M cone genes are adjacent to each other and high frequencies of recombination between these two genes form the basis for red-green colour vision (Nathans et al., 1986).

Several tests are available to screen and quantify the colour vision deficiencies in the clinic. The disadvantage of these tests is that the patient has to report the results subjectively which may not always be accurate.

Post receptoral neurons

1.3.3 Horizontal cells (HCs)

Horizontal cells are the interneurons that form the first synaptic plexus in human and other mammalian retinae. As their name suggests they spread their visual signals horizontally and contribute to lateral inhibition, feedback and feed-forward interactions with photoreceptors and bipolar cells. By these mechanisms they play a key role in the initiation of spatial and spectral opponency (Werblin and Dowling, 1969, Baylor et al., 1971). Horizontal cells make contact with multiple cones and receive excitatory input from them (Lee et al., 1999, 2010). There are three types of horizontal cells in the retina: HI, HII and HIII cells (Ahnelt and Kolb, 1994; Kolb et al., 1994; Kolb, 1974).

(A) HI horizontal cell

HI cells have a small-field cell with a dendritic tree of 15 µm in the fovea and 80-100 µm in the peripheral retina. HI cells have comparatively larger cell bodies, thick and bushy dendrites giving rise to round and donut shaped terminals. The use of neurobiotin injections and immunocytochemical staining has resulted in better understanding of cone-selective interactions of HI cells (Chan and Grunert, 1998; Goodchild et al., 1996). The HI horizontal cells receive lateral excitatory input from the L- and M- cones but lack significant input from S- cones and rod photoreceptors (Lee et al., 1999; Dacey , 1999). These cells contact cones with their dendrites and rods with their axon-like processes (Verweij et al., 1999).

This arrangement is suggestive of the HI cells role in the rod vision alongside cone mediated responses. A recent report by Crook et al (2011) suggested that when L- and M- cones of macaque retinas were stimulated, synaptic conductances were measured in the midget ganglion cells and they observed that the L-M cone opponency occurred presynaptic to the midget cell. They assumed that L-M cone opponency might arise via horizontal feedback which does not provide cone type selective inhibition. These results propose that horizontal cells may play a key role in L-M opponency that form the basis for red-green colour vision in midget ganglion cells.

(B) HII horizontal cells

These cells are referred to as 'wooly looking' types with larger dendritic tree diameter and indistinct and indistinct terminals leading to the difficulty of assessing the collaboration with the number of cone pedicles (Kolb et al., 1989). The axon of HII cells is short and curled and makes contact with cone pedicles by means of wispy dendrites (Kolb et al., 1994). HI cells are more in number when compared to the HII cells at all eccentricities of the retina. Although these cells contact L- and M- cones, they receive strong S- cone input from S- cones (figure 1.12) (Kolb et al., 1989).

(C) HIII horizontal cells

The HIII cells resemble HI cells in appearance but have a large dendritic field and have asymmetrical dendritic trees (Ahnelt and Kolb, 1994). The axonal terminals of HIII cells are not clearly demarcated and it is still not clear about the type of photoreceptors they connect with. However, it is assumed that HIII cells make lateral connections with a mixture of rods and cones (see figure 1.12) (Kolb et al, 1994).

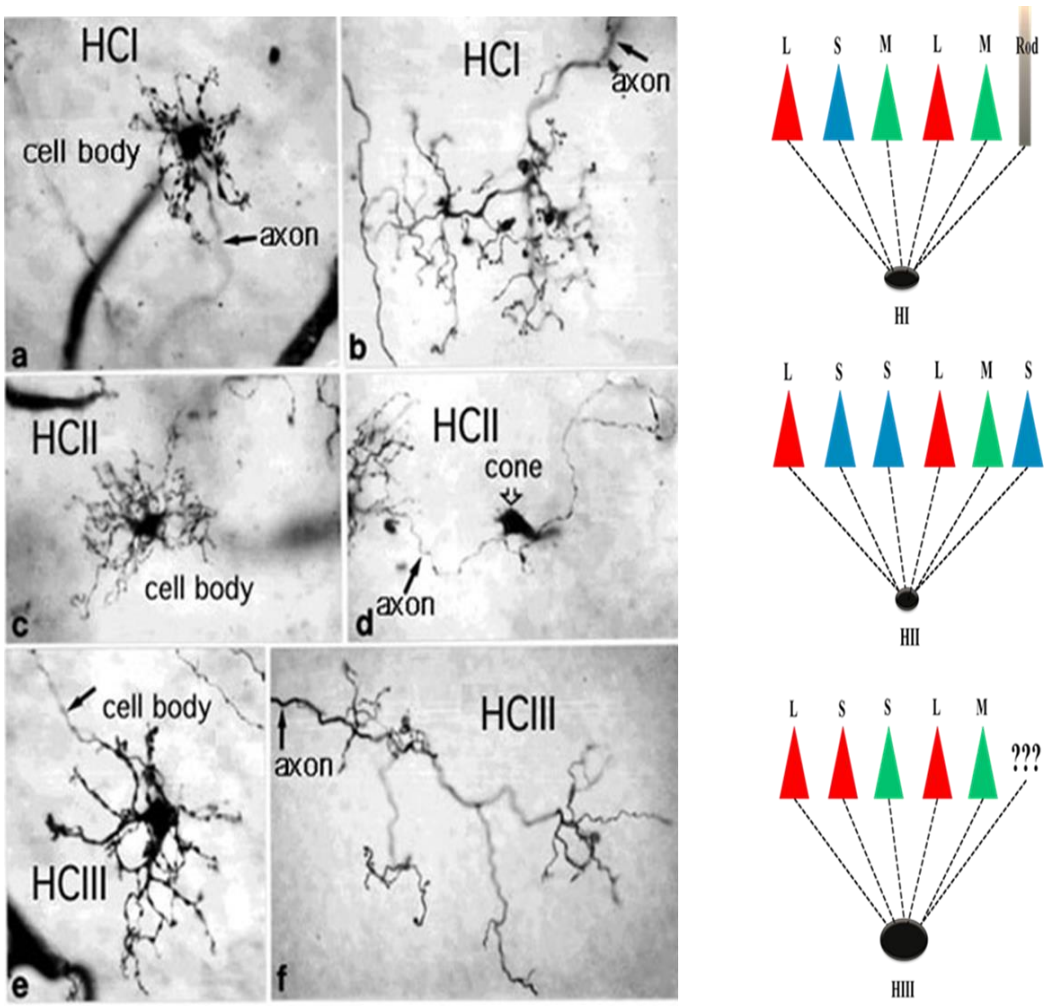

Figure 1-12 showing light micrograph of different types of human horizontal cells from Golgi stained whole mounts (left) lateral connection of different types of horizontal cells with different types of photoreceptors (right).

Source: http://webvision.med.utah.edu/imageswv/LM3HChu.jpeg

1.3.4 Bipolar cells

Bipolar cells are the second order neurons or sometimes referred to as mediating cells that collect, compare and convey information from photoreceptors to ganglion cells. These cells function through the assistance of complex networks of horizontal and amacrine cells in the collection and comparison of visual information received from cones.

Two types of bipolar cells have been identified based on their response to stimulus of their receptive fields (Joselevitch, 2008) (see figure 1.13):

(A) **OFF bipolar cells:** these cells polarize the same way as cones polarize, i.e., when stimulated by light, these cells hyperpolarize. The axons of these cells terminate in sublamina- a. These cells are also referred to an invaginating type based on their contact with the cone pedicles and their axonal stratification in the vitreal half of the IPL. OFF bipolar cells use ionotropic (iGlyRs) receptors, which are non-specific cationic channels that allow influx of currents in the dark, keeping them depolarized (Kaneko and Saito, 1983).

(B) **ON- bipolar cells** or the flat type BPCs polarize in the opposite direction i.e, depolarization in reaction to light. Rod photoreceptors were proved to have an exclusive connection with them and their axons end in the in the sublamina b (see figure 1.13) (Famiglietti, 1981; Kolb et al., 1981). The metabotropic receptos/mGlur-driven channels remain closed in the dark, preventing the influx of ions causing ON- bipolar cells to hyperpolarize.

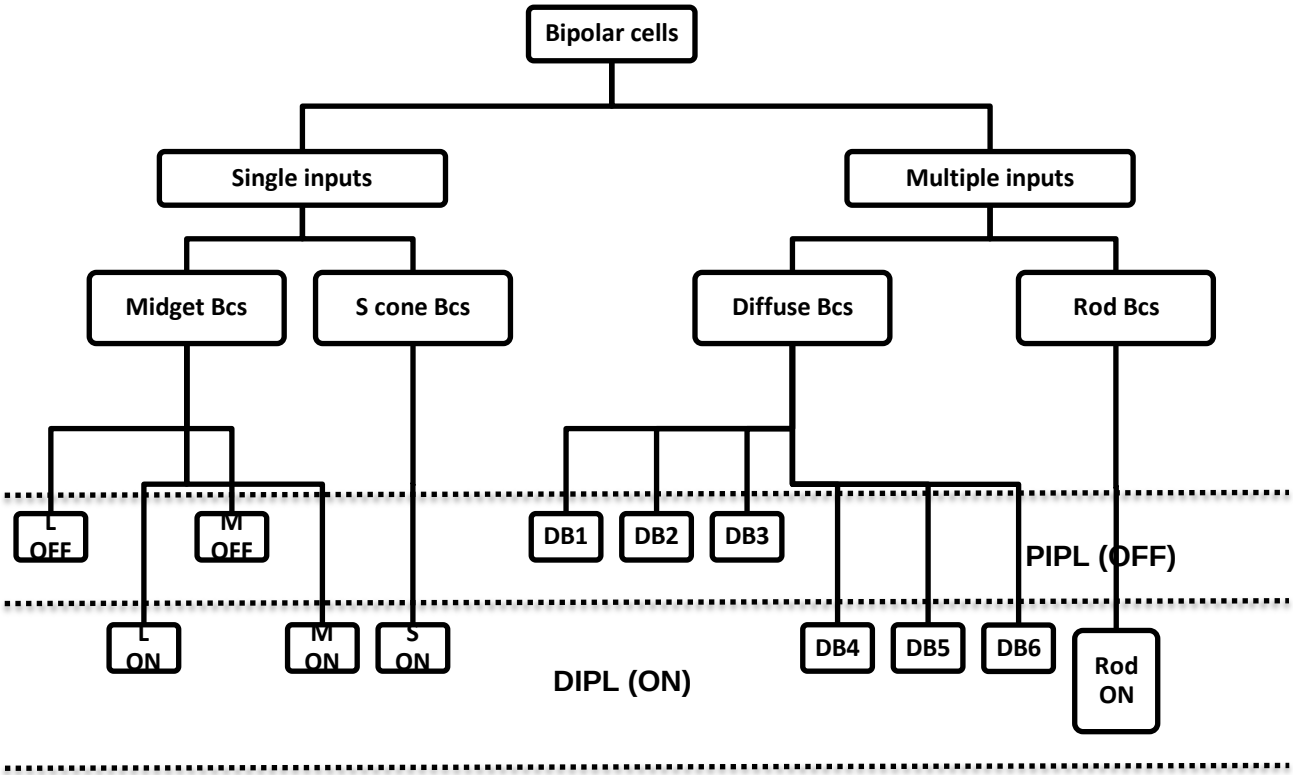

Figure 1-13 Classification of bipolar cells based on their response of their receptive fields and stratification in the proximal (PIPL) and distal strata (DIPL) of the inner plexiform layer (adapted from Joselevitch, 2008).

There are about 20 types of bipolar cells identified in the human retina which were further categorised based on their extent of the dendritic arbour into four types (Kolb, 1970) (see figure 1.13):

(A) Midget bipolar cells (MBCs) usually make contact with one cone and one ganglion cell however in the periphery some of these cells communicate with few cones. Based on stratification of axon terminals in the IPL, the type of pre- and postsynaptic connections and their receptive field these cells are further classified into four types: L-ON, L-OFF, M-ON and M-OFF.

This one-to-one relationship between photoreceptors, midget bipolar cells and midget ganglion cells (Polyak, 1941) form the basis of high spatial visual acuity (Calkins et al., 1999).

(B) Diffuse bipolar cells (DBCs) make contact with multiple cone photoreceptors. DBCs are further classified into six subtypes based on depth of stratification. DB1-3 stratify in the scleral half of the IPL while DB4-6stratify in the vitreal half of the IPL (see figure 1.13). This arrangement suggests the involvement of DB1-3 and DB4-6 being included in OFF and ON bipolar cell categories respectively (Boycott and Wassle, 1991).

(C) S cone bipolar cells

Like midget bipolar cells, S-cone bipolar cells also contact single S-cone in the central retina (Kouyama and Marshak, 1992). The axon terminals of the S-cone bipolar cells end in the distal strata of IPL (see figure1.13).

(D) Rod bipolar cells

The results of the immunocytochemical study conducted by Grunert and Martin (1991) provided the evidence of selective Rod BCs to amacrine cells rather than to the ganglion cells. The maximum density of Rod BCs at 1-3 mm eccentricity corresponds to the presence of high number of rods. In this area, the number of rods that are connected to the rod bipolar cells increase, ranging from about 20 to 60 rods per each rod bipolar cells at 2-7 mm eccentricity.

1.3.5 Amacrine cells

These are the laterally connecting interneurons that interact with the direct vertical pathways of photoreceptor-bipolar-ganglion cell chain with multiple subcircuits in the inner retina. Amacrine cells produce significant direct input to ganglion cells, in addition to lateral processing. In human retina midget ganglion cells receive equal synaptic input from both amacrine cells and bipolar cells (Pang et al, 2002). Approximately 24 to 60 types of amacrine cells is assumed to contact ganglion cells (Masland, 2012. The function of many subcircuits of ACs is still unknown. Based on measurement of their dendritic field diameters ACs are classified into narrow-field (30-150 µm), small-field (150-300 µm0, medium-field (300-500 µm) and wide-field (>500 µm) amacrine cells (Kolb, 1981, 1997).

Kajal's (1892) five strata subdivision of the IPL led to the classification of ACs based on their stratification. Sublamina-a and –b has 1-2 and 3-5 substrata respectively (Famiglietti and Kolb, 1976). Sublamina- a contains axons of bipolar cells and ganglion cell connections that guide the OFF-center ganglion cell pathway while sublamna-b is composed of bipolar and ganglion cell connections providing the basis for the ON- center ganglion cell pathway (Nelson et al., 1978). The broadly stratified types of amacrine cells lie in sublamina-a, the bistratified type cells stratify in 1 and 5 strata. The monostratified type amacrine cells are restricted to any one of the five strata and dendrites of the diffuse type amacrine cells stratify at all the strata.

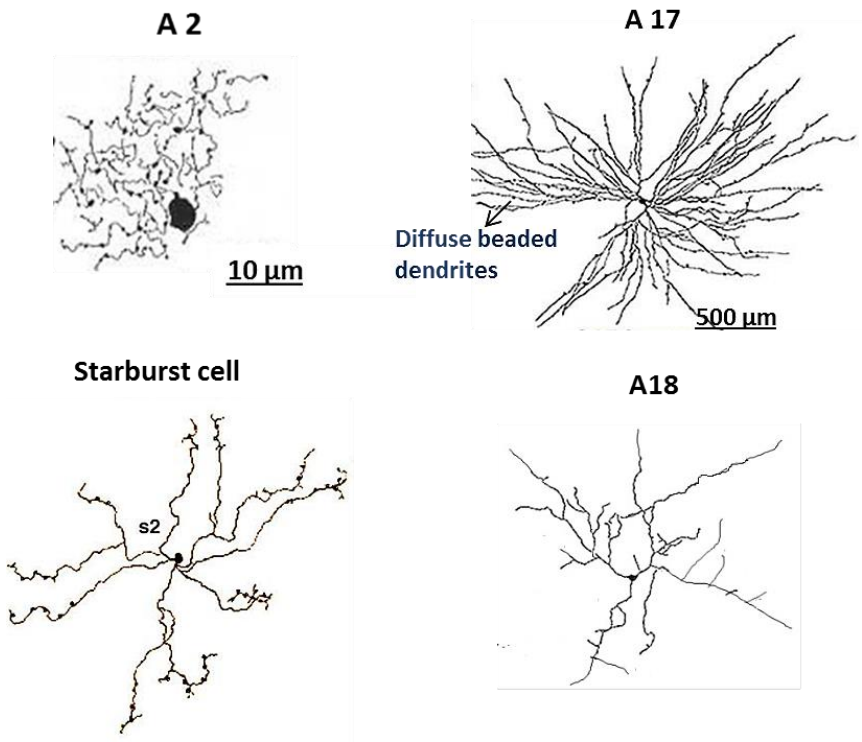

Figure 1-14 Golgi drawings of amacrine cells in human retina

Source

http://webvision.med.utah.edu/book/part-iii-retinal-circuits/roles-of-amacrine-cell

In-vitro studies by Dacey (1999) have resulted in the determination of cone inputs and light responses of ACs of two types: AI and AII cells.

The **AI cells** bear a distinct axon like arbor with dendritic tree that stratify across ON-OFF subdivision of the IPL (Dacey, 1989). The ON- and OFF- components of the receptive field receive additive input from L- and M- cones, resulting in photopic luminosity function. These cells do not transmit a cone specific inhibitory signal to second and third order neurons. Response of AI cells to S-cones is still not evident.

AII ACs are more in number than the rest of the amacrine cell types in the retina and are known to be involved in the rod pathway (Kolb and Famiglietti, 1974; Wassle et al., 1989). They contact rod bipolar cells directly and communicate with cone bipolar cells through gap junctions and probably form a link between scotopic and photopic vision (Demb and Singer, 2012). AII amacrine cells pass rod driven signals through ON- center cone bipolar axons in distal strata of IPL to ON- center ganglion cells by means of gap junctions (Kolb, 1997). Field et al (2009) suggested that even S- cone bipolar cells receive rod signals through these gap junctions. AII amacrine cells communicate with other AII ACs via gap junctions in sublamina-b of the IPL. The distribution of AII amacrine cells is high across the retina (Vaney, 1990) and contact with several rod bipolar cells and as Zrenner (1990) suggested that AII amacrine cells may have a key contribution to the pattern ERG.

Besides AI and AII three other types of amacrine cells play a key role in cone and rod vision (Kolb, 1997).

A17 amacrine cells

These are very wide-field, diffusely branching amacrine cells with fine beaded dendrites that pass through IPL terminating in the lower sublamina-b receiving synapses at intervals from axon terminals of rod bipolar cells. A single A17 amacrine cell can receive signal inputs from about 1000 rod bipolar cells and hypothesised to act as an integrating unit that assists in setting sensitivity over a very large area of rods and rod bipolar cells ((Nelson and Kolb, 1985). These cells have a reciprocal synaptic relationship with rod bipolar cells from which it receives signal input.

A17 amacrine cells are highly sensitive at low light levels and assumed to play a role in convergence and amplification of rod signals from large areas of the retina. These cells depolarise in response to light and produce a GABA-ergic (inhibitory) type of neurotransmission (Pourcho and Goebe, 1983).

A18 amacrine cells

This class of amacrine cells have wide-field with extreme dendritic arborisation in sublamina-a with thin dendrites that contact two major (AII and A17) and some other minor amacrine cells that mediate rod vision. These are dopaminergic neurons that are thought to play a role in circadian cycle by modulating changes in adaptation from dark to light (Pourcho, 1982).

Starburst amacrine cells

These cells are categorised based on their appearance and are classified into two types based on their dendritic branching in sublamina-a and sublamina-b (Famiglietti, 1991). These cells help in directing the ganglion cell responses through their synaptic transmission and thereby play a key role in information processing (Yoshida et al., 2001).

1.3.6 Ganglion cells

The axons of ganglion cells travel from the retina to the lateral geniculate nucleus (LGN) in the thalamus and then to the primary visual cortex (V1). Ganglion cells are the terminating and most complex neurons of the neurosensory retina which receive their visual information from bipolar cells and amacrine cells. The chemical information relayed from the second order neurons are detected by receptors on the ganglion cell membrane. Further transformation of these chemical messages into intracellular electrical signals occurs with the help of transmembrane receptors. Within ganglion-cell dendrites and cell body these signals are combined and probably in the early segment of the ganglion-cell axon, are converted into nerve spikes. These nerve spikes also referred to as action potentials are a time-coded numerical form of electrical signalling used to convey neural information over long distances. In the human visual system, these neural spikes are transferred to the higher order neurons in the brain visual centers through optic nerve.

Like bipolar cells, ganglion cells can be classified based on their receptive field responses to light as ON- centre or OFF centre and ON- surround or OFF-surround. Based on the morphology of their dendritic terminal, GCs can be subdivided into four major classes:

(A) Biplexiform ganglion cells: This is the class of ganglion cells that connects directly to the rod photoreceptors (Zrenner et al., 1983). The Golgi studies by Waessle et al (2000) suggested that these cells represent the misplaced HII cells. There is also some evidence supporting that these cells involve in relay of cone signals probably through gap junctions. Their direct contact with rods and communication with cones may suggest their involvement in responses that change with illumination and they could probably play a role in circadian rhythms (Rodieck, 1998).

(B) Bistratified ganglion cells (non- P, non-M cells): As the name indicates have their dendritic fields stratified near both inner and outer borders of the inner plexiform layer. They are small in size (Dacey and Petersen, 1992) and their dendritic field diameter ranges from approximately 50 µm in the central retina and about 400 µm in the periphery. In vitro preparations of human and macaque retina using injections of Neurobiotin and horseradish peroxidase led to characterise the anatomy, depth of stratification and distribution of small bistratified ganglion cell (Dacey, 1993; Dacey and Lee, 1994). These cells were found to receive strong excitatory input from S- cones and this was supported by the observations such as membrane depolarisation of these cells upon exposure to S-cone isolating stimuli and associated action potentials which were in phase with the S- cone modulation. Anatomically, the dendritic field of these cells stratify at the same depth as the axon terminals of S- cones probably forming a synaptic relationship for excitatory S-cone signals in the retina (Dacey and Lee, 1994).

They are least in number and respond only at high illumination levels. Spatial opponency cannot be determined in this class but they show blue-yellow spectral opponency. The chromatic opponent signals of S- cones and combined L- and M- cone signals are antagonistic in nature and arise from the inputs derived from the ON- center bipolar cell that contacts S- cone and the OFF- bipolar cells that contact L- and M- cones (Dacey et al., 1996; Packer et al., 2010; Lee and Dacey, 1995).

(C) Midget ganglion cells (A cells/P-beta cells or P cells); Midget cells have smaller dendritic fields with highest density at the fovea (Dacey and Peterson, 1992). They are most numerous among all the classes of ganglion cells. They show spatial opponency and are assumed to be involved in red-green chromatic opponency. Polyak (1941) rightly pointed out that midget ganglion cell demands a specific mention as it selectively receives all of its input from a single midget bipolar cell. Two types of midget ganglion cells are classified based on the spread of their dendrites: dendrites which bifurcate in the lower portion of the IPL while the dendritic trees of others arborize in the upper part of IPL. This arrangement suggests the existence of two types of midget ganglion cells that convey nerve spikes to the LGN in the thalamus and then to the visual cortex. Of these two types of midget GCs, one most likely signals when exposed to increment in illumination (ON- response) while the other signals with decrement in illumination (OFF- response) (Kolb and Marshak, 2003).

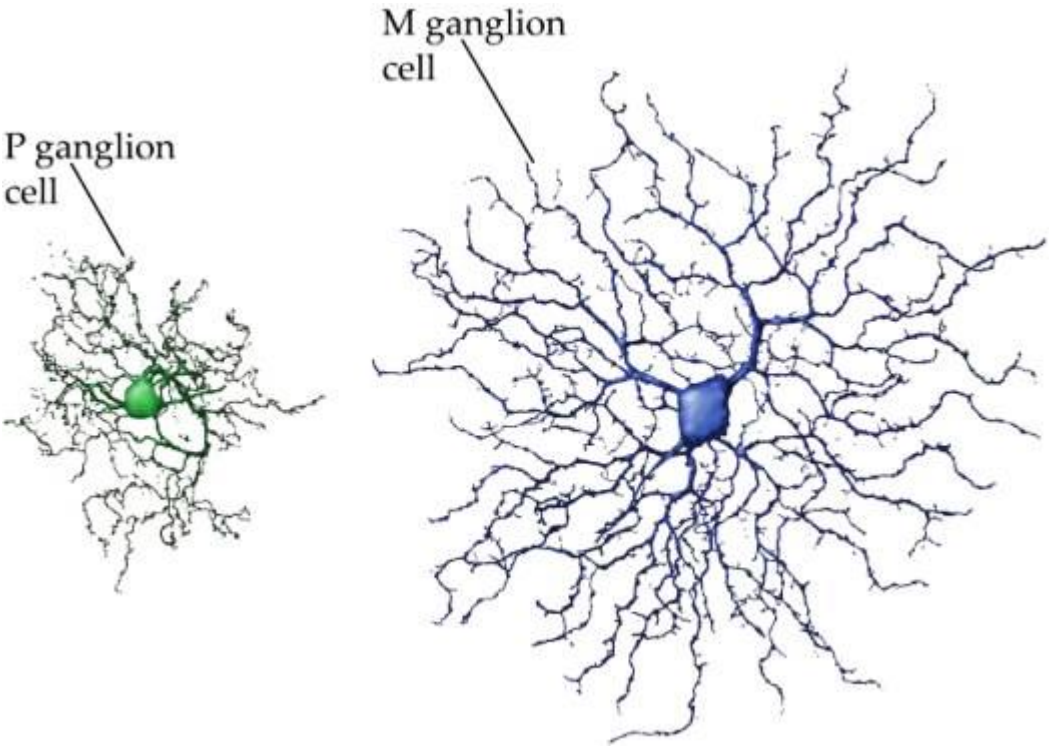

Figure 1-15 P and M ganglion cells that project to layers 3, 4, 5 or 6 of parvo- and layers 1 or 2 of magnocellular layers

Source:http://www.rci.rutgers.edu/~uzwiak/AnatPhys/Vision.htm

(D) Parasol ganglion cells (B cells/P alpha cells/ M cells) Dendritic trees of parasol cells have larger diameter and a lower spatial density (Dacey and Petersen, 1992). This class of GCs remain active at low illumination levels. They show spatial opponency but not spectral opponency. Parasol GCs are categorised into two types based on their size; (a) small parasol GCs which carry broadband, tonic luminance signals to parvocellular layers of lateral geniculate nucleus (LGN) and (b) large parasol GCs carry the broadband, phasic signals to the magnocellular layers of the LGN.

Both P and M cells, which comprise of the 80% and 10% are made up of a heterogeneous group with small axonal fibers. Some of these fibers project to the LGN (Conley and Fitzpatrick, 1989) while rest of them to the superior colliculus (Perry and Cowey, 1984).

1.4 Postreceptoral retinal pathways

Modern anatomical, physiological and psychophysical studies in human and nonhuman primates have identified three major postreceptoral pathways that involve in signal transmission from retina to the brain for further analysis and interpretation of visual image.

1.4.1 The L-M cone (Red-Green) opponent pathway

The L-and M- cones constitute of about 90% of the whole cone population. Both L- and M- cones are arbitrarily arranged with respect to one another in the cone mosaic (Roorda and Williams, 1999 , Roorda et al., 2001 , Dacey and Packer, 2003). In about a central 10 degrees of primate retina, a single midget bipolar cell draws all its input from either a single L or M cone and connects inturn exclusively to a single midget ganglion cell. Therefore, this one to one connectivity in the retina is often referred to as 'private-line' from single cone to the cortex (Dacey and Packer, 2003). Paulus (Paulus and Krogerpaulus, 1983) stated that this private-line pathway may attribute to create L versus M cone opponency. L-M cone opponency is known to be restricted to the midget system of the central retina, where an individual cell is controlled by the excitatory input from a single cone. This pathway accommodates the signals derived from the opposite interaction of the L- or M- cones which, then, are conveyed to the primary visual cortex through the parvocellular layers of the LGN. The receptive field centre of a midget ganglion cell receives excitatory input from either L or M cone via the ON-center midget bipolar cell and the surround receives inhibitory signals from the opposing cone type to that of the center from the OFF-center bipolar cells (Dacey and Packer, 2003)(see figure 1.6 for example) leading to the strong center-surround antagonistic mechanism.

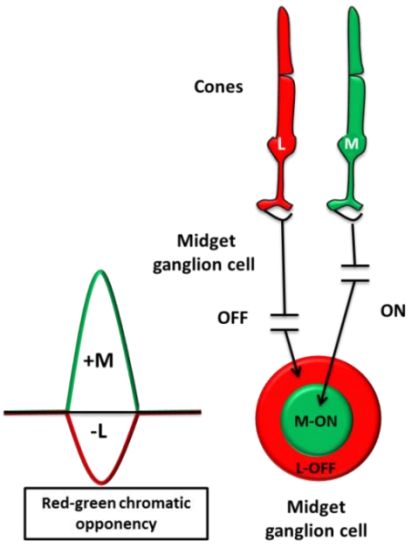

Figure 1-16 L and M cone opponent pathway in the human retina

L- and M- cones contact OFF- and ON- center bipolar cells respectively resulting M- ON center and L- OFF surround resulting in red-green chromatic opponency in the midget ganglion cell.

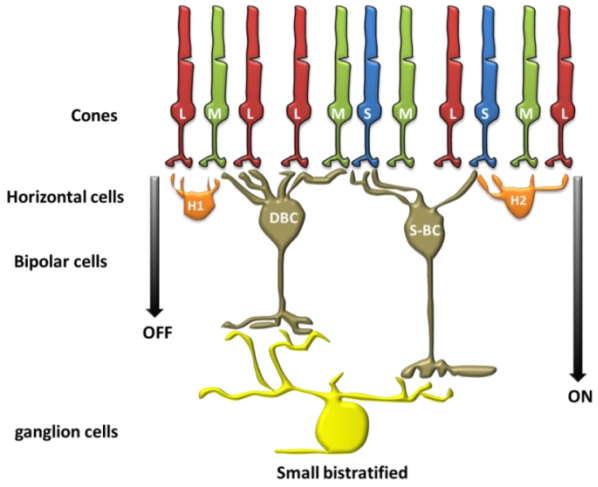

Figure 1-17 The blue- yellow pathway in the retina.

HII horizontal cells communicate with L-, M- and S- cones and are also assumed to be the probable basis for a surround in the S- cone bipolar cell leading to the origin blue-yellow opponency. Small bistratified ganglion cells non-selectively receive input from the L- and M- cone diffuse bipolar cells via the outer stratifying dendrites and a selective input from the S- cone bipolar cell. HI cells communicate with L- and M- cones and could probably act as the basis for an inhibitory surround in the diffuse bipolar cell. The input from wither of these bipolar cell pathways result in the S- ON, (+L+M) OFF opponent receptive field (Dacey, 2000).

1.4.2 The S/(L+M) (Blue-Yellow) Pathway

The S- cones make up only 5-10 % of whole cone population and it has been difficult for several years to distinguish the characteristics of the S-cone pathway due to their sparse distribution throughout the retina. Colour discrimination in dichromats is due to signals generated from the combination of any of the two types of cones. In trichromats, this process is similar apart from the existence of another set of cones, which split the colour spectrum further. The antagonistic interaction of the signals derived from the blue or short wavelength sensitive cone with a combination of signals derived from addition of outputs from long- and middle- wavelength sensitive cones of the trichromatic species enables blue-yellow discrimination (Dacey et al., 2000a, Sher and DeVries, 2012). Small bi-stratified ganglion cells receive excitatory input from the S- ON cone and inhibitory input from the combination of L- and M- OFF cones (+S-(L+M)) (Dacey and Lee, 1994, Sher and DeVries, 2012). These ganglion cells also receive weak 'OFF' input signals from diffuse bipolar cells connected to L- and M- cones which could contribute to the S- versus L+M opponent response (see figure 1.17). These cells receive input from a distinct 'blue cone' bipolar cell that makes selective connections with S- cones. A distinct type of horizontal cell type, the HII cells receive robust inputs from the S- cones and the weaker inputs from both L- and M- cones (Dacey et al., 1996). HII cells are also predicted to provide a basis for L- and M- cone L- and M- cone signals (+L+M) feedback to the S- cones forming the receptive field surround by the combination of L- and M- cones of the S- cone bipolar cell (Dacey and Packer, 2003). The principal basis of the circuitry involved in the S- OFF pathway is still not clear as no evidence with regard to the selective S- cone- OFF-bipolar cell connectivity is known as of yet.

1.4.3 +L+M non-opponent (luminance) pathway

The luminance pathway is mediated by the parasol ganglion cells. Parasol ganglion cells are composed of mono-stratified dendritic trees of medium diameter that subdivide at either one-third or two-thirds of the depth of the inner plexiform layer. These unique characteristics of the dendritic tree distinguish parasol cells from the other types of ganglion cells. The responses derived from this cell is contributed by the L cone output (Diller et al., 2004). These cells receive additive input from the diffuse bipolar cells that synapse with both L- and M- cones forming the non-opponent luminance pathway (see figure 1.18). Furthermore, this pathway also partakes in spatial opponency.

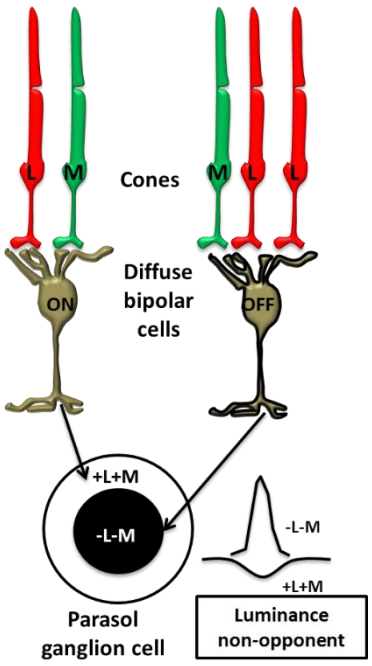

Figure 1-18 L and M cone opponent pathway in the human retina

1.5 Lateral geniculate nucleus

The LGN is subdivided into three distinct laminae based on the signals they receive from retinal ganglion cells through distinct parallel pathways: (Magnocellular (M-), Parvocellular (P-) and Koniocellular (K-) (see figure) and from there signals are transferred to the primary visual cortex (V1). These subsystems in the LGN possess distinct physical and spatiotemporal characteristics. The dorsal four layers (3-6) receive signals from midget ganglion cells (DeValois et al., 1958; Reid and Shapley, 1992) and are composed of P cells. Parasol ganglion cells project to the ventral 2 layers (1&2) of the LGN to form magnocellular channel (Leventhal et al., 1981). This channel is composed of M cells. The koniocellular pathway if formed in between inter-laminar regions and receive signals from the bistratified ganglion cells. The neurons in these layers possess distinct neurophysiological and anatomical properties that form the basis of chromatic and achromatic vision.

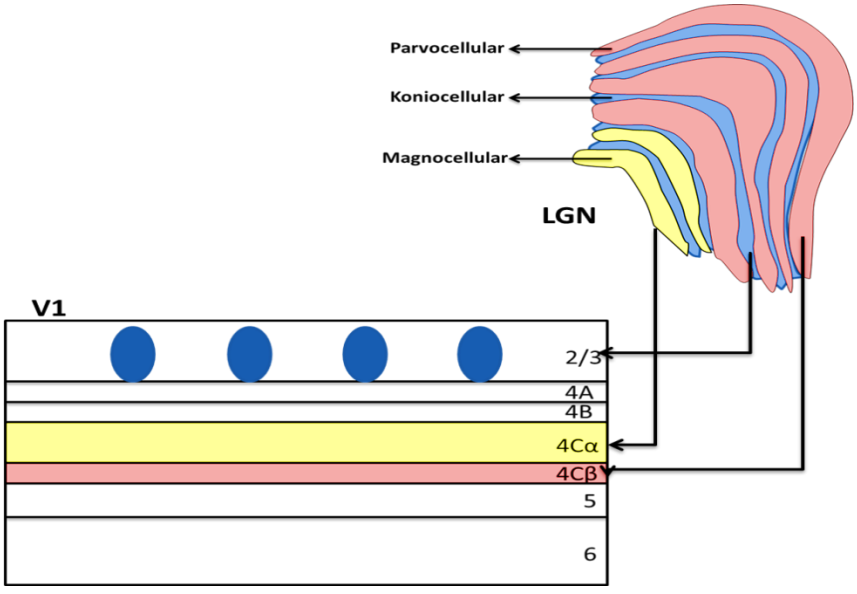

Figure 1-19 showing different layers of human lateral geniculate nucleus (LGN) and innervation of LGN in the primary visual cortex.

1.5.1 Magnocellular pathway

Cells in the magnocellular (M-) layer obtain signal inputs from retinal M- cells which in-turn receive signals from diffuse bipolar cells that carry synergistic inputs from L- and M- cones (Derrington et al., 1984).The signals derived from this pathway are transient and show band-pass response characteristics. They constitute about 10% of the total ganglion cell population (Parry et al., 2012). These cells receive additive input from L- and M- wavelength sensitive cones and form the basis for achromatic (luminance) vision (Wiesel and Hubel, 1966; Demonasterio and Gouras, 1975; Parry et al., 2012). These cells are less numerous and mediate achromatic vision. M cells respond to low spatial and high temporal frequencies. The conduction velocities of magnocellular neurons is higher than parvo- and konio- cellular neurons and it is assumed that this could be because of higher convergence of their neural circuits that could probably produce responses that start early.

1.5.2 Parvocellular pathway

This pathway is the composed of projections from the midget ganglion cells which account to about 70% of the total ganglion cell population. The receptive field of midget ganglion (P) cells has a center made of single L- or M- cones and surround by a specific cone type (either L- or M- cone) (Reid and Shapley, 1992; Martin et al., 2011). P cells contribute to about 80% of total retinogeniculate projections (Perry et al., 1984). These cells respond to the stimulus in a sustained fashion and possess low temporal frequency response characteristics and receive opponent inputs from L- and M- wavelength sensitive cones forming the L-M cone opponent mechanism (Parry et al., 2012). Evidence suggests that the PC layer forms the key substrate for red-green colour vision (Derrington et al., 1984; Demonasterio and Gouras, 1975).These cells show sustained temporal

responses, low contrast gain, good spatial resolution and also reported to respond to achromatic contrast (Gegenfurtner and Kiper, 2003).

Based on the structure of their receptive field, LGN neurons are classified into several colour opponent cells. For instance the P- layers as described in macaque retina is composed of three types of colour opponent cells:

1) Type I or colour opponent center-surround cells
2) Type II or colour opponent (no center-surround) cells
3) Type III or non-opponent or broadband cells

Type I cells constitute of around 65% of the cell population in dorsal geniculate layers. When stimulated the receptive field of these cells exhibit center-surround organisation and based on this arrangement, these cells are further subdivided into five types (see figure): L-ON, M-OFF; L-OFF, M-ON; M-ON, L-OFF; M-OFF, L-ON; S-ON, M-OFF (Weisel and Hubel, 1966).

Type II cells receive both excitatory and inhibitory inputs from different cone classes but lack a distinct center-surround organisation (see figure 1.21). This type of arrangement is assumed to indicate that colour coding can exist independently without any role in spatial vision (Dacey, 1996).

Type III cells are arranged in a concentrated center-surround fashion with cone types of identical spectral sensitivities (see figure 1.22)

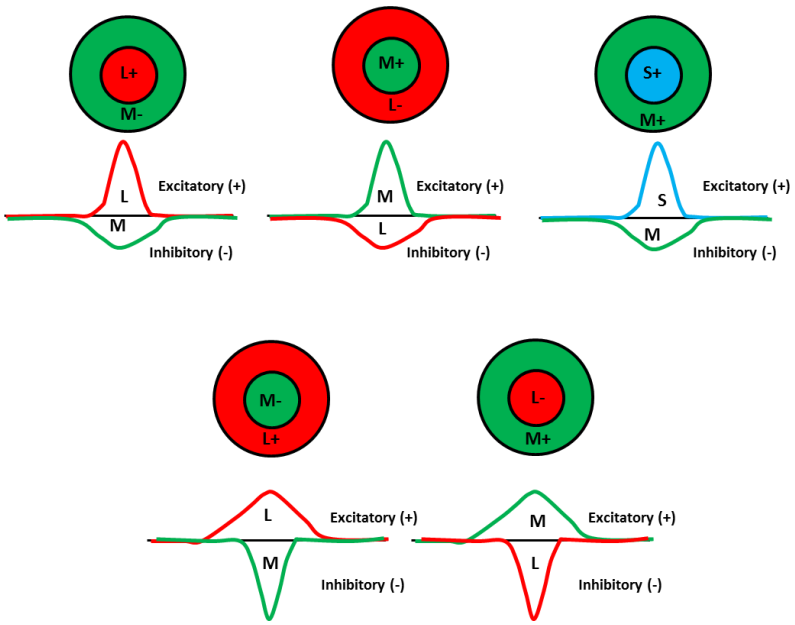

Figure 1-20 Types of type 1 LGN cells. upper half of the panel show L-ON, M-OFF, M-ON, L-OFF, S-ON, M-OFF and the lower half of the panel shows M-OFF, L-ON and ; L-OFF, M-ON receptive fields respectively.

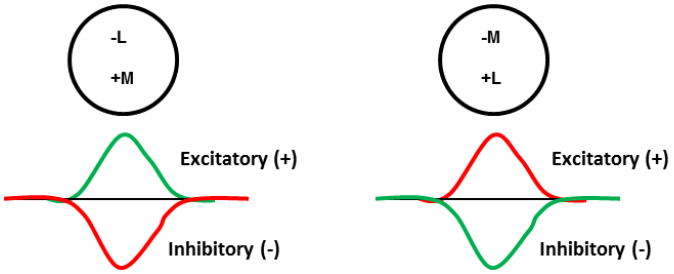

Figure 1-21 Type II cells of human lateral geniculate nucleus.

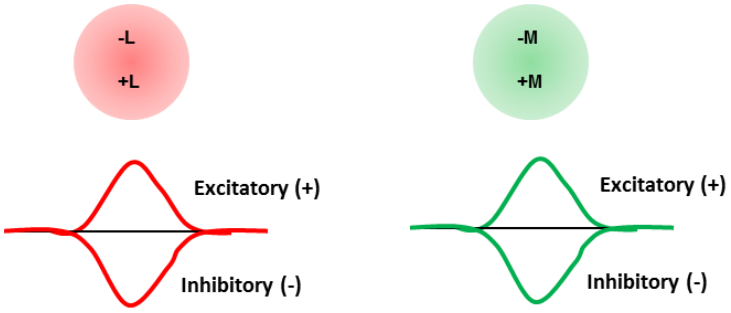

Figure 1-22 Type III cells of human lateral geniculate nucleus

1.5.3 Koniocellular pathway

This pathway contains signals transferred from bi-stratified ganglion cells. These are small neurons that are identified to mediate blue-yellow colour vision. The receptive field of bi-stratified ganglion cells receive opponent inputs from S- cones for center and the additive input from L- and M- cones for the surround (Dacey and Lee, 1994; Dacey, 2000; Parry et al., 2012).

1.6 Visual cortex

The projections from the magno-, parvo- and koniocellular pathways end in different layers of the primary visual cortex (V1).

Using functional magnetic resonance imaging, Zeki and Marini (1998) classified three cortical stages for colour processing that mediate V1, V2, V4, inferior temporal and frontal cortices (see figure 1.23).

1.6.1 V1 and V2 cells

The magnocellular neurons project to layer 4Cα and layer 6. Parvocellular fibers innervate in layers 4A, 6 and 4Cβ and koniocellular fibers end in the cytochrome oxidase- (CO-) rich blobs in layers 1, 2 and 3 (Hubel and Wiesel, 1972; Fitzpatrick et al, 1985). 4Cβ are the type-I cells that have a center-surround arrangement that forms colour opponency. These pathways remain separated in V1 and extrastriate cortex (Livingstone and Hubel, 1987a and b, 1988; DeYoe and Van Essen 1985; Roe and Ts'o, 1999).

In V2, magnocellular pathway correspond with the thick CO- rich bands which also form the basis for motion and depth (Hubel and Livingstone, 1987), the parvocellular pathway with the pale interbands which also subserve form. The thin CO- rich bands correspond with both parvocellular and koniocellular pathways and form the basis for colour (Gegenfurtner and Kiper, 2003).

The neurons of the primary visual cortex (V1) can respond to the spatially uniform stimuli, some of V1 neurons can be stimulated by spatially uniform stimuli, chromatic and respond little or none to achromatic modulation. Most of these cells are selective for the orientation of edges. About 5-10% of these neurons respond to purely chromatic modulation among which colour preferences are widely distributed.

Despite being four or more synapses away from cone photoreceptors, chromatic responses of receptive fields in V1 can be determined by linear combination of cone input at this level (De Valois et al 2000; Conway and Livingstone, 2006). The function of V1 and probably V2 is to document the presence and intensity of different wavelengths (λ) and difference in wavelengths of light (λ_1- λ_2) (Bramao et al., 2010).

1.6.2 V4

The posterior fusiform V4 cells involve in colour constancy operations (Barbur and Spang, 2008). Colour constancy is the ability to allot colours to objects irrespective of change in light levels. In other words, it is the true colour of the object. Memory, learning and perceptual judgement has shown to have no influence on this area (Zeki and Marini, 1998). This area is commonly referred to as center for colour perception (Lueck et al., 1989; Bartels and Zeki, 2000; McKeefry and Zeki, 1997) as it helps in recognition of object colour (Martin et al., 1995; Zeki and Marini, 1998), colour knowledge (Simmons et al., 2007) and colour imagery (Howard et al., 1998) but not wavelength discrimination (Wild et al., 1985). While the area V4 deals with colour perception, storage of colour information is reported to take place in the left inferior temporal gyrus (Kellenback et al., 2001). Chao and Martin (1999) debated that areas in the cortex that deal

with colour information can be divided into two types, first, form the basis for colour perception and second, subserve colour knowledge.

1.6.3 Inferior temporal and frontal cortices

These are the areas of brain that mediate memory operations, perceptual judgement and learning and helps in processing of chromatic information of naturally coloured objects (example: fruits and animals) (Zeki and Marini, 1998).

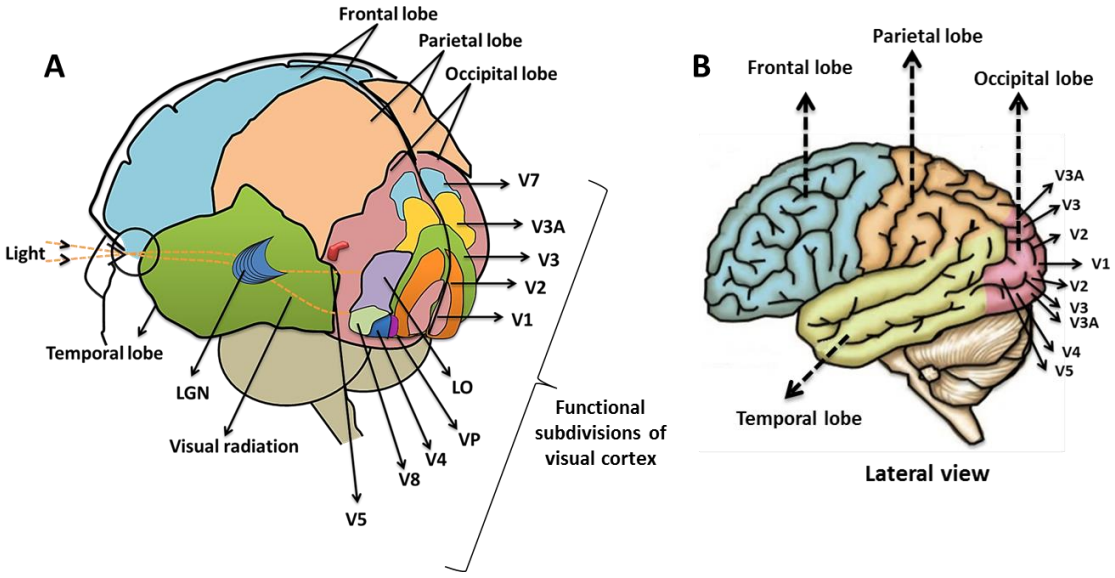

Figure 1-23 (A) Representation of different types of lobes and vision centers in the human brain and (B) lateral view of human brain showing different cortical areas that are responsible for vision.

(Source adapted from Logothetis, N.K., 2006)

1.7 Research Rationale

Although accurate data on global visual impairment and blindness due to hereditary retinal disorders is not available, previous reports on animal models suggest that the underlying cause of inherited retinal diseases is usually associated with the dysfunction or death of photoreceptors (Pacione et al, 2003, Francis, 2006, Veleri et al., 2015). On the other hand, colour vision deficiency although is not a sight threatening problem but has a significant impact on lifestyle and limits the career possibilities of an individual (Tagarelli et al., 2004; Steward and Cole1989).

The aim of this thesis was to develop an objective method for colour vision testing by assessing signals derived from different classes of photoreceptors using electroretinograms in healthy individuals so that this data can be used as a tool to monitor functional changes of individual photoreceptor class in retinal disease.

Chapter 2 - Introduction to Electroretinogram

Experiment 1 (Chapter 4)

Aim: To measure L- and M- cone ERGs as a function of temporal frequency using sinusoidally modulated triple silent substitution stimuli.

Hypothesis: It is expected that at low temporal frequency, L- and M- cone ERGs display similar amplitudes and at high temporal frequencies amplitudes of L-cones are predominant in comparison to M- cone ERGs.

Experiment 2 (Chapter 5)

Aim: To describe L- and M- cone specific ERG waveforms obtained using silent substituted square wave stimuli.

Hypothesis: The profile of the isolated L- and M- cone ERG waveform using silent substitution technique is comparable to conventional Flash ERG.

Experiment 3 (Chapter 6)

Aim: To obtain rod isolated ERGs using silent substitution method and understand how these responses vary with change in temporal frequency and retinal illuminance.

Hypothesis: The amplitude of rod ERGs decrease with increase in temporal frequency and retinal illuminance.

2.1 Introduction

The electroretinogram (ERG) is usually recorded using an active electrode attached in contact with the eye under examination and a reference and ground electrode attached to the skin of the patient. It is the bioelectrical potential that arises in the retina that can be recorded using differential amplifier when stimulated by a flash of light. It is a simple objective and non-invasive approach to investigate the activity of retinal epithelium, glia and neurons (Stockman and Slaughter, 1989).

To make effective use of electroretinography, it is necessary to have the knowledge about the appropriate stimuli that elicits these signals, anatomic origins of these potentials, recording technique and measurement of the signal responses (Schiefer et al., 2007).

2.2 History of ERG

DuBois-Reymond was the first to discover potential of about 6 mV in excised tench (fish) while Holmgren (1865) was the first to discover this as a retinal response to light in a frog's eye. Dewar and McKendrick (1873) independently reported the change in amplitude of electrical response with change in stimulus intensity. Dewar (1877) reported the first successful recording of a human ERG while Kahn and Lowenstein (1924) published the first human ERG waveform using a string galvanometer.

2.3 Electrical basis of the electroretinogram

The response of the ERG to a light stimulus is the measurement of potential differences that arise from the electrical currents that stream across the retina as a result of neuronal signaling and the various ocular structures that serve as electrical resistors (Arden and Brown, 1965). The change in illumination results

in a synchronous activity of retinal neurons like photoreceptors and bipolar cells that are radially oriented with respect to cornea which make major contributions to the ERG waveform in comparison to laterally oriented cells like horizontal and amacrine cells (Frishman and Wang, 2011). Human photoreceptors relay visual information via parallel retinal neuronal pathways which enable the flow of current **(I)** through photoreceptors to ganglion cell pathways that algebraically sum up and generate radial extracellular currents (see figure 2.1 (i)). These currents flow along two principal pathways: (A) local (within retina) and (B) remote (includes extracellular ocular tissues **(R)** like cornea, sclera, choroid, crystalline lens, vitreous and the retinal pigment epithelium).

According to **Ohm's law**, voltage **(V)** between two points is independent of the pathway through which the current flows. Therefore the potential difference between local (A) and remote (B) pathways can be shown as:

$$\mathbf{I_A R_1 = I_B(R_2+R_3+R_4+R_5+R_6)} \quad \textbf{Equation 1}$$

Since the summed resistances on the right side of the equation 1 i.e., ($R_2+R_3+R_4+R_5+R_6$) is greater than the left side (R_1) and as Ohm's law suggests that the resistance is inversely proportional to current, the current I_A produced in the local pathway must be greater than that of current I_B that flows in the remote pathway. Therefore, the ideal site to place the electrode when recording ERG would be at point A as the results obtained at this site would have larger potential. However, it is not practically possible to insert electrodes on the retina while recording ERGs in a clinical setup. Therefore, ERGs can be recorded using an alternative pathway (B) (figure 2.1 (i)) by placing the active electrode on or close to cornea between points C and D on remote pathway as shown in figure 2.1 (ii).

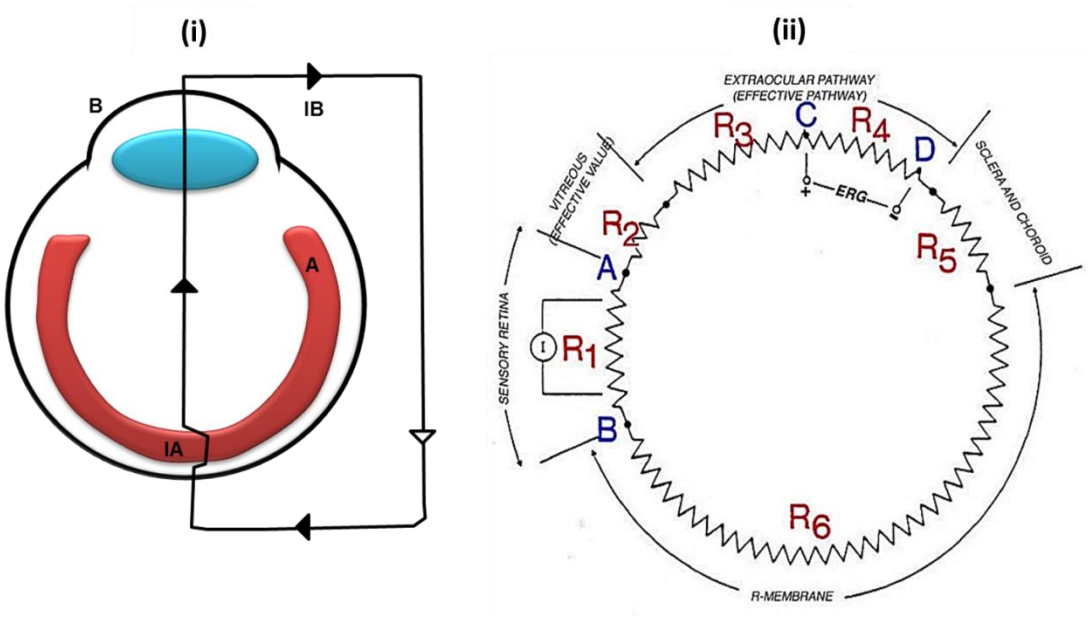

Figure 2-1 Schematic representation of electrical basis for corneal electroretinogram

(i) the currents IA and IB flow through several resistors (R) across the eyeball via two routes when stimulated by light. (ii) The local (intraretinal) route denoted by A and remote route (beginning at retina, passing through the vitreous, lens, cornea, extraocular tissues and back to retina through sclera, choroid and retinal pigment epithelium acting as resistors) denoted by B.

(Source:http://webvision.med.utah.edu/book/electrophysiology/the-electroretinogram-erg/)

2.4 Granit's analysis of cat ERG

The extensive experimentation by Granit (1933-1947) using improved techniques helped in the analysis of the components of the cat ERG and is still in use. He used chemical agents to investigate ERGs and postulated the existence of three potentials which he referred to as PI, PII and PIII components (see figure 2.2), after observation of the sequence of disappearance under ether anaesthesia. His work suggested that the fast-developing corneal negative PIII forms the a-wave. The corneal positive PII then develops post PIII, the additive resultant of PIII and PII produces the b-wave. As PII decreases, PI develops resulting in the production of c-wave. He postulated that the origin of PII evolved from the neural

pathways between photoreceptors and ganglion cells. This hypothesis was later confirmed by Bartley (1937). The short latency of PIII indicated that the origin was probability at the level of photoreceptors.

The slow and rapid changes of the ERG components associated with the retinal illumination were first recorded by Noell (1954). His work suggested that the c-wave is derived from the RPE. He also suggested that the negative PIII could be differentiated into two components based on their time constants a) early and b) late components of which, one arising faster was said to be originating from the photoreceptors. Using microelectrodes, Brown (1968) concluded the origin of PIII to be from photoreceptors after the experiment on blockage of the central retinal artery, which does not supply blood to the foveola and constitutes of only cone photoreceptors. Steinberg et al., (1985) while working in Brown's laboratory suggested that the reduction in potassium ion concentration in the subretinal space led to the production of the c-wave.

Hence, his team proved the origin of these slower responses was from the RPE. The positive and negative waves of the human ERG originate from the summation of the overlapping of positive and negative components from various stages of retinal circuitry.

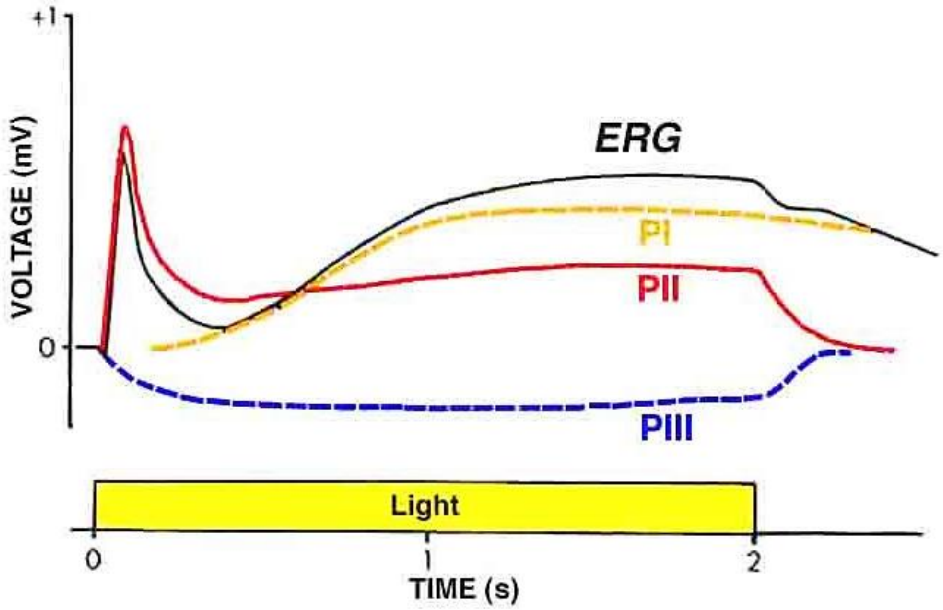

Figure 2-2 The ERG recordings from the anesthetised cat retina with a 2 second light stimulus.

The dotted lines PI, PII and PIII indicate the components of ERG that appeared with the deepening of the ether anesthesia (Granit, 1933). The red line represents the ERG response with the combined components to the same stimulus of light.

(Source: http://webvision.med.utah.edu/imageswv/ERGFig2.jpg)

2.5 The Human Flash ERG

The human flash ERG is typically evoked by a single flash of light. It is a transient and highly repeatable wave response that can be classified into four major components: an initial transient negative deflection called as a-wave that appears after the onset of stimuli proceeded by a large positive deflection referred to as b-wave which is then followed by a broader positive c-wave and finally a smaller positive d-wave (see figure 2.3). Nevertheless, not all these components can be observed in all flash ERGs as the characteristics of waveform depends on various factors like stimulus luminance, duration, wavelength, extent and location and also the state of retinal adaptation (Frishman, 2006).

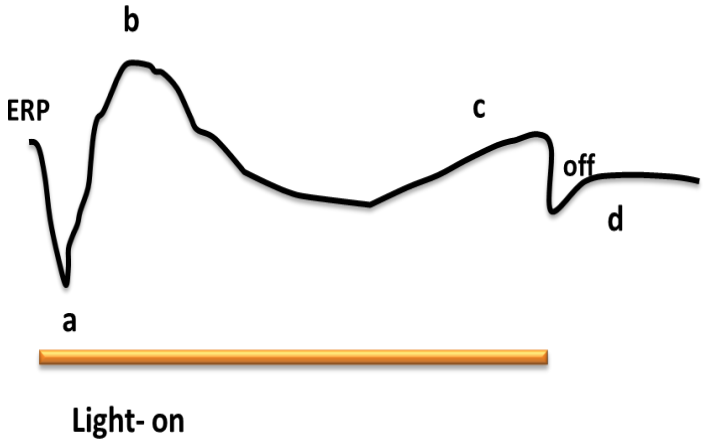

Figure 2-3 Theoretical flash ERG waveform showing all components when stimulated by a long pulse of light

2.5 (i) Origins of components of ERG

Historically, several different strategies have been used to define the cellular mechanisms and neuronal origins of generation of the flash ERG. In this section, the origin of the four major components (see figure 2.4) of the flash ERG will be briefly discussed.

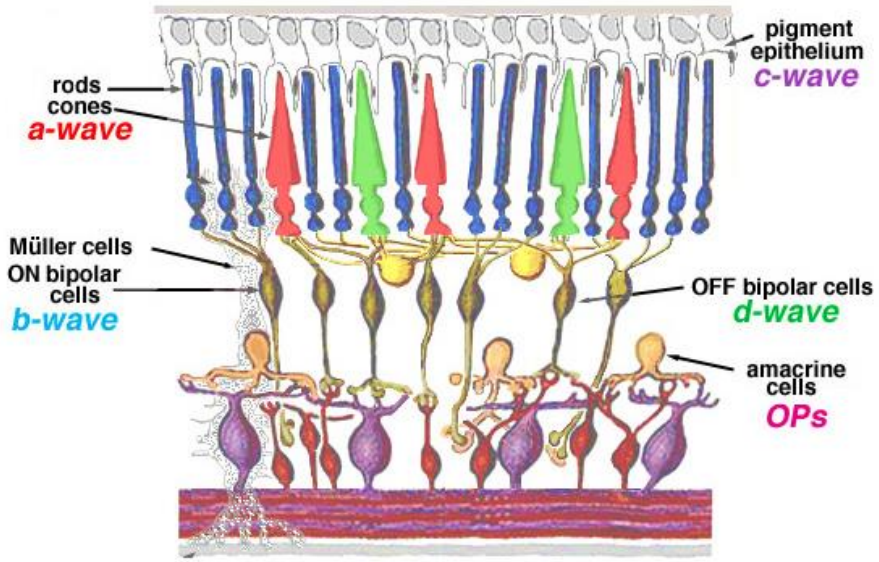

Figure 2-4 Diagram showing the retinal cellular origin of major components of ERG

(Source: http://webvision.med.utah.edu/imageswv/DONFig3.jpg)

a- wave

The a-wave of the human ERG is also known as the leading part of the Granit's PIII component. As mentioned in the previous section, the PIII component can be further divided into two subcomponents: a fast and a slow PIII (Sillman et al., 1969). The results obtained from ERG recordings with intra-retinal microelectrodes suggested the activity of photoreceptor layer as the origin of the fast PIII component of the ERG (Brown and Murakami, 1964). Bloomfield and Dowling (1985a) used pharmacological approach to study the a-wave component of the ERG by blocking the synaptic transmission from the photoreceptors to the post-receptoral processes by using intravitreal injection of L-glutamate or 2-amino-phosphonobutyric acid (APB) (Massey et al., 1983; Bloomfield and Dowling, 1985b) into one eye (A) and saline into the control eye (B) of monkey retina resulted in successful elimination of the PII component, thus revealing the PIII component through the entire course (see figure 2.5).

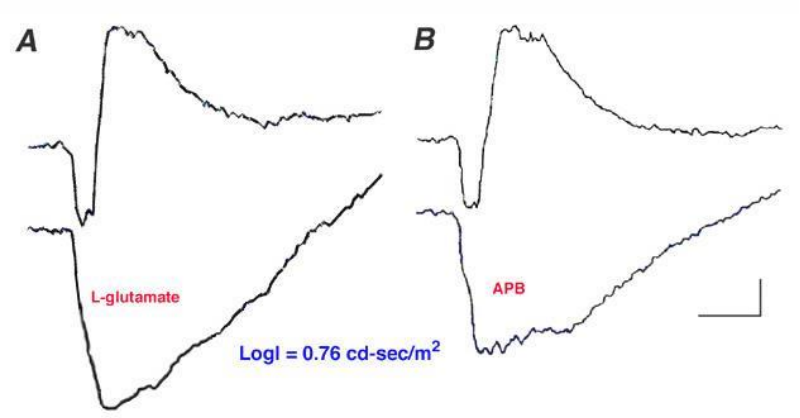

Figure 2-5 Effect of L-glutamate and APB on ERG b- wave

The obvious demolition of the b-wave of the ERG by intravitreal injection of (A) L-glutamate or (B) 2-amino-phosphonobutyric acid (APB) in the right eye of the rabbit retina (lower trace) with saline filled in the other eye that served as control (upper traces) revealing just the a-wave alone.

(Source: http://webvision.med.utah.edu/imageswv/ERGFig6.jpg)

As described in chapter 1, absorption of light by visual pigment initiates a sequence of molecular events leading to the hyperpolarization (negative alterations in intracellular electrical potential) of outer segments of the photoreceptors. This change in intracellular potential results from a light induced reduction in entry of Na^{2+} currents across the plasma membrane of the outer segment. This change in currents can be clinically measured as the corneal negative a-wave of the flash ERG. Early studies in amphibians using compounds like $Co^{2+,}$ Mg^{2+} and Na^{+} that block transmission from photoreceptors to postreceptoral neurons had shown the demolition of b-wave indicating the loss of postreceptoral activity thereby producing the a-wave whose origin is assumed to be due to activity of rod photoreceptors only (Furukawa and Hanawa, 1955). This was further supported by intra-retinal recordings of mammalian retinae (Brown and Wiesel, 1961a, b) and experiments on isolated rat retina where light induced suppression of dark currents of photoreceptors (Penn and Hagins 1969, 1972 and Hagins and Penn, 1970) led to the conclusion that the origin of a-wave is from rod receptor photocurrent.

On the contrary, light adapted a-wave is smaller than dark adapted a-wave and probably this discrepancy reflects the difference in the relative densities of rods and cones. Using glutamate analogs in macaque retina (Bush and Sieving, 1994) reported that much of the a-wave originates in the postreceptoral neurons with response up to about first 5ms after onset of flash stimulus originating in cone photoreceptors (Robson et al 2003).

b-wave

The b-wave is the largest positive deflection recorded at the cornea elicited by a diffuse flash stimulus. This component corresponds to the additive result of PIII and PII components as demonstrated by Granit's ERG recordings from the cat retina. Several scientists conducted experiments on vertebrate retinae and stated that the activity of the depolarizing (ON-) bipolar cells contribute to the dark adapted b-wave (Knapp and Schiller, 1984; Gurevich and Slaughter, 1993; Robson and Frishman, 1995, 1996; Frishman et al., 1996; Stockton and Slaughter, 1989). Initially the origin of the b-wave was thought to be from the neural retina proximal to the photoreceptors. The evidence obtained using compounds like Mg^{2+} and Na^{2+} aspartate (Dowling and Ripps, 1972; Shimazaki and Oakley, 1984) and the occlusion of the central retinal artery that supplies oxygen to all nerve fibers of the neurosensory retina (Noell, 1954; Brown et al., 1965) supported the idea that b-wave originates in the postreceptoral neurons as under these conditions the annihilation of the b-wave but preserved photoreceptor responses was observed. Intra-retinal depth recordings of local ERGs to identify the cells that precisely contribute to generate the b-wave demonstrated the initial negative deflection appeared closer to the outer plexiform layer (OPL) followed by a reversal in the amplitude that developed across the inner nuclear layer (INL) (Arden and Brown, 1965).

Using pharmacological agents like APB (2-Amino-4-Phosphonobutyric Acid), a glutamate analogue that results in loss of light responsiveness of ON-bipolar cells which led to the complete loss of b-wave of the photopic flash ERG whilst the remaining signal derived from photoreceptors, horizontal and OFF-bipolar cells

which remained unaffected post application of APB (see figure 2.6) (Slaughter and Miller, 1981; Sieving et al., 1994).

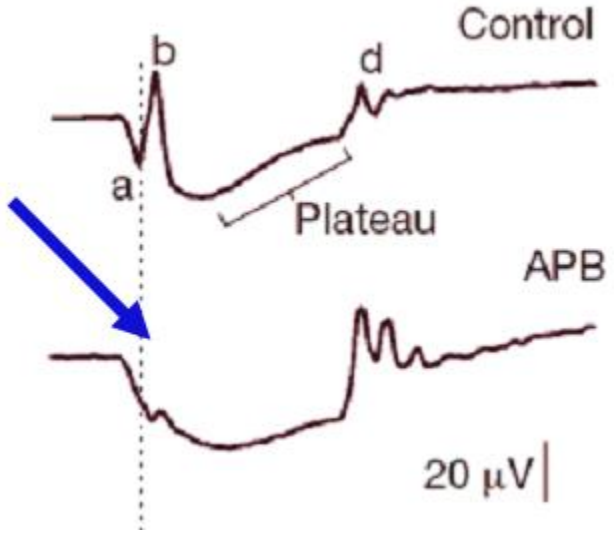

Figure 2-6 Normal macaque flash ERG showing a-, b- and d-waves (upper trace) and the demolition of photopic b-wave post application of glutamate analogue (APB) (lower trace)

(Source: Sieving et al., 1994)

However, few other studies also mentioned that Muller cells also contribute to the generation of b-wave (Robson and Frishman, 1995 and Robson et al., 2004). By employing current source density analysis, Faber (1969) proposed that the ionic fluxes across the Muller cell membrane generate the b-wave. This hypothesis was further supported by Miller and Dowling (1970) who used intra-retinal recordings in mudpuppies and observed that the latency, time course and dynamic range of Muller cell response was similar to that of b-wave response suggesting that Muller cells may probably generate the b-wave by a K+ regulated mechanism. A report by Bonaventure et al (1981) suggested that when intravitreal injection of DL-alpha aminoadipic acid, a Muller cell toxin was used in frog and chicken retinae, a complete loss of b-wave was observed. In addition to previous report, these results also supported the assumption that Muller cells

generate b-wave. However, there is also evidence that acute application of DL-α-aminoadipic acid may also affect other retinal neurons (Stockton unpublished).

Conclusions drawn from these results indicated that the b-wave is propagated by flow of ions through radially oriented cells with a bipolar nature. However, on the other hand, contribution of Muller cells (also bipolar in terms of entrance and exit of K^+ ions) to the b-wave is still debated as they are also radially oriented cells that span the entire retina extending from the Internal limiting membrane (ILM) to external limiting membrane (ELM) (Asi and Perlman, 1992).

c-wave

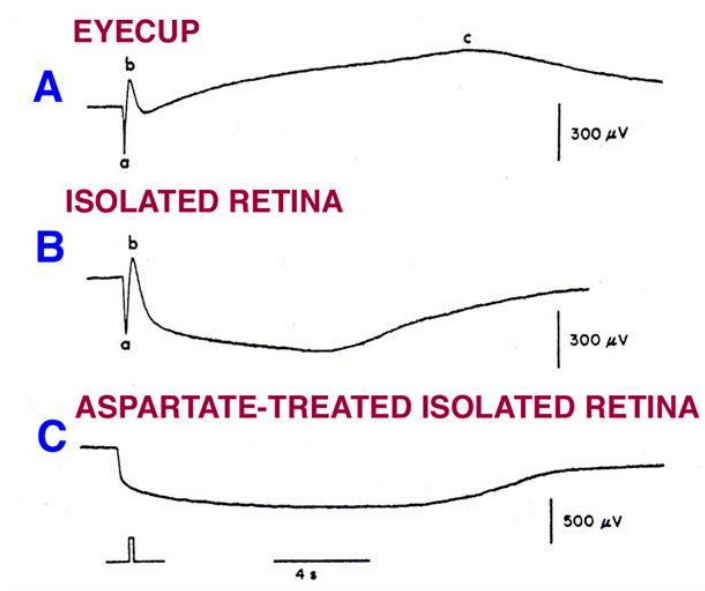

Figure 2-7 ERG recordings from skate retina.

(A) ERG recording from the whole skate eyecup (B) ERG recording derived from the neural retina detached from the retinal pigment epithelium clearly demonstrating the demolition of the c-wave (C) After treating the retina with aspartate, which is known to block the transmission from the photoreceptors to the bipolar cells that led to the cessation of the b-wave.

(Source: taken from Pepperberg et al., 1978)

This wave is known to originate in the retinal pigment epithelium. Noell's experiments showed that after systemic injection of sodium azide, a potential evoked from the retina which appeared similar to the PI component of ERG recordings obtained by Granit in cat retina (Noell, 1954). This azide induced response was not manipulated by iodoacetic acid, which has the potential to demolish the photoreceptors. Also the response did not disappear even after disconnection of optic nerve which consists of the bundles of ganglion cell axons. The ERG responses from the isolated skate neural retina revealed both a- and b- waves but the c-wave ceased. Therefore, this experiment strongly recommended that the c-wave is derived from the pigment epithelium (see figure 2.7) (Pepperberg et al., 1978).

d-wave

The fourth component of the flash ERG is more of a stimulus influenced response and can either be positive or negative depending on the type of stimulus and/or species studied. The d-wave is considered to be largely generated by OFF bipolar cells, which was known from the results obtained from the current source-density analysis studies and the pharmacological studies, using selective blockers for ON bipolar cell glutamate metabotropic receptors and OFF bipolar cell α-amino-3-hydroxy-5-methyl-4-isoxazolepropionic acid/kainate abbreviated as AMPA/KA type receptors in amphibian retinas (Stockton and Slaughter, 1989; Gurevich and Slaughter, 1993; Szikra and Witkovsky, 2001) and in primates (Sieving et al., 1994).

These pharmacological studies have shown that the d-wave of the ERG solely depends on AMPA/KA type synaptic transmission (synaptic plexus between

photoreceptors and OFF- bipolar cells). This component is observed when the ON and OFF phases of the ERG response are differentiated in time, by presenting the light stimuli of longer duration (>100 ms). The ERG recordings obtained using microelectrodes in the distal retina revealed the opposite polarities of the waves (opposite wave deflections to the conventional ERG responses recorded with electrodes places anterior to the retina when compared to the active recording at the cornea i.e., the a- wave is positive while b and d waves are negative).Various researchers (Dong and Hare, 2000; Awatramani et al., 2001) studied the effect of DNQX (6,7-dinitroquinoxaline-2,3-dione), an antagonist for AMPA/KA type glutamate receptors that led to the reversal of polarity of the d-wave, amplification of the b-wave and decrease in the amplitude of a-wave, providing the basis for the origin of the d-wave from the OFF- center bipolar cells. Awatramani et al., (2001) reported the contribution of third order neurons to the ERG d-wave. The d-wave can be recorded when the retina is exposed to prolonged light stimuli while it tends to couple with the b-wave when exposed to stimuli presented with a shorter duration.

Oscillatory potentials (OPs)

When a bright light stimulus is used to elicit an ERG in humans, low amplitude rhythmic wavelets are identified on the ascending limb of b-wave. Depth recordings by use of mciroelectrodes in frog retina to study OPs indicated their importance in diagnosing early changes in the circulatory disturbances in the inner retina (Yanagida et al., 1986). The frequency of OPs range from 100-150 Hz and can be best isolated by digital filtering to eliminate the a- and b- waves which are slow when compared to these potentials (Asi and Perlman, 1992). This filtering also helps in the amplification and isolation of these wavelets. With the

help of the Fast Fourier Transform (FFT), quantitative assessment of the amplitude and frequency of these potentials is possible (see figure 2.8).

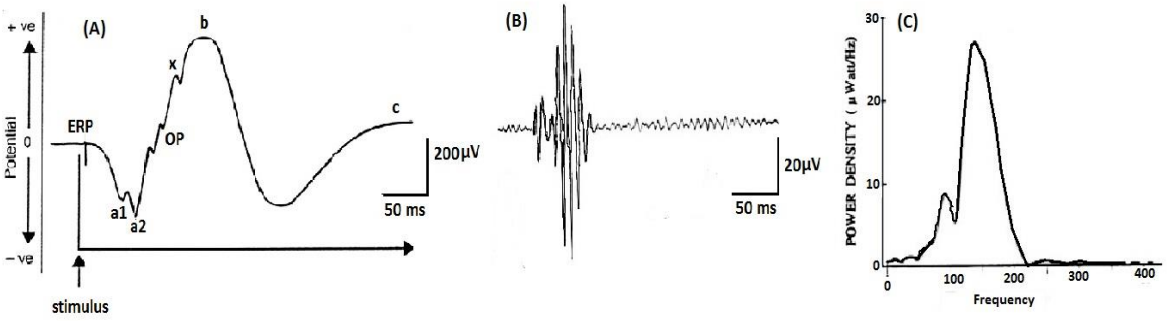

Figure 2-8 (A) Location of Oscillatory potentials on the ascending limb of the b-wave, (B) Isolation of these wavelets by using FFT and (C) Power spectrum of OPs

(Source: Asi and Perlman, 1992)

2.5 (ii) Amplitudes and Implicit times- measures of ERG

Two principal components, a- and b- waves are distinct and easily recognizable in an ERG waveform evoked by a single flash of light in both dark and light adapted ERGs. Amplitudes and time interval between onset-to-peak are two important measurements that help us understand the difference between a normal and an abnormal retinal function. The a-wave amplitude is measured from baseline to the trough or lowest point of the a-wave. The b-wave amplitude is usually measured from the baseline to the peak of b-wave in the absence of a-wave and from trough of the a-wave to the crest of the b-wave when a-wave is present. Time taken for the appearance of the a-wave followed by the onset of the flash stimuli is referred to as latency of the a-wave response and implicit time is a measure of the time interval between the crest of the b-wave from the onset of strong flash stimulus (see figure 2.9).

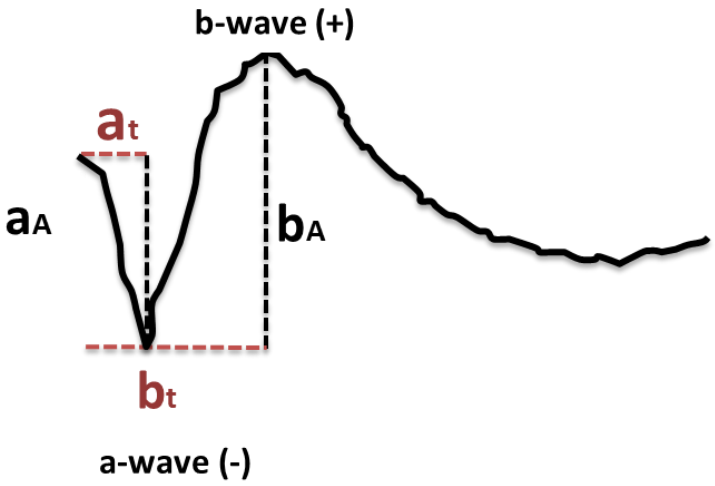

Figure 2-9 Typical ERG waveform showing signal amplitudes (aA and bA represented by black dotted lines) and onset-to-peak times (at and bt represented by red dotted lines) of a- and b- waves respectively.

2.6 The Clinical full-field ERG

To record comparable ERGs across the world, fundamental aspects of light and dark adapted retinal function have been described by International Society for the Clinical Electrophysiology of Vision (ISCEV). ISCEV develops standard stimuli parameters that accommodates different types of light sources like light emitting diodes (LEDs) and gas discharge lamps and specifies six protocols based on different stimulus strengths to record clinical ERGs under both dark (scotopic) and light (photopic) adapted conditions (McCulloch et al., 2015).

2.6.1 Scotopic ERG assessment

As per ISCEV standards, ERGs under scotopic conditions is examined using four stimulus conditions. Patients are dark adapted for atleast 20-30 minutes before recording scotopic ERGs (see figure 2.10).

Dark adapted 0.01 ERG (Isolated rod response)

This is the first signal to be recorded post dark adaptation as this measurement could be affected with light adaptation. To record this signal, a dim white flash with a photopic strength of 0.010 photopic cd.s.m^{-2} (0.025 scotopic cd.s.m^{-2}) is

presented on a dark background with a minimum interval of 2 s. This stimulus elicits responses from rod photoreceptors only as cones do not respond to this stimulus strength. The waveform obtained in response to this stimulus is a single, slow positive b-wave which peaks at about 90-100 ms and is assumed to be derived from rod depolarizing bipolar cells (Pardue et al., 1998).

Dark adapted 3 ERG (maximal combined cone and rod response)

To record this response a brighter stimulus of 3.0 photopic cd.s.m^{-2} (or 7.5 scotopic cd.s.m^{-2}) is presented at an interval of about 10 s between stimulus flashes on a dark background. The initial 25 milliseconds of the dark adapted combined response have been thought to be rod dominated while the rest of the waveform is assumed to have postreceptoral origin (Hood and Birch, 1990 a, b). However, Robson et al (2003) suggested that the leading edge of the dark adapted a-wave is the direct reflection of currents from both rod and cone photoreceptors.

Dark adapted 10.0 ERG (combined responses to stronger flash)

This step is the brighter version of DA 3 ERG. To achieve this a stimulus strength of 10 photopic cd.s.m^{-2} (25 scotopic cd.s.m^{-2}) is presented on a dark background whilst ERGs are recorded in the dark adapted conditions. The waveform derived in response to this stimulus is characterized by a larger and distinct a-wave that reflects rod and cone activity, shows a shorter peak time than dark adapted 3.0 ERG. This response is observed to be more reliable in conditions like opaque media and immature retinae (McCulloch et al., 2015).

Dark adapted 3.0 oscillatory potentials

In response to dark adapted 3.0 photopic cd.s.m^{-2} and post hoc filtering (high-pass filter <75 Hz and low pass filter >300 Hz), small wavelets can be recorded

on the ascending limb of the dark adapted b-wave called as oscillatory potentials. These are a chain of high frequency low amplitude wavelets obtained in response to strong stimuli. The origin of these wavelets is assumed to be in amacrine cells. Wachtmeister (1998) suggested that OPs may be a useful indicator in investigating the neuronal adaptive mechanisms in the retinal vascular and degenerative diseases.

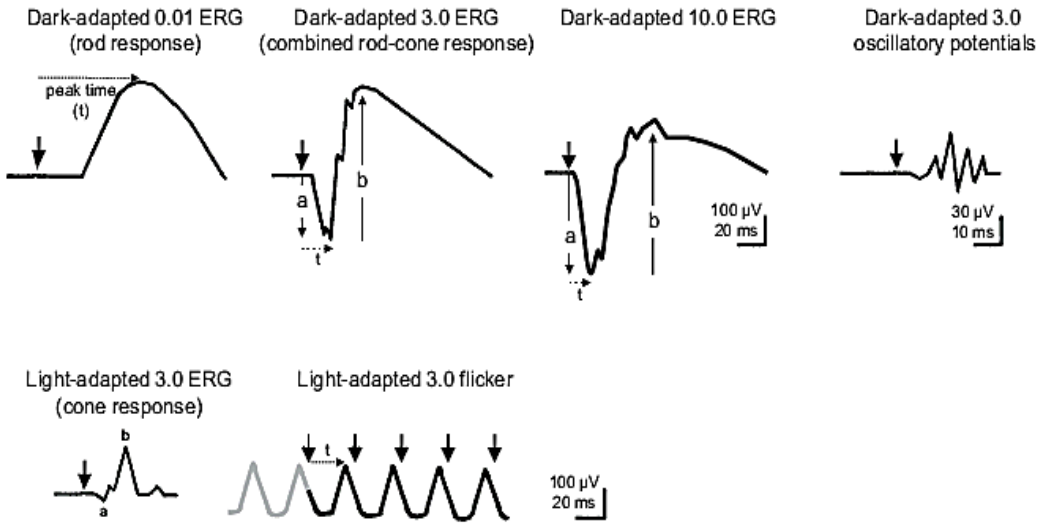

Figure 2-10 shows six normal waveforms elicited by ISCEV standardized full-field ERG.

The top four responses show scotopic responses and lower two ERG responses represent photopic responses.

(Source: Taken from McCulloch et al., 2015)

2.6.2 The Photopic ERGs

This protocol requires the patient to light adapt for atleast 10 minutes prior to the testing of photopic ERG responses in order to record stable and reproducible responses from the cone system minimizing signals from the rod system.

Light-adapted 3.0 ERG (Single flash cone ERG)

This signal is recorded in response to stimulus flashes (3.0 photopic cd.s.m^{-2}) presented on a full-field background luminance of 30 photopic cd.s.m^{-2} at an interval of about 0.5 s between flashes. This waveform is characterized by a negative a-wave followed by a larger positive b-wave. The a-wave is known to arise from hyperpolarization of cone photoreceptors and hyperpolarizing bipolar cells (Frishman and Wang, 2011) whilst the b-wave was reported to originate from ON- cone bipolar cells with no contribution from rod bipolars (Heynen a and b).

The photopic b-wave evoked in response to light adapted single flash is formed as a result of brief, opposite polarity contribution of OFF and ON bipolar cells creating ‘push-pull effect’ (Sieving et al., 1994).The typical implicit times of a- and b- waves are 15 and 30 ms respectively.

Light-adapted 30 Hz flicker ERG

Like light-adapted single flash stimuli, 30 Hz flicker uses a train of brief 3.0 photopic cd.s.m^{-2} flashes presented on a background luminance of 30 photopic cd.s.m^{-2}. These flashes are presented at a flickering rate of approximately 30 stimuli per second. The flicker ERG also referred to as steady state ERG is characterized by positive to negative oscillations that are repeatable and match the temporal frequency of the stimulus. This response has been shown to be purely cone dominated. (Conner an MacLeod, 1977).

2.7 Factors effecting ERGs

While recording ERGs, we need to consider factors like size of pupil, age, sex, refractive error (high myopia), duration of stimulus, inter-flash interval, diurnal fluctuations, size of the retinal area illuminated, and clarity of ocular media as these factors could affect the response amplitudes and may delay signal implicit times which may give us a wrong impression of a retinal disease (Perlman, 2015).

2.8 Full-field Flash ERG applications

In conditions like Retinitis Pigmentosa (RP) and Congential stationary night blindness (CSNB) where the disease have a significant effect on phototransduction cascade, the a- and b- wave amplitudes and implicit times of scotopic isolated rod responses and mixed cone and rod responses provide a basis of differential diagnosis that allows us to perform a non-invasive examination of normal or abnormal functioning of the visual cycle (Creel, 2015).

Prior to photographic evidence, Oscillatory potentials can be used to identify retinal dysfunction in cases like Juvenile diabetic retinopathy (Juen and Kieselbach, 1990) and can also be used a predictor of progression of severe proliferative retinopathy (Bresnick et al., 1984; Bresnick and Palta, 1987; Kizawa et al., 2006).

In several types of inherited retinal dystrophies, a diffuse type of damage occurs in the cone photoreceptors where complete loss or reduction of a- and b- wave amplitudes of single-flash cone ERGs accompanied by a delay in their latencies can be observed (Hamel, 2007). Noma et al (2012) determined the correlation between inflammatory factors and different components of the ERG and found that the implicit time of 30 Hz flicker ERG can be used to identify patients who were at a higher risk of ischemia secondary to branch retinal vein occlusion (BRVO) with macular edema. Larsson and Andréasson (2001) suggested that photopic 30 Hz flicker ERG can be used as a good predictor for neovascularization of central retinal vein occlusion (CRVO). The implicit time of 30 Hz flicker ERG could also be used for a valuable predictor of retinal recovery process, long-term visual outcome after macular hole surgery and may also serve

as a useful tool in selection of patients suitable for surgery (Andréasson et al., 2013; Andréasson and Ghosh, 2014).

Several reports also showed that flash ERGs can serve as a useful tool in investigation of certain psychiatric disorders (Lavoie et al., 2014a, b). In conditions like the seasonal affective disorder where patients experience recurrent depressive episodes especially during fall and winter when the length of photoperiod is shorter than in summer, flash ERGs were observed to be affected (Lam et al., 1992; Hébert et al., 2002). These results were presented with decreased cone and rod b- wave amplitudes which upon patient receiving light therapy were shown to be improved therefore suggesting that flash ERG could be used to examine retinal sensitivity to diagnose patients with SAD during fall or winter and also could be used to monitor effect of light therapy given that both the ERGs recordings on pre- and post- therapy visits are recorded at the same time of the day (Lavoie et al., 2009). High-risk offspring of patients with Schizophrenia and Bipolar disorder were shown to have diminished rod b- wave with delayed implicit time long before the incidence of disease in these individuals indicating that ERG can be used for identification of individuals who are at higher genetic risk and may be used as a biomarker for early investigation of these neuropsychiatric disorders (Hébert et al., 2010).

2.9 Methods to achieve isolated rod and cone ERGs

A variety of strategies can be applied to obtain isolated rod and cone ERGs, some of which are discussed in this section.

2.9.1 Coloured stimuli

The peak spectral sensitivities of rods and cones is around 510 nm and 560 nm respectively represented by grey and yellow lines as shown in the figure 2.11A. These numerical values indicate that the rods are sensitive to blue wavelengths but are relatively insensitive to the red wavelength of the visible spectrum. Using this information, separate rod and cone ERGs can be obtained by means of coloured filters like Kodak blue and red Wratten filters or coloured flashes produced by LEDs. After dark adaptation for 20-30 minutes, when test eye is presented with a low-intensity blue flicker stimulus, the resultant ERG response is purely rod-dominated and lack involvement of cone responses (An et al., 2012). Similarly, when test eye is presented with a bright red light stimulus, a biphasic waveform with an initial fast response elicited by cones and the second, slow response contributed by rods can be observed (see figure 2.11B) (Fishman, 1985). Under such stimulus conditions, the rod response is equal to that of cones despite them outnumbering cones in the retina. This discrepancy in rod's contribution to the ERG waveform reflects the relative lack of sensitivity of rods to red wavelength of the spectrum.

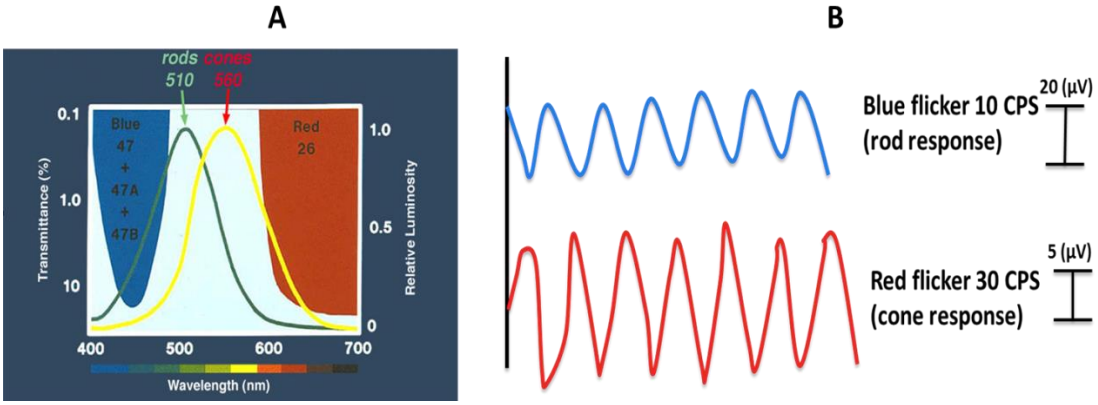

Figure 2-11 (A) blue and red filters that can be used to obtain separate rod and cone components of ERG using weak flashes under scotopic conditions (B) coloured stimuli that can aid the isolation of rod and cone ERGs.

(Source A: http://webvision.med.utah.edu/imageswv/DONFig9a.jpg & source B: taken from Fishman 1985).

2.9.2 Flicker ERGs

The temporal response characteristics of rod and cone systems are different as rods do not operate above approximately 15 cycles per second i.e., at a flickering rate of 30 Hz. The ERGs recorded at this frequency are purely cone dominated and therefore flicker ERGs of different temporal frequencies can be used to obtain separate rod and cone responses (McCulloch et al., 2015).

2.9.3 Paired-flash paradigm

In a number of in vitro studies, this method has been shown to rely on rod response property or rod photocurrent saturation. This method involves a test flash stimulus (typically around 2.1 log cd.s.m^{-2}) and a bright probe flash of fixed intensity presented rapidly in a sequence of trials and can be used to obtain cone-driven ERG responses. The interstimulus interval (t_{probe}) varies between trials. The test stimulus elicits a mixed cone and rod response that saturates the rods. The second brighter probe flash is presented in a rapid succession (ISI between 200-1000 ms) in the duration of which rods are still not recovered therefore, producing a cone response alone (Birch et al., 1995). The hypothetical rod response can be obtained by computational subtraction of the cone component generated by probe flash from the mixed rod-cone response achieved in response to test flash (Pepperberg et al, 1997; Phipps et al., 2004).

2.9.4 Manipulation of adaptation

This approach involves changing level of luminance and state of adaptation (light vs dark adaptation). Under scotopic conditions, following 20-30 minutes of dark adaptation, isolated rod ERGs can be recorded using a dim flash as cones cannot operate under these circumstances. To achieve cone responses alone, different light adaptation levels are required where rods saturate producing purely cone driven ERG signals. This method takes advantage of the fact that cones and rods operate best at different state of adaptation. This approach has been adopted by ISCEV for testing cone and rod full-field ERGs (McCulloch et al., 2015).

2.10 Isolation of cone isolated ERGs

The isolation and comparison of rods, L-, M- and S- cone signals may be essential in understanding the fundamental physiological processes in the human retina. Furthermore, the knowledge of the response characteristics driven from each cone type becomes important in order to study the interactions between different cone ERGs and to quantify the signal strengths of each distinct cone type independently. Cones responses can be further isolated into subtypes, L-, M- and S- cone ERGs using selective adaptation and silent substitution paradigms.

2.10.1 Chromatic adaptation

Chromatic adaptation is a method of selective desensitization of different cone classes using coloured backgrounds. This can be achieved by selectively adapting a single or more cone classes to specific coloured background in order to reduce their sensitivities to an adapting background whilst favouring the responses from the remaining cone type(s) (Eisner and MacLeod, 1981; Evers and Gouras, 1986; Kremers, 2003). This method is similar to the adaptation strategy described in the previous section except for the fact that this method uses manipulation of coloured stimuli instead of just black and white stimuli and allows classification of cone signals into long-, middle- and short- wavelength sensitive ERG signals. Using this technique, isolation of S- cone driven ERGs can be attained with less difficulty in comparison to L- and M- cone responses as their absorption spectra are quite different to those of L- and M- cones (Norren & Padmos, (1973); Padmos & Norren (1971).

Limitations

The spectral sensitivities of L- and M- cones overlap extensively, which makes the isolation of responses from either cone photoreceptor types difficult as adapting one cone type may certainly adapt the other. Besides their similarities in spectral sensitivities, L- and M- cone ERGs exhibit similar flash ERGs which makes the quantitative as well as qualitative assessment of the respective cone driven ERGs challenging (Kremers 2003). Additionally, chromatic adaptation also induces nonlinearities in the response properties of a cellular system. The underlying reasons for these nonlinearities could be due to inter-individual differences in lens pigment absorption (Norren, 1972), pigment bleaching in the photoreceptors, adaptation of the post-receptoral cellular processes like horizontal and retinal ganglion cells (Lee et al., 2008) that contribute to an ERG waveform. Furthermore, this method also have a disadvantage of using varying adapting fields as background to obtain isolated responses from different classes of photoreceptors. Meaning that the measurements obtained using this method cannot be compared quantitatively since the cone driven signals are significantly affected by change in state of adaptation (Kremers, 2011).

2.10.2 Silent Substitution

In the recent past, it has been shown that it is now possible to isolate responses of a specific cone photoreceptor type without altering the sensitivities of any of the cones through adaptation mechanisms using silent substitution. The silent substitution paradigm was first introduced by Donner and Rushton (1959) and was later introduced into electrophysiological experiments by Estevez and

Spekreijse (1982). The excitation of photoreceptors post absorption of light obeys the Principle of Univariance and colorimetric principles.

According to the Principle of Univariance, three properties hold important for photopigment transduction and for the excitation in the photoreceptors (Estevez and Spekreijse, 1982): proportionality, additivity and transitivity (Kremers, 2003).

Proportionality: When two different wavelengths λ_1 and λ_2 produce the same number of isomerizations in a specific photoreceptor, then we can say that $\lambda_1=\lambda_2$. By changing the intensities of both λ_1 and λ_2 by a factor n also results in the same number of isomerizations ($n\lambda_1=n\lambda_2$).

Additivity: If a different combination of wavelengths λ_3 and λ_4 produce the same number of photoisomerizations as λ_1 and λ_2, then replacing either λ_3 or λ_4 with λ_1 or λ_2 also produce identical number of isomerizations (example: $\lambda_1+\lambda_3=\lambda_1+\lambda_4$ or $\lambda_2+\lambda_3=\lambda_2+\lambda_4$ can be used as interchangeable combination of wavelengths that produce excitation required to study a responses of a particular photoreceptor type while suppressing the activity of others).

Transitivity: If a different wavelength λ_5 is added to both wavelengths λ_1 and λ_2, the resultant will still be identical in the number of their isomerizations. (Example: $\lambda_1+\lambda_5=\lambda_2+\lambda_5$ since $\lambda_1=\lambda_2$).

The principle of silent substitution is that under identical states of adaptation when alternating between two lights of different wavelengths that produce equal excitation (no net excitation) for one photoreceptor type, yield different excitation for another photoreceptor type. For example, when a monochromatic light of 520 nm is replaced by 575 nm, results in negligible or no excitation to the M cones whilst producing a different excitation to the L cones for the same modulation. In other words, M cones are suppressed and cannot detect the difference whilst L cones are stimulated and isolated L cone responses are achieved (see figure 2.12) (Kremers, 2003).

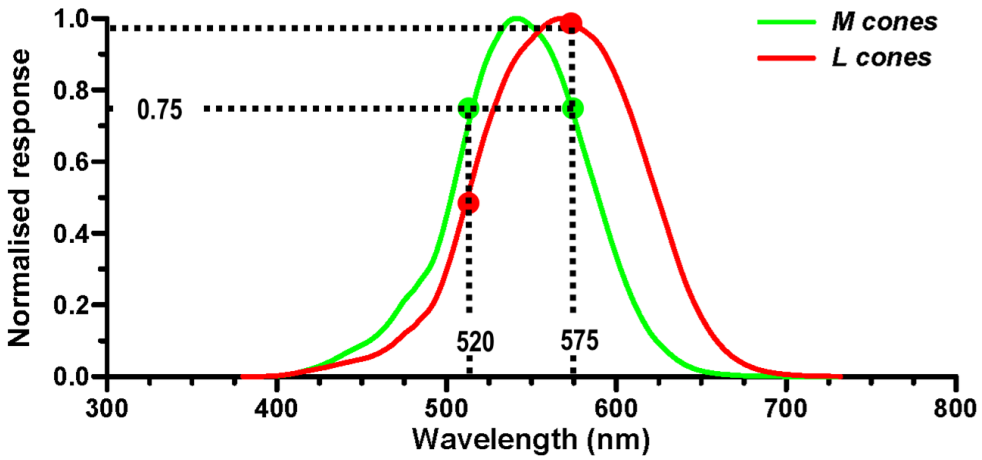

Figure 2-12 An example of silent substitution paradigm using spectral distributions of L- and M-cones.

The 530 and 575 nm lights give no (insignificant) excitation to the M cones while a different excitation to the M cones. This graph suggests that when alternating between wavelengths 520 nm and 575 nm M cones cannot be activated allowing us to achieve isolated M cone responses (Image courtesy: Parry NRA)

The number of photoreceptor classes that can be suppressed for a specific condition depend on the number of independent light sources used for the stimulus. At least four primaries or independent light sources are required in order to elicit responses from a single photoreceptor class while silencing the remaining three types of human photoreceptors (Murray et al., 2008). The number of light sources should be equal to the number of photoreceptors, which allows us to isolate and study all signals from all classes of photoreceptors and their contribution independently. Recent use of four-primary (LED) ganzfeld stimulator have been proven to be a great tool in measuring all the four photoreceptors separately (Kremers, 2003 and Murray et al., 2008). The stimulus strength of each photoreceptor can calculated in terms of either cone or rod contrast (Michelson contrast).

Michelson contrast = (Lmax-Lmin)/ (Lmax+Lmin) *100 % …… Equation 2

Lmax is the maximal output and Lmin is the minimal output from the LEDs

The cone isolated response can be measured in terms of its cone excitation strength (Usui et al., 1998 , Kremers, 2003). The cone excitation strength of each cone type is obtained by multiplying emission spectra of the primaries with the psychophysically determined cone fundamentals and integrating over a range of wavelength (Stockman et al., 1993).

Calculation of the cone excitation strength is given below:

$$E_{L,R}(t) = F_R . L_R(t) . \int I_R(\lambda) . A_L(\lambda) . d\lambda \quad \text{…… Equation 3}$$

Where L_R = luminance of the red LED

$E_{L,R}$= L cone excitation by the red LED

t= changes as function of time

I_R (λ)= emission spectrum of red LED at unit luminance

A_L (λ)= L cone fundamental

F_R= conversion factor for Red LED involving the photometric measurements to the cone fundamentals.

Total excitation of L cones depends on the sum of the excitations produced by each LED.

The calculations used to produce stimuli used in our experiments will be described in the methods chapter.

Advantages of silent substitution

Application of this method helped in better understanding of the characteristics of a specific cone type and their interactions with other photoreceptors and post-receptoral processes (Challa, 2010; Kremers 2011). The responses elicited by this paradigm were suggested to give reliable results as the time averaged luminance and chromaticity remains same for all stimulus conditions. As a result, the responses obtained by this method, makes it possible to compare results attained by the different stimuli (Kremers, 2003; Murray 2008).

Table 2-1 : Summary of studies that have used silent substitution

Authors	Smith and Pokorny 1995	Usui et al 1998	North et al 2004	North et al 2005	Challa et al 2010	Haueisen etal 2010	Kremers et al 2015	Jacobs et al 2015	Maguire et al 2018
Silent substitution paradigm	Psychophysics, counter-phase and in-phase sine wave stimuli	30 Hz square wave Phosphors Green, red and blue (40, 20, 6 cd/m^2) ;5 trichromats	ERG response to 200 ms red pulse at 2500 Td on a blue background. 18 in each group normotensive and POA glaucoma	650 nm – bleaching L cones 450 and 535 nm presented in counter phase; 21 Type 1 and 32 Type 2 Diabetes	CRT stimulator, Double silent substitution, 12- and 30 Hz Sine wave stimuli recorded in healthy individuals	Green, red and blue (282, 117, 47 cd/m^2); 39 Glaucoma patients	RETIport system; green orange blue and red LEDs	4 primary-LED ganzfeld stimulator using sine wave stimuli; 8 healthy participants	Green (514 nm), amber (590 nm) blue (460 nm) and red (635 nm) LEDs
Study purpose	To study L- and M-cone signals and their contribution t o postrecepto ral pathways	L and M cone specific ERGs studied as a function of temporal frequency	Post receptoral pathway specific (S, L+M) ERGs in Glaucoma and ocular hypertension	Role of S-cones in Diabetes studies through ERGs	L- and M-cone ERGs studied as a function of temporal frequency and retinal eccentricity	To objectively diagnose POAG using silent substitution paradigm	Role of spatial arrangement of L and M cones ERGs	Spatial arrangement of L- and M-cone ERGs	Characterisin g S cone using Silent substitution paradigm
Key results	Chromatic channel and achromatic channels sensitive at low and high temporal frequencies respectively .	Demonstration of heterochromatic flicker stimuli to record photoreceptor specific ERGs	Late photopic negative wave reduced in OHT and glaucoma patients compared to normals	Poor S-cone ERGs may be attributed for impaired colour vision	Results indicate the existence of cone selective inputs to ERGs vary across human retina and temporal frequency.	S-cone VEP wave form profile significantly different from normal	For a full field stimulus, L cone ERG amplitudes are larger than M cone ERGs	Using triple silent substitution, it is possible to study spatial arrangement of L- and M-cone ERGs and the data further agrees to the assumption that these signals reflect postreceptoral pathways.	S- cone ERG obtained using SS method is reflective of S cone function

2.11 Summary

Electroretinographic testing plays an important role in physiological examination of retina and provides us the basis for differential diagnosis of several hereditary retinal diseases. These methods also allow us to assess the effect of treatment strategies and help us monitor changes in retinal function on follow-up cases. In our experiments we used flash and flicker ERG stimuli to obtain isolated rod, L- and M- cone ERGs using silent substitution whose data could be used to assess how these responses are affected in disease.

Chapter 3 - General Methods

3.1 Introduction

As discussed in chapter 1, human trichromatic vision relies on L-, M- and S-wavelength sensitive cones, each of which yield a univariant, colour-blind signal with different spectral peak sensitivities. To understand both normal and reduced forms of colour vision (colour vision deficiency), an unequivocal knowledge about colour matching functions and spectral sensitivities of different photoreceptors is essential. Since our experiments involved manipulation of coloured stimuli generated on a four-primary ganzfeld stimulator, a precise knowledge and understanding of different colorimetry concepts like colour matching functions and cone fundamentals is required.

3.2 Colour matching functions and spectral sensitivities

Colour matching functions provide the quantitative links between different wavelengths of electromagnetic spectrum i.e., pure colours and human physiological perception of colour. The colour matching function can be defined as the ability of a normal trichromatic observer to match a test light of a fixed wavelength to a combination of three independent primaries (red+green+blue) of equal energy (figure 3.1A). Wright (1928-29) and Guild (1931) conducted matching experiments independently and were the first to define colour matching functions and referred them as $\bar{\boldsymbol{r}}(\boldsymbol{\lambda}), \bar{\boldsymbol{g}}(\boldsymbol{\lambda}), \bar{\boldsymbol{b}}(\boldsymbol{\lambda})$ (see figure 3.1B). These CMFs provided the basis for the derivation of the CIE (International Commission on Illumination) 1931 standard observer.

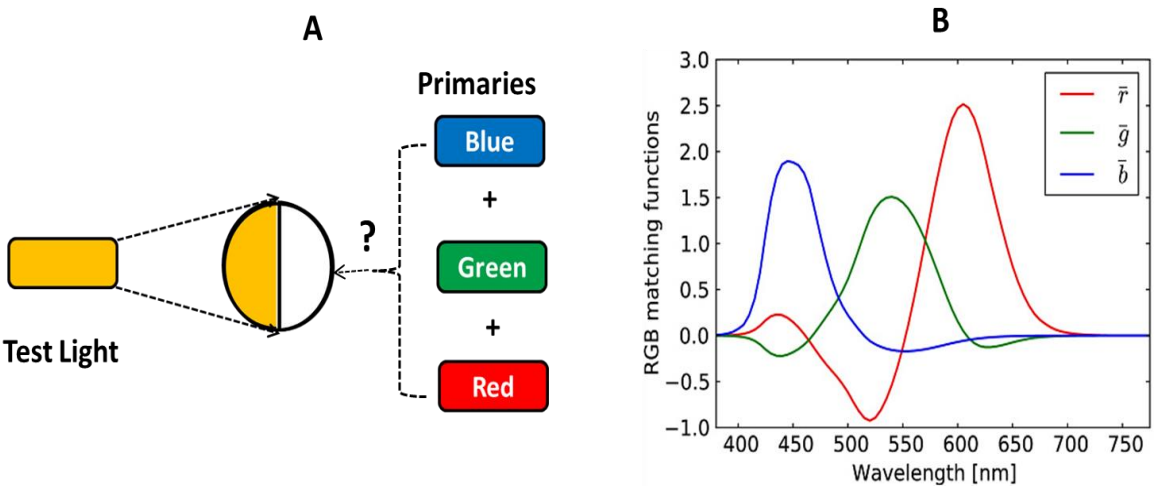

Figure 3-1 (A) Example of a colour matching function derived using red (700 nm), green (546.1nm) and blue (435.8 nm) primaries against yellow test light.

The question mark indicates the amount of each primary requires producing yellow that matches the test light. (B) Graph showing colour matching functions plotted as a function of wavelength (nm). In other words, the amount of each of the three primaries required to match each wavelength of the spectrum.

To solve certain drawbacks in the original set of CMFs, the CIE reviewed, developed and recommended the advanced CMF values defined as $\bar{x}(\lambda), \bar{y}(\lambda), \bar{z}(\lambda)$ (see figure 3.2). These modified version of CMFs satisfied factors like elimination of the negative values in the CMFs value (for example, around 500 nm, the colour matching function was shown to be negative (see figure 3.1B)) and incorporation of photopic luminous efficiency function V(λ) into the CIE system of colorimetry. These modified sets of CMFs had to follow the rules described below:

1) $\bar{x}(\lambda), \bar{y}(\lambda), \bar{z}(\lambda)$ values should be positive real integers
2) $\bar{z}(\lambda)$ should be zero for long wavelengths i.e., >650 nm
3) The value of $\bar{y}(\lambda)$ should coordinate with V(λ) (luminosity function) of the standard observer
4) 3 equal proportions of $\bar{x}(\lambda), \bar{y}(\lambda), \bar{z}(\lambda)$ should result in equal energy white light.

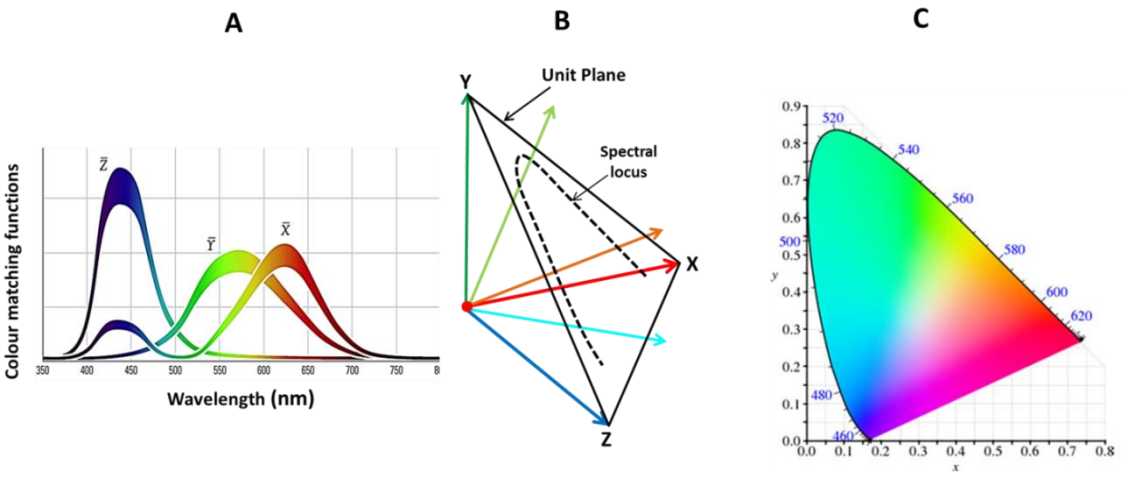

Figure 3-2 x,y,z colour matching functions plotted as a function of wavelength (nm),

Panel (B) plotted on a unit plane (plane where at any point the sum of three primaries is equal to 1) which can be further elaborated as shown on graph as (C) The CIE 1931 xy color space chromaticity diagram. The outer curve shows the spectral locus and the numbers denote the wavelengths of the visible spectrum in nm. The bottom straight line connecting the curve on either ends is line of purple where no colour can be produced by a monochromatic source or a single wavelength of light spectrum.

These CMFs can be linearly transformed into other sets of real or imaginary primaries such as the X, Y and Z primaries chosen by the CIE or to the cone fundamentals that underpin the normal trichromatic colour matches. This transformation can be achieved by multiplication of CMFs by a 3x3 matrix specified in CIE standards as shown in the equation below (Fairman et al 1997):

$$5)\ \begin{bmatrix} X \\ Y \\ Z \end{bmatrix} = \frac{1}{0.176,97} \begin{bmatrix} 0.490 & 0.310 & 0.200 \\ 0.176 & 0.812 & 0.010 \\ 0.000 & 0.010 & 0.990 \end{bmatrix} \begin{bmatrix} R \\ G \\ B \end{bmatrix}$$

where X, Y and Z are the revised CMFs but retain all colour matching properties whilst satisfying the drawbacks of the Wright–Guild data (1928,1931) and R, G, B, are spectral power distributions of the three primaries and the digits shown in the 3x3 matrix satisfy the drawbacks as

suggested by the CIE. The second row of the matrix describes the ratio of the luminance coefficients normalised to a value of 1 (see figure 3.2A).

3.2.1 CIE 1931 xyL colour space

Since the human photoreceptors can detect a wide range of wavelengths in the visible spectra, all these visible colours can be plotted and shown as a chromaticity diagram (figure 3.2C). However, perception of colour is based on two components 1) chromaticity and, 2) brightness. Considering the change in brightness with constant chromaticity can have an effect on the appearance of the surface colour, CIE XYZ colour space was intentionally devised in a way where the Y parameter defined the measure of /brightness of a colour.

As per CIE standards, all the tristimulus values were converted into positive values and were denoted as $x = \frac{X}{X+Y+Z}, y = \frac{Y}{X+Y+Z}, L = Y$. The values of both x and y determine the chromaticity of a colour (see figure 3.2C) and L defines the luminance. The L can be assumed as the line perpendicular to equal energy point at the center of the colour space. The curved area is called the spectral locus and all the colours in this area are monochromatic and the bottom straight line is called the line of purples and these colours are not produced by a monochromatic source.

3.3 Cone fundamentals

Twenty years after the 1931 standard observer was established, Stiles and Burch conducted experiments to redefine the CMFs using 2^0 and 10^0 heterochromatic intensity matching bipartite visual fields presented on a custom designed colorimeter (Stiles and Burch, 1955). Their results suggested experimentally significant differences between the standard observer data and 2^0 pilot data but those differences were reported to be not large enough to influence the standard

data for practical colorimetry (Wyszecki and Stiles, 1982). The stimuli we used in our experiments are based on modified Stockman and Sharpe (2000) fundamentals which account to pre-receptoral filtering and adjustment in optical density of photopigments derived from the Stiles and Burch 10^0 CMFs that accommodate large field testing and S- cone sensitivity measurements.

The cone fundamentals as described in chapter 1 are the human colour matching properties defined by the sensitivity of individual cone class to the visible spectrum. The three cone fundamentals derived from L-, M- and S- cone populations' overlap to a great extent throughout the visible spectrum. This overlapping of spectral sensitivities makes isolation of cone responses difficult. This issue was addressed by experiments conducted by Vos and Walraven (1971), Smith and Pokorny (1975), and Stockman et al (1993) by using protanopes and deuteranopes to obtain normal M and L cone sensitivities respectively. Stockman and Sharpe (1998) furthered the experiments by deriving the normal human S-, M- and L- cone fundamentals by examining dichromats and monochromats of known genotypes (Stockman and Sharpe, 2000).

The Stockman and Sharpe fundamentals use a heterochromatic flicker photometry with a 2^0 diameter test light and a 2^0 reference light presented on a 18^0 diameter steady background. The reference light is usually set at 560 nm while test light varied randomly between 400 to 700 nm in 5 nm presented in opposite phase at 16 Hz on a conventional Maxwellian-view optical system. To measure these sensitivities, firstly, flicker reference light is adjusted to the threshold and after the mean threshold value is calculated, reference light is set at $0.2\log_{10}$ unit above this value. The subject is then required to alter the intensity of the flickering test field until the flicker disappears. This is performed as a

function of randomly picked wavelengths of light thereby producing isolated cone spectral sensitivities.

3.4 Transformation of cone fundamentals into CMFs

Although cone fundamentals are the direct measures of the spectral sensitivities of each cone class, for convenience and precision they are usually defined in terms of CMFs (Stockman and Sharpe, 1998). The basis for a colour match between the test and the mixture of primaries can be determined at the level of cone photoreceptors as the quanta absorbed in the photopigments of all photoreceptors for both the fields (test and mixture) would be identical. Given that the quantal catch in both the test and mixture of primaries is equal, we can express their relationships in equations as given below:

$$\bar{l}_R\bar{r}\,(\lambda) + \bar{l}_G\bar{g}\,(\lambda) + \bar{l}_B\bar{b}\,(\lambda) = \bar{l}(\lambda)$$

$$\bar{m}_R\bar{r}\,(\lambda) + \bar{m}_G\bar{g}\,(\lambda) + \bar{m}_B\bar{b}\,(\lambda) = \bar{m}(\lambda)$$

$$\bar{s}_R\bar{r}\,(\lambda) + \bar{s}_G\bar{g}\,(\lambda) + \bar{s}_B\bar{b}\,(\lambda) = \bar{s}(\lambda)$$

Where $\bar{l}_R$, $\bar{l}_G$ and $\bar{l}_B$ are L cone sensitivities to red (R), green (G) and blue (B) primaries, $\bar{m}_R$,$\bar{m}_G$ and $\bar{m}_B$ M cone sensitivities and $\bar{s}_R$,$\bar{s}_G$ and $\bar{s}_B$ S cone sensitivities respectively. Since S- cones are relatively insensitive to the longer wavelengths of the spectrum, it can be assumed that $\bar{s}_R$ is effectively zero for a red primary (R) (Stockman and Sharpe, 1998). The remaining eight unknowns can be linearly transformed as shown in the equations below:

$$\begin{bmatrix} \bar{l}_R & \bar{l}_G & \bar{l}_B \\ \bar{m}_R & \bar{m}_G & \bar{m}_B \\ \bar{s}_R & \bar{s}_G & \bar{s}_B \end{bmatrix} \begin{bmatrix} \bar{r}(\lambda) \\ \bar{g}(\lambda) \\ \bar{b}(\lambda) \end{bmatrix} = \begin{bmatrix} \bar{l}(\lambda) \\ \bar{m}(\lambda) \\ \bar{s}(\lambda) \end{bmatrix}$$

Where $\bar{r}(\lambda)$, $\bar{g}(\lambda)$ and $\bar{b}(\lambda)$ represent the CMFs and the first, second and third row in the 3x3 matrix indicates sensitivities of L, M and S cones to red (R), green (G) and blue (B) primaries respectively.

$$\begin{bmatrix} \bar{l}_R & \bar{l}_G & \bar{l}_B \\ \bar{m}_R & \bar{m}_G & \bar{m}_B \\ 0 & \bar{s}_G & \bar{s}_B \end{bmatrix} \begin{bmatrix} \bar{r}(\lambda) \\ \bar{g}(\lambda) \\ \bar{b}(\lambda) \end{bmatrix} = \begin{bmatrix} \bar{l}(\lambda) \\ \bar{m}(\lambda) \\ \bar{s}(\lambda) \end{bmatrix}$$

Since we are concerned with relative spectral sensitivities of L, M and S cones rather than their absolute values, the eight unknowns' can be further disintegrated into five.

$$\begin{bmatrix} \bar{l}_R/\bar{l}_B & \bar{l}_G/\bar{l}_B & 1 \\ \bar{m}_R/\bar{m}_B & \bar{m}_G/\bar{m}_B & 1 \\ 0 & \bar{s}_G/\bar{s}_B & 1 \end{bmatrix} \begin{bmatrix} \bar{r}(\lambda) \\ \bar{g}(\lambda) \\ \bar{b}(\lambda) \end{bmatrix} = \begin{bmatrix} k_l\bar{l}(\lambda) \\ k_m\bar{m}(\lambda) \\ k_s\bar{s}(\lambda) \end{bmatrix}$$

Where k_l,k_m and k_s are the scaling coefficients that determine the type of normalization of cone fundamentals. Using the results from their experiments, Stockman et al. (1999) suggested a new transformation based on Stiles and Burch 10^0 CMFs into cone fundamentals as shown below:

$$\begin{bmatrix} 2.802296 & 10.973728 & 1 \\ 0.167289 & 8.235906 & 1 \\ 0 & 0.010600 & 1 \end{bmatrix} \begin{bmatrix} \overline{r}\,(\lambda) \\ \overline{g}\,(\lambda) \\ \overline{b}\,(\lambda) \end{bmatrix} = \begin{bmatrix} k_l \overline{l}\,(\lambda) \\ k_m \overline{m}\,(\lambda) \\ k_s \overline{s}\,(\lambda) \end{bmatrix}$$

Where $\overline{l}\,(\lambda), \overline{m}\,(\lambda)$ and $\overline{s}\,(\lambda)$ are the relative cone receptor sensitivities and $\bar{r}$, $\bar{g}\ and\ \bar{b}$ are the Stiles and Burch 10^0 CMFs.

3.5 Four Primary ganzfeld stimulator

Shapiro & Pokorny, (1996) were the first to postulate that four-primary colorimetric system can be used to independently manipulate the excitation of the four classes of photoreceptor populations in the human eye. According to their hypothesis, this method allows us to examine individual photoreceptor class contributions to various post-receptoral pathways.

Compared to conventional methods for recording ERGs, the four-LED ganzfeld stimulator offers a number of advantages like 1) it allows recording responses from one class of photoreceptor while maintaining the other three constant, 2) permits independent control of stimulation of three types of cones and rods at the same chromaticity, light level and retinal locus (Shapiro et al, 1996 and Pokorny et al, 2005) and 3) examination of rod-cone interactions under mesopic conditions (Zele and Cao, 2014).

We generated all of our experimental stimuli on a commercially available four-primary ganzfeld ERG system (ColorDome and Espion E^2, Diagnosys, Cambridge, UK). To investigate the interactions between four classes of photoreceptors, four different LED types are essential to examine each photoreceptor type in isolation. To accomplish this, we used the method of silent substitution (Estévez & Spekreijse, 1982). Using our photostimulator and employing silent substitution (as discussed in chapter 2) allowed us to silence

upto 3 photoreceptor classes. This was possible by adjusting the excitation of remaining photoreceptor population and altering the radiances of wavelengths of four classes of LEDs The L-, M- and S- cone and rod excitations for any given light source with the spectral distribution of $E_{X,Y}$ can be calculated as shown below:

$$E_{X,Y}(t) = F_R.L_Y(t). \begin{bmatrix} \sum_\lambda I_R(\lambda)A_l(\lambda) & \sum_\lambda I_R(\lambda)A_m(\lambda) & \sum_\lambda I_R(\lambda)A_s(\lambda) & \sum_\lambda I_R(\lambda)A_r(\lambda) \\ \sum_\lambda I_G(\lambda)A_l(\lambda) & \sum_\lambda I_G(\lambda)A_m(\lambda) & \sum_\lambda I_G(\lambda)A_s(\lambda) & \sum_\lambda I_G(\lambda)A_r(\lambda) \\ \sum_\lambda I_B(\lambda)A_l(\lambda) & \sum_\lambda I_B(\lambda)A_m(\lambda) & \sum_\lambda I_B(\lambda)A_s(\lambda) & \sum_\lambda I_B(\lambda)A_r(\lambda) \\ \sum_\lambda I_A(\lambda)A_l(\lambda) & \sum_\lambda I_A(\lambda)A_m(\lambda) & \sum_\lambda I_A(\lambda)A_s(\lambda) & \sum_\lambda I_A(\lambda)A_r(\lambda) \end{bmatrix}$$

$E_{X,Y}$ = photoreceptor excitation (X) by a particular class of LED (Y)

F_Y= conversion factor for a class of LED involving the photometric measurements to the fundamentals.

L_Y = luminance of a particular class of LED

t= changes as function of time

$I_Y(\lambda)$= emission spectrum of a LED at unit luminance

$A_X(\lambda)$ = photoreceptor fundamental

Total excitation of each class of photoreceptor depends on the sum of the excitations produced by each LED.

Using the above equation (equation 3.1), we calculated numerical values of the photoreceptor sensitivities to individual LEDs relative to the total sensitivity as shown in the 4x4 matrix shown below:

$$E_{X,Y}(t) = \begin{bmatrix} 0.000229445 & 0.08157226 & 0.2870788 & 0.00307697 \\ 0.015093494 & 0.32595908 & 0.18308088 & 0.20938359 \\ 0.984467308 & 0.2919551 & 0.11793258 & 0.7624646 \\ 0.000209753 & 0.30051356 & 0.41190773 & 0.02507484 \end{bmatrix} \ldots . Eq\ 3.2$$

The inverse of equation is then multiplied by the desired LED contrast (L_c) to achieve cone or rod isolating stimuli for the desired photoreceptor contrast (P_c). For example to obtain a desired L cone contrast of 11%, remaining photoreceptor contrasts are set at zero and to generate this stimulus condition, desired LED values were multiplied by the inverse $(E_{X,Y})^{-1}$ of the 4x4 matrix as shown in equation (equation 3.2)

$$Lc=\begin{bmatrix} L \\ M \\ S \\ R \end{bmatrix} \rightarrow Lc = \begin{bmatrix} 0.11 \\ 0 \\ 0 \\ 0 \end{bmatrix}$$

$$Pc=Lc*(E_{X,Y})^{-1}$$

The stimulus parameters obtained using these calculations was then modulated at different temporal frequencies assuming that the pupil diameter is 8 mm. we used a software to generate script files that comprised of details like luminance, modulation depth and phase of each stimulus condition which were then transferred to the Espion ganzfeld stimulator where all these stimuli were presented to obtain ERGs.

The numerical values used in the matrix are taken from Prof Jan Kremers calculations on photoreceptor sensitivities to individual LED classes used in our laboratory.

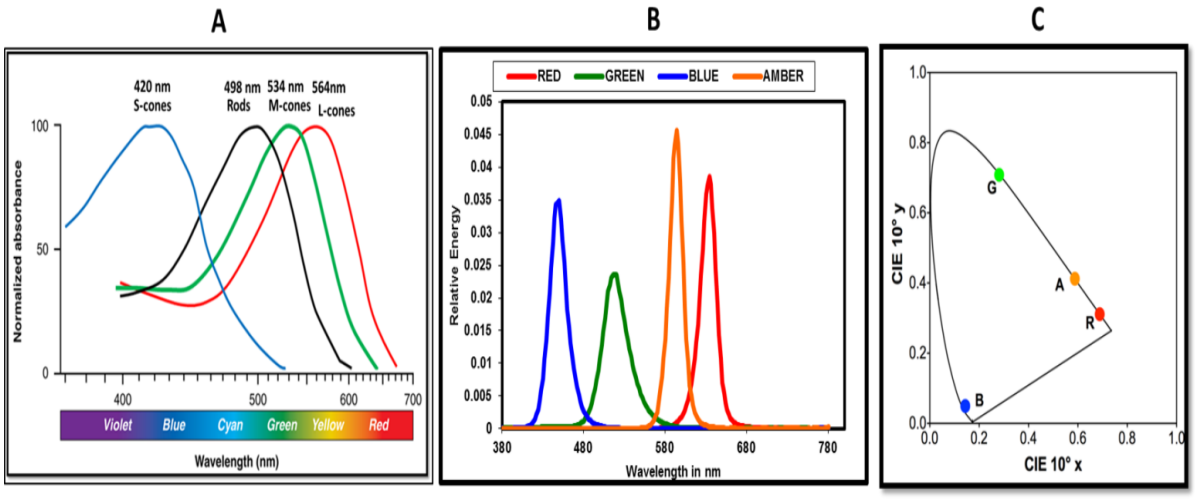

Figure 3-3 (A) The relative (normalised) spectral sensitivities of rods, S-, M-, and L cones plotted as a function of wavelength, (B) LED spectral distributions of our equipment and (C) LED chromaticities in 1964 CIE 10^0 space.

The Espion 2 ColorDome system has two LED units, one attached on either side of the front hole, which contains red, green, blue and amber LEDs. The circuit as shown on (see figure 3.4 (left)) contains three rings of LEDs, a bright ring, a dim ring and a low dim ring that allows a dynamic stimulus range and offers a resolution of 64000 steps per ring. The calibration of these LEDs is supported by the internal system with an integrated calibration routine which requests for auto-calibration when we switch on the Diagnosys system.

We used PR650 spectrophotometer (Photo Research Inc, Chatsworth, California, USA) to calibrate spectral characteristics, chromaticities and luminances of each class of LED. The peak wavelengths (± half-bandwidth at half-height) of blue, green, amber and red LEDs of our ganzfeld stimulator as measured using this instrument were observed to be at 460 nm (±15), 514 nm (±20), 590 nm (±8), and 635 nm (±10) respectively (see figure 3.3B and 3.3C).

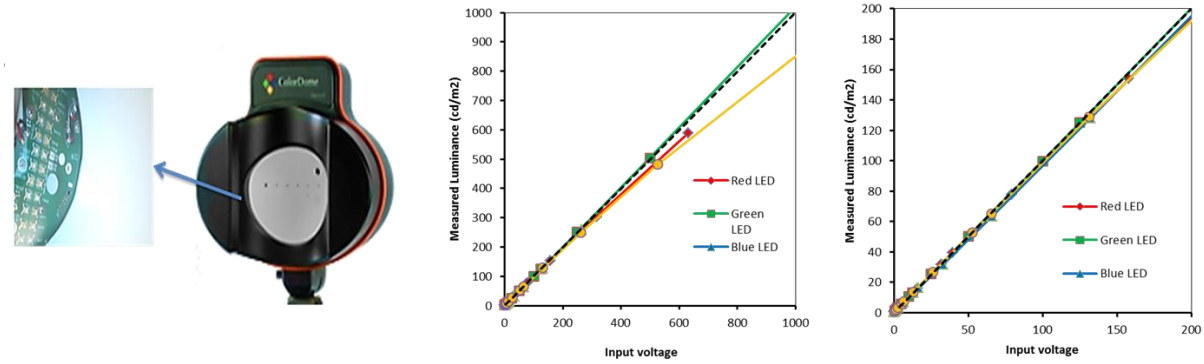

Figure 3-4 shows circuit board comprising of LEDs located on either side of the front hole (left).

Luminances measured as a function of input voltage for each class of LEDs (right).

3.5.1 Calibration of photostimulator

Calibration of the ganzfeld stimulator was performed by measuring the luminance and spectral output of the LED output as well as characterisation of each LED output as a function of voltage input (Pokorny et al 2004). The spectral output of each LED was measured at 5 nm intervals with a PR-650 spectroradiometer positioned at the front port hole of the ganzfeld stimulator. The mean luminance of our stimuli was maintained below 238.73 cd/m^2. Above this luminance level, red and amber LEDs were shown to deviate from linearity which could impact cone isolation. Luminances of the LEDs were set by voltage input. The relationship between LED voltage and luminance was linear below 300 candela/m^2 (see figure 3.4(right)).

3.6 General experimental procedures

Subject preparation

All the ERG recordings were carried out in the Visual Electrodiagnostic unit of School of Optometry and Vision Sciences at University of Bradford. The number of participants who took part in different experiments varied and the informed consent was obtained after nature and possible consequences of the study were explained to all the participants. All the experimental protocols adhered with the tenets of the Declaration of Helsinki and all experiments were approved by the Institutional ethics committee.

3.6.1 (A) Colour vision tests

To confirm their colour vision status, all participants were tested using Ishihara pseudoisochromatic chart, Farnsworth-Munsell 100 Hue test and HMC anomaloscope *(Oculus* Optikgeräte GmbH, Germany). These tests were performed prior to the first recording session on all participants to evaluate their colour vision. Based on these results we categorised our participants into dichromats and normal trichromats whose results allowed us to compare cone ERGs of our interest for both conditions and to see if isolation was complete (described in detail in chapter 4 and 5).

(a) Ishihara pseudoisochromatic plates

We used Ishihara test as a screening tool to detect colour vision deficiency. Ishihara test has the most complex design layout with isoluminant circular discs that vary in brightness, color and sizes with differently coloured numerals and tracing lines on a uniformly coloured background. The coloured dots that are chosen based on the axis of confusion of colour deficient observers are arbitrarily arranged on these plates in such a way that a normal trichromat can identify numerals or tracing lines within the array of dots while a dichromat or an anomalous trichromat may not identify or misread the number. Although it is an inexpensive, easy and quick way to evaluate colour vision deficiencies, tritan defects cannot be detected using this test and another drawback of this test is that it cannot provide the degree of dichromacy (Birch, 1993). Reading error of <4 and >4 out of 24 plates of the 38 plates Edition (1979) was considered as normal and colour defective observers respectively. We used this test for screening and identifying participants with normal and reduced form of colour vision.

(b) Farnsworth-Munsell 100 hue test

This test evaluates the ability to discriminate hue and is an effective way to detect moderate and severe forms of colour vision deficiency. This test consists of 85 caps with their surface covered by Munsell colour paper. The caps are grouped into four sets. Each of these boxes constitutes a quadrant of the circle in the chromaticity diagram. In each tray, two caps are fixed on either end and the observers are instructed to arrange the randomly presented pigmented caps with a gradual progression in their hue composition between these two fixed caps.

Each cap has a number beneath it which allows the examiner to know its position relative to the adjacent caps. This test was performed under room illumination

with the measurement of 410 lux using illuminometer (Model 5200, Robin electronic Ltd). Once the observer is done with arrangement of caps, we noted the numbers for calculation of error score. Error score was calculated by the sum of differences between two adjacent caps. This test was repeated twice on each subject to check the accuracy of the results. Hue discriminating ability of an observer could be evaluated depending on his/her total error score and the nature of colour deficiency could be assessed based on their corresponding hue plots. The total error score of 50 or less was considered as normal and anything above this value was considered as abnormal. This test has proven to show 'learning effect' and also since we performed this test under room illumination and not according to colour vision standards, we wanted to ensure that the diagnosis of colour vision deficiency was accurate and so, we further obtained results from anomaloscope, as performing FM- 100 hue test under room illumination as reported in literature showed overestimation of the total error score (Zahiruddin et al 2010).

(c) Anomaloscope

This is considered to be the most accurate test to detect and classify dichromacy and differentiate dichromats from anomalous trichromats. The stimulus is composed of a bipartite circular field with upper half composed of a ratio of two wavelengths- 670 nm (red) and 546 nm (green). The mixture of these two wavelengths is adjusted by the examiner and the total luminance of this area remains constant for all red: green ratios. The lower half is called the test field and the participant's task is to adjust the knob to change the ratio of red to green wavelengths in order to match the upper field. According to the range of colour matching by an individual observer, the status of their colour vision can be

described. When the ranges of the values had fallen within the normal limit, they were regarded as normal trichromats.

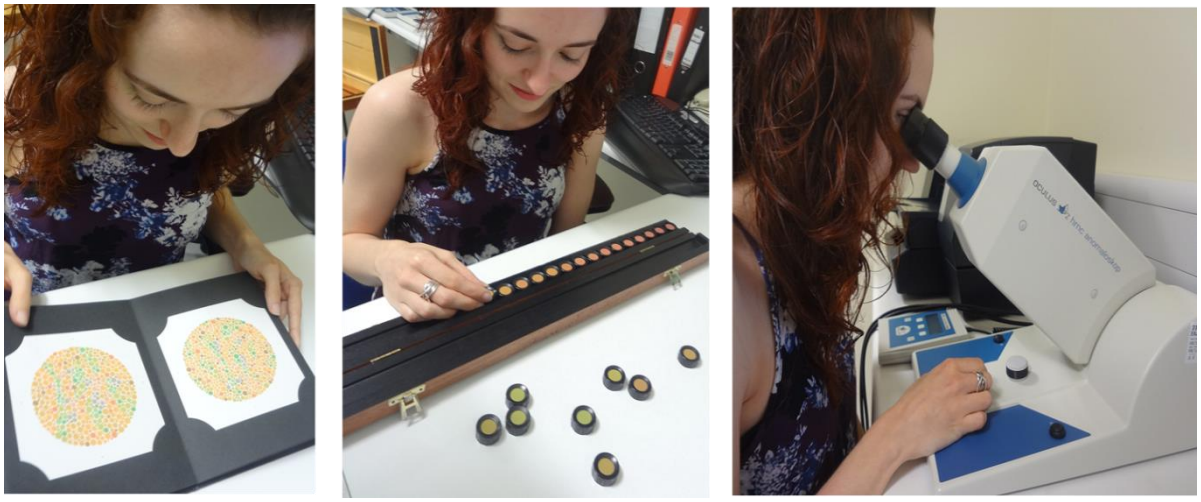

Figure 3-5 a participant performing all three Colour vision tests (left to right) Ishihara pseudoisochromatic plates, Farnsworth-Munsell 100 Hue test and Anomaloscope prior to the recording session.

In the beginning of each experimental procedure, pupillary dilatation in one eye (either right or left) of all observers was achieved using 1% Tropicamide. Stimuli were presented to each observer only after measuring pupil diameter (approximately 8 mm) to ensure uniform retinal illuminance across subjects. The head of the participant was held stable with the forehead rest. All the observers were encouraged to fixate at the central red LED subtending 1 degree of angle throughout the session.

3.6.2 Electrodes

The recording of ERG signals requires active, reference and ground electrodes. The difference in voltage between reference and active electrodes is sensed and amplified by a differential amplifier. Upon stimulus presentation, the electrical signal recorded as a consequence of the light-induced retinal activity is detected by the active electrode whilst both active and reference electrodes detect myogenic activity and the background noise. The electrical activity recorded from retina can be monitored on the computer monitor as shown in figure 3.7.

(i) Active electrode

In all our experiments we used Dawson, Trick and Litzkow (DTL) electrode which is a low-mass nylon fibre impregnated with silver and is a monopolar electrode. To achieve signal measurement of maximum amplitude, the DTL electrode was placed along the tear prism above the lower lid margin close to cornea. Adhesive sponge pads secure the DTL electrode to the temporal and nasal canthi. (Hébert, M. and Lachapelle, 1999). Although the recordings made with DTL electrode tend to be smaller in amplitude, these measurements were shown to be similar to the contact lens electrode (Vaegan, 1996). DTL electrode addresses limitations by other electrodes like gold-foil, Burian-Allen and skin electrodes and has several advantages like patient comfort (Yin and Pardue, 2004) increase in recording time, no use of corneal anaesthesia and lubrication, produces large and repeatable signals (Heberta et al., 1999), electrode stability, minimal impedance, good signal quality (McCulloch et al., 1998; Marmor and Zrenner, 1999) and optics of the eye remain unaffected.

ERGs recorded in our experiments are smaller in comparison to the signals recorded from neurological and myogenic activity that form background noise. The use of a differential amplifier allowed amplification of the signal thus reducing the effect of background noise.

(ii) Reference and Ground electrodes

Skin area on the temporal orbital rim near lateral canthus of ipsilateral and forehead was prepped using *Nuprep abrasive* skin preparation *gel* (D.O. Weaver, USA) prior to the positioning of reference and ground electrode respectively. This was to ensure least resistance between skin and electrodes. Surface silver-silver chloride electrodes attached adjacent to the lateral canthus of the test eye and forehead with electrode paste served as reference and ground electrodes (see figure 3.6 (left)). Impedances between electrodes were maintained below 5kΩ and were monitored throughout each experimental session. We recorded ERGs from right eyes of all participants for all the study protocols in this thesis.

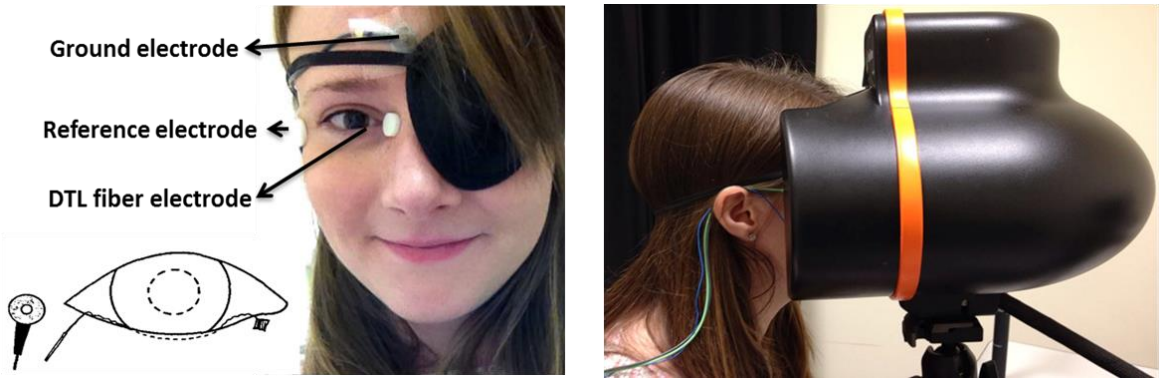

Figure 3-6 Electrode placement for monocular ERG recording with left eye occluded (left). Observer presented with stimulus on ColorDome ganzfeld stimulator (right).

3.6.3 The Stimulus presentation

A commercially available full field ganzfeld stimulator (Diagnosys LLC, Lowell, Massachusetts, USA) (see figure 3.6 (right)) was used for presentation of light stimuli in all the experiments. This instrument has been reported to have several advantages over other stimulators like conventional three primary CRT monitor (Brainard et al, 2002) as this system allows stimulation of wider area of retina, produces uniform intensity of retinal illumination, permits swift changes in luminance, generation of higher photoreceptor contrasts , narrow-band spectral emission and higher retinal illuminances. It also allows triple silent substitution, enables precise control of light output and increased depth of modulation (Shapiro et al., 1996; Murray et al, 2008).

We used sine and square wave modulation of amber, blue, red and green LEDs for different experiments with pre-defined Michelson contrasts (as described in Chapter 2). ERG responses were amplified and filtered at a bandwidth of 1 to 300 Hz and sampled at a rate of 1000 Hz. Epochs varied according to the stimulus used and ranged from 100 ms (for transient stimulus) to 4 s (for steady-state stimulus).

3.6.4 ERG recording and analysis

Prior to the recording session, we made sure the impedances between the electrodes were 5kΩ. An inbuilt infra-red camera allowed us to monitor participant's fixation during the recording session. After ERGs were recorded, artifacts caused by blinks and eye movements were manually eliminated before averaging the signals as they may influence the measurements of the ERGs recorded. For all stimulus conditions, responses were averaged and the number of sweeps for each step in all experimental protocols varied and addition of sweeps depended on the signal quality.

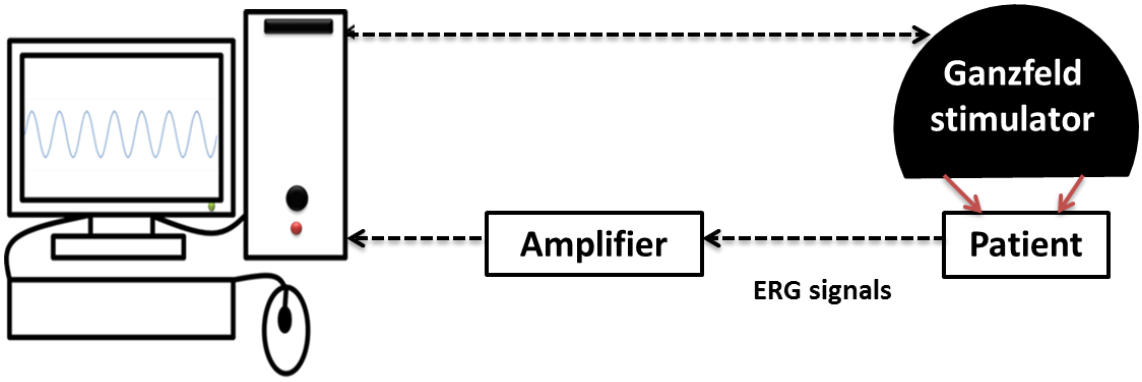

Figure 3-7 showing experimental set-up with patient positioned facing the front of the ganzfeld stimulator.

Upon stimulus presentation, the electrodes sense the signals obtained from the retinal photoreceptors and relay the signals to the amplifier and then to the PC where ERG signals could be monitored.

Post signal acquisition, for steady-state ERGs, the averaged traces underwent two stage offline analyses. 1) Resampling of averaged ERG traces was necessary as the signal epoch was 4 seconds resulting in 4000 sampling points. To make the signal waveform compatible for the fast Fourier transform analysis, we had to resample the signal at a sampling frequency of 1024 Hz to achieve 4096 points

and 2) these modified signals were further subjected to FFT analysis to extract signal amplitude and phase information at a temporal frequency of interest. The averaged signals obtained from each observer were subjected to Fourier analysis using a ED1401 plus interface running Signal (version 2.16) software (Cambridge Electronic Design, Cambridge, UK) for the extraction of amplitude and phase information in experiments where sinusoidal modulation was used. A measure of noise was obtained at a frequency below the fundamental response amplitude (n-1). For example (see figure 3.8), for fundamental response amplitude at 30 Hz (n), noise was measured at 29 Hz (30-1 Hz).

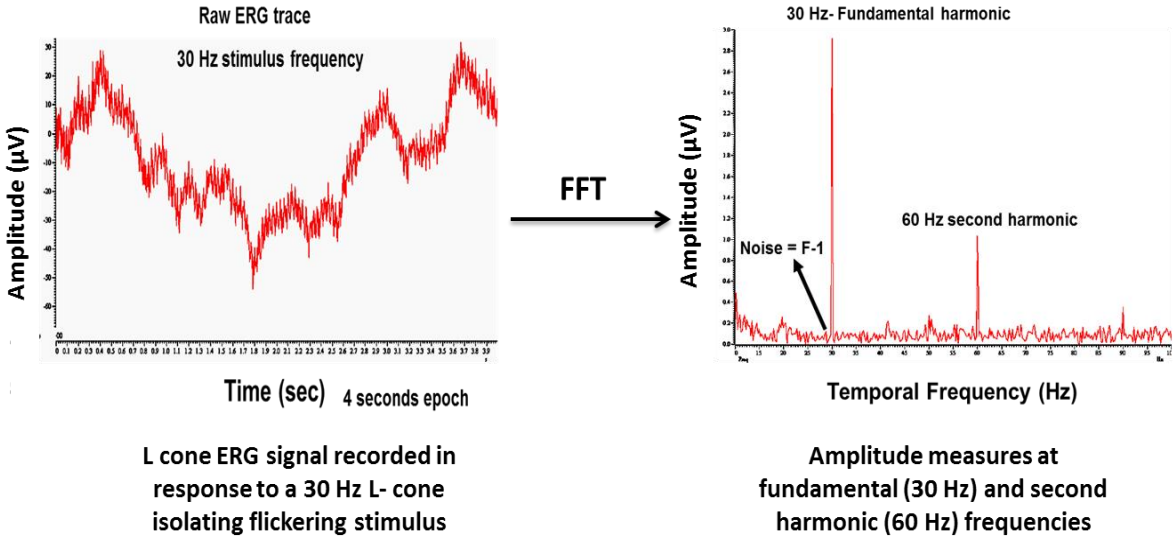

Figure 3-8 showing L cone driven ERG signal as a function of time

The signals are obtained at a stimulus frequency of 30 Hz (left) with subsequent Fourier transform (right) showing amplitude of fundamental (F) and second harmonic (2F) with F-1 as a measure of noise as a function of frequency plotted as a function of temporal frequency.

3.7 Repeatability of steady state cone isolated ERG

Since the biological measurements vary from time to time, it is essential to consider the effect of these variations when assessing clinical and research data. We conducted a pilot study to assess repeatability measures of L- and M- cone isolating ERGs derived in response to sinusoidally modulated L- and M- cone isolating stimuli presented on the Espion 2 ColorDome system. A total of five participants (one male and four female) with age ranging from 19-33 years (Mean±Stdev=27.2± 5.40) were recruited in this experiment. All the participants had best corrected visual acuity of 6/6 Snellen acuity in both eyes and normal colour vision with no ocular pathology or medical history that would affect ERGs. L- and M- cone ERGs were recorded on two different occasions (two weeks apart) by the same examiner. Before each recording session, left eye pupils of each participant were dilated using 1% Tropicamide and we made sure that the pupils were fully dilated to about 8 mm and also that the participants were not pre-exposed to bright light.

The first peaks recorded in response to onset and offset stimuli that were comparable to components on a conventional Flash ERG were marked up on L- and M- cone ERGs elicited by square-wave pulse stimuli

The average time taken for colour vision testing and recording ERGs were about 20-25 minutes in a given session. To record ERGs from different photoreceptor classes on the same subject, participants were called upon their convenience.

The steady state L- and M- cone isolating stimuli we used in this experiment was of 4s duration and presented at a flickering rate of 30 Hz. All the ERGs were recorded under similar testing conditions in two different experimental sessions. The responses were acquired using a DTL electrode that served as an active electrode placed closed to the lower limbus. The waveforms were averaged over 24 sweeps for both the stimulus conditions and signals were filtered from 0.3 to 100 Hz. Large artefacts due to blink and eye movements were manually rejected. The signals were analysed using fast Fourier transform to obtain amplitude and phase information. These signals were sampled at a frequency of 1024 Hz. We used Wilcoxon matched-pair sign rank to test to assess intersession reliability of L- and M- cone isolated ERGs. Our null hypothesis is that there is no difference in ERG measurements obtained in both recording sessions where the alternative hypothesis was assumed to have a difference in ERG signals recorded in both sessions for both L- and M- cone isolating stimuli. Correlation coefficients (R) were calculated for amplitudes and phase of both L- and M- cone isolated ERGs and the r values are shown in table 3.1 and the R^2 values shown in figure 3.9. We used Excel for statistical analysis to analyse test-retest reliability signal amplitudes and phase for both stimulus conditions.

The Pearson correlation coefficient provides a measure of linear association between two variables. Values of correlation coefficients (R) as shown in table 3.1 are close to +1 indicating that both L and M cone amplitudes and phase obtained from two sessions are perfectly related in a linear sense, in other words these measurements were shown to be highly repeatable therefore supporting the null hypothesis.

Table 3-1 R^2 and R values for 30 Hz L and M cone amplitudes and phase

30 Hz steady state cone isolated ERGs	R^2	R (Correlation coefficient)
L cone amplitude	0.9422	0.970682
M cone amplitude	0.9208	0.959606
L cone phase	0.9828	0.991379
M cone phase	0.9575	0.978499

The test-retest L- and M- cone mean amplitudes and phase and the mean of the differences in their amplitudes and phase are shown in Table 3.2 (A&B). Our results using Wilcoxon matched-pair signed rank at p=0.05 showed no significant differences (p>0.05) in both amplitude and phase of L- and M- cone isolated ERGs. These results were plotted as test against retest amplitudes and phase for both the conditions (figure 3.9). The p-value for all the measures also support the hypothesis that the test-retest L- and M- cone amplitude and phase difference is not statistically significant and thereby, we assume these differences may not necessarily are clinically significant as well.

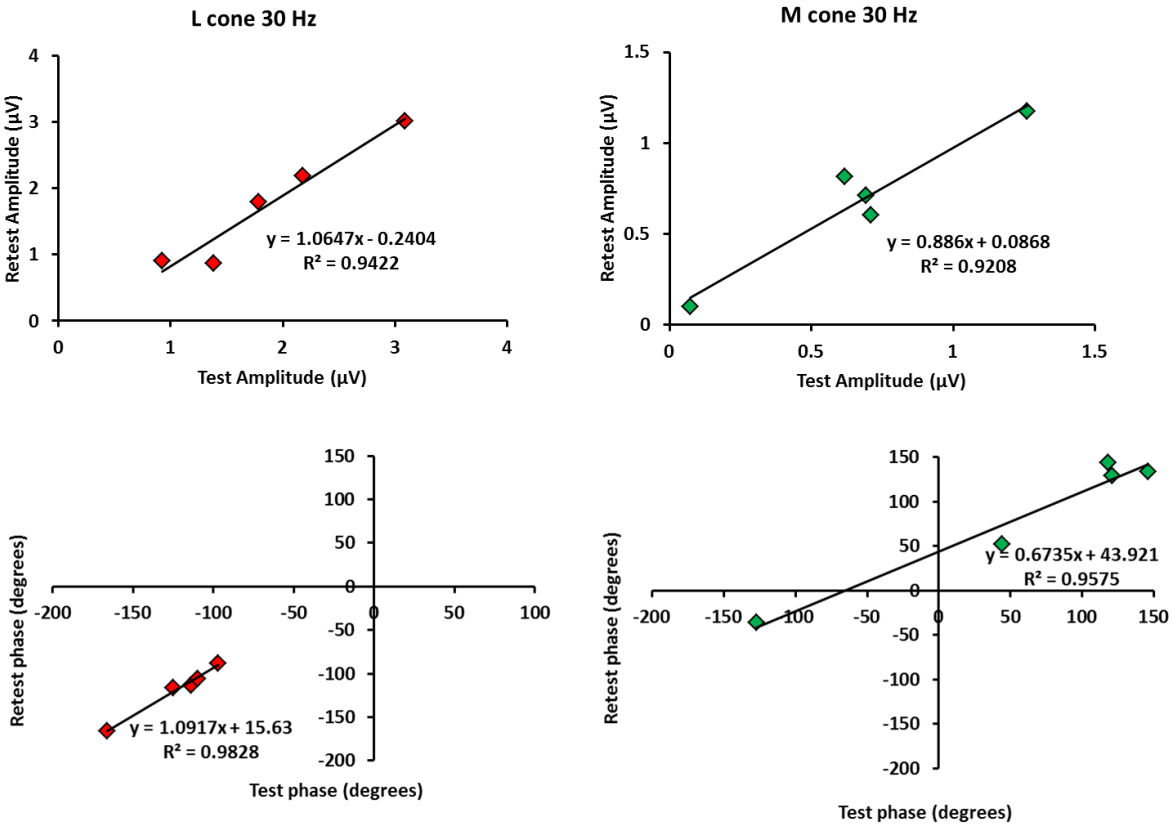

Figure 3-9 showing test vs retest 30 Hz flicker L- and M- cone driven ERG signal amplitudes (top row) and phase (bottom row) with the straight line showing perfect correlation.

Table 3-2 (A) Cone isolated ERG amplitudes for retinal illuminance of 10,000 trolands (mean luminance=198.94 cd/m^2)

30 Hz steady state ERG	Mean Amplitude (SD)		Mean Test-Retest difference (SD)	95% CI of Test-Retest Difference	Sig (p-value)
	Test	Retest			
L cone	1.872(0.824)	1.753(0.904)	0.119(0.079)	0.196	**0.584**
M cone	0.670(0.421)	0.680(0.389)	-0.010(0.032)	0.104	**0.584**

Table 3.2 (B) Mean Phase and Mean Test-Retest difference 30 Hz L- and M- cone isolated ERG amplitudes for retinal illuminance of 10,000 trolands (mean luminance=198.94 cd/m^2)

30 Hz steady state ERG	Mean Phase(SD)		Mean Test-Retest difference (SD)	95% CI of Test-Retest Difference	Sig (p-value)
	Test	Retest			
L cone	-122.4(26.349)	-118(29.017)	-4.4(4.505)	3.949	**0.371**
M cone	60.4(111.47)	84.6(76.725)	-24.2(39.68)	34.788	**0.361**

Test-retest difference was computed by the subtraction of test from retest amplitude (as shown in Table 3.2A) and phase (as shown in Table 3.2B). p-value was calculated using Wilcoxon match-pair signed rank at p=0.05.

A limitation of this experiment is that we only included small sample (n=5) for assessment of intersession reliability. Although the sample used in this experiment is small, our results showed remarkably little variation. Considering good test-retest reliability, we suggest that the ERG signals obtained in response to these stimuli seem to be consistent over a period of time and therefore probably can be used to monitor and compare normal and abnormal ERGs on two different sessions.

Chapter 4 - Incremental and decremental L- and M- cone isolated ERGs derived using square-wave pulse stimulation

4.1 Introduction

The retinal circuitry mediates transfer of light induced potentials via parallel pathways involving depolarising (DBCs) and hyperpolarising bipolar cells (HBCs) (Sterling et al., 1992). To investigate the properties of these pathways and their contribution to the typical photopic flash ERG, conventionally, a brief white increment flash presented on a rod-suppressing white background, is used. The ERG obtained in this manner is typically composed of three prominent wave components- a, b and d (Miller and Dowling, 1970; Newman, 1980; Massey et al.,1983; Heynen and van Norren, 1985a,b; Sieving et al., 1994; Xu and Karwoski, 1994; Frishman, 2006) (see figure 4.1). The a-wave is an initial negative response that appears immediately after the onset of stimulus and is reported to have contributions from different retinal cellular origins. The initial portion of the a-wave reflects cone photoreceptoral activity Brown and Wiesel, 1961; Hood and Birch, 1990a,b, 1993; Pugh et al., 1998) while the origin of the later portion is in hyperpolarising bipolar cells (HBCs) (Bush and Sieving, 1994; Sieving et al., 1994; Robson et al., 2003). Also there is evidence on the involvement of amacrine and ganglion cells to the photopic- a-wave (Friedburg et al., 2004; Ueno et al., 2006). The b-wave is the first positive peak that appears after the onset of flash stimulus and is suggested to have its origin in the depolarising bipolar cells (DBCs) (Sieving et al., 1994).

Furthermore, in the same experiment it was also shown that the amplitude and shape of the b-wave is determined by the feedback mechanisms of horizontal cells and activity of hyperpolarising bipolar cells (HBCs), and Muller glial cells.

When a longer duration white increment flash is used, another positive deflection appears around 30-40 ms after the cessation of the stimulus known as d-wave (Sustar 2006) (see figure 4.1). Many studies suggest that the rapid early phase of the d-wave reflects activity of HBCs and the origin of late slow phase component of d-wave in the cone photoreceptors (Yanagida et al., 1986). These results also stated that the DBCs influence the modelling of d-wave (Sieving et al., 1994; Ueno et al., 2006).

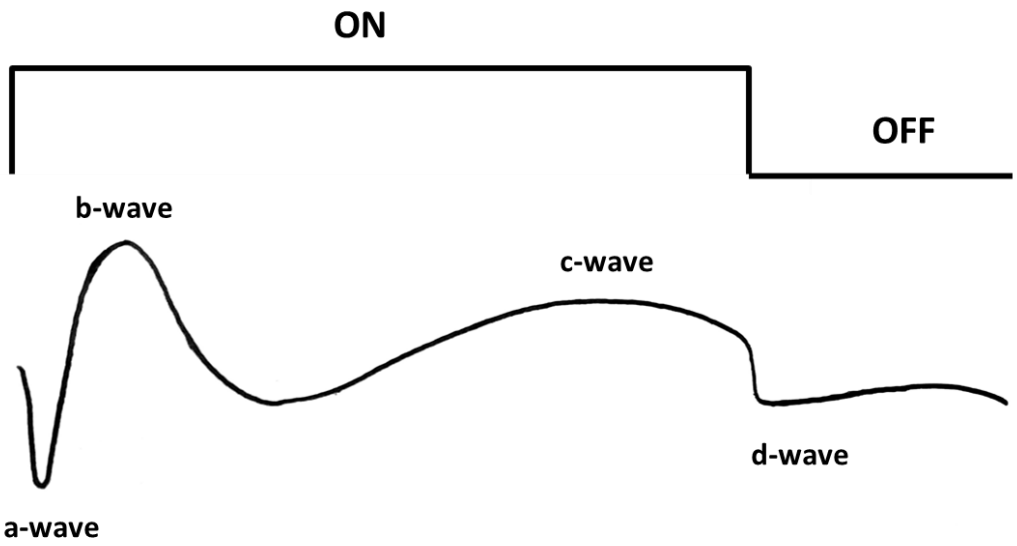

Figure 4-1 Hypothetical Human ERG waveform elicited using long duration flash stimuli. a-, b- and c- waves as observed in response to ON- stimuli and d- wave elicited in response to OFF- stimuli.

As mentioned above, ERGs provide information about the light evoked signals originating in different classes of photoreceptors and the activity of the inner retinal cells (Sieving et al., 1994; Bush and Sieving, 1996; Viswanathan et al., 2002; Kremers and Link, 2008; Friedburg et al., 2004). For chromatic processing, L- and M- cone inputs combine in an opponent manner (+L-M (L-On center, M-Off surround) or (+M-L (M-on center and L-Off surround receptive fields)) to form red-green colour vision (Lee et al., 1987; Dacey, 2000). These interactions first occur in the midget bipolar cells producing signals that are conveyed to the parvocellular pathway via midget ganglion cells. Conversely, for luminance vision, L- and M- cone inputs combine in a non-opponent, additive manner (+L+M) and these signals are transferred to the magnocellular layers of LGN via parasol ganglion cells (Derrington and Lennie, 1984; Shapley and Perry, 1986; Lee, 1996; Lee et al., 1990; Parry et al., 2012).

In the current study, we wanted to advance this knowledge by generating L- and M- cone isolating incremental and decremental square wave pulse stimulation. Literature suggests that the responses evoked by luminance increments and decrements are quite different and mediate two distinct pathways (on- and off-) that underpin these responses in the retina (Biersdorf,1968; Sieving, 1993). It has also been demonstrated that the On- and Off- cone ERGs are not to be considered as mirror-images of each other as the neuronal pathways involved in generating these signals are quite complex and contain substantial nonlinearities causing response asymmetries of these signals (Viswanathan et al., 2000; Simpson and Viswanathan, 2007; Rodrigues et al., 2010).

In order to achieve temporal separation of responses elicited by both onset and offset stimuli, several studies recommended that the flash duration of at least 100 ms and approximately until 250 ms (Evers and Gouras, 1986; Seiple and Holopigian 1994; Viswanathan et al., 1999, 2000; Kondo et al., 2000; Sustar et al., 2006; Horn et al., 2011) should be used. As a substitute to flash increments, it has been suggested that decrement square wave profiles can be used to examine d-wave as these flashes produce d-wave at the onset of the stimulus and avoids any response contamination due to blink artifacts and myogenic activity as observed in offset-d waves (Horn et al., 2011).

The rationale behind the need for functional isolation of photoreceptor specific ERGs is that each of these photoreceptor types interact with the postreceptoral neurons in a different manner and these interactions form the physiological substrate for chromatic and luminance vision. Furthermore, each of them may have different susceptibilities to different disease processes and the knowledge of the isolated responses from these photoreceptor classes may allow us to assess functional changes in each photoreceptor class in various acquired and hereditary retinal disorders and also in monitoring the effectivity of treatment strategies (Miyake et al., 1987; Sieving, 1993; Viswanathan et al., 1999; Kremers et al., 1999; Khan et al., 2001; Barnes et al., 2002).

The objectives of this study were to: (i) evaluate the feasibility of using transient square-wave pulse stimuli in achieving isolated L- and M- cone ERGs, (ii) assess to what extent L- and M- cone ERGs can determine the operation of cone-opponent, chromatic and cone-non-opponent, luminance pathway mechanisms, and (iii) validate the use of silent substitution in obtaining L- and M- cone isolated ERGs by using dichromats as controls.

4.2 Methods

4.2.1 Subjects

A total of 19 healthy human subjects (12 male and 7 female) with age ranging from 11 to 64 (Mean age=32.6 years) and four dichromats (all males) (2 protanopes and 2 deuteranope) with age ranging from 22 to 60 years (mean age= 38.7 years) participated in the study. All participants recruited in this experiment had normal visual acuity and healthy eyes and were not on any medication that could affect colour vision. The dichromats were classified as deuteranopes (missing M-cone function) or protanopes (missing L-cone function) based on their Rayleigh colour matches and other basic colour vision tests (as described in chapter 3). They otherwise had normal visual acuity with no other ocular pathologies.

4.2.2 Stimuli

Full field pulse stimuli were generated on a ColorDome ganzfeld stimulator (Diagnosys LLC, Lowell, Massachusetts, USA) using the manufacturer's scripting language which provided a temporal resolution of 1 ms. Luminance of the LEDs were modulated with increment or decrement square wave pulses with duration of 500 ms (for experiment 1) and 250 ms (for experiment 2) to generate L- and M- cone isolating stimuli. Figure 4.2 illustrates the method of generation of L-cone excitation increment stimulus (+L or L-ON) and L- cone excitation decrement stimulus (-L or L-OFF). We manipulated LED luminance outputs in the similar manner as for L-cone stimuli to generate M cone excitations increment and decrement stimuli. We used a total cone contrast of 11% (see Table 4.1) and a retinal illuminance of 12000 trolands for both L- and M- cone isolating stimuli as this permits comparison of both L- and M- cone driven ERGs under identical stimulus conditions. We chose a cone contrast of 11% as this value is the maximum achievable M cone contrast on our ganzfeld stimulator whilst maintaining silent substitution. The peak wavelengths ($\pm$half-bandwidth at half height) as measured by PR650 spectrophotometer (Photo Research Inc., Chatsworth, California, USA) of the blue, green, amber and red LEDs of our stimulator were 460 nm ($\pm$15), 514 nm ($\pm$20), 590 nm ($\pm$8), and 635 nm($\pm$10) respectively. The ratio of red:amber:green:blue LED luminances was kept constant (4:7:2:2) for all stimuli (see figure 4.2, 4.3 and 4.4). The use of four-LED ganzfeld stimulator has an advantage over traditional CRT monitors in that the ganzfeld stimulator used in this study have LED emission spectra of narrow bandwidths that we assume would allow better functional isolation of signals derived from individual classes of photoreceptor populations (Murray et al., 2008).

Table 4-1 Photoreceptor contrasts (%) of the isolated L- and M- cone, luminance and compound stimuli.

Stimulus	Photoreceptor Contrast			
	L- cones	M- cones	S- cones	Rods
L- cone isolating	11	0	0	0
M- cone isolating	0	11	0	0
Luminance (LUM)	11	11	11	11
Compound (+L-M and/or +L+M)	5.5	5.5	0	0

Experiment 1 Equal mark:space ratio (250 ms: 250 ms)

In Experiment 1 full field square wave pulsed stimuli were generated on a ColorDome ganzfeld stimulator (Diagnosys LLC, Lowell, Massachusetts, USA) using the manufacturer's scripting language which provided a temporal resolution of 1 ms. Here, we used square wave temporal profiles to provide luminance increments and decrements of equal amplitudes and a time duration of 500 ms (250 ms increment & 250 ms decrement) but with opposite polarity.

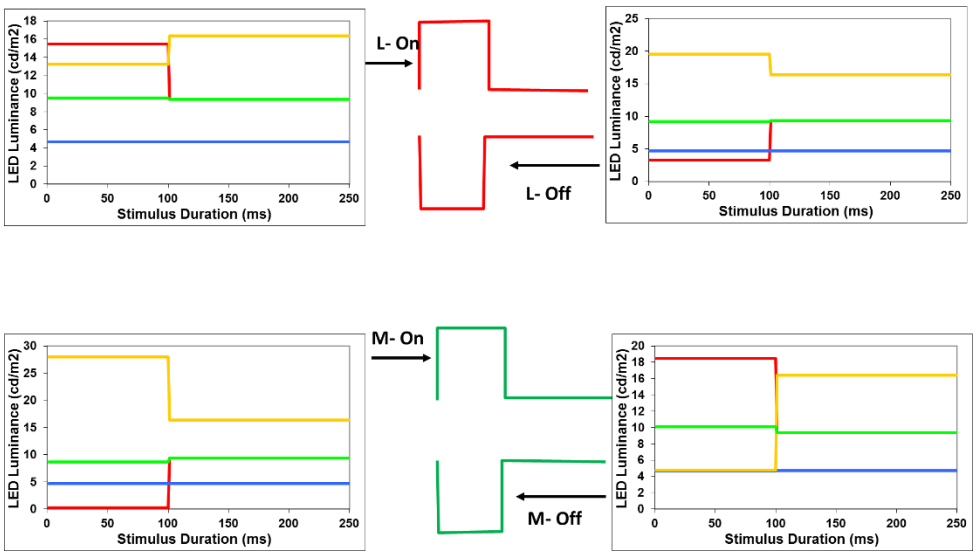

Figure 4-2 Luminance profiles of red, green, blue and amber LEDs to generate L and M cone excitations.

L-cone excitation increment (L-On), L- cone excitation decrement (L-Off) (as shown in top row), M- cone excitation increment (M-On) and M- cone excitation decrement (M-Off) (bottom row) square wave pulse stimuli with a stimulus duration of 100 ms onset and 150 ms offset (Experiment 2). Similar profiles were

used to generate 250 ms onset and 250 ms offset L- and M- cone isolating On-Off and Off-On pulse stimuli (Experiment 1).

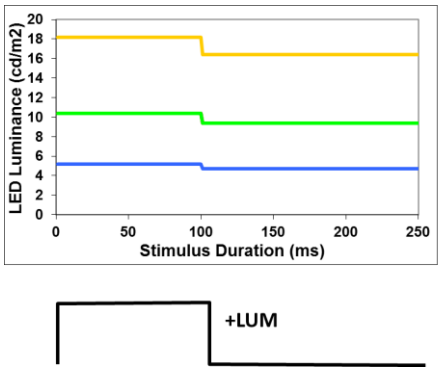

Figure 4-3 shows luminance outputs of different classes of LEDs required to generate incremental luminance flash (LUM-On) stimulation

Note that to produce these stimuli we used similar contrast (11% for each LED class) with the same polarity and are excited simultaneously.

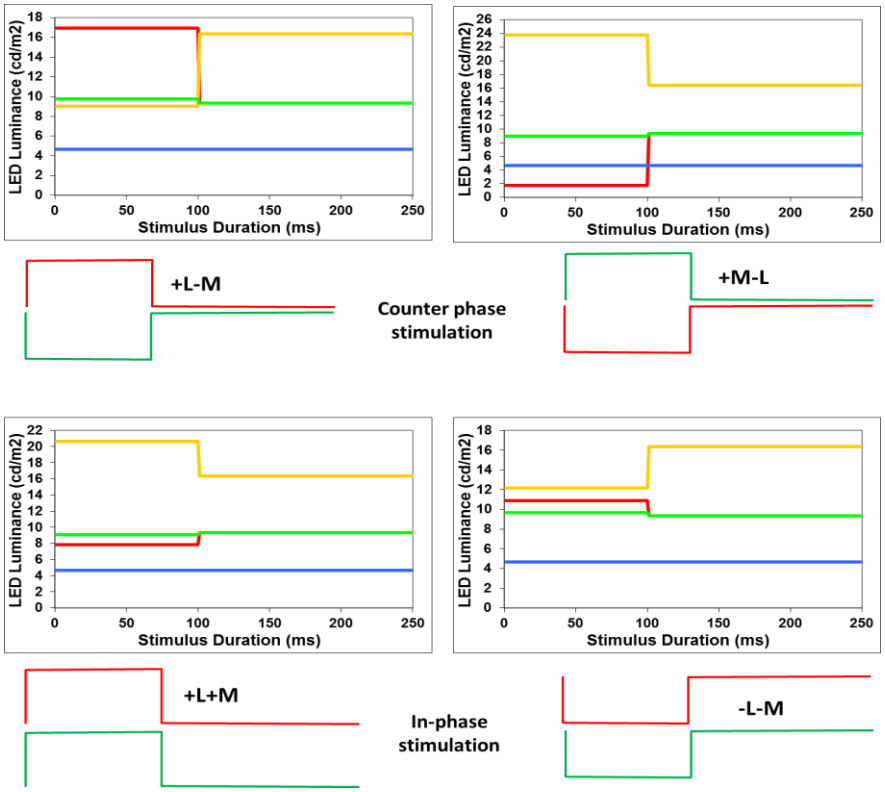

Figure 4-4 Temporal profiles of compound L- and M- cone isolating square wave pulse stimuli created using different luminance outputs of four LED classes.

The top row shows counter-phase stimulation (L-On/M-Off and M-On/L-Off) and the bottom row in-phase stimulation (L-On/M-On and L-Off/M-Off). Note that the cone contrast used to generate these stimuli for these stimuli was L=5.5% and M=5.5% respectively owing to a total contrast change of 11%.

Experiment 2 (Unequal mark:space ratio (100 ms:150 ms))

In addition to 250 ms increment and 250 ms decrement L- and M- cone isolating stimuli, we used 100 ms increment to 150 ms decrement square wave pulsed stimuli to record ERGs from L- and M- cones (figure 4.2 LED temporal profiles of square-wave pulsed L- On, L-Off, M-On and M-Off cone isolating stimuli). In addition to cone isolating stimuli, we also generated luminance square-wave stimuli (+LUM) where luminances of all four classes of LEDs increased simultaneously (see figure 4.3). Furthermore, we also generated compound stimuli counter-phase (+L-M or –L+M) and in-phase (+L+M or –L-M) L and M modulations to probe the activity of chromatic, cone opponent and non-opponent, luminance system respectively (see figure 4.4).

4.2.3 Recording

Full field ERGs were obtained for all stimulus conditions from the right eye of each participant using DTL fibre electrode (Diagnosys LCC). Twenty minutes before the commencement of the experiment, pupillary dilatation was achieved using 1% Tropicamide. An eye patch was worn over the left eye to provide comfort and to reduce blinks and photophobia when presented with stimuli. Electrodes were placed as described in chapter 3. At the beginning of the experiment, we made sure that the pupils were fully dilated (to approximately 8 mm diameter) and that the electrode impedance was below 5KΩ.

4.3 Results

4.3.1 Experiment 1 (Equal mark:space ratio (250 ms: 250 ms))

In this experiment, we used square-wave temporal pulses to stimulate L- and M-cone specific ERGs with an onset followed by an offset with stimulus duration of 250 ms each respectively with a total duration of 500 ms. Implicit times of N_{Li}, P_{Li}, P_{Mi}, a- and b-waves of L-, M- cone and luminance isolated ERGs were measured from onset of stimuli (zero) to the first negative trough and the implicit times of P_{Ld}, N_{Md}, P_{Md} and d-waves were measured from the time point of stimulus offset to the second positive peak.

Table 4-2 shows components of L- and M- cone increment and decrement ERGs that have similar response characteristics as a, b and d waves of photopic flash Electroretinogram

Components of photopic flash ERG	L cone On- Off/Off-On components	M cone On-Off/Off-On components
a-wave	N_{Li}	N_{Md}
b-wave	P_{Li}	P_{Md}
d-wave	P_{Ld}	P_{Mi}

L- & M- cone onset/offset response characteristics in normal trichromats

ERGs generated in response to L- cone isolating cone excitation increment produced an early negative component followed by a positive wave which we termed as N_{Li} and P_{Li} followed by a negative potential (LN_{Li}) that has similar features as Photopic negative response (PhNR) (see figure 4.5) which has been reported previously in primate and human photopic ERGs and is known to reflect the spiking activity of ganglion cells (Viswanathan et al., 1999; 2000; Colotto et al., 2000; Gotoh et al., 2004). When the L- cone onset stimulus terminates, we observe a positive wave (P_{Ld}) in response to the decrement flash and appears to be similar to the d-wave of the luminance ERG. Also the implicit time measurements support the argument that N_{Li} and P_{Li} wave components reflect a and b- waves of luminance ERG respectively (see table 4.2). In response to L-cone decremental stimulus, a small positive wave (PL_d) followed by a negative response (N_{Ld}) are observed (see figure 4.5).

When stimulated with M- cone isolating square wave stimuli, the ERGs obtained from these observers showed similar wave components as of luminance and L-cone ERGs. However, these responses appeared to be out of phase or in other words, M- cone response inversion was observed (see figure 4.6 and 4.9). The ERGs generated in response to the M- cone onset stimuli exhibits a small positive deflection (P_{Mi}) that mimics P_{Ld} of L- cone offset response, followed by a small negative response (N_{Mi}) that is similar to the d- wave of the luminance ERG. The decremental M- cone isolating flash stimuli generates small negative wave component (N_{Md}) followed by a positive wave (PMd). This wave then continues as a late negative potential (LN_{Md}) similar to LN_{Li} component of L-ON ERG and a PhNR of photopic flash ERGs (see figure 4.5). The implicit times of all these components are measured and displayed in table 4.3.

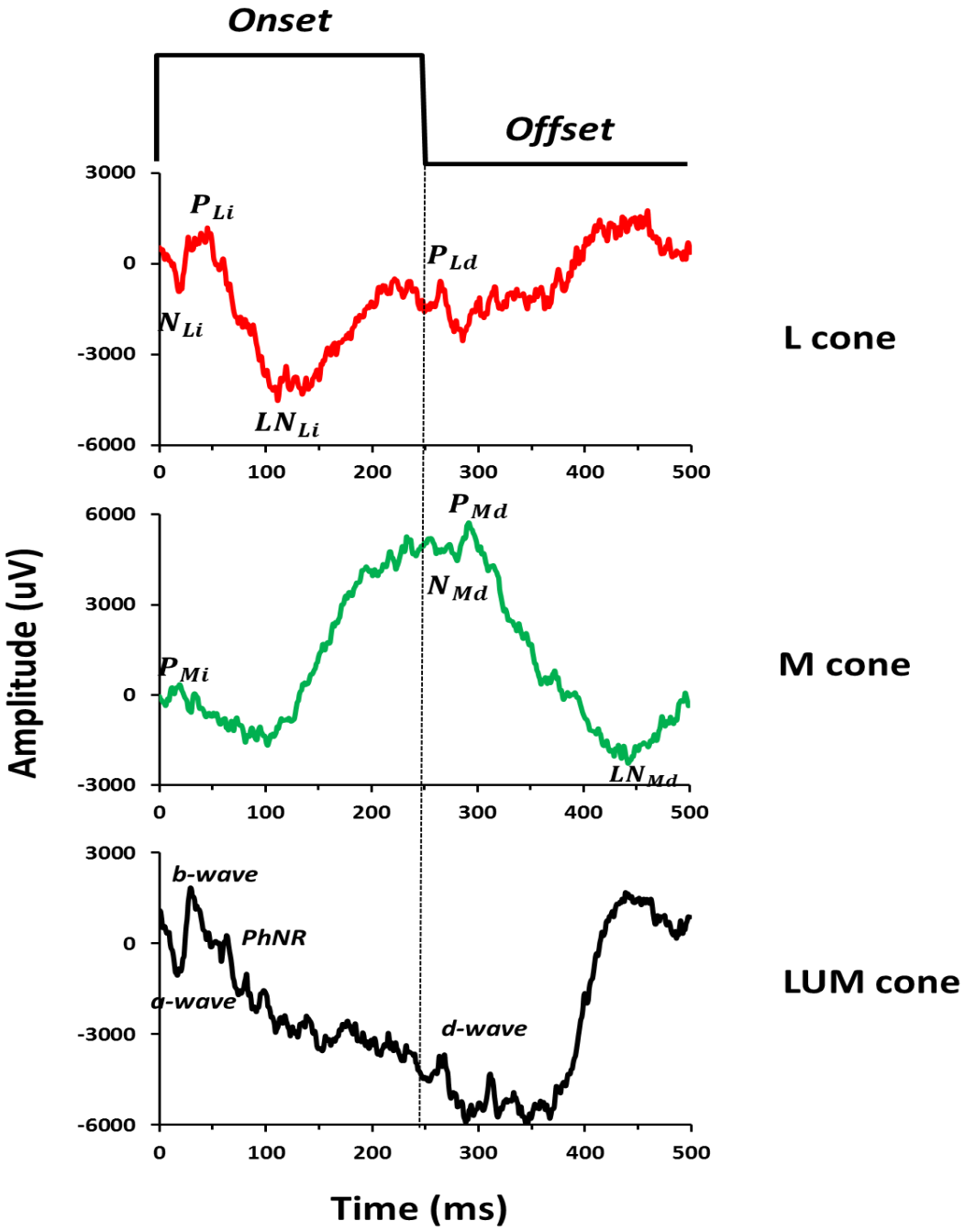

Figure 4-5 Group averaged ERGs (n=11) elicited in response to L-On/Off, M-On/Off and Luminance-On/Off equal spaced square-wave pulse stimuli with a stimulus duration of 250 ms onset and 250 ms offset.

(P=positive, N=negative, M=M- cone, L=L- cone, i=increment and d=decrement)

Table 4-3 Measured implicit times of different components of luminance, L- and M- cone isolating ERGs in normal trichromats (n=19).

ERG	Components	Implicit time (ms)	95% CI
Luminance	a-wave	16.62	15.52-17.72
	b-wave	30.09	29.05-31.13
	d-wave	17.60	15.71-19.5
L- cone	N_{Li}	17.73	16.23-19.25
	P_{Li}	34.8	31.25-38.35
	P_{Ld}	15.82	14.71-16.95
M- cone	P_{Mi}	17.26	15.8-18.73
	N_{Md}	19.85	17.05-22.66
	P_{Md}	34.40	30.61-38.21

4.3.2 Experiment 2

Unequal mark:space ratio (100 ms:150 ms)

(A) L- and M- cone isolating ERGs

Johnson and Massof (1982) reported that the offset responses to increment flashes are usually contaminated when presented with high intensity stimulus flashes by a photomyogenic reflex. However, they reported that this was rarely demonstrated when subjects were presented with decrement flashes. Since we used bright flashes in our experiments, to reduce contamination of signals from such artifacts and also to condense recording time, we further manipulated the phase of the L- and M- cone excitation increments and decrements. This approach also allowed us to examine the apparent L-M cone inversion also preserving offset responses.

Figures 4.2, 4.3, 4.4 show the LED luminance profiles used to generate L- and M- cone isolating stimuli, both as incremental and decremental stimuli. Cone isolating stimuli as described in figure 4.2, are presented with a cone excitation increment followed by a cone excitation decrement (on-off stimulus) or vice versa, i.e., an initial cone excitation decrement followed by a cone excitation increment (off-on stimulus). The top row of figure 4.6 exhibits the averaged L- cone ERG responses (n=6) to the on-off and off-on versions of the stimulus. The individual responses elicited by the L- cone on-off stimulus and L- cone off-on stimulus are displayed in figures 4.7 (left panel) and 4.8 (left panel) respectively with N_{Li} and P_{Li} generated in response to increment stimulus flash and P_{Ld} component to the cone excitation decrement (see top left panel of figure 4.6).

The L- cone off-on stimuli elicits similar response but with opposite polarity (see top right panel of figure 4.6) to that of L- cone on-off response with components P_{Ld} and N_{Ld} being elicited with the stimulus offset followed by the components that are elicited by the increment i.e., N_{Li} followed by P_{Li}. For the M- cone on-off stimulus, response inversion relative to L-cone on-off responses is observed with a positive P_{Mi}, a negative N_{Mi} component elicited by M- cone onset and N_{Md} followed by P_{Md} components to L- cone decrement (see bottom left panel of figure 4.6) and M- cone offset responses exhibited similar properties to those elicited by L- cone onset, with N_{Md} followed by P_{Md} to offset (and a P_{Mi} elicited by M- cone onset (see bottom right panel of figure 4.6). All these responses were obtained from normal trichromats.

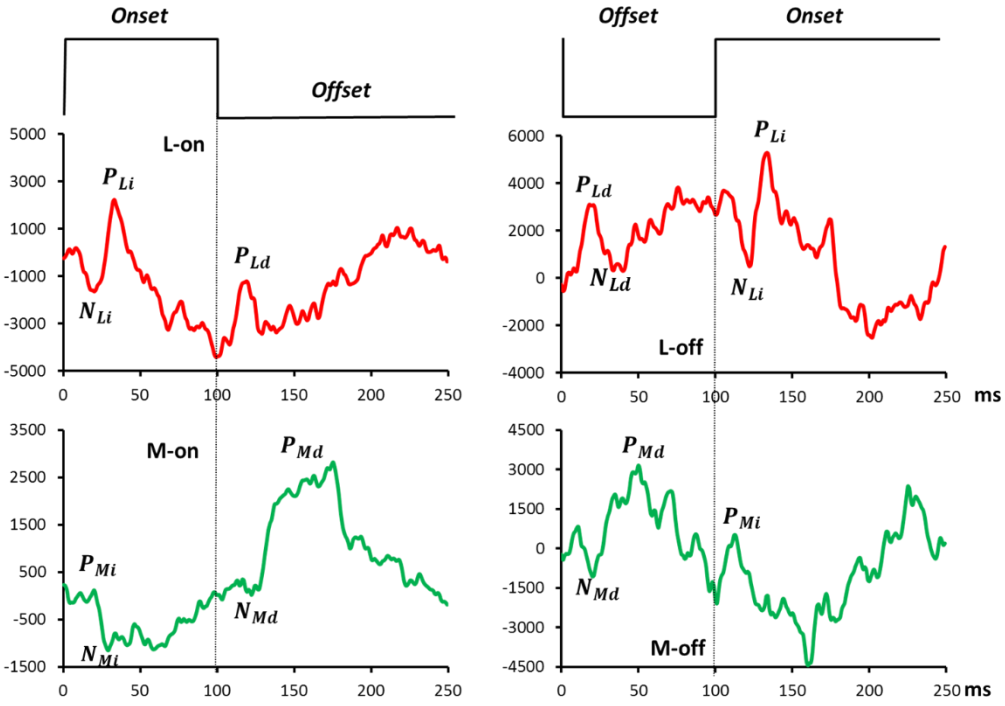

Figure 4-6 On-Off response inversion of the M- cone ERG in normal trichromats.

Mean L- and M- cone driven ERGs (n=6) elicited in response to L- and M- cone on-off (increment followed by a decrement) and off-on (decrement followed by an increment) square-wave pulse stimuli.

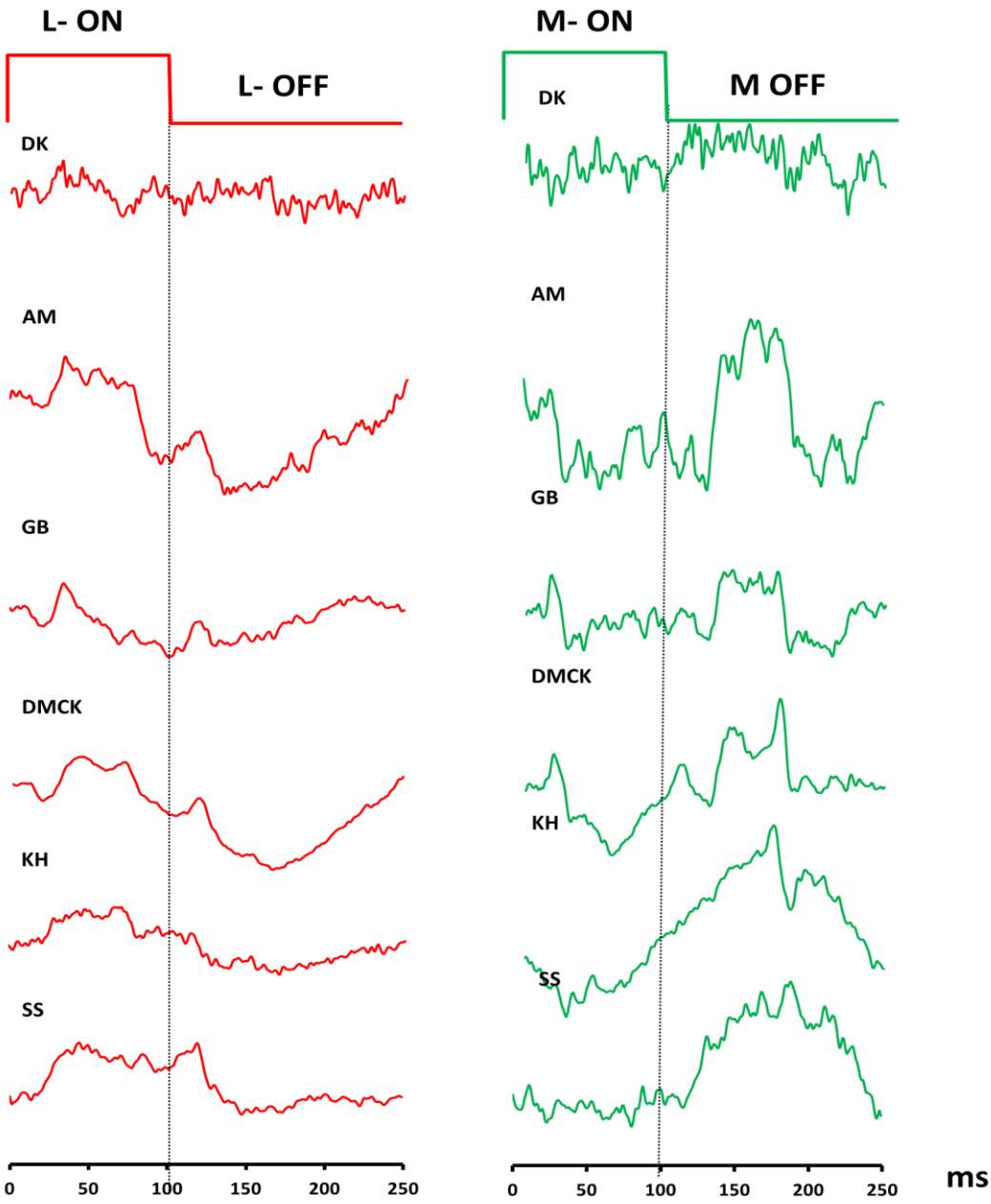

Figure 4-7 Individual L-On and M-On driven ERGs obtained in response to 100:250 ms on/off transient, square- wave pulse stimuli.

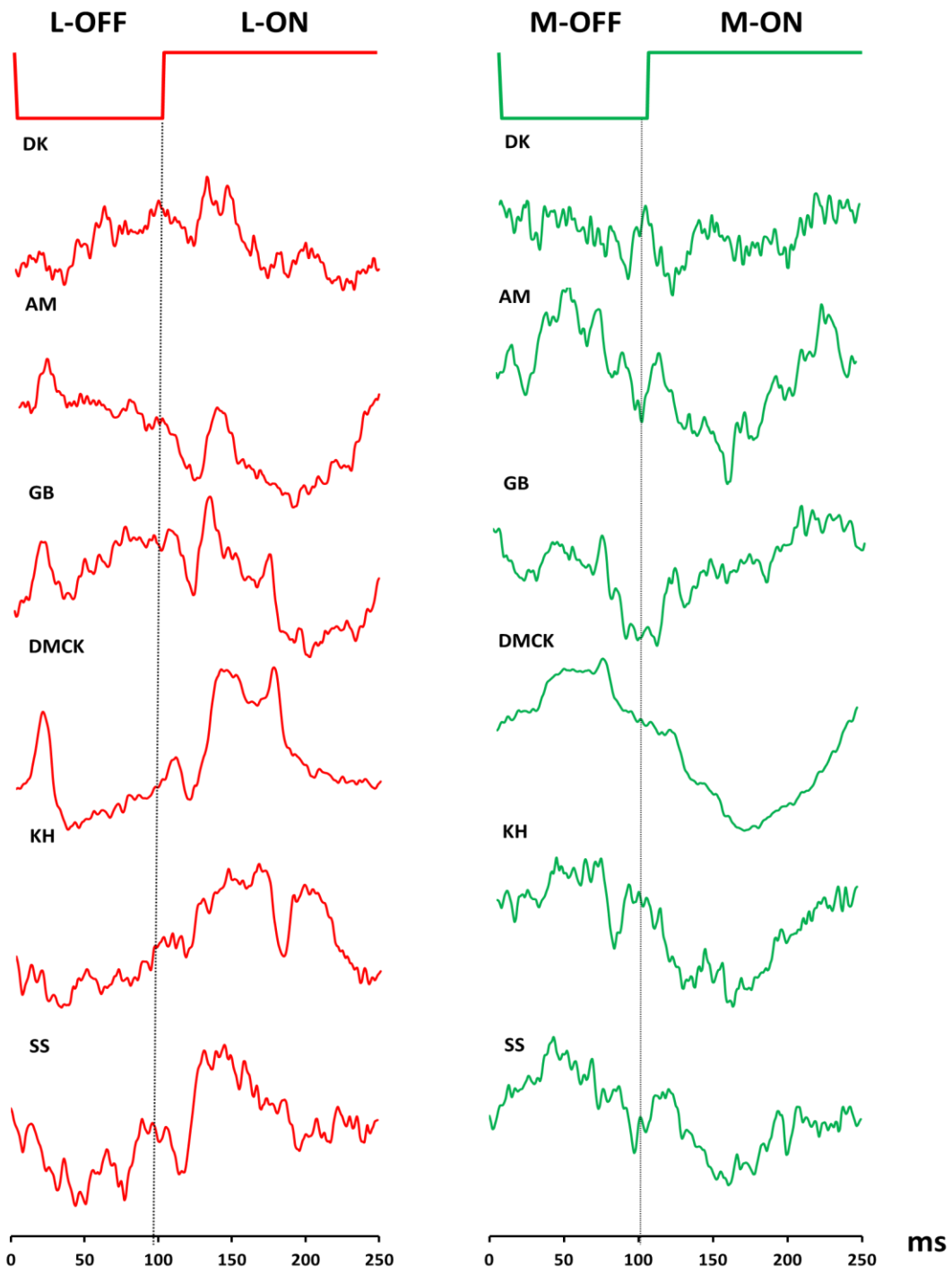

Figure 4-8 Individual L-Off and M-Off driven ERGs obtained in response to L- and M- cone isolating decrement/increment transient, square- wave pulse stimuli.

From figures 4.6, 4.7 and 4.8 and tables 4.2 and 4.3, we infer that L- cone increment responses (Li) were observed to be similar to those of M- cone decrement responses (Md). We also compared the mean implicit times (n=19) of

the early negative components of L- onset and M- offset responses and noticed that although both responses appear similar, the implicit time of M-off early negative response (N_{Md}) were found to be longer than that of the L-on early negative wave (N_{Li}) (see table 4.3). Similarly when L-off (Ld) responses were compared to M-on responses (Mi), we observed that the implicit time of P_{Mi} were longer than that of P_{Ld} (see table 4.3 and figure 4.6). Our findings suggest that early negative (N_{Ld} and N_{Mi}) and the first positive (P_{Li} and P_{Md}) components of L- and M- cone isolated flash ERGs are comparable to a- and b- waves of photopic flash ERGs but the key feature here is that these components possess opposite polarity (see figure 4.6). Also their measured implicit times are found to be similar, suggesting these components could have a common cellular origin.

(B) Dichromatic Controls

Here we were interested in examining to what extent these ERG responses were cone-specific and free from contaminant contributions from other photoreceptor types. In this experiment, we used the same approach as proposed in literature to verify the extent to which the stimuli used in this study were cone-selective (Smith et al., 1995, Usui et al., 1998; Kremers et al., 1999; Albrecht et al., 2002; Kremers 2003; Parry et al 2002). In protanopic observers, SH and IP, ERGs displayed no signals in response to L- cone isolating stimuli but displayed robust signals in response to M- cone isolating onset-offset stimuli.

Another interesting feature of the M- cone ERGs recorded from the Protanopic observers SH and IP (as shown in figure 4.9) is that the On-Off response inversion was absent, unlike what was observed in the M- cone driven ERGs in normal trichromats (as shown in figure 4.6). The N_{Mi} and P_{Mi} components elicited by M- cone increments in normal trichromats which resemble the a- and b- waves seen in the luminance ERG, were shown to be elicited by M- cone decrements in protanopes. It is more likely that in the absence of the normally functioning L- cones in protanopes, the M- cone ERGs exhibit onset-like responses to increments and offset-like responses to decrements.

Conversely, in deuteranopes, L- cone responses were present and no measurable M- cone mediated responses were observed. However, ERGs obtained in response to M- cone isolating stimuli in one of the deuteranopes (IB), displayed some residual late responses with an implicit time around 80-85 ms (see figure 4.10) and thus are unlikely to have derived from primary sensory responses. We assume these responses could probably be the analogues of the LN responses marked in figure 4.6.

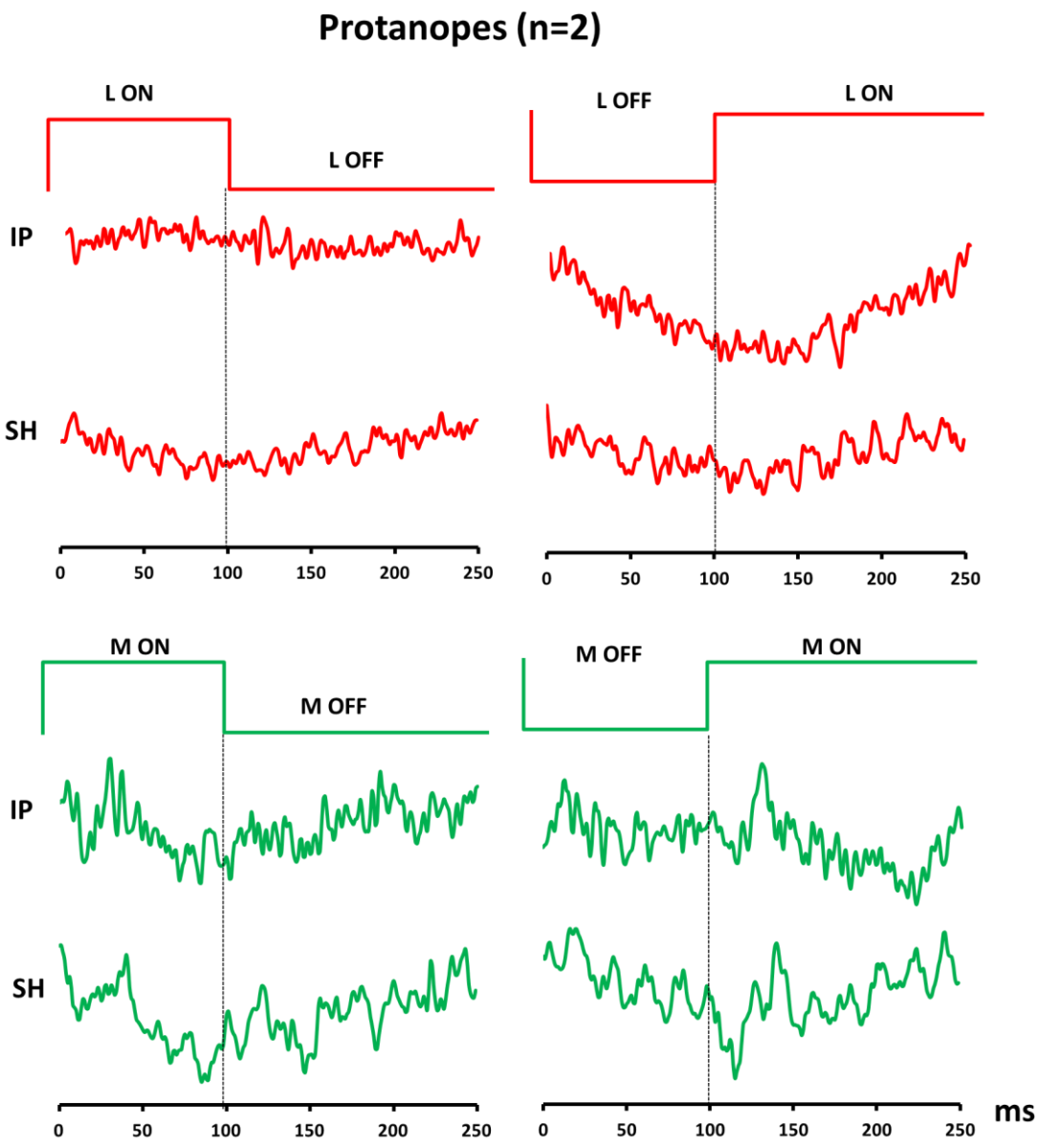

Figure 4-9 L- (upper traces) and M- cone (lower traces) driven ERGs of two Protanopic observers (IP and SH) elicited in response to L- and M- cone isolating increment flash followed by a decrement transient flash stimulation.

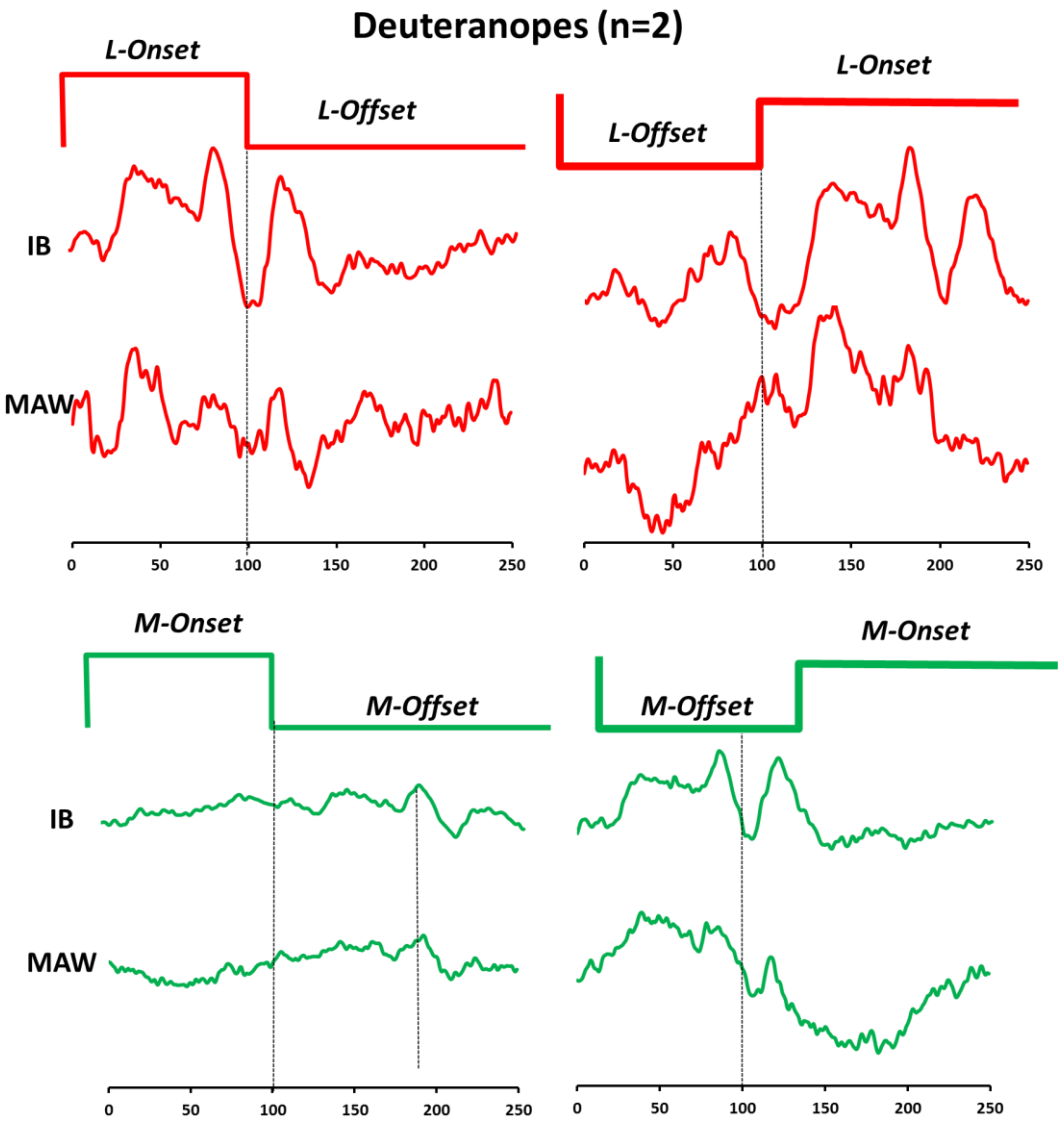

Figure 4-10 L- (upper traces) and M- cone (lower traces) driven ERGs of 2 deuteranopes (IB and MAW) elicited in response to L- and M- cone isolating increment flash followed by a decrement transient flash.

4.4.3 Counter-phase and in-phase L/M cone Stimulation

We speculate that the ERG responses elicited by L- and M- cone onset and offset stimuli provide a measure of contribution to the postreceptoral pathways in addition to the functional response of the individual photoreceptor classes. . To explore the notion that has been previously reported in psychophysical and single-cell electrophysiological studies (Lee et al., 1989; Dacey, 2000; Parry et al., 2012), we further examined ERG waveforms elicited by compound L/M cone stimuli. Here, we used Luminance (+LUM or –LUM) and linearly combined L- and M- cone compound stimuli. In order to create compound stimuli, we manipulated L- and M- cones either in counter-phase (+L-M) or (-L+M) and/or in-phase (+L+M) or (-L-M) to investigate how these stimuli could affect the ERG waveform in a dichromatic observer (IP) and in normal trichromats (see figures 4.12 and 4.13).

It is interesting to note that luminance responses elicited by luminance (LUM) stimuli were observed to have similar amplitudes and implicit times to those of the signals obtained from the linear combination of L- and M- cone isolating stimuli (see figure 4.11) confirming what has been long established that the additive inputs from L- and M- cones form the basis of luminance vision (Lee et al., 1989; Dacey, 2000; Parry et al., 2012).

The +L+M and –L-M conditions as shown in figure 4.12 elicited responses similar to on- and off- responses elicited by L- cone increments and decrements respectively. On the other hand, the –L+M stimulus condition generated responses similar to components observed in response to L-cone decrements and M- cone increments and +L-M stimulus elicited response components as seen in L- cone increments and M- cone decrements.

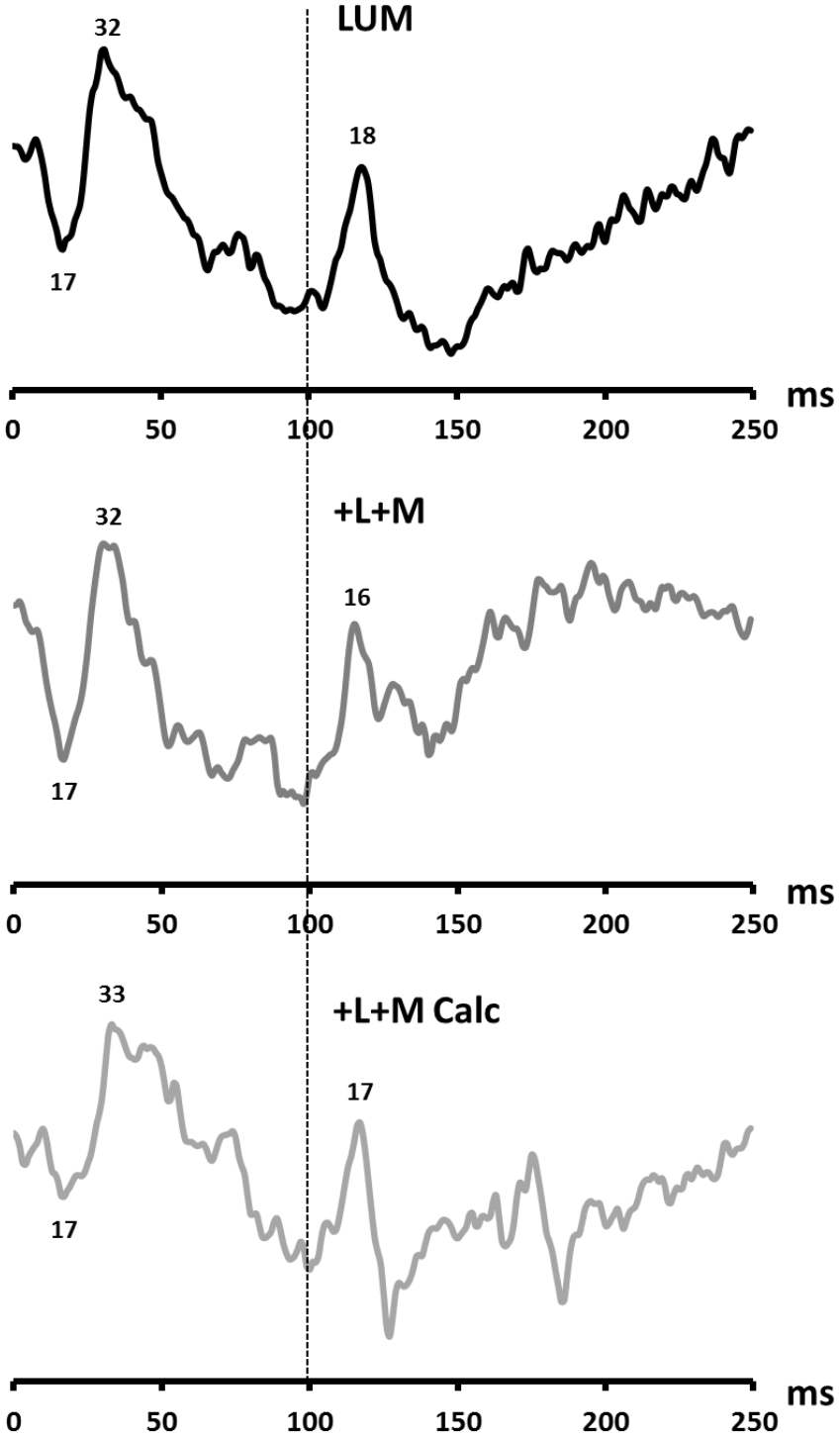

Figure 4-11 illustrates group averaged Luminance, actual +L+M response and computed +L+M responses obtained by linear addition of L- and M- cone ERGs using brief on/off pulse stimulation.

The total cone contrast change of 11% and a retinal illuminance of 12000 Td was used for all stimulus parameters. The numerical values displayed on the graph indicates implicit times of a-, b- and d-waves as measured at 17 ms, approximately 32 ms and 17 ms respectively for all three responses.

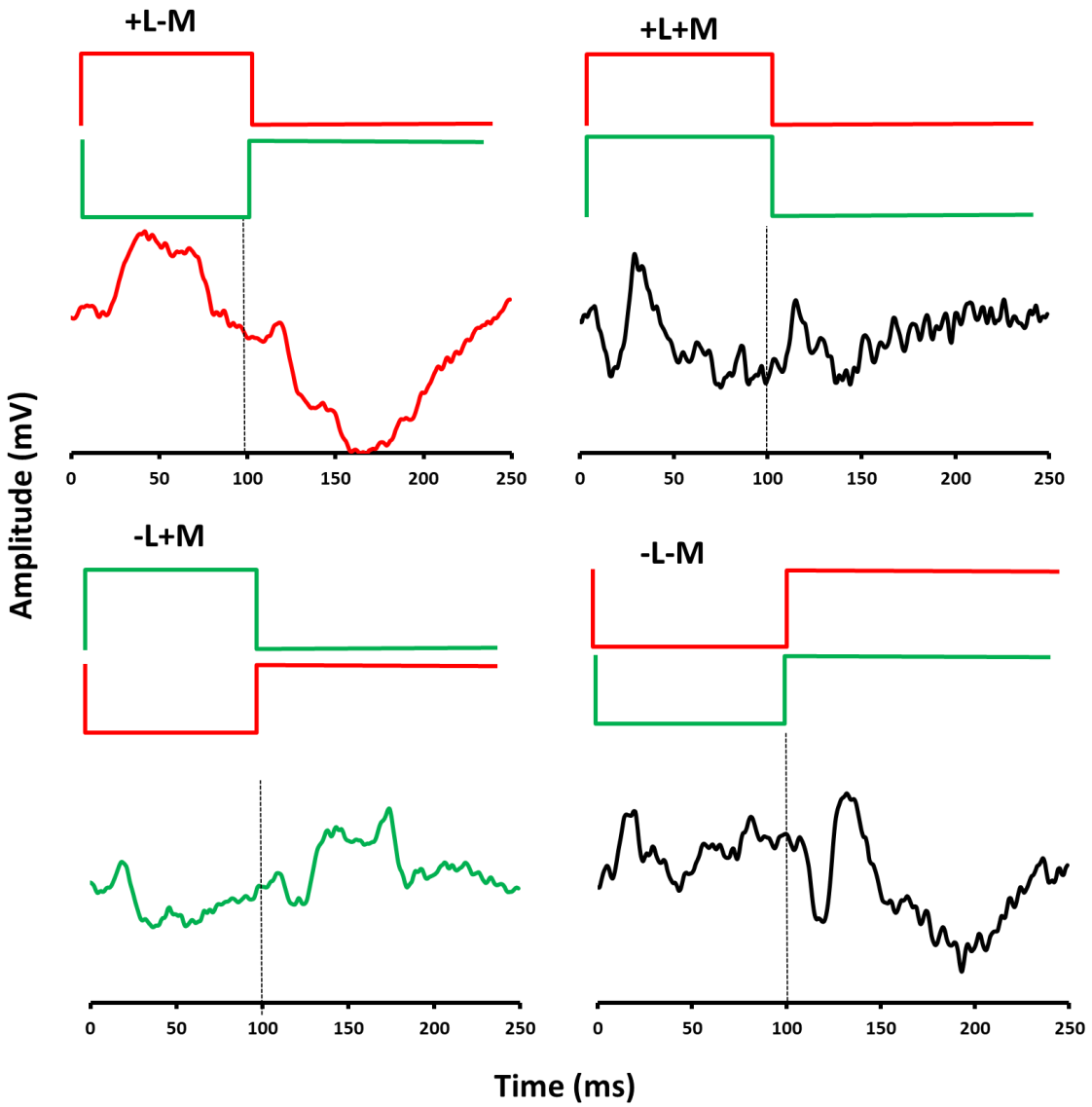

Figure 4-12 Group averaged ERGs elicited in response to counterphase (left panel) and in-phase (right panel) stimulation in normal trichromats (n=6) using 100 ms onset followed by a 150 ms offset square wave profile.

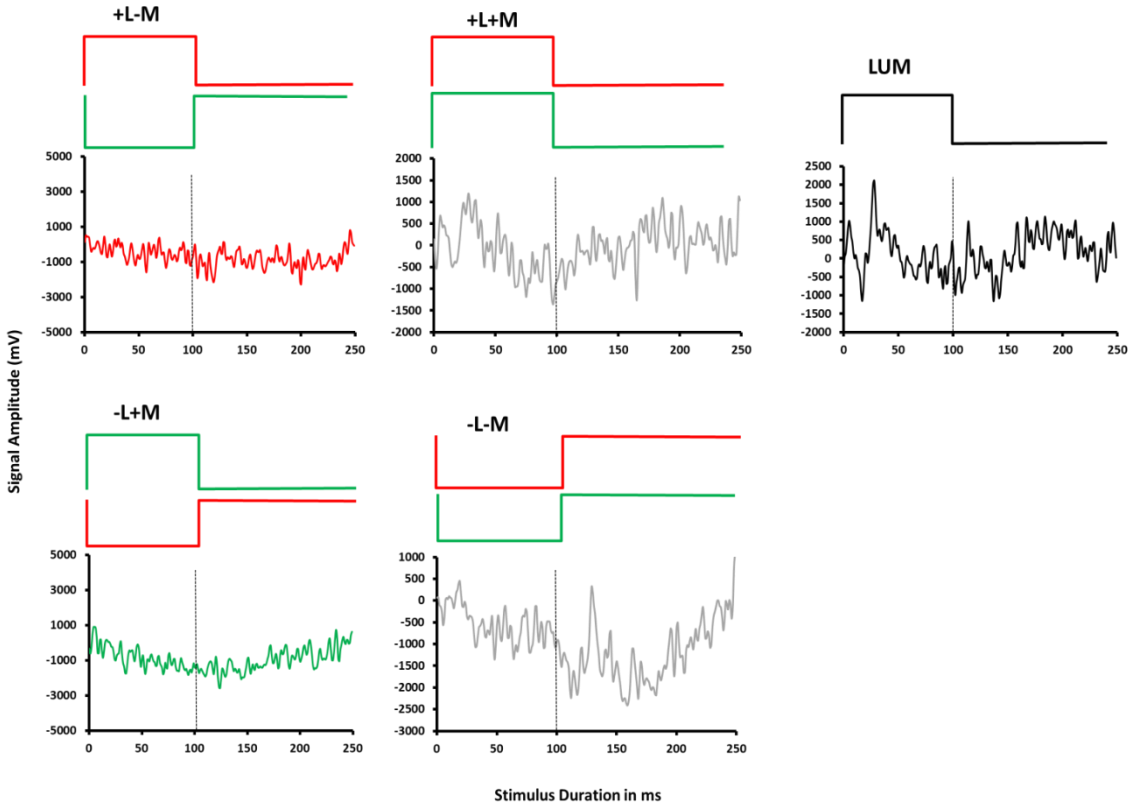

Figure 4-13 ERGs recorded in a protanopic observer (IP) to inphase (+L+M and –L-M), counterphase (+L-M and –L+M) and luminance (LUM) stimulation.

4.4 Discussion

In this study we sought to determine the response characteristics of L- and M-cone driven ERGs elicited by transient, square-wave pulse stimulation in normal trichromats as well as dichromats using silent substitution.

4.4.1 Validation of L- and M-cone silent substitution Stimuli

Here we used square-wave temporal profiles generated on a four primary photostimulator to elicit L- and M- cone driven transient, ERG responses using silent substitution method. Our results are in accord with results reported previously (Kremers and Pangeni, 2012) and as described in Chapter 5 & 6 in this thesis where silent substitution was used in recording steady state ERGs to sinusoidally modulated stimuli. Although absorption spectra of the optical media and eccentricity dependent alterations in the cone photopigments may result in residual signals in the silenced photoreceptors, we observed that L- and M- cone

ERG responses in dichromatic observers broadly confirm the cone- selective nature of these stimuli. The absence of L- cone responses in protanopes strongly validates that the substitution method effectively excites only the photoreceptor type of particular interest. However, deuteranopes displayed small, residual responses to M- cone isolating stimuli. We observed this in our experiments where sine-wave modulation is used and the cause of these residual responses is unclear but we assume that the inter-individual differences in lens absorption spectra and eccentricity dependent changes in photoreceptor absorption may have attributed to such residual signals (Foster 2010).

4.4.2 L- and M- cone isolated ERGs

Since the M- cone onset-offset response depart from the conventional flash ERG waveform, we had two questions, 1) at what level of retina were these signal generated? and 2) what is the basis of this phase reversal? The answer to the first question could be that L- and M- cone ERGs generated at low temporal flicker rates, reflect the properties of L- and M- cone opponent mechanisms. This is in line with the results provided by previous psychophysical experiments where detection of cone-isolating stimuli was found to vary with change in temporal frequency. i.e., at low temporal frequencies, the detection of stimuli is mediated by cone-opponent, chromatic channel whilst at high temporal frequencies, it is mediated by cone-non-opponent, luminance channel (Kelly and van Norren, 1977; Smith et al., 1995).

In answer to second question, the foregoing section clearly indicates that the basis for the L-M cone response inversion originates at the postreceptoral level. The findings that support this hypothesis are 1) the presence of L/M cone response inversion observed only in normal trichromatic observers, 2) absence of M- cone on-off inversion relative to L-cone responses in protanopic observers (who lack L-cones) and the waveform here adopts a conventional flash ERG like appearance with a- and b- wave like components present when elicited by M-cone increments (N_{Mi} and P_{Mi}) (see figure 4.9), 3) manifestation of phase inversions could be at the level of single cellular level of cone-opponent ganglion cells considering that it has been already shown in the previous experiments that it is at the cone-opponent (parvocellular) ganglion cell level, where the L- and M-cone responses are about 180 degrees out of phase (Smith et al., 1992).

Cone opponency is often regarded as the property of midget ganglion cells which receive opposite and distinctly separate inputs from L- and M- cones to the center and surround of their receptive fields (De Monasterio and Gouras, 1975; Lee et al., 1989; Smith et al., 1992) (see figure 1.1.6 of Chapter 1). In contrast to this, parasol ganglion cells receive combined inputs from L- and M- cones to their center and surround receptive fields (Dacey, 1999) (see figure 1.1.8). There is evidence that the cone antagonism could begin in the more distal layers, with the inhibitory feedback from the horizontal cells to photoreceptors and bipolar cells (see figure 1.12) (Verweij et al., 2003). It is thought that this feedback results in reversal in response polarity. While these feedback mechanisms are noted to influence the opponency in lower vertebrates (Dacey, 1999), it is still not clear how this mechanism would explain the M- cone response inversion relative to L-cone responses in mammals.

Also, there is evidence on contribution of bipolar cells to luminance ERG response (Sieving et al., 1994). There exists two types of bipolar cells, diffuse and midget, of which, diffuse bipolars transmit signals to parasol ganglion cells while midget bipolar cells, to midget ganglion cells (Polyak, 1941). These cells are assumed to form precursors for the functional pathways of chromatic (parvocellular), and achromatic or luminance (magnocellular) vision (Schiller et al., 1990; Smith et al., 1992). Although there is clear evidence on functional segregation at the level of bipolar cells in non-primate mammalian retina (Li and DeVries, 2006; Breuninger et al., 2011 and Puller and Haverkamp, 2011), this functional dichotomy in the primate retina has been less forthcoming (Dacey, 2003).

However, we continue to believe that midget and diffuse bipolar cells at low temporal frequencies contribute to L- and M- cone driven ERGs and midget cells to luminance ERGs at high temporal frequencies (Kremers and Link, 2008).

4.4.3 Counter-phase and in-phase L/M cone Stimulation

With compound stimuli, i.e. L- and M- cones presented in either inphase (+L+M, -L-M) or counterphase (+L-M, -L+M), ERGs obtained reproduced responses that reflect cone non-opponent, luminance and cone-opponent, chromatic pathway activity. A crucial feature of these signals is that they are elicited by simple linear combinations of onset and/or offset cone isolating stimuli (Derrington et al, 1984). In this regard, our results add to previously reported physiological and psychophysical evidence in support of an opponent model of visual processing (Derrington et al., 1984; Schiller et al., 1990). Moreover, our data demonstrates the usefulness of ERG in providing a functional index of early visual processing of L- and M- cone opponent (+L-M), chromatic and +L+M cone non-opponent postreceptoral mechanisms.

4.4.4 L/M cone Ratios

Furthermore, the data shown here provides the quantitative description of normal L- and M- cone ERGs which can be used in the future to study the isolated L- and M- cone responses in different retinal disorders. The L- cone isolated response components were found to be larger than their M- cone counterparts in response to both increment and decrement flash stimulation across all observers. This is possibly due to higher L:M cone ratios in all observers. Furthermore, we also noticed that the L- cone response components derived in response to L- cone isolating increment stimuli has similar response characteristics and implicit times as that of a, b and d waves of luminance ERGs (see figure 4.6 and 4.11 for comparison). This finding could also suggest that it is because of higher L:M cone ratios in the retina that L- cones may offer stronger input to the luminance ERG. In the absence of such strong inputs from L- cones for example as seen in the protanopes (see figure 4.9) where L cones are absent, no M- cone response

inversion was noticed to M- cone stimulus onset as we observed in normal trichromats (as shown in figure 4.6). Therefore, we suggest that the L-M cone phase reversal witnessed in normal trichromats could be due to higher number of L- cones dominating the M-on responses. It would be interesting to see if this property of L-M cone response inversion is also noticed in individuals with high M:L cone ratios. In that case, we will be able to conclude that its numerical superiority of L- cones that cause phase reversal in cone opponent mechanisms.

4.5 Conclusion

In summary, the results demonstrated in this study suggest that L- and M- cone isolating ERGs can be obtained from trichromatic human retina using transient, square wave pulse stimulation. The novel finding of the L-M cone inversion and the identical response nature of the luminance signals to that of the computed L and M cone signals by linear addition suggest that the origin of these responses probably are derived from the postreceptoral L- and M- cone opponent and non-opponent mechanisms respectively. The similar response characteristics of L-ON and M-OFF components and L-OFF and M-ON components and their similar implicit times could possibly imply that these components have common cellular origin. We conclude that methods employed in this study may prove a powerful tool in characterization of retinal diseases where mutations silence L- and M-cone associated neural components and can be compared to the normative data.

Chapter 5 - Temporal response characteristics of L- and M-cone isolated flicker ERGs using sine wave stimuli

5.1 Introduction

In addition to flash ERGs routinely used in the clinic (Penn & Hagins, 1969; Lamb & Pugh, 1992; and Hood & Birch, 1996), ERGs are also generated using sinusoidally modulated light in a train of repetitive flashes, called flicker ERGs. When responses are obtained in this manner, they provide useful insights into the temporal properties of the retinal circuitry. The application of flicker ERG has proven to be indispensable in examination of the frequency-response relationship of the retina as the responses were found to vary in shape and/or amplitude from cycle to cycle (Burns et al., 1992). Furthermore, it also allows us to gauge linearity of the responses derived from the retina (Burns et al., 1992; Odom et al., 1992; Crevier and Meister, 1998; Kondo and Sieving, 2001; Krishna et al., 2002; Viswanathan et al., 2002; Alexander et al., 2005; Qian et al., 2008; 2010).

Clinically, the 30 Hz flicker ERG recommended by ISCEV is used in examining cone activity. At this frequency rod photoreceptors are inactive and the response derived is purely cone driven (Marmor et al., 2004; 2009 and McCulloch et al., 2015). This technique is used in differential diagnosis of several retinal disorders (Miyake et al., 1987; Cideciyan and Jacobson, 1993; Fishman, 1985; Molday et al., 2000) and in monitoring the efficiency of treatment strategies. Although this protocol provides information of global cone activity it does not offer enough information to understand the contribution of different classes of photoreceptors to flicker ERG.

The ERG is typically known to provide the measure of the outer retinal function (Baker et al., 1988). However, there is growing evidence that the origin of these signals are likely to be in different retinal cells and may reflect the activity of postreceptoral processing mechanisms arising from the activity of spiking retinal ganglion cells or bipolar cells (Bush and Sieving, 1996; Kondo and Sieving, 2001; Viswanathan et al., 2002; Qian et al., 2008; 2010). Flicker ERGs have been previously recorded in combination with the application of pharmacological agents in both the primate and non-primate retina (Seiple et al., 1986; Odom et al., 1992; Burns et al., 1992; Kondo and Sieving, 2001; Krishna et al., 2002; Qian et al., 2008; 2010). The striking feature of all these studies is that the temporal characteristics to luminance stimuli in different primate species share similar properties. The results obtained in all these experiments showed similar response functions with two distinct response regions (see figure 5.1) where the amplitude of the first harmonic falls to a minimum at around 10-12 Hz and then reaches a peak in amplitude between 30 to 40 Hz that is followed by a gradual decrease in response up to 100 Hz (Kondo and Sieving, 2001; Krishna et al., 2002; and Qian et al., 2010). Kondo and Sieving (2001) suggested that this characteristic shape of the ERG temporal response is attributed to frequency-dependent phase cancellation of ON- and OFF- pathways.

In this study we furthered this knowledge and reinvestigated the temporal frequency response functions of cone isolated ERGs in response to L- and M-cone isolating stimuli. As discussed in chapter 3, the isolation of responses from individual cone populations presented something of a challenge in view of their large degree of overlapping spectral sensitivities of all four photoreceptor classes.

In studies where chromatic adaptation was used to obtain either L- or M- cone isolated ERGs, the signals were contaminated by M- or L- cone intrusion and complete isolation was reported to be not entirely possible (Kremers 2003). It was shown to be more difficult to derive isolated responses from these two cone classes as their spectral sensitivities overlap extensively as the genetic composition and biochemical properties of their photopigments are about 98% identical (Neitz & Neitz, 2011).

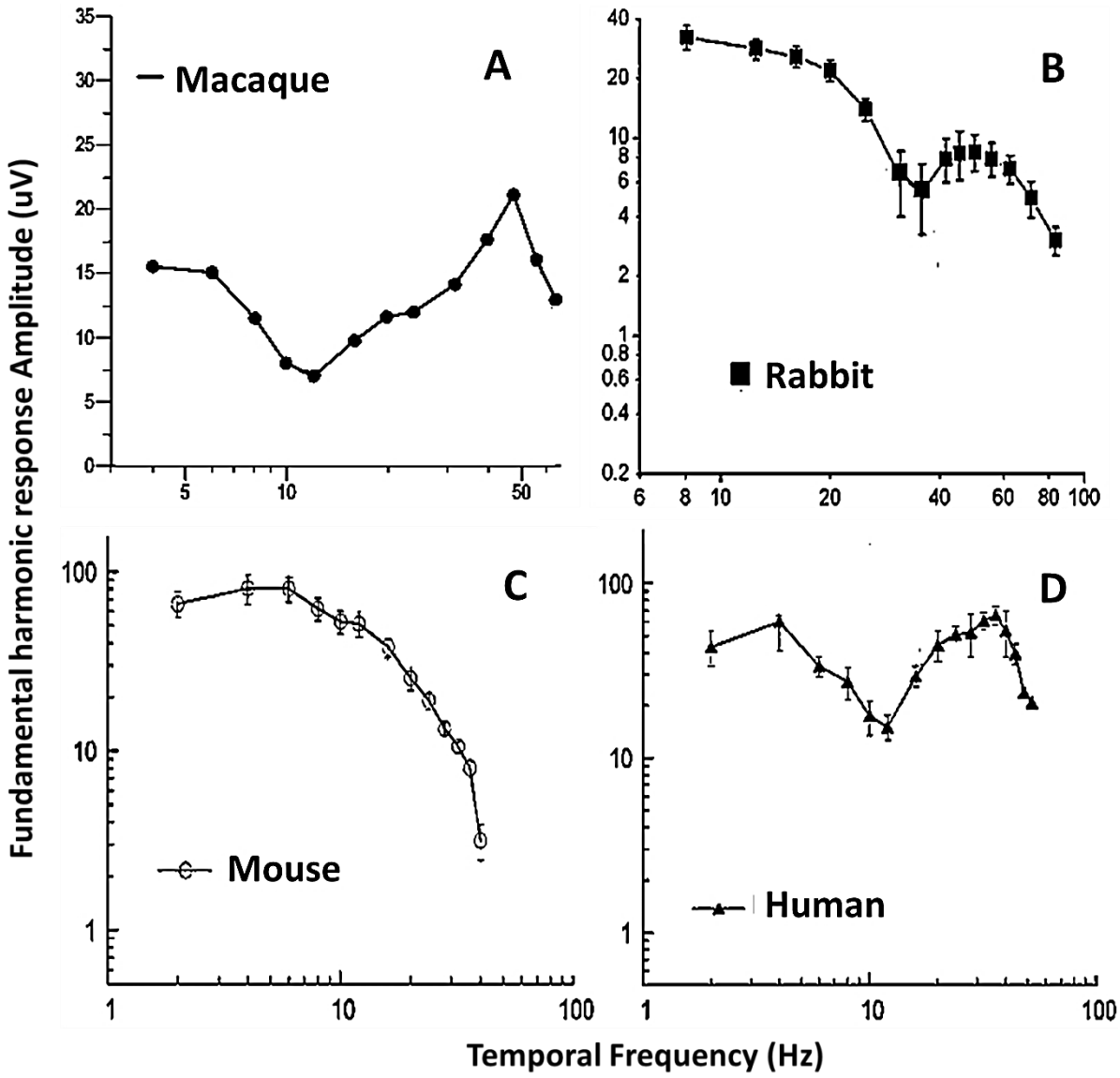

Figure 5-1 Fundamental harmonic flicker ERG responses plotted as a function of temporal frequency in (A) Macaque (Kondo & Sieving, 2001); (B) Rabbit (Qian et al., 2010); (C) Mouse and (D) Human (Krishna et al., 2002) retina.

A number of studies have used silent substitution stimuli to study isolated cone populations in psychophysical studies (Lee et al.,1990; Lee, 2011). This has led to the assumption that the responses derived do not necessarily reflect the activity of individual cone classes alone, but that the underlying mechanisms may have a postreceptoral origin (Smith et al., 1995; Sun et al., 2001; Kremers et al., 2003). These studies suggest that response sensitivity at low and high temporal frequencies are determined by cone-opponent, chromatic and cone non-opponent, luminance processing pathways respectively.

Previous cone isolating ERGs demonstrated similar results and supported the proposal that there are temporal frequency dependent contributions from different post-receptoral mechanisms in the human retina (Kremers and Pangeni, 2012; Kremers and Link, 2008; Kremers et al., 2010; Kremers,2011; Challa et al., 2010; Parry et al., 2012). At low frequencies (<12 Hz), both L- and M- cone driven signals demonstrate similar response amplitude but with a phase difference of 180 degrees. On the other hand, at high temporal frequencies (30 Hz), L-cone mediated signals showed higher response amplitudes in comparison to M- cone mediated ERGs with a phase difference of about 90 degrees and the response function at these frequencies exhibit V_λ-like spectral sensitivity characteristics (Jacobs et al., 1996). All these response characteristics are consistent with the notion that low- and high- frequency flicker ERGs are mediated by the chromatic, cone-opponent and the achromatic, cone non-opponent processing pathways, respectively (Kremers and Link, 2008).

In the present study, we describe the temporal frequency response characteristics of human L- and M- cone isolated ERGs by using harmonic analysis which has allowed us to examine how signal amplitude and phase varied with stimulus flicker rate. The purpose of this study was to provide further evidence to the hypothesis that L- and M- cone responses recorded at low and high temporal frequencies reflect the mechanisms that are thought to underlie the properties of chromatic and luminance vision respectively. In order to achieve this, we adopted two different approaches: first, we examined the L- and M- cone response amplitudes plotted as a function of temporal frequency in normal trichromats and dichromats. The dichromatic observers served as controls in this experiment to examine if the silent substitution stimuli used in this study is effective in obtaining isolated cone ERGs. The L:M cone ratios were also measured in the control participants to assess how they depart from the measurements acquired in normal trichromats. Secondly, we examined how L- and M- cone phases varied with change in temporal frequency. In this study, temporal frequencies were sampled intensively in comparison to previous studies (Kremers and Pangeni, 2012). This permitted the calculation of apparent latencies which would further allow us to study the time delay in L- and M- cone responses and how they vary as a function of temporal frequency (Regan, 1966). Previous psychophysical and single-unit studies suggested that the delay between L- and M- cone response differ in their magnitude depending upon whether they convey their inputs to either chromatic or luminance postreceptoral mechanisms. It was found that for the chromatic, cone-opponent system, the delay between L- and M- cone responses was found to be minimum (Smith et al., 1992).

In contrary to this finding for the luminance system, L- and M- cone responses demonstrated substantial delay which according to HFP studies is due to the apparent phase shifts that are necessary to eliminate residual flicker at isoluminance between cone isolating stimuli. These findings indicate that if there are temporal frequency-dependent contributions to the ERG from luminance and chromatic postreceptoral processing mechanisms, then such contributions would be revealed by varying delays in the L- and M- cone derived latencies as a function of temporal frequency. In this study we sought out to determine whether such variations were evident in the steady state ERGs obtained using silent substitution method.

In addition to the L-M cone opponent channel, we know that there exists another chromatic channel in which signals from S-cones interact in an opponent fashion with a combined signal from L- and M- cones (L+M) (Dacey, 1996). There is evidence that S- cones in comparison to other cone types are particularly sensitive to disease and trauma (Marré, 1973; Zrenner, 1982; Mollon, 1982; Pacheco-Cutillas et al., 1999; Cho et al., 2000). It would, therefore be useful to have a protocol or Electroretinographic method for examination of S cones. The S- cones represent about 5-15% of the total cone population (Stiles, 1949; Brindley, 1954; Marc and Sperling, 1977; DeMonasterio et al., 1981; Ahnelt et al., 1987; Williams et al., 1981; Curcio et al., 1991; Solomon and Lennie, 2007) and less than 0.5% of the total photoreceptors (Osterberg, 1935; Sawusch et al., 1987). Thus, silent substitution may prove to be a better method in extracting of these small signals considering their low numerosity relative to other receptors in the retina.

Therefore, in addition to examining L- and M- cone driven ERGs, we also measured isolated S- cone driven ERGs as a function of temporal frequency under similar stimulus conditions as for measuring L- and M- cone mediated responses.

5.2 Methods

5.2.1 Subjects

In total, 18 subjects participated in the current study. Three experiments were conducted 1) where isolated L- and M- cone ERGs were recorded in eleven normal trichromats (four female observers and seven male observers, aged between 12 and 47 years) and six male observers (aged between 19 and 40 years) with colour vision deficiencies at larger intervals of temporal frequencies (non-intensively sampled data), 2) where temporal responsivity of L- and M- cone driven ERGs were examined in detail with smaller intervals between stimulus frequencies in five normal trichromats (four male observers and a female observer, aged between 20 and 47 years) (intensively sampled data) and 3) S-cone mediated ERG signals were obtained from five normal trichromatic observers (one female and four male observers, aged between 21 and 47). The right eye of each participant was dilated to approximately 8mm for testing purposes using a 1% Tropicamide minim. Prior to the experimental session, informed consent was obtained from all the participants and the experiments conducted were in accordance with the tenets of the Declaration of Helsinki.

5.2.2 Visual stimulation

Full-field, sinusoidally modulated flicker L-, M- and S- cone isolating stimuli were generated on four-primary ColorDome ganzfeld stimulator (Diagnosys LLC, Lowell, Massachusetts) using calculations described in chapter 3. We used temporal frequencies from 5 to 100 Hz and the stimuli were equated in terms of cone contrast (11%) and retinal illuminance (12000 Td) with a mean luminance of 238.732 cd/m^2 for all stimulus conditions (L-, M-, S- cone and Lum or L+M cone stimuli) (see figure 5.2 for temporal profiles of LED classes for L- and M-cone isolating stimuli at 5- and 30- Hz). ERG traces were recorded over a block of 4 seconds generating over 1000 data points. For non-intensively sampled data, we recorded ERGs over eight temporal frequencies (5,10, 15, 20, 30, 40, 75, 100 Hz) and for intensively sampled data, ERGs were over a wider range of stimulus frequencies (5, 6, 8, 10, 12, 15, 18, 20, 24, 28, 30, 32, 34, 36, 40, 42, 44, 46, 52, 56, 60, 62, 64, 66, 70, 75, 100 Hz).

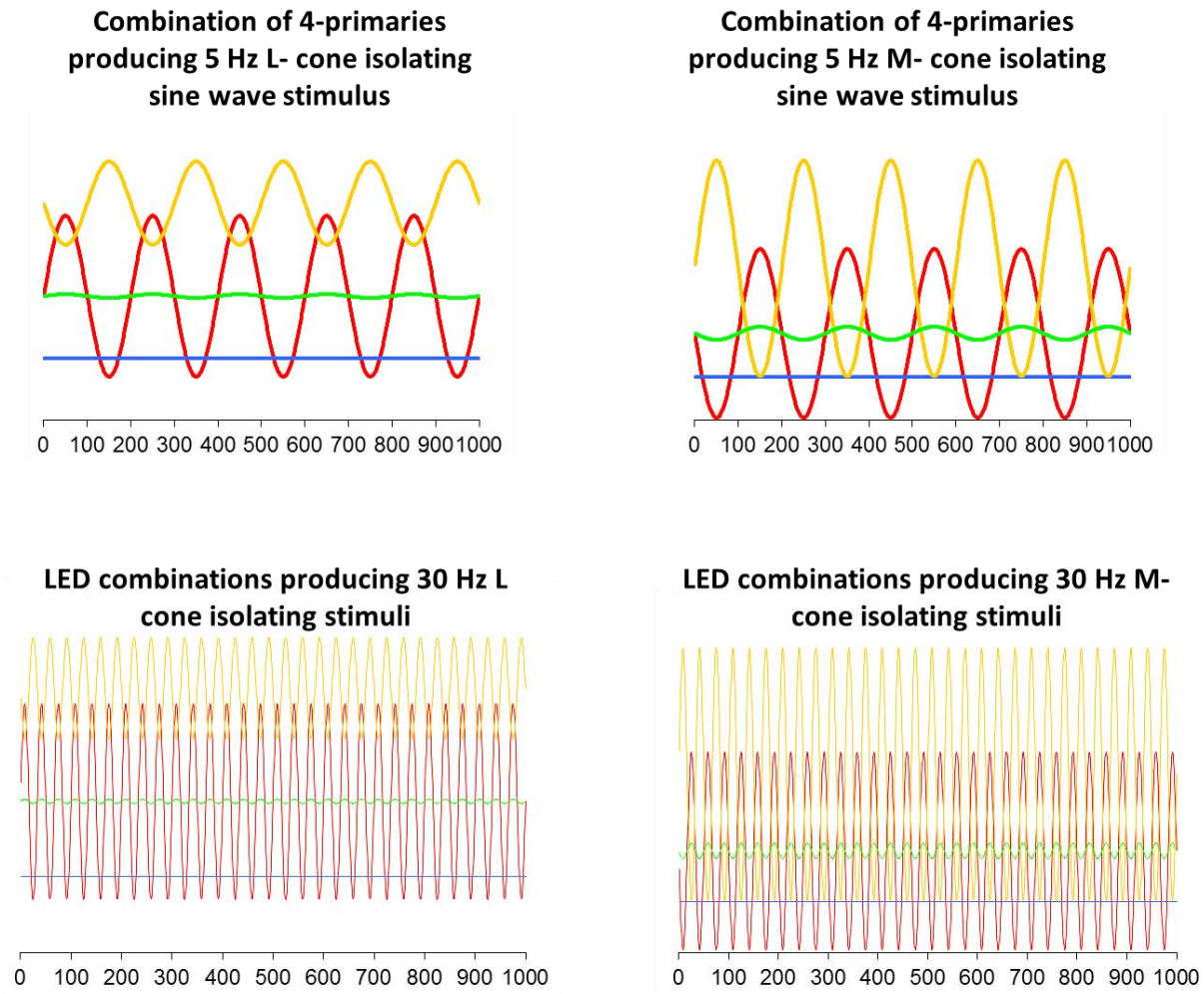

Figure 5-2 showing combination of four LED outputs used in the generation of L and M cone isolating stimuli at 5- (top row) and 30- (bottom row) Hz using modified Stockman fundamentals.

5.2.3 ERG recordings

Electrodes were placed as described in chapter 3. All participants were positioned on a chin rest and at a viewing distance of 10 cm from the central point of fixation which subtended approximately 0.5^0 and were instructed to maintain steady fixation throughout the experiment. ERG signals were amplified and band pass filtered (cut off frequencies 1 and 300 Hz) and sampled at 1000 Hz. The responses to each stimulus were recorded over 36 seconds in 8 blocks of 4 seconds producing 4000 data points. These were further subjected to offline analysis using fast Fourier transform to extract amplitude and phase information. The rod contrast was set at 0% for all stimulus conditions. A minimum of eight recordings were collected at each stimulus frequency. In case, if some of the recordings had to be excluded due to the occurrence of biological artifacts, we collected an additional eight recordings, i.e, 16 epochs per step to achieve better signal quality.

5.2.4 Data analysis

Following data acquisition, the averaged ERG traces were further subjected to a two-stage offline analysis. 1) Resampling of the traces and 2) subjecting these resampled signal traces to Fourier analysis (described in chapter 3). Note that the raw ERG traces as demonstrated in figure 5.3 show irregular traces for both L- and M- cone ERGs at 5 and 10 Hz whilst at 40 Hz, both L- and M- cone isolated signals display pointed, simple triangle like responses. These responses appeared linear and were shown to be reduced in size and with increase in temporal frequency. It is known from previous studies that flicker ERGs

demonstrate a linear, fundamental or first harmonic (1F) and a non-linear, second harmonic (2F) components (see figure 5.3) (Odom et al., 1992; Burns et al., 1992; Porciatti et al., 1993; Falsini et al 1999; Qian et al., 2008; Parry et al., 2012). These results were vector averaged to understand frequency-response amplitude and phase changed across subjects (Vector averaging explained in appendix).

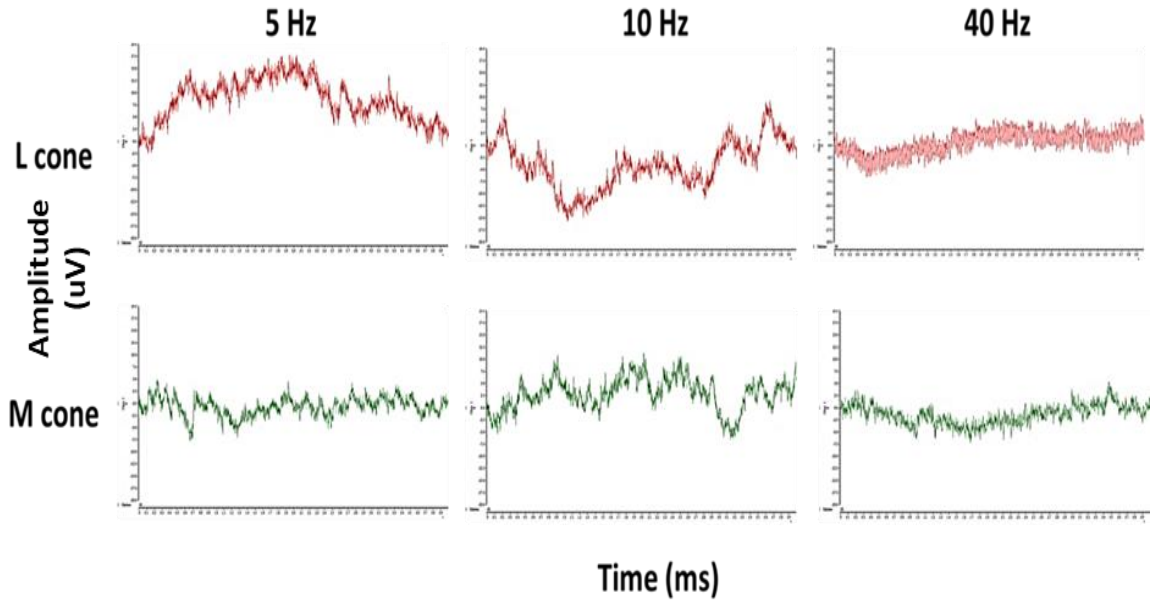

Figure 5-3 Examples of original ERG waveforms elicited from one observer by sinusoidally modulated L- (top row, red coloured traces) and M- (bottom row, green coloured traces) cone isolating stimuli at 11% cone contrast, presented at temporal frequencies 5-, 10- and 30 Hz. Each trace represents the average of at least 16 sweeps.

5.3 Results

5.3.1 Experiment 1 (Non-intensively sampled data)

Figure 5.4 displays L- and M- cone driven first harmonic response amplitudes obtained from eleven normal trichromatic observers plotted as a function of temporal frequency. Our results show similar response function to what has been previously reported (Burns et al., 1992; Odom et al., 1992; Kondo and Sieving, 2001; Krishna et al., 2002). The temporal response functions for the L- and M-cone first harmonic amplitudes exhibit three distinct regions: a low frequency region (<10 Hz) where the response amplitudes of the fundamental component of both L- and M- cone ERGs showed similar signal strengths, an intermediate frequency region (10 Hz), where the response falls to a minimum and a high frequency region (>10 Hz) where the fundamental response amplitude of L-cones reaches maximum at approximately 30 Hz, falling to noise levels around 100 Hz. The M- cone response amplitudes were shown to have weaker signal strengths in comparison to L- cones in this frequency region and this could be attributed to the lower number of M- cones present in the retina (Brainard et al., 2000; Neitz et al., 2002; Carroll et al., 2002; Hofer et al., 2005).

(A) Temporal response characteristics of the fundamental components of L- and M- cone ERGs in trichromats

Figure 5.4 shows variation in the fundamental component amplitude as a function of temporal frequency from eleven normal trichromatic observers (age±stdev; 32.63±15.23 years) for L- (red solid lines) and M- (green solid lines) cone isolating stimuli at a constant cone contrast (11% each) and a retinal illuminance of 12000 Td.

We observed that L- cone signals demonstrate similar response characteristics of luminance ERGs as reported in other mammalian ERG studies. We compared the temporal responsivity of L- and M- cone response amplitudes of the fundamental component for the non-intensively sampled temporal frequencies (5, 10, 15, 20, 30, 40, 50, 75, 100 Hz). The common observation amongst all observers is that L- cone responses are predominant at high frequencies with attenuated M- cone signal strengths above 10 Hz and L- cone response amplitude reaching maximum at around 30 Hz and the signal amplitude was shown to decline steeply and fall down to noise levels at around 75 Hz. In contrast to this, at low frequencies (<10 Hz), L- and M- cone responses displayed similar response amplitudes with the exception of responses observed in participants ST, AM and JM. To address this issue, we conducted another experiment where the signals were recorded at frequencies at shorter intervals and defined the data as intensively sampled (results shown under section 5.3.2).

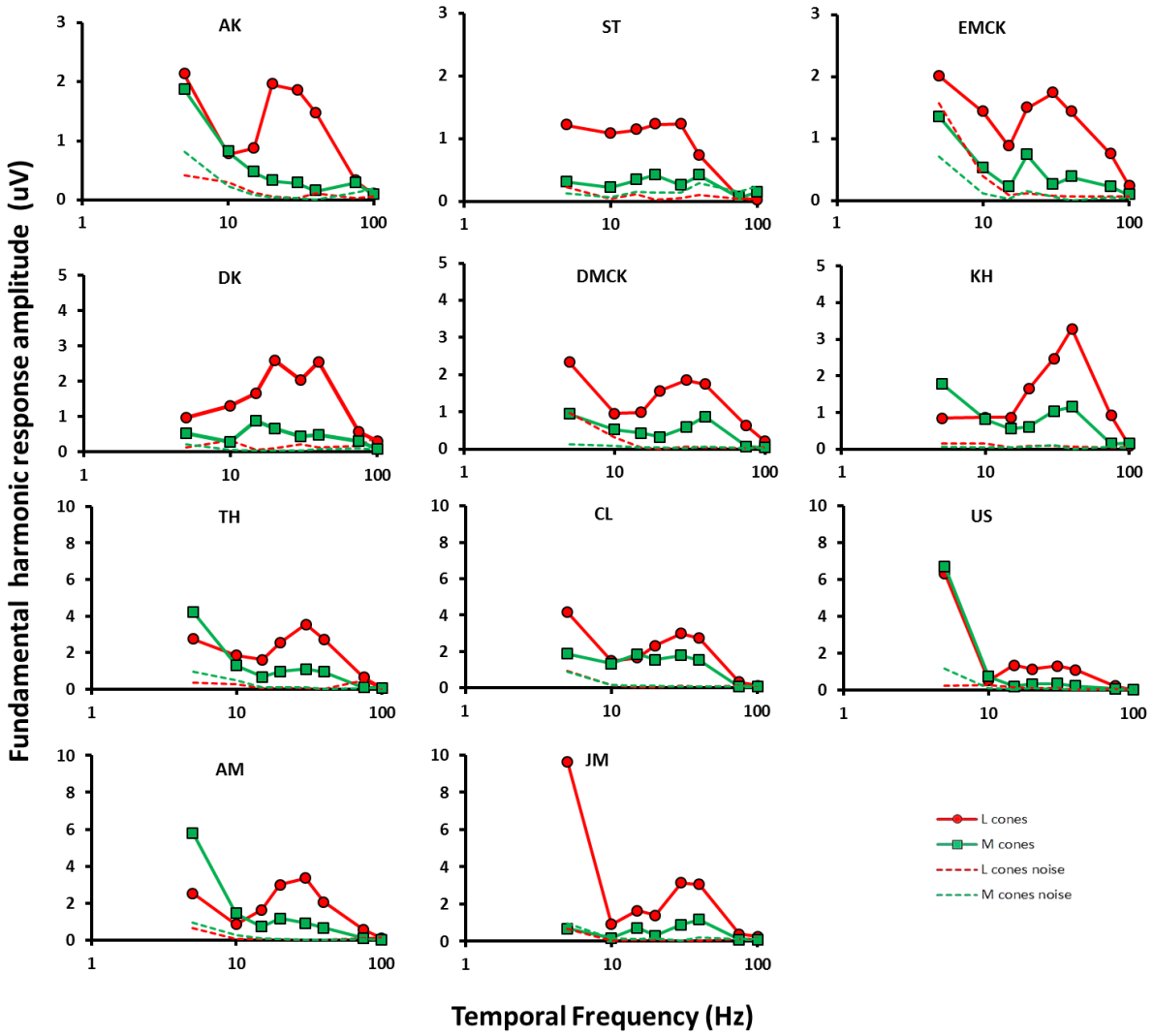

Figure 5-4 Fundamental component amplitudes of individual L- and M- cone isolated flicker ERGs plotted as a function of temporal frequency.

(B) Temporal response characteristics of the fundamental components of L- and M- cone ERGs in dichromats

Figure 5.5 shows L- and M- cone isolated steady state ERGs obtained from four dichromats (male observers; mean age+stdev;35.2+16.0 years) and anomalous trichromats (n=2; two male observers aged 20 and 21). The colour vision status in these participants was established based on the colour vision tests described in chapter 3. These observers served as controls as we wanted to establish if

the stimuli we used in this study has the ability to silence the cone populations that are not of our interest.

In protanopic observers, IP and SH, we observed robust M- cone signals across all frequencies with response energy of L- cones below noise levels especially at low frequencies and close to noise at high frequencies suggesting that the stimuli used in this study satisfy the criteria for using silent substitution method.

On the other hand, in deuteranopic observers, we observed pronounced L cone responses similar to that observed in normal trichromats. In contrast to the loss of L- cone response energy as observed in protanopes, we noticed weaker M-cone responses at low frequencies and small but measurable signals at high frequencies (between 15 and 40 Hz). The presence of M cone signals in deuteranopes (in which case M- cones are absent) could be due to the use of full field stimuli eliciting responses from peripheral cone populations where cone fundamentals used may not be applicable. Another explanation could be individual-dependent departures of M- cone absorption spectra in terms of inter-individual differences in pre-retinal absorption factors such a crystalline lens pigment density and macular pigment (Foster, 2010).

In protanomalous observers (third column in figure 5.5) L- cone ERG signals were shown to be weaker in comparison to M cones, however, it is interesting to note that L- cone responses in observer SS exhibited stronger signal strengths in comparison to observer LM and we assume this could be attributed to the severity of their protanomaly.

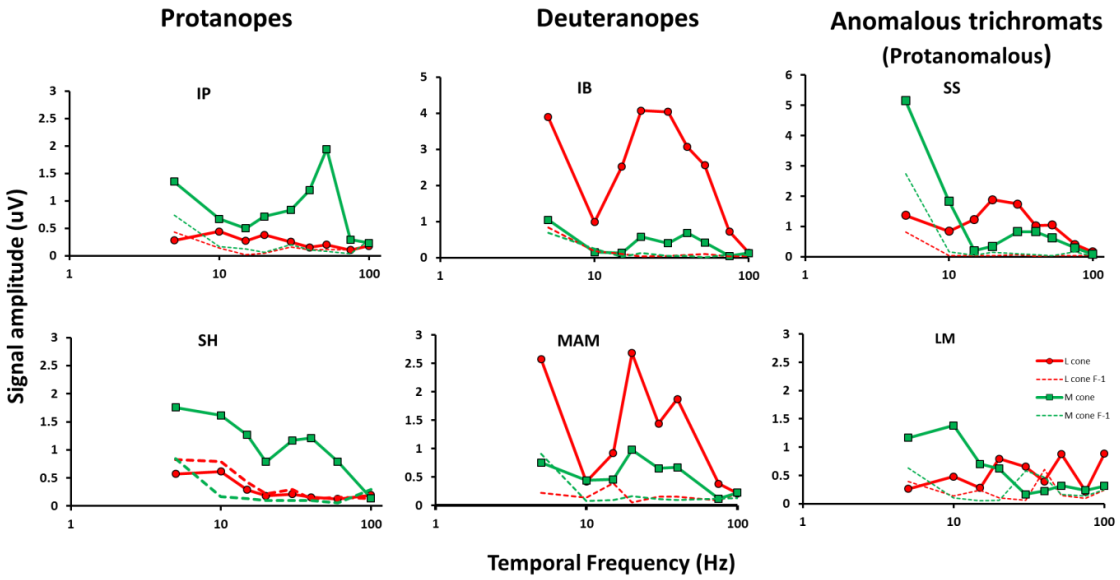

Figure 5-5 Temporal responsivity of the first harmonic (F) signal amplitudes of L- and M- cone steady ERGs obtained in four dichromats, protanopes (n=2) (first column), deuteranopes (n=2)(middle column) and two anomalous trichromats (last column).

5.3.2 Experiment 2 (Intensively sampled data)

We sampled temporal frequency response functions of L- and M- cone ERGs more intensively in a subgroup (n=6) of the trichromatic observers (see figure 5.7) in order to investigate further how response energies vary from low to high temporal frequencies in terms of amplitudes and phase. The vector averaged first (F) and second harmonic (2F) response amplitudes of L- and M- cone driven ERGs are shown in figure 5.6. These response functions were shown to be of a similar form to those observed in less intensively sampled data. Note that error bars at low frequencies for both L- and M- cone driven fundamental and second harmonic signals were shown to be higher in comparison to responses obtained at high frequencies. This may be suggestive of high inter-individual differences in numerosity of foveal L- and M- cones (Brainard et al., 2000; Carroll et al., 2002; Hofer et al., 2005, Challa et al., 2010).

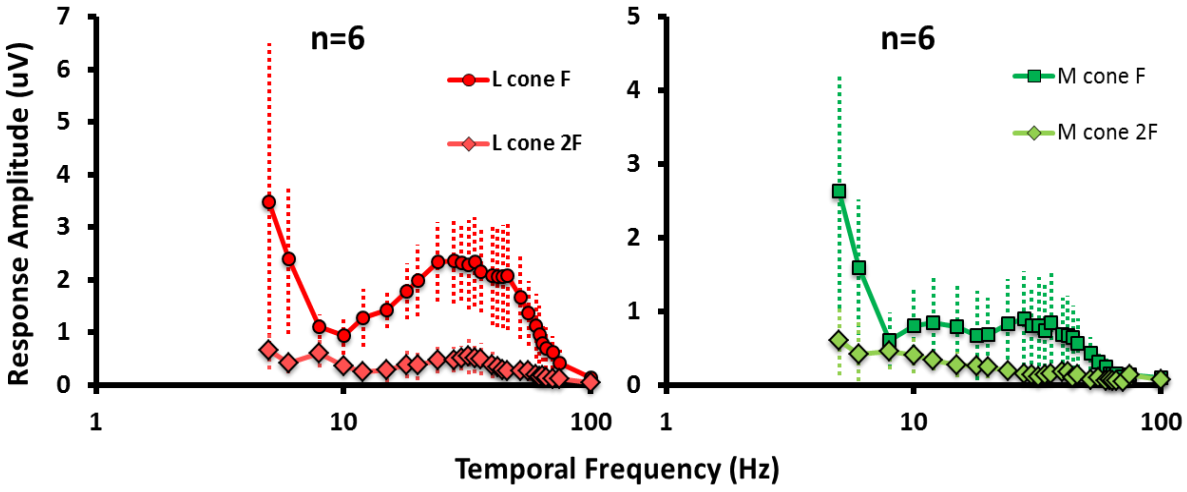

Figure 5-6 Vector averaged fundamental and second harmonic ERG amplitudes obtained in response to L- (left) and M- cone isolating sine wave stimuli in normal trichromatic observers plotted as a function of temporal frequency.

Dotted lines indicate error bars representing standard deviation of response amplitudes at the given stimulus frequency.

The second harmonic (2F) response amplitudes derived from both L- and M-cone driven ERGs were shown to contain little response energy barely rising above noise levels demonstrating a high degree of response linearity compared to the response derived from their first harmonic counterparts.

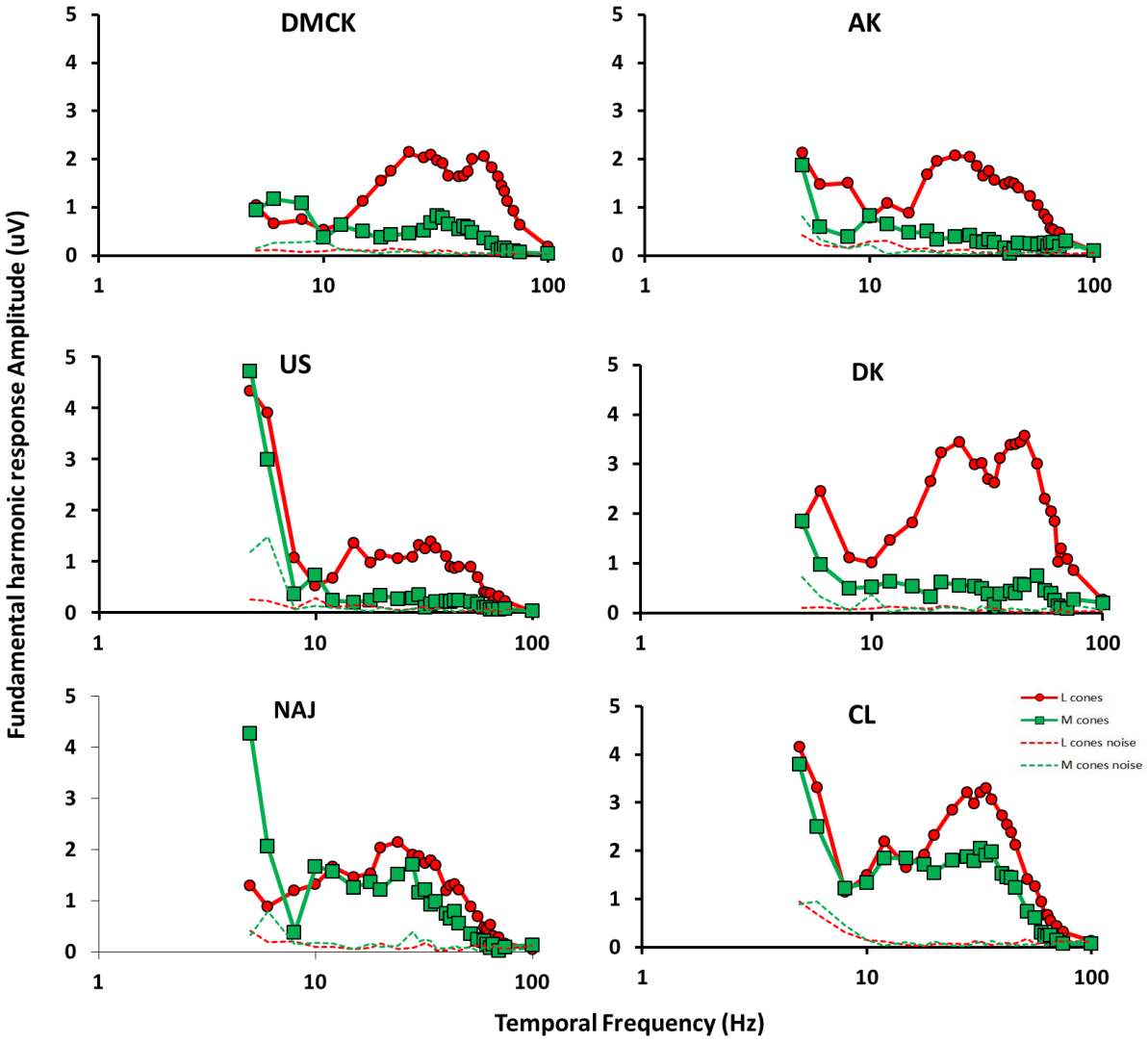

Figure 5-7 Graphs showing individual L- and M- cone amplitudes plotted as a function of temporal frequencies

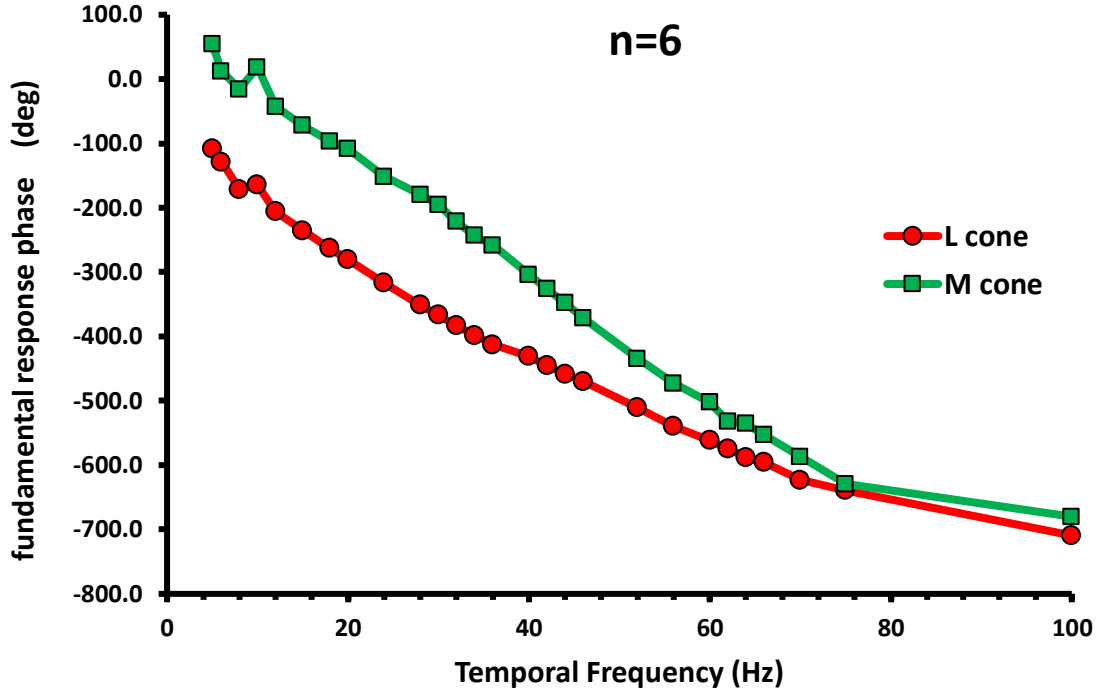

Figure 5-8 Vector averaged L- and M- cone phase data plotted as a function of temporal frequency (n=6).

Figures 5.8 and 5.9 show how phases of L- and M- cone ERGs vary with change in temporal frequency. Such data is a sensitive indicator of the temporal stability of underlying L-, M- cone mediated response mechanisms. When slopes appear parallel as shown in both graphs, they represent involvement of mechanisms with similar temporal response characteristics. On the other hand, these slopes appear to converge at high temporal frequencies and may reflect mechanisms with different temporal characteristics.

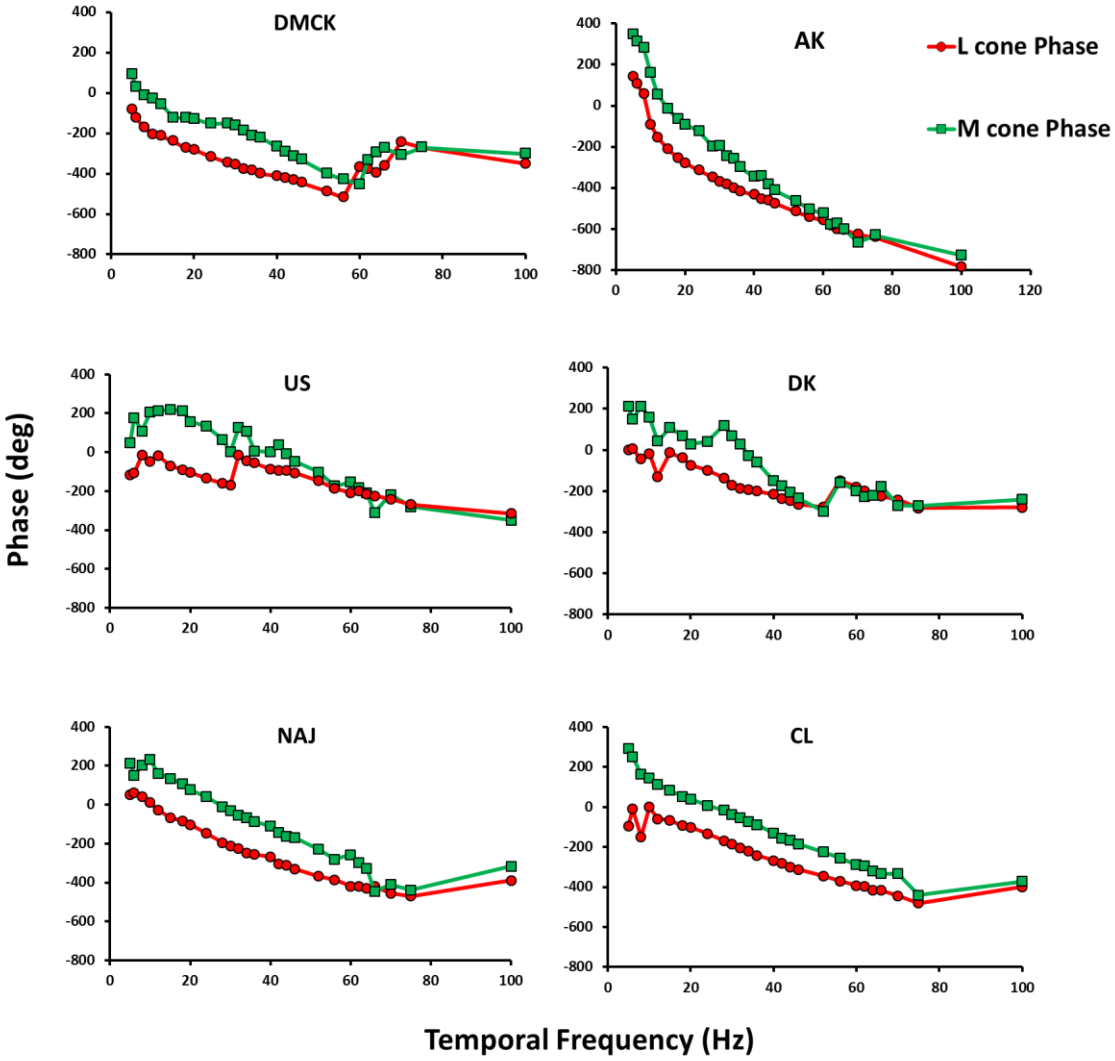

Figure 5-9 Individual phase data obtained from six normal trichromatic observers plotted as a function of temporal frequency.

Apparent latency

Apparent latency (τ) provides a measure of response delay based on the slope of the response phase as a function of temporal frequency (Van Der Tweel and Lunel, 1965; Regan, 1966; Odom et al., 1992). Apparent latencies are conventionally used in VEP studies that provides a measure of response delay based on the slope of the phase versus frequency function (ΔΦ/Δf) where

$$r = (1/360) * (\Delta\Phi/\Delta f)$$

The apparent latencies were calculated for both L- and M- cone ERGs plotted as a function of temporal frequency. Each data point on the graph is characterised by the local apparent latency, calculated by performing regression analysis on discrete portions (for instance five points in this case) of the L- and M- cone phase functions.

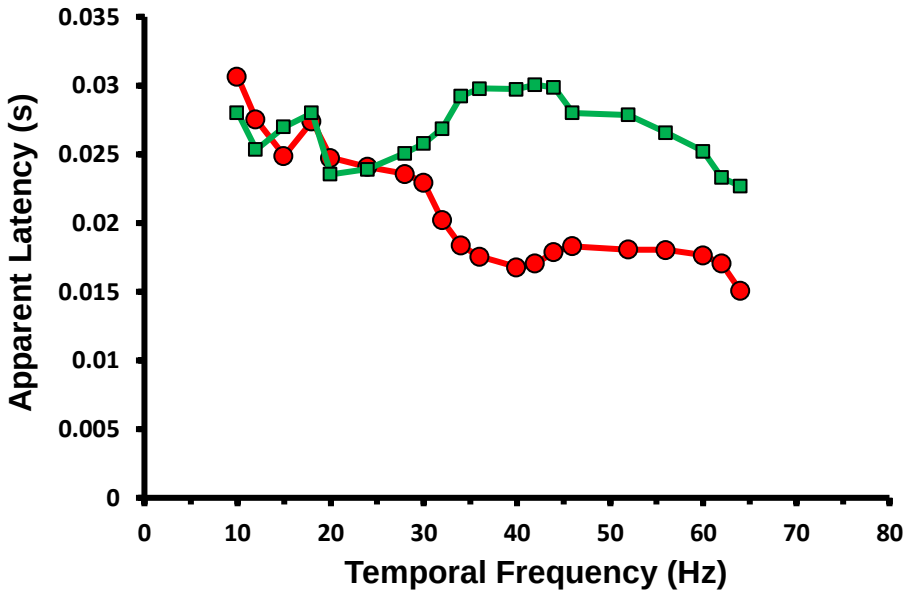

Figure 5-10 Apparent latencies of vector averaged L- and M- cone driven steady state ERGs plotted as a function of temporal frequency.

The apparent latency values derived at low temporal frequencies were shown to be similar with a mean difference between L- and M- cone responses below 20 Hz of 1.76 ms, with a maximum difference of 2.6 ms at 10 Hz. On the other hand at high temporal frequencies (>20 Hz), the apparent latencies were shown to diverge with M-cone apparent latency being greater than that for L-cones (see figure 6.11). There is a mean difference of 9.6 ms between 30 and 60 Hz, with a maximum 13.01 ms at 42 Hz (see figure 5.10).

The response amplitudes of the fundamental component of L- and M- cone ERGs were used to compute L:M cone ratios plotted as a function of temporal frequency (see figure 5.11). On the x-axis we used a scale up to 60 Hz as beyond this frequency M- cone responses were shown to fall to noise levels. Note that when L:M cone ratios are plotted in this manner, they demonstrate a near 1:1 ratio at low temporal frequencies (<10 Hz) with error bars representing small inter-individual differences. In contrast to this, when there is an increase in temporal rates beyond 20 Hz, L:M cone ratios appear to increase with high inter-individual differences. This finding is consistent with previous reports on L:M cone ratios obtained in response to fast flicker ERGs and to those ratios obtained using imaging techniques, psychophysical and electrophysiological methods (Brainard et al., 2000; Kremers et al., 2000; Carroll et al., 2002; Neitz et al., 2002).

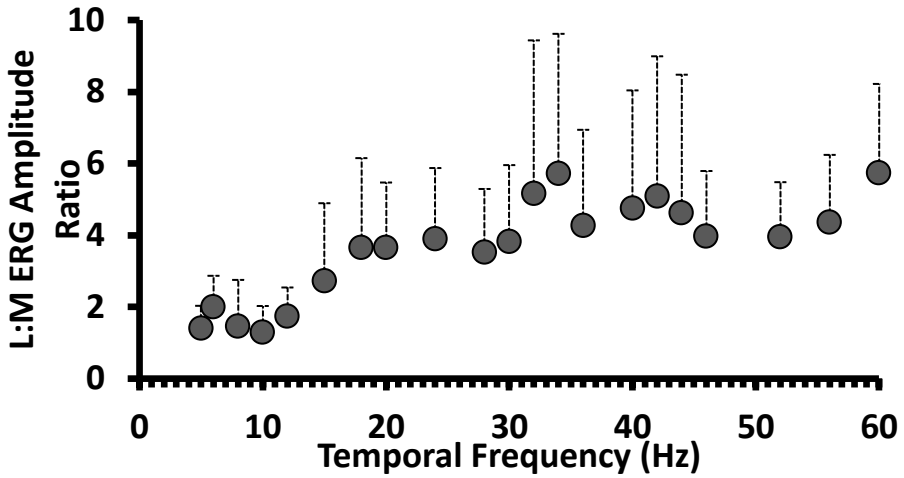

Figure 5-11 L:M cone ERG signal amplitude ratios plotted as a function of temporal frequency.

Data obtained from six normal trichromats from the intensive sampling group. Dotted error bars indicate standard deviation of the mean at each temporal frequency. Error bars indicate standard deviation and represents inter-individual variability in L:M cone ratios.

5.3.3 Experiment 3 (S- Cone Intensively sampled data)

Figures 5.12(A) and 5.13 demonstrate the group averaged and individual S- and L+M cone fundamental component (F) response amplitudes derived from five normal trichromats. We can see from the data that at all frequencies L+M cone responses are greater in their magnitude in comparison to S- cone signals. Furthermore, distinct L+M cone responses can be observed up to about 75 Hz whilst S- cone responses appear sluggish and attenuate above 10 Hz. These findings are consistent among all five observers (see figure 5.13). S- cone responses displayed a low-pass function with a rapid decline of response amplitudes above 28-30 Hz as shown in figures 5.12 (A) and 5.13 whilst the L+M cone responses exhibit a band-pass function with peak responses at around 5-, 28- and 44- Hz. It is interesting to note that both S- cone and L+M cone responses showed a dip in their amplitudes at around 10 Hz similar to what we observed in L- and M- cones responses with higher signal amplitude at 5 Hz.

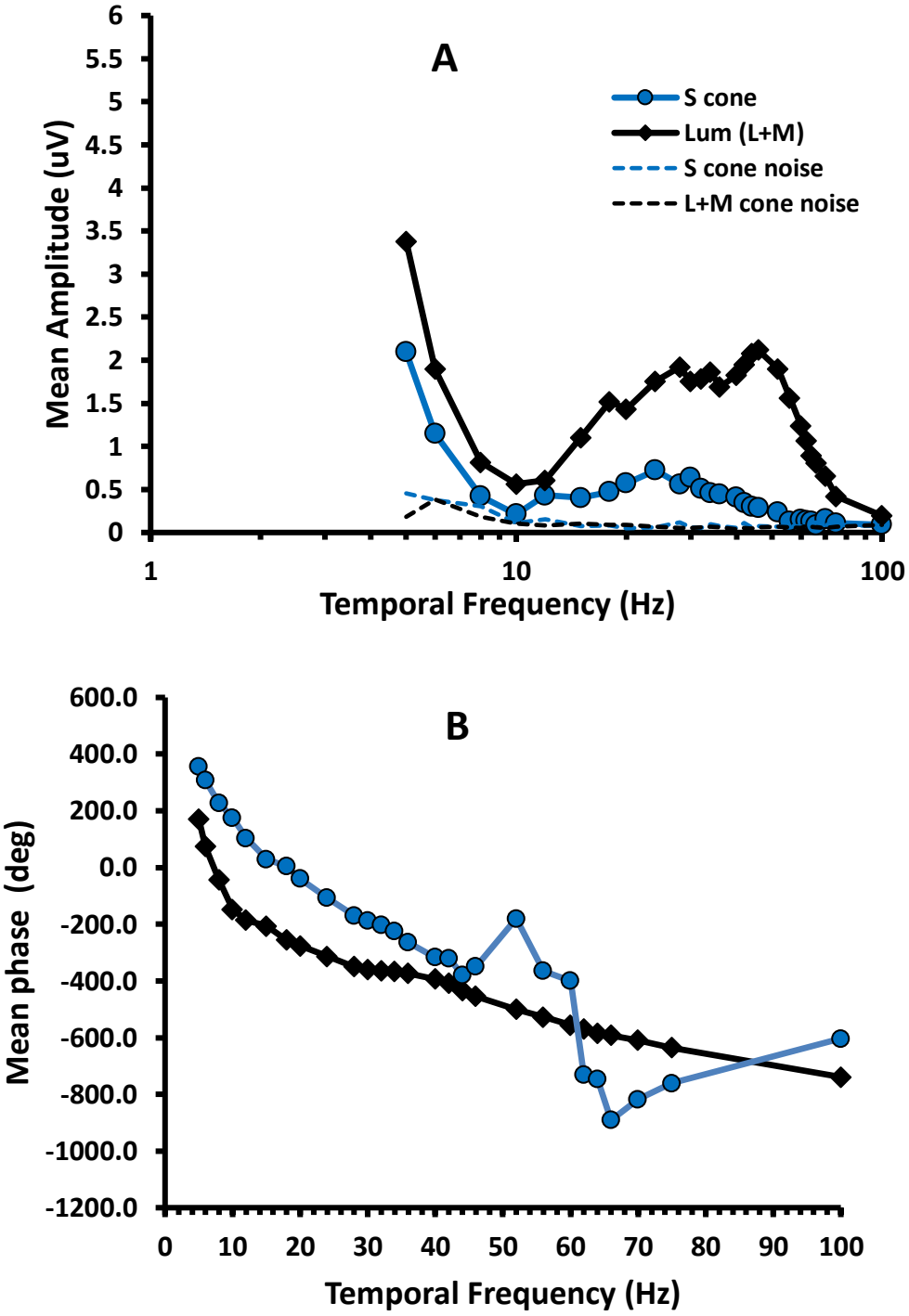

Figure 5-12 (A) Group average data of Fundamental component (F) amplitudes of S- and L+M cone driven ERGs plotted as a function of temporal frequency. (B) Vector averaged S- and L+M cone phase data plotted as a function of temporal frequency obtained from normal trichromats (n=5).

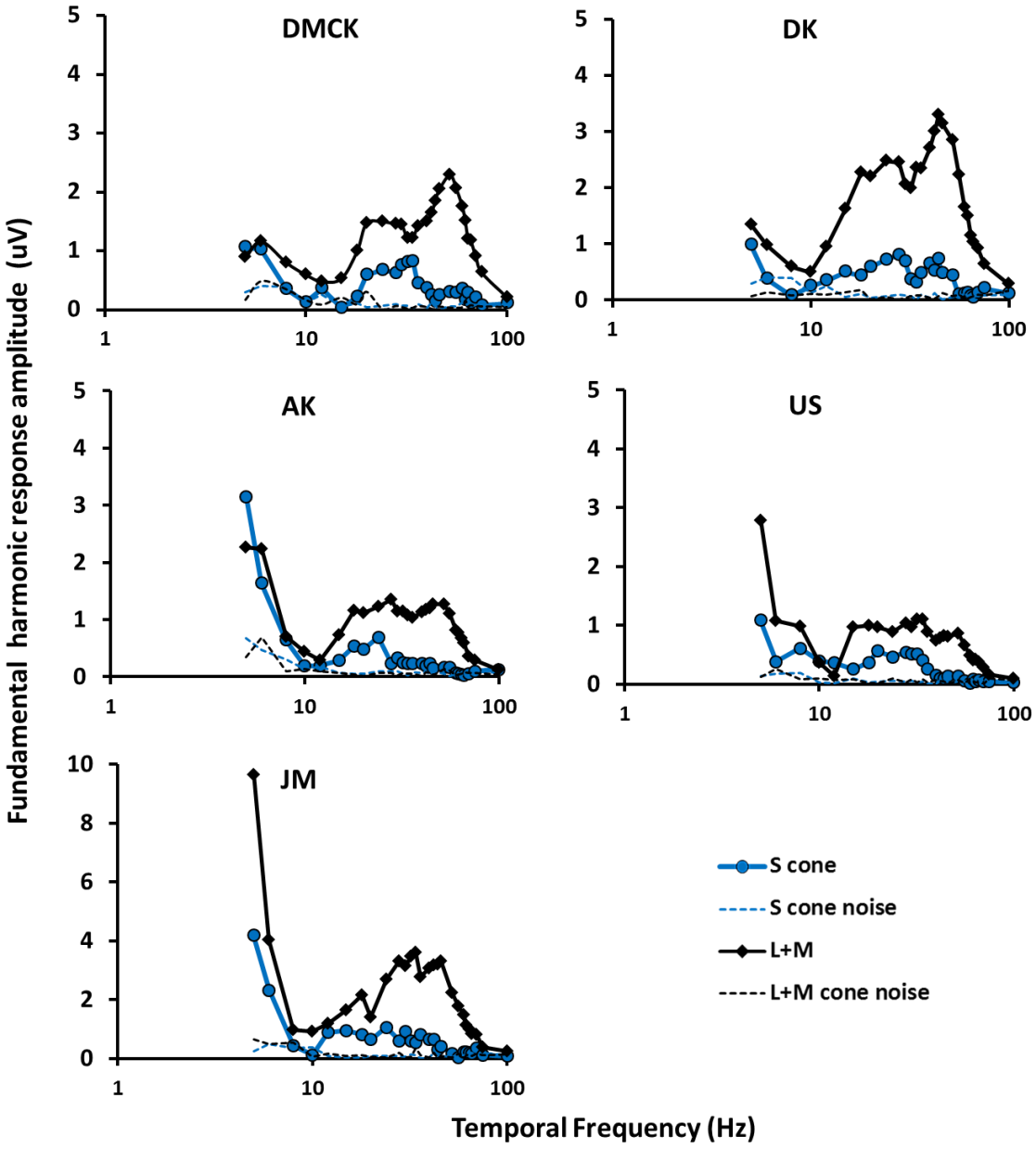

Figure 5-13 Graphs showing individual S- and L+M cone amplitudes obtained from normal trichromatic observers plotted as a function of temporal frequency (n=5).

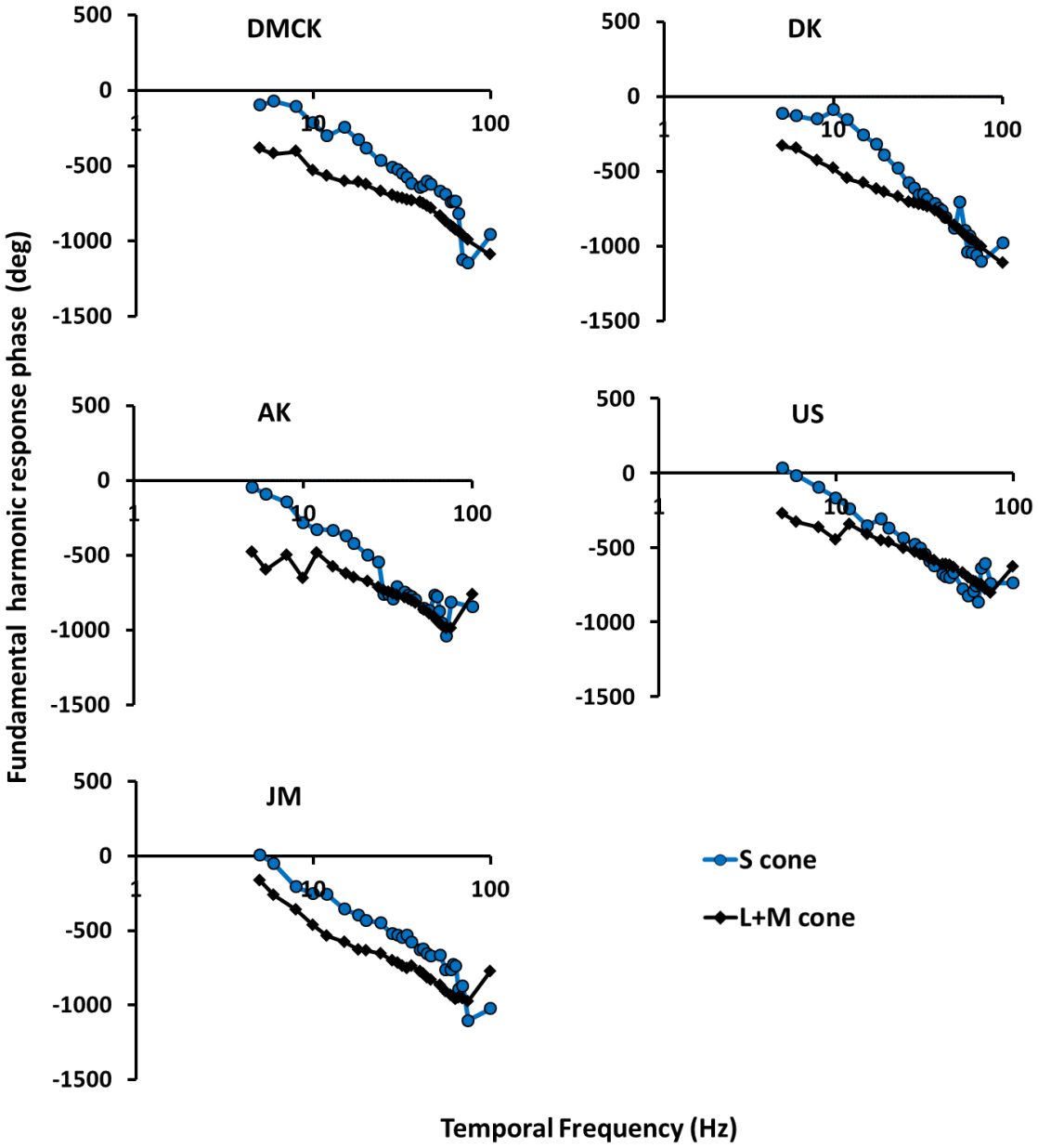

Figure 5-14 Individual phase data obtained from five normal trichromatic observers plotted as a function of temporal frequency.

Figures 5.12 (B) and 5.14 show vector averaged and individual S- and L+M cone first harmonic response phases obtained in five normal trichromats. We observe from the data that the phase difference between these signals is about 180 degrees and were shown to converge with decrease in phase difference with increase in temporal frequency. Note that phase data of S-cones at higher frequencies (>10 Hz) display irregular trend and cannot be used for interpretation since the responses saturate beyond about 28 Hz.

5.4 Discussion

(A) L- and M- cones

The main aim of this study was to retest the hypothesis that L- and M- cone driven ERGs at low and high temporal frequencies reflect properties of post-receptoral mechanisms and to reassess if the silent substitution stimuli used in our experiment is effective in acquiring isolated L- and M- cone ERGs. Here we draw parallels between our results and previously published electrophysiological and psychophysical data.

Our L- and M- cone ERG response amplitudes are similar to luminance ERG response functions reported by previous electrophysiological studies (Kremers, 2011). These response functions can be divided into two distinct regions: 1) a low frequency region (<10 Hz), where both L- and M- cone ERGs are balanced in terms of their signal strengths leading to L:M cone ratios close to unity. This is supported by phase data where the phase difference between signals derived from both cone classes were shown to be about 180 degrees and have similar apparent latencies, and 2) a high temporal frequency region (>20 Hz) where the L- and M- mediated ERGs displayed differing response properties. At these frequencies, L- cone ERGs are of larger amplitude than their M- cone counterparts with a phase difference of about 90 degrees and their apparent latencies are different. These response properties at low and high temporal rates are consistent with what has been described earlier in previous studies (Kremers, 2003; Challa et al., 2010; Kremers and Pangeni, 2012).

(B) L:M cone ratios

Few studies in the past have provided an estimation of actual cone counts and distribution of L- and M- cones in the human retina (Roorda and Williams., 1999; Brainard et al., 2000; Roorda et al., 2001; Hofer et a;., 2005). These results were well correlated to psychophysically (Vos and Walraven, 1971; Williams et al., 1981; Pokorny et al., 1991) and electrophysiologically (Caroll, 2002) determined estimates of human L:M cone ratios. Results from these experiments suggested a preponderance of L- cones over other cone types across the human retina with a high inter-individual variability in L:M cone ratios. Estimates of relative number of L- and M- cones have ranged from 0.3:1-3:1 (Rushton and Baker, 1964); 1:1.5 to 3.79 (Roorda and Williams., 1999) and L:M cone ratios as high as 12:1 have also been observed in the human retina (Dobkins et al., 2000; Carroll et al., 2000). Challa et al (2010) conducted an experiment using L- and M- cone isolating low (12 Hz) and high (30 Hz) stimuli presented with varying spatial configuration and demonstrated that L:M cone ratios obtained in response to 12 Hz stimuli were 1:1 irrespective of eccentricity. This was not the same for responses obtained at 30 Hz as at this frequency, L:M cone ratios were shown to increase with eccentricity. A possible explanation could be that at low temporal frequencies, it is L-,M- cone mediated midget cells that respond to stimuli at low temporal rates producing closely matched response amplitudes obtained from both cone classes (i.e., the L:M cone ratio is close to unity). This balanced response contribution of L- and M- cones at low temporal frequencies could reflect the activity of midget cells within parvocellular system that underpin the chromatic, cone-opponent processing mechanisms (Lee et al., 1990; Kremer et al., 1992; Lee, 2011).

A key feature of this finding is that these 1:1 L:M cone ratios were shown at low frequencies irrespective of the actual relative count of L- and M- cones that exist in the retina as a whole (Brainard et al., 2000). On the other hand, L:M cone ratios derived at high flicker rates with a high inter-individual variability were shown to be remarkably close to what has been reported by imaging studies (Hofer et al, 2005).

An interesting observation of the trichromatic L- and M- cone ERGs at low temporal rates is that the responses obtained from these two cone classes is nearly equal in amplitude whereas this is not the case in responses obtained in dichromats. Figure 5.15 illustrates the ERG derived L:M cone ratios obtained in both trichromatic and dichromatic observers at 5- and 30- Hz. The measured L:M cone ratios derived from protanopes and deuteranopes at 5 Hz were not close to unity as shown in normal trichromats. The departure from the 1:1 L:M cone ratio at this frequency could reflect the absence of either L- or M- cones from their respective retinae and may be suggestive of abnormal cone input to the chromatic pathway. Thus, at low temporal frequencies the L:M can provide an assay of functional integrity of L-M cone opponency in the human retina. Our results indicate that the comparison of L- and M- cone steady state ERGs at low temporal frequencies may provide an objective, electrophysiological method for testing red-green colour deficiencies.

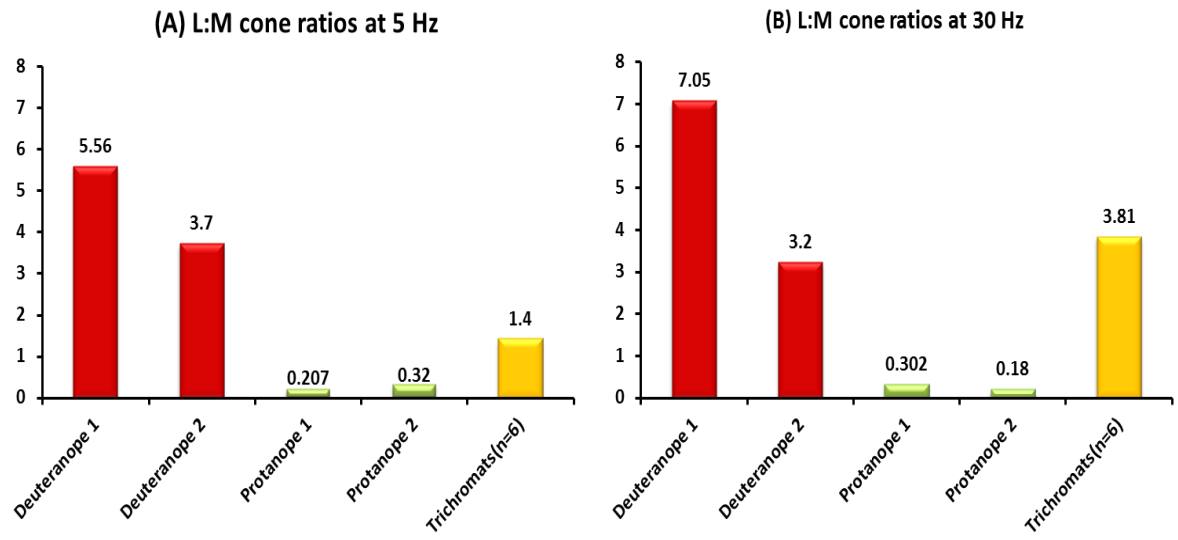

Figure 5-15 L:M cone ERG response amplitudes measured at a temporal frequency of (A) 5 Hz and (B) 30 Hz respectively.

The graph shows the measured values from two deuteranopes (red bars), two protanopes (green bars) and a mean L:M amplitude ratios obtained in six normal trichromats (yellow bars).

The link between cone opponency at low temporal frequencies mirrors the use of the ERG elicited at higher flicker rates as a functional assay of cone into postreceptoral mechanisms that underpin luminance vision (Jacobs et al., 1996; Jacobs and Deegan, 1997; Kremers et al., 2000; Brainard et al., 2000). As observed in figure 5.15, the L:M cone ratios measured at 30 Hz are greater than those found at 5 Hz in normal trichromats. This could be attributed to the presence of a relatively higher number of L- cones than M- cones present in the human retina (Hofer et al., 2005).

An important addition to this study is the calculation of apparent latencies of L- and M- cone ERGs (see figure 5.10). This data provides further evidence for the existence of functional dichotomy of L- and M- cone mediated ERGs elicited in response to low and high flicker rates. Below 20 Hz, latencies for the L- and M- cone mediated ERGs are similar with the largest difference between the two cone responses being 2.6 ms. This value is similar to the latency difference between the L- and M- cone inputs to the parvocellular ganglion cells recorded in the macaque retina (Smith et al., 1992). This finding reiterates the hypothesis that L- and M- cone driven steady state ERGs at low flicker rates demonstrate the chromatic, non-opponent processing pathway mechanisms, only presenting with a small difference in the apparent latency. Our results showed that at above 20 Hz, L- and M- cone apparent latency responses were shown to diverge with L- cone ERGs demonstrating shorter latencies than the M- cone responses. The maximum latency difference was observed to be high at 42 Hz (13.01 ms). This value is remarkably close to the latency differences determined in the psychophysical experiments using heterochromatic flicker photometry (HFP). HFP is a technique where the observer is presented with two lights modulated in counter-phase, the luminance differences between light stimuli can be eliminated by minimizing the perceived flicker.

Lee et al (1988) suggested that results from HFP reflects luminance vision in the primate visual system and underpins the activity of non-opponent neurons of the magnocellular systems. When observers perform HFP, residual flicker of the counterphase modulated lights is frequently reported at isoluminance, and this can only be eliminated by altering the relative phases of the lights (De Lange, 1958; Swanson et al., 1987). The phase difference obtained in this manner has been taken as evidence for the existence of a delay between the L- and M- cone inputs to the luminance system (Walraven and Leebeek, 1964; Drum, 1977; Swanson et al., 1987a, b). An important feature is that the delays reported in this study between L- and M- cone driven ERGs at high temporal flicker exhibited similar values to those measured psychophysically. This correlation would provide additional evidence in support for the view that fast flicker ERGs provide an index of the contribution of L- and M- cones to postreceptoral luminance processing pathways.

Our results highlight the potential use of silent substitution stimuli in achieving cone isolated steady state ERGs which may provide a measure of activity of individual cone class within the parvo- and magno-cellular processing pathways. These pathways have been widely acknowledged as forming the respective physiological substrates for L-M chromatic and L+M luminance vision in the primate subcortical visual system (Wiesel and Hubel, 1966; De Monasterio and Gouras, 1975; Dreher et al., 1976; Hicks et al., 1983; Derrington and Lennie, 1984; Shapley and Perry, 1986; Lee et al., 1987; 1989; Stockton and Slaughter, 1989; Schiller et al., 1990; Kaiser et al., 1990; Boycott and Wassle, 1991; Valberg et al., 1992; Wassle et al., 1994; Bush and Sieving, 1996; Dacey, 2000; Lee et al., 2010; Parry et al., 2012).

The parvo- and magno-cellular pathways constitute major functional subdivisions and receive input from midget and parasol ganglion cells of the inner retinal layers (Lee, 2011). The parvo- and magno-cellular pathways constitute major functional subdivisions and receive input from midget and parasol ganglion cells of the inner retinal layers (Lee, 2011). However, it is unlikely that the ERGs elicited in response to low and high temporal frequency flicker rates directly reflect the activity of these two cell populations. Instead, there are reports that suggest that these responses are more likely to reflect the operation of bipolar cell activity in the generation of these signals (see figure 5.16) (Stockton and Slaughter, 1989; Boycott and Wassle, 1991; Wassle et al., 1994; Morrone et al., 1994; Bush and Sieving, 1996; Dacey, 2000; Kremers, 2009).

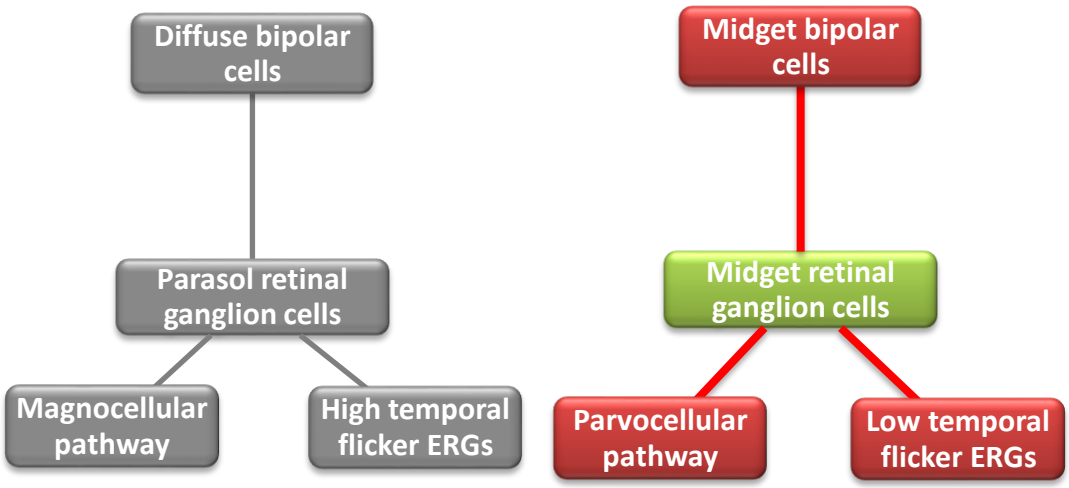

Figure 5-16 Contribution of flicker ERGs at high (left) and low (right) temporal frequencies reflecting activity of magno- and parvo-cellular pathway mechanisms of human visual system and their contribution to steady state ERGs.

A model proposed by Kremers et al (2009).

Although there is clear evidence on segregation of chromatic and luminance signals at bipolar cells in non-primate retina, there is little information in supporting this view in the primate retina. In fact, anatomical studies in the marmoset retina suggests that midget and parasol ganglion cells may not directly inherit response properties from their midget and diffuse bipolar input (Erikoz et al., 2008). An alternative explanation for the temporal response functions of L- and M- cone ERGs in the absence of clear cut evidence of functional segregation of chromatic and luminance mechanisms at the level of bipolar cells is the temporal-dependent on- and off- bipolar cell interactions that may attribute to these response functions. Such interactions between ON- and OFF- bipolar cells contributing to luminance ERGs has been previously described using pharmacological agents (Bush and Sieving, 1996; Kondo and Sieving, 2001). Contributions from other retinal cells like horizontal cells, amacrine cells and retinal glial cells to these response functions cannot be ruled out (Lee et al., 2010).

S- cone

The fundamental response amplitudes of L+M cones were shown to be larger than signals derived from S- cones. This finding reiterates the fact that the normal human retina has relatively less number of S- cones and is dominated by L- and M- cones. From the literature, data from psychophysical experiments report that S- cones exhibit a lower critical flicker fusion frequency (Brindley et al., 1966; Marks and Bornstein, 1973; Stockman et al., 1991) and our data further adds to the evidence that the temporal resolution of S- cone is below 28 Hz (Kelly, 1974; Wisowaty and Boynton, 1980; Stockman et al., 1991).As it is known S- cone system convey their signals via two pathways, our data suggests that the isolated S- cone signals recorded in this experiment may reflect the activity of brisk and sluggish S- cone pathway. We assume so, 1) because we noticed a loss of responsivity at high frequencies, 2) rapid decline of signal amplitudes above 30 Hz, 3) a phase difference of about 180 degrees between S- cone, chromatic and L+M, achromatic data at frequencies below 18 Hz, may suggest the properties of blue-yellow cone-opponent, Koniocellular pathway activity. We suggest that more data is required from different age groups to see how age related ocular changes may affect these signals and using S- cone monochromats as controls to examine the validity of the stimuli used in this experiment would be beneficial.

5.5 Conclusion

The preceding discussion has attempted to explain the temporal-frequency dependent changes in L-, M- and S- cone isolated steady-state ERG response characteristics. Although the interpretation of the data remains unclear at present, it is apparent that there are clear correlations between ERG response properties at high and low temporal frequencies and their contributions to postreceptoral luminance and chromatic processing pathways respectively. With careful choice of stimulus parameters, L-, M- and S- cone isolated steady state ERGs may have the potential to provide an objective measure of chromatic and luminance vision.

Chapter 6 - The effect of temporal frequency and retinal illuminance on Rod and Cone driven Human ERGs using Silent Substitution

6.1 Introduction

Together, rods and cones enable retinal sensitivity over a 50 billion-fold dynamically changing light intensity encountered in the transition from night or scotopic to day or photopic light conditions. In addition to photopic or scotopic vision where only either cones or rods are active, mesopic vision is more complex as it involves both rod and cone activity. Previous psychophysical evidence show that rod activation at mesopic light levels influence many cone-dependent functions such as chromatic discrimination (Stabell & Stabell, 1977), colour appearance (Buck et al., 2000; Cao et al., 2005; 2008) and temporal processing (Cao et al., 2006, 2007; Zele et al., 2008).

Although human cone photoreceptors offer an exquisite resolution of spatial detail, detection and discrimination of millions of hues contributing to majority of daily vision, nearly 95% of the total photoreceptor population comprise of rods. Rod photoreceptors respond under low light levels as they are sensitive to single photons (Baylor, 1987; Rieke, 2000) and are also believed to contribute to colour vision under mesopic light levels (Zele and Cao, 2015). Understanding the physiology of rod photoreceptors becomes important in view of a clinical perspective as in comparison to cone dysfunction, rods have shown to have a devastating effect on vision in several congenital retinal disorders including retinitis pigmentosa (RP), congenital stationary night blindness (CSNB), rod-cone dystrophy and Vitamin- A deficiency.

In addition to this, there is growing evidence suggesting that rods precede cone photoreceptor loss in early stages of age related macular degeneration (ARMD) which is the most common cause of legal blindness in the elderly population in the developed world (Curcio et al., 1996; 2000; Adler et al., 1999) and more arguably in glaucoma (Kendell et al., 1995; Nork et al., 2000).

To measure ERG signals, a variety of strategies can be used such as the manipulation of the chromatic, luminance and temporal characteristics of the stimulus as well as the observer's state of adaptation. In a clinical setting, rod isolated ERGs are recorded in response to a set of brief light stimuli of low intensities after rod sensitivity is maximised by a 20-30 minute dark adaptation as recommended by International Society for Clinical Electrophysiology of vision (ISCEV). However, in recent years with the evolution of four and five primary stimulators there has been increasing evidence of obtaining rod mediated signals using silent substitution (Shapiro et al., 1996; Pokorny et al., 2004). This method takes advantage of the knowledge of spectral sensitivities of each photoreceptor class (as described in chapter 3) and provides a means of achieving isolated responses from individual photoreceptor populations (Estévez and Spekreijse, 1982).

In this study we wanted to examine the temporal processing of the human rod system using silent substitution paradigm in response to sinusoidally modulated flicker stimuli. In addition to this, we wanted to provide the objective measure of rod critical flicker frequencies as a function of retinal illuminance using our stimuli and if these measures are comparable to previously established data. Here we report rod isolated responses obtained over a range of temporal frequencies and

retinal illuminances in normal subjects and compare them to L-, M- and S- cone isolated responses.

The main aim of this study was to examine the temporal response characteristics of rod driven ERGs obtained using silent substitution method. Our main focus was to examine ERGs obtained using rod-isolating stimuli in terms of temporal frequency, compare these responses to cone temporal response functions and investigate how low- and high temporal frequency rod mediated ERG responses vary with change in luminance characteristics. Previous studies reported that rods exhibit low-pass function and their critical flicker frequencies can reach up to 28 Hz at high scotopic light levels (Ives, 1922; Conner, 1982; Stockman et al., 1991). From previous experiments, we know that cones respond to temporal frequencies up to 100 Hz as observed in normal trichromats. Therefore, we could use this knowledge of different rod and cone temporal dependent responsivities in investigating the rod responses elicited using our silent substitution stimuli. To measure rod responses in the light adapted eye using high intensity stimuli, we should be careful in ensuring that rod selectivity is maintained and cone intrusions are reduced. Acquiring ERG responses as a function of retinal illuminance will help us gauge the extent of such intrusions. Furthermore, we took advantage of the fact that rods do not contribute to photopic vision and used this information in validating if the stimuli used in this experiment are rod isolating.

6.2 Methods

In this chapter, we focus on the examination of temporal processing of isolated human rod driven ERGs and how these responses change with variation in retinal illuminances using silent substitution method. In doing so, we speculate that we could define stimulus parameters that have the potential to isolate rod function without cone intrusion under photopic conditions without the need for dark adaptation. This approach could provide with an alternative to currently available techniques and may be more time-efficient and probably provide improved rod selectivity in both normal and disease conditions. We performed this experiment using a four LED ganzfeld stimulator (as described in Chapter3)

6.2.1 Stimuli

We generated sinusoidal, full-field flicker stimuli, where the luminances of the LED classes were modulated with sinusoidal temporal profiles ranging from 5 to 100 Hz in Experiment 1 and 5 to 40 Hz in Experiment 2 (4, 6, 8,10, 12, 15, 18, 24, 30 and 40 Hz). All the measurements were recorded at retinal illuminances of 120 Td, 1200 Td and 12000 Td (Experiment 1) and 1 Td to 10000 Td (Experiment 2) ranging from mesopic to photopic light levels. We used a four-primary ColorDome ganzfeld stimulator (Diagnosys LLC, Lowell, MA) to control rod and cone responses independently. To excite rods alone, a Michelson contrast of 11% was used while maintaining L, M, and S cone contrast at zero and vice versa. We used photopic trolands instead of scotopic trolands to avoid confusion as we examined responses from both rods and cones across a wide range of retinal illuminances and when changing units from low to high intensities of light stimulus it would be easier for us to understand the rod response transition from mesopic to photopic light levels.

For our convenience, we used photopic trolands instead of scotopic trolands as in other studies for easier comparison of rod responses to those of cones. Photopic trolands, when multiplied by a factor of 2.489 produce scotopic trolands (Wyszecki and Stiles, 1982) and vice versa, we used this knowledge in understanding of our results in comparison to results obtained in other studies. Besides, these two experiments, we also examined how 8- and 30 Hz responses elicited in response to rod isolating stimuli varied with change in retinal illuminance in Experiment 3.

6.2.2 Subjects

A total of seven healthy observers with normal colour vision (assessed by colour vision tests described in chapter 3) with a best corrected visual acuity of 6/6 and no ocular pathology participated in the study with an age ranging from 23 to 48 years (four males and three females; 31.42+ 8.32 years (mean age$\pm$stdev)). Informed consent was obtained from all our participants prior to recruiting the participants. No individual observer calibration measurements were taken in this study. The protocols were approved by the Institutional Review Board of University of Bradford and adhered to the tenets of the Declaration of Helsinki.

6.2.3 ERG recording

ERGs were recorded from the right eyes of all participants using a silver/nylon corneal fibre electrode (Department of Physics and Clinical Engineering, Royal Liverpool University Hospital, UK). We placed electrodes as described in detail in chapter 3. Pupil diameter was measured to about 8 mm to ensure constant retinal illuminance across all subjects and was observed to consistent throughout the experimental session. After the placement of electrodes, impedance was measured until this was < 5kΩ. The ERG signals were amplified and band-pass filtered between 1 and 30 Hz and sampled at 1000 Hz. For each recording, atleast 16 sweeps were averaged based on the signal quality. If ERG traces were contaminated with blink artefacts, they were manually rejected. To minimize onset effect, first recording was automatically rejected. The order of presentation of temporally flickering stimuli was randomised in order to avoid any systematic adaptation effects across all the experimental sessions. Note that in both experiments we only included signals with SNR of 2.

6.2.4 Data Analysis

The averaged waveform for each stimulus condition was subjected to a fast Fourier transformation to extract the amplitudes of first and second harmonic and phase of the fundamental component. Noise was defined based on the amplitudes of the adjacent frequency 1 Hz below the test frequency. For instance, for the test frequency 8 Hz, the amplitude at 7 Hz was for estimation of noise. We defined signal as a pronounced response only when the fundamental response amplitude was about 2x greater than that of the noise amplitude for that frequency. Phase values extracted from Fourier analysis ranged from 0 to 360^0 - large differences between adjacent temporal frequencies were minimized as described in chapter 5.

6.3 Results

6.3.1 Experiment 1 Temporal properties of isolated rod ERGs under mesopic and photopic conditions

Conventionally, Rod ERGs are recorded using low intensity stimuli (Marmor et al., 2009; McCulloch et al., 2015) in the dark adapted eye. In this experiment, temporal response function of the fundamental component of ERGs derived using rod isolating silent substitution stimuli at retinal illuminances 120 Td and 12000 Td. The upper and lower plots as shown in figure 6.1, displays the vector averaged amplitudes and phases respectively.

At 120 Td, we observed a low-pass response function with peak responses of signal amplitudes at lower frequencies (<10 Hz). Figure 6.1 also demonstrates a steady decline of rod responsivity to noise levels at about 30 Hz. On the other hand, when the sine wave modulated rod isolating stimulus was presented at a retinal illuminance of 12000 Td (Photopic light levels), we observed a band-pass temporal function that extends up to higher frequencies with a peak response at about 30 Hz. At this retinal illuminance, the temporal response function was shown to be similar to that of cones (see experiment 1 for cone temporal function). This clearly indicates a loss of rod selectivity at 12000 Td and demonstrates that cones dominate ERG responses despite using rod isolating stimuli at these light levels.

The vector averaged phase data obtained from five healthy individuals as shown in figure 6.1 exhibit similar response phases as a function of temporal frequency regardless of the retinal illuminance used. However, we believe that at much lower retinal illuminances, the phase data could be different what is shown here in figure 6.1.

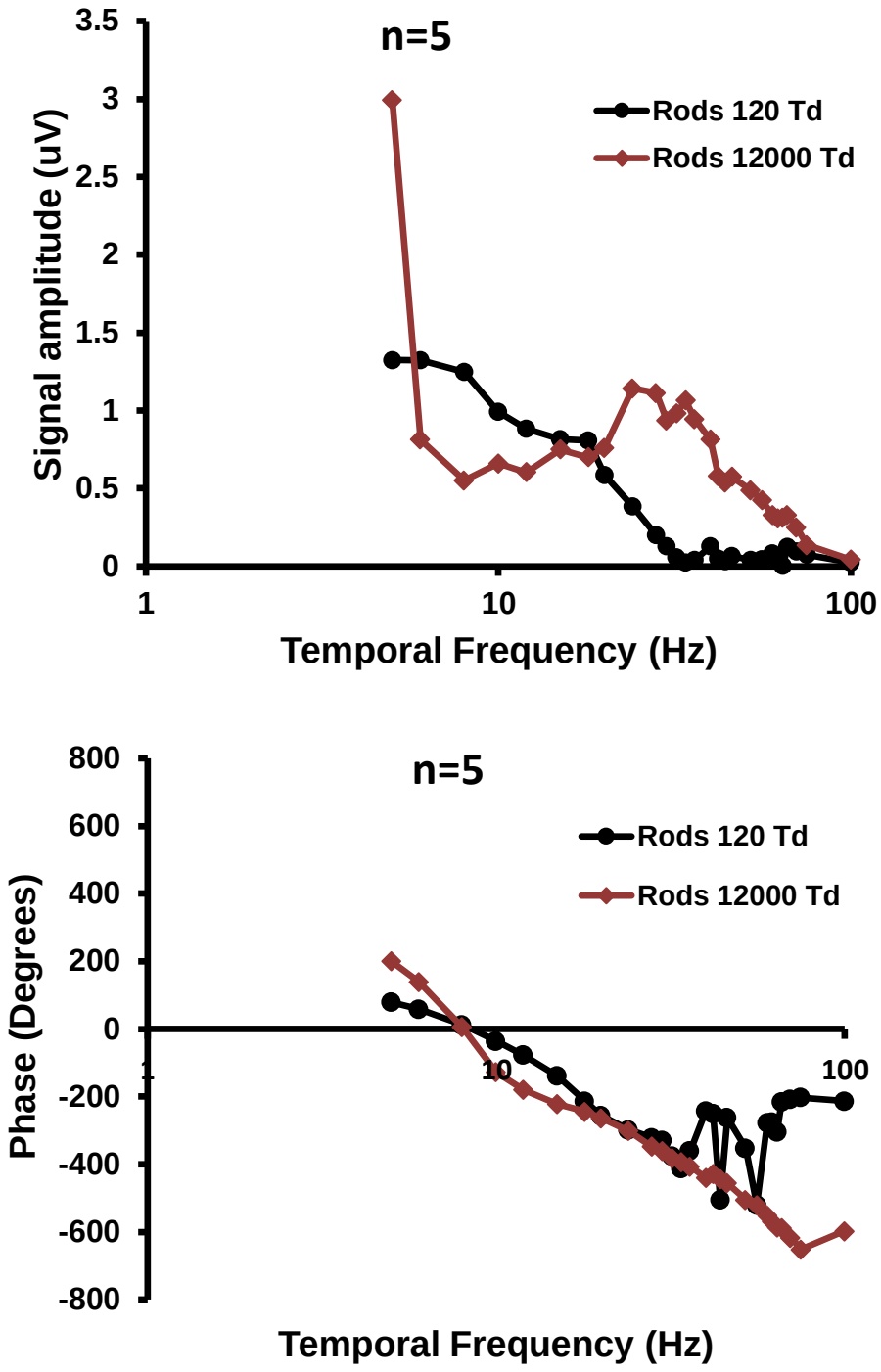

Figure 6-1 Vector averaged Fundamental (F) rod responses (n=5) plotted as a frequency of temporal frequency, derived at retinal illuminances 120 Td (mesopic) and 12000 Td (photopic).

The upper and lower plot demonstrates averaged signal amplitudes and phases respectively.

6.3.2 Experiment 2

Rod, L- and M- cone ERGs as a function of Temporal Frequency at different Retinal Illuminances

To investigate more closely and to examine how rod responses change with the transition from mesopic to photopic light levels, we used stimulus intensities with retinal illuminances ranging from 1 Td to 10000 Td. Furthermore, we examined the temporal properties of L-, M- and S- cones at these light levels and compared them to rod responses for stimulus frequencies ranging from 5- to 40- Hz.

Figures 6.2, 6.3, and 6.4 show ERG amplitudes derived in response to rod-, L- and M- cone isolating sinusoidally modulated stimuli in observers MK, DK and GG (two females and one male) with an age (STDEV) of 29 (3.09) who were all normal trichromats with a best corrected visual acuity of 6/6 with no ocular or systemic pathology that could affect the measurements.

We noticed that rod ERGs in all three participants were shown to have a low-pass function from 1-100 Td with peak responses observed at 4 Hz. Another interesting point is that rod responses were measurable until 100 Td above which the rod function seemed to saturate. In data obtained from all three observers, rod signal amplitudes were shown to be high at 4 Hz at a retinal illuminance of 10 Td.

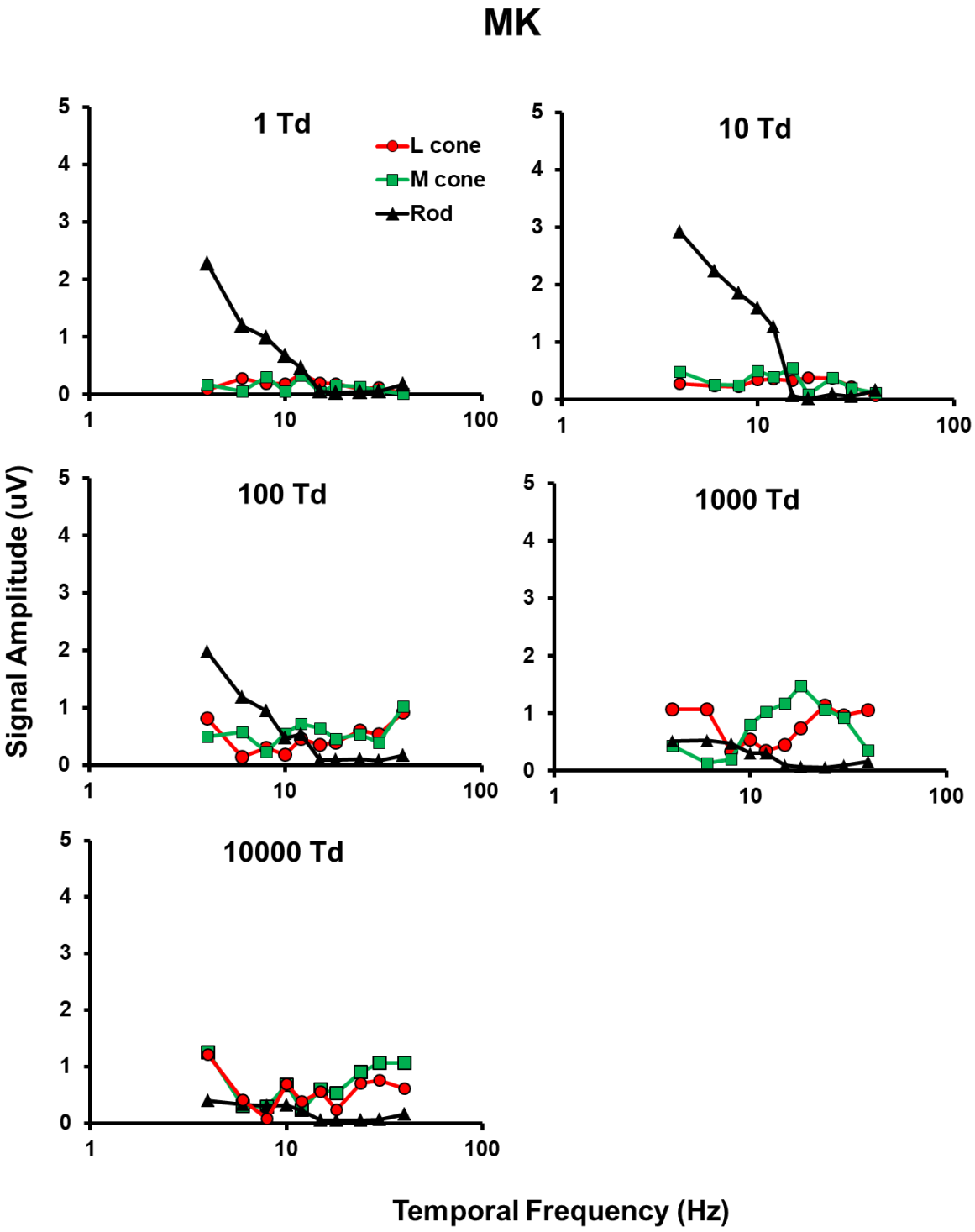

Figure 6-2 Temporal response characteristics of rods, L- and M- cone isolated ERGs for five stimulus conditions ranging from low mesopic to photopic light levels (1 Td, 10 Td, 100 Td, 1000 Td and 10000 Td) recorded in observer MK.

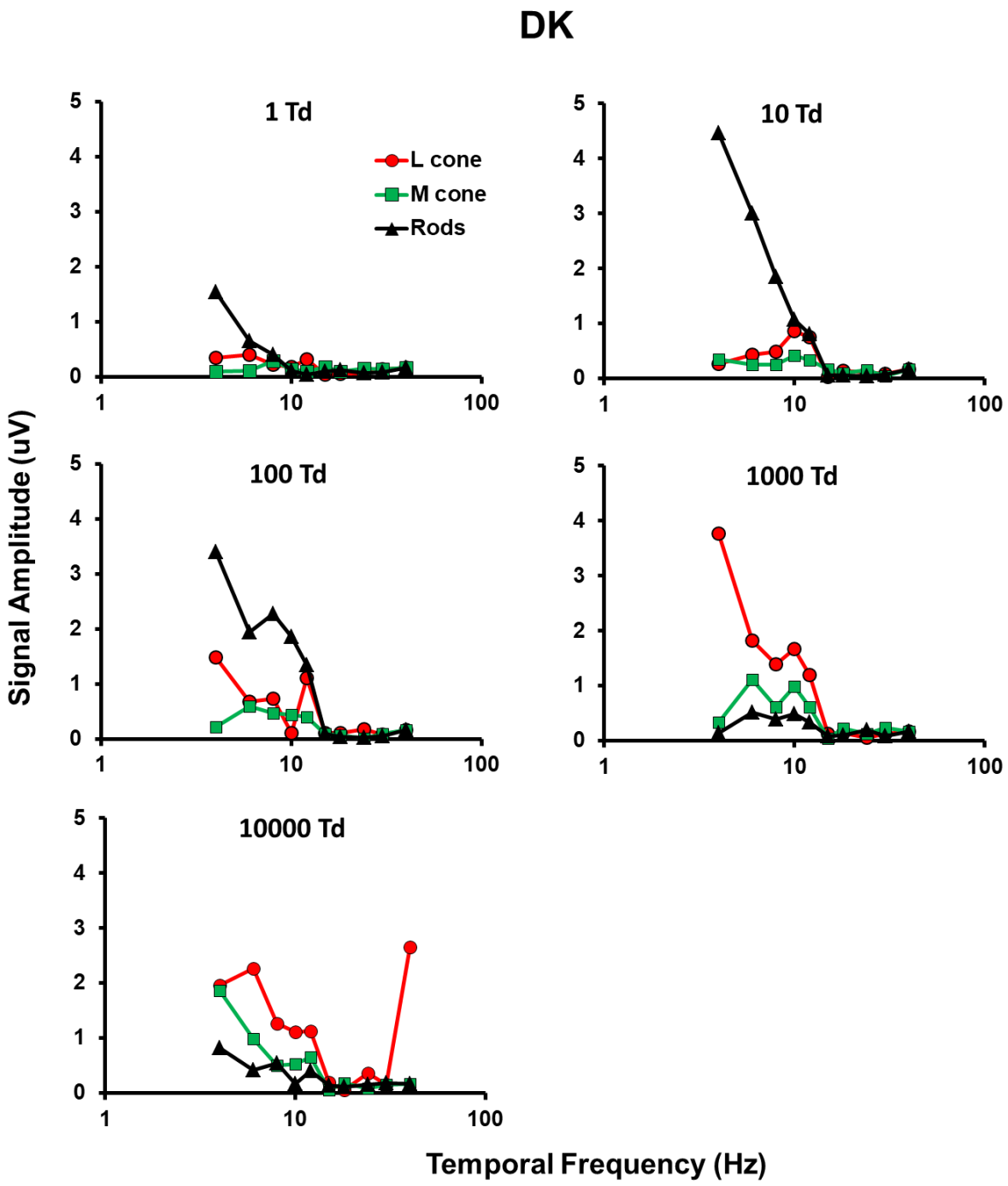

Figure 6-3 Temporal response characteristics of rods, L- and M- cone isolated ERGs for five stimulus conditions ranging from low mesopic to photopic light levels (1 Td, 10 Td, 100 Td, 1000 Td and 10000 Td) recorded in observer DK.

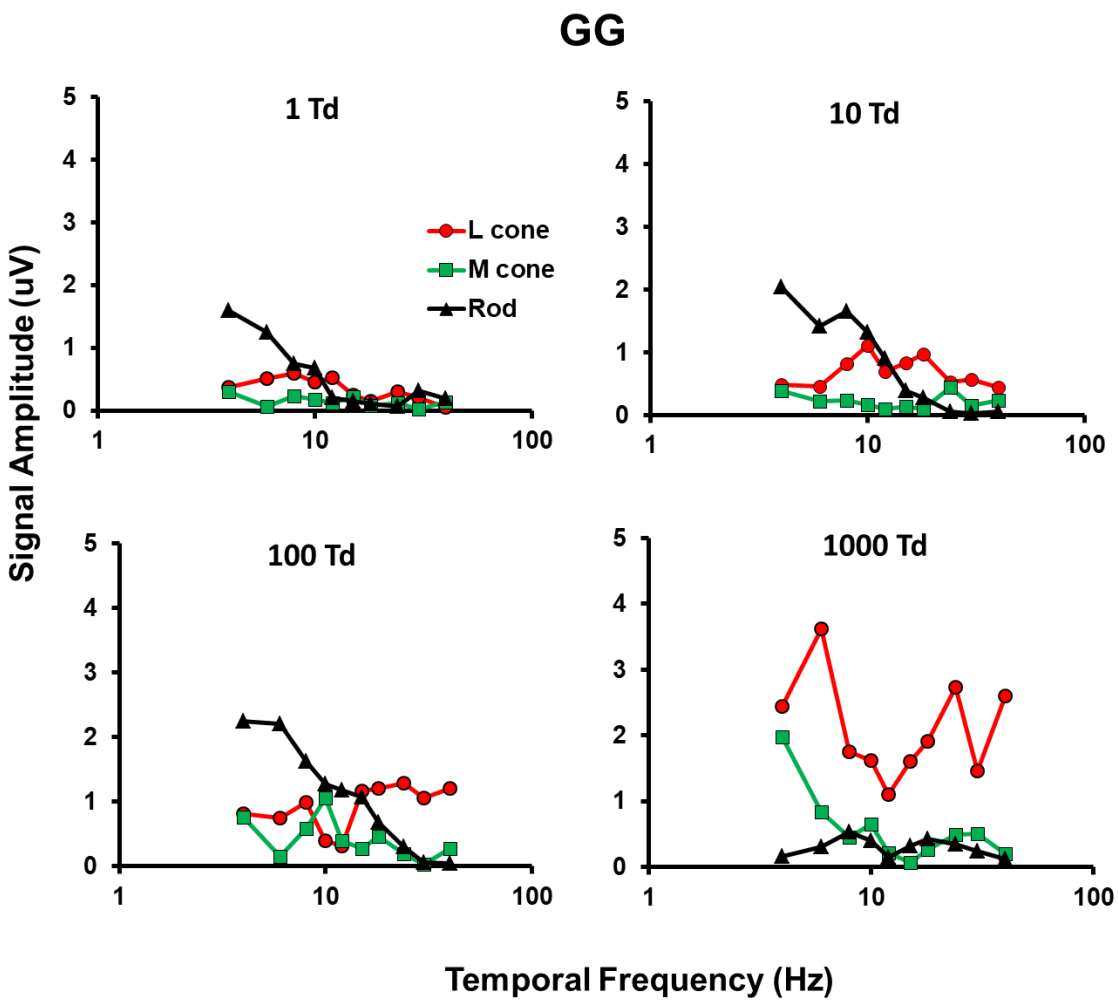

Figure 6-4 Temporal response characteristics of rods, L- and M- cone isolated ERGs for five stimulus conditions ranging from low mesopic to photopic light levels (1 Td, 10 Td, 100 Td, and 1000 Td) recorded in observer GG.

Note that responses at 12000 Td are not included since the participant was reported photosensitivity and therefore, had to discontinue the experiment.

Although data obtained from S- cones is not shown in the current chapter, an interesting observation was made as at 100 Td, like rods, S cone responses exhibited a low-pass function with peak responses dominating responses derived from other photoreceptor classes at 4 Hz and extending measurable responses up to about 30 Hz after which these signals fall to noise (data not shown here due to inadequate data available).

On the other hand, at 100 Td and above, we notice measurable L- and M- cone response amplitudes which increase in magnitude with increase in retinal illuminance. At higher retinal illuminance, 10000 Td, both L- and M- cone ERGs elicited in response to substitution stimuli begin to demonstrate the signal properties much like a band-pass function as described in the previous chapter.

Note that ERGs recorded in subjects MK and DK displayed measurable rod-driven responses only up to 10 Hz at 1 Td (see figures 6.2 & 6.3). The phase data shown in subjects MK and DK (figure 6.5) show that rod- driven responses at 1 Td and 10000 Td below 10 Hz show different trends. This might be suggestive of different underlying mechanisms although the stimuli used is rod-selective may not be so and the responses shown are luminance dependant. Apparent latencies were calculated since the sample included in this study is small in size.

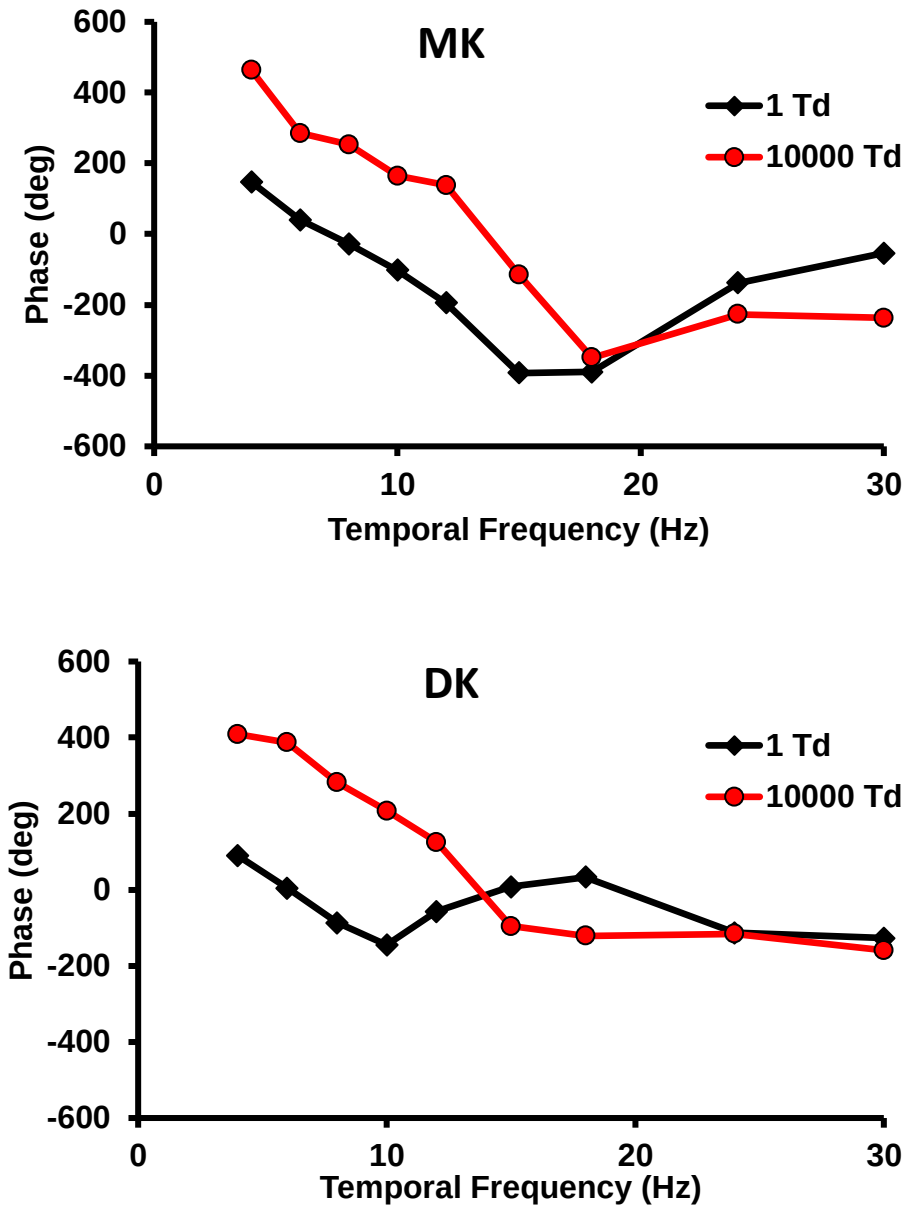

Figure 6-5 Response phase characteristics of rods driven ERGs recorded at 1 Td (mesopic) & 10000 Td (photopic) retinal illuminances plotted as a function of temporal frequency for subjects MK and DK.

6.3.3 Experiment 3

8- and 30- Hz Rod isolated flicker ERGs versus Retinal Illuminance

The purpose of this study was to see how 8- and 30- Hz rod specific ERG responses varied with change in retinal illuminance. We chose to examine rod mediated responses at these frequencies 1) because at about 8 Hz, we noticed a response minimum of L- and M- cone ERGs and 2) as rods saturate at 30 Hz (McCulloch et al., 2015). We recorded responses at these frequencies as a function of retinal illuminance to test to what extent rod isolating stimuli can elicit rod responses alone.

Figure 6.6 illustrates the group averaged fundamental response amplitudes (top plot) and phase (bottom plot) measured with an 8 Hz and 30 Hz rod-isolating stimulus plotted as a function of retinal illuminance ranging from 120 to 12000 Td (120, 240, 600, 1000, 1200, 2400, 6000, 10000, 12000 Td). At low retinal illuminances (<600 Td) prominent 8 Hz responses with attenuated 30 Hz responses were observed. In contrast to this finding, at high retinal illuminances (>600 Td), 8 Hz responses show minimum response energy whereas 30Hz responses are shown to increase in amplitude.

It is interesting to note that the 8- Hz and 30- Hz phase data crossover at 600 Td similar to what we have noticed with respect to their response amplitudes. As temporal resolution of rods limit to about 28 Hz, we should not see any response at 30 Hz. However, with increase in retinal illuminance, we found that despite using rod isolating stimuli, ERGs could be recorded at 30 Hz temporal frequency at high retinal illuminances which is suggestive of cone intrusion (see figure 6.6).

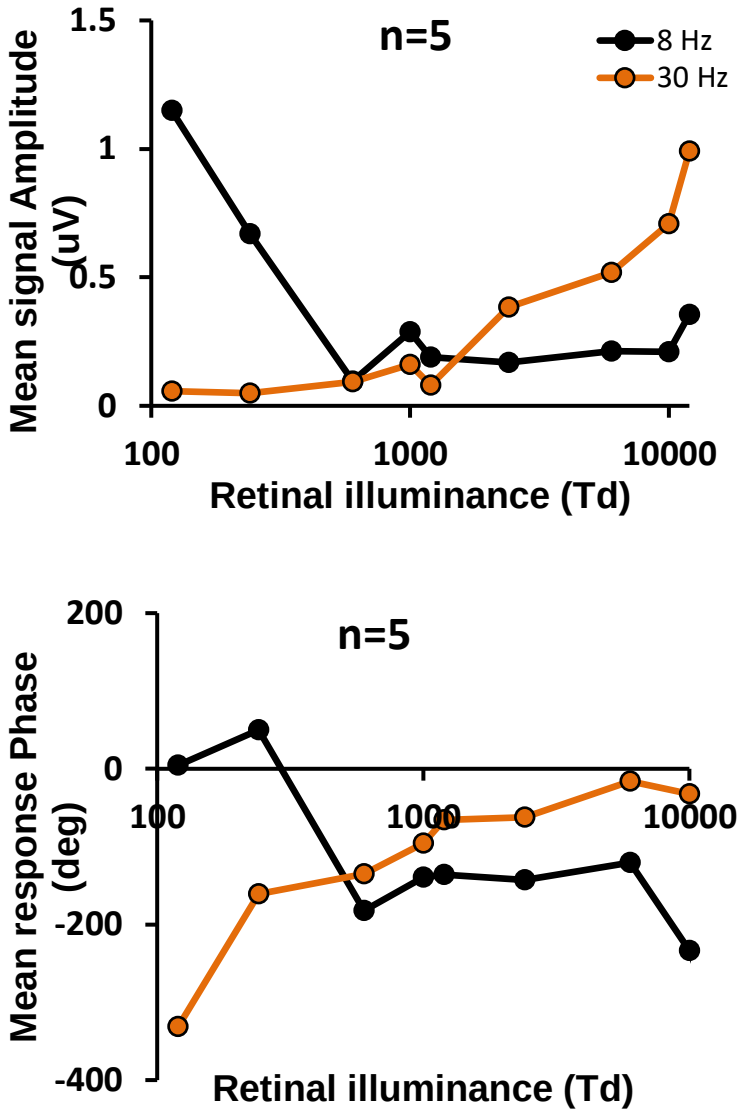

Figure 6-6 Group averaged 8- and 30- Hz rod isolated flicker ERG amplitudes (top graph) and phase (bottom graph) plotted as a function of temporal frequency.

6.4 Discussion

In this study, we have characterized the temporal properties of rod ERGs elicited by silent substitution steady-state stimuli. Here, we examined the influence of temporal frequency and retinal illuminance on rod- driven ERGs. In addition to measuring rod responses, we recorded L- and M- cone driven ERGs under the same stimulus conditions (as described in Experiment 2).

The activity of rods varies from threshold i.e., absorption of few quanta until saturation of rods at about 3000 scotopic trolands. It is known from literature that at higher intensities of light (approximately >1 Td), human vision is dominated by the cone system. However, it is believed that for the rods to be completely saturated, a light level of several hundred trolands is required (Aguilar and stiles, 1954).

From our data, we suggest that optimal stimulus parameters that can be used in measuring rod mediated ERG responses is between 4- to 10- Hz temporal frequencies and 1- to 100- Td retinal illuminances. A key feature of our results is that rod isolated ERGs can be obtained without prior dark adaptation and the stimuli used may not be restricted to low light intensities like those used in standard testing protocols.

A number of studies demonstrated that the rod signals exhibit a low-pass temporal response limit (Ives, 1922; Gouras and Gunkel, 1964; Conner, 1982). Our data is in agreement with this finding as we observed that until about 1000 Td, rod- responses could be measurable with the temporal resolution of about 30 Hz.

Another crucial observation is that despite employing rod isolating stimuli, functional selectivity of these photoreceptors is only maintained at light intensities ranging from mesopic to low photopic levels. At 12000 Td (photopic), responses elicited by rod isolating stimuli took more of a band-pass like appearance. This finding is in line with other studies that rods saturate and cones dominate vision at high intensity light levels (Hornstein et al., 2005; Seeliger et al., 2011; Zele and Cao, 2015). To confirm this, we further recorded ERGs in response to rod isolating stimuli at 8 Hz (where L- and M- cones displayed response minimum as described in Chapter 5) and 30 Hz (where rods saturate and L- cone exhibit peak response) (see figure 6.6). We found that 8- Hz ERGs fall to noise above 600 Td while it is above this retinal illuminance (RI) 30-Hz response that appears more like an L- cone response begins to increase in amplitude with increase in retinal illuminance. It is interesting to note that the phase data showed similar switch in their responses as a function of retinal illuminance. We assume that it is around this RI, rod-mediated vision switch-over to cones, and however, more data is required to confirm this hypothesis.

In the literature it has been established that the human rod system in itself has an internal duality (Conner and MacLeod, 1977; Conner, 1982) where the signals are carried in two luminance dependent pathways:

(1) Slow rod pathway (Famiglietti and Kolb, 1975, Dacheux and Raviola, 1986; Demb et al., 2012), via which rods send signal input to On- rod bipolar cells, AII amacrine cells and ON- and OFF- cone bipolar cells. This pathway is reported to mediate activity of rods under low light conditions and

(2) Fast rod pathway (Dacheux and Raviola, 1986, Raviola and Gilula, 1973) rod signals are conveyed via cone-rod gap junctions and ON- and OFF bipolar cells. This pathway is hypothesised to mediate rod activity under mesopic and high scotopic light levels (Stockman et al., 1991).

A key question here is whether ERGs elicited by rod isolating stimuli exhibit properties of these pathways. Examination of response amplitudes in all observers MK, DK and GG (in experiment 2) displayed that the temporal resolution varied with change in retinal illuminance i.e., at 1 Td, the upper temporal response limit was shown to be 12-15 Hz while at 10 Td and 100 Td, it was 15-30 Hz. Furthermore our phase data as shown in figure 6.5 demonstrates that at low temporal frequencies, responses elicited by rod isolating stimuli at low and high retinal illuminances show distinct trends. This finding may be interpreted as that the responses at high and low retinal illuminances are derived from different pathways; however, further investigation is needed to comment on whether and how these pathways contribute to these rod-signals.

Rod responsivity was shown to be maintained at low retinal illuminances (<10 Td). However, above 100 Td, the reduction in rod-response amplitude for substitution stimuli was observed. It is interesting to note that these illumination levels coincide with the previously reported light intensities at which rod saturation begins (Aguilar and Stiles, 1954; Stockman and Sharpe, 2006). Results from previous studies where non-isolating luminance flickering stimuli was used, rod-response amplitudes were reported to decrease with increase in stimulus frequency. These reports explain that destructive interference may result in phase cancellation between rod and cone signals and attribute to such reduction in response amplitudes (Sharpe et al, 1989; Stockman et al, 1991; Sharpe and Stockman, 1999). However, this may not be the case with silent substitution stimuli since the cone modulation for rod isolating stimuli is minimal and it is not very likely that such interference would occur between rod and cone driven responses. Moreover, the reduction in rod ERG for stimuli >10 Td was observed at all frequencies.

There is growing evidence on morphological and pathophysiological changes in rod and rod-mediated in the early stages of ARMD (Walter et al., 1999; Owsley et al., 2000; Chen et al., 2004; Feigl et al 2011. This condition is reported to be a one of the leading causes of acquired vision loss in the elderly population (as described in Priority Eye Diseases by WHO), this, therefore, prompts the need for the development of effective testing methods that could selectively assess the function of rods and help monitoring the efficiency of treatment strategies.

Our data demonstrates that it is possible to elicit rod-mediated steady-state ERGs using triple silent substitution. These results are in accord with previously established properties of rod-mediated vision using this paradigm. Furthermore, we recommend optimal stimulus parameters that could be used in a light adapted eye to derive rod-driven ERGs using this isolation method.

From the viewpoint of a clinician, this technique offers potential advantages over currently used testing methods for assessment of rod function. Most importantly, this approach provides a time-effective testing method for assessment of human rod function without having the subjects sit through the adaptation period that lasts about 30 minutes. Another advantage with this method is that signals derived from rods in this manner can be conveniently compared to signals obtained from other photoreceptors. Therefore, this could provide an understanding on how each photoreceptor type is susceptible to different retinal diseases.

Chapter 7 - General discussion, Conclusions, Limitations and Future work

7.1 General Discussion

In Chapter 4 (Experiment 1), the on- and off- responses elicited by transient, square-wave L- and M- cone isolating stimuli were obtained from human trichromatic (n=19) and dichromatic (n=4) observers. Full-field stimuli were generated on a four-primary LED stimulator and were equated in terms of a total cone contrast of 11% and a retinal illuminance of 12000 Td. The amplitudes and implicit times of L- and M- cone isolated ERGs elicited by onset- and offset- stimuli were analysed. L- and M- cone driven ERG responses exhibited similar waveforms to those observed for luminance ERGs. However, M- cone driven signals displayed a phase reversal in their responses to onset and offset stimuli in comparison to L- cone isolated ERGs. A key feature of these findings is that this on-off phase reversal was only observed in normal trichromats but absent in dichromats. In addition to isolated L- and M- cone ERGs, responses elicited by simultaneous inphase (+L+M; -L-M) and counterphase (+L-M; -L+M) stimulation further strengthened our argument that these responses provide not the measure of the photoreceptoral activity but reflect the contribution of individual photoreceptor classes to postreceptoral chromatic and luminance processing. Furthermore, we foresee the potential use of these cone-isolating stimuli in the objective assessment of colour vision status of an individual.

In Chapter 5 (Experiment 2), sinusoidally modulated cone isolating stimuli were used to assess the temporal properties of L- and M- cone steady-state ERGs in normal trichromatic (n=11), dichromatic (n=4) and anomalous trichromatic observers (n=2) human observers. We used stimuli with temporal frequencies ranging from 5 to 100 Hz, equated in terms of cone contrast of 11% and a retinal illuminance of 12000 Td. All the ERGs were subjected to fast Fourier transform analysis for the extraction of response phase and amplitudes. At low temporal frequencies (<10 Hz), the L- and M- cone ERGs exhibited similar response amplitudes and showed minimal differences in apparent latency. At higher flicker rates, M- cone responses were shown to be attenuated in comparison to responses obtained from L- cones, which were shown to have higher signal amplitudes. Here, L- cone responses exhibited shorter apparent latencies than the latencies obtained from M- cones. These findings are consistent with the previous findings and add up to the large pool of data reported in the literature that these differences in L- and M- cone ERGs reflect the properties of the chromatic and luminance postreceptoral processing pathways at low and high temporal frequencies, respectively. In addition to recording L- and M- cone driven responses, we also used S- cone isolating stimuli to assess the temporal response characteristics of S- cone ERGs in normal trichromats (n=5). We found that unlike L- and M- cone ERGs, S- cone driven signals displayed a low-pass function and is in agreement with previously reported data (Stockman et al, 1991). These results demonstrate that triple silent substitution can be used to generate ERGs that may provide a functional index of L-, M- and S- cones.

In Chapter 6 (Experiment 3), rod isolating stimuli were used to assess the temporal frequency and retinal illuminance response characteristics of rod mediated ERGs in healthy observers (n=7) without subjecting the participants to dark adaptation. Here, we observed that rod ERGs exhibited a temporal resolution of 30 Hz with peak response at 4 Hz. A key feature of this experiment is that at 8 Hz, rod- driven responses were shown to have considerably higher amplitudes unlike what we have observed in L- and M- cone driven ERGs (as shown in Chapter 4) where a response minimum was observed at this frequency, therefore, suggesting these signals are more likely to be rod- selective. More data is required to understand the underlying mechanisms of these responses and to validate the rod-isolating stimuli used in this study, for example using rod monochromats as controls could be beneficial. In this study, the substitution technique had proven to be an effective method in achieving rod driven ERGs and therefore, could provide an alternative to conventionally used, time-consuming testing protocols in the clinic with improved selectivity.

7.2 Conclusions

Appropriate choice of stimulus parameters can provide functional properties of individual receptoral and postreceptoral pathway processing mechanisms.

In summary, we conclude that silent substitution can-

- be employed in examination of temporal characteristics of L-, M-, S-, and rod photoreceptors
- be used to demonstrate isolation of individual receptoral and post receptoral response mechanisms
- be used to compare responses from individual photoreceptor classes under identical states of adaptation
- be used in obtaining rod isolated ERGs without dark adaptation
- probably be used as a tool for objective assessment of the colour vision status.

7.3 Limitations

The limitations of these experiments are 1) that we have not taken individual observer calibration into account and 2) the sample size is relatively small and therefore, we will be unable to comment on the variability of these measurements across the population.

7.4 Future work

This thesis further enhanced the fundamental understanding of how cone or rod isolating electroretinograms does not just provide the index of the photoreceptoral activity but reflect their contribution to the postreceptoral processing mechanisms. Furthermore, this work validates the using of silent substitution paradigm in the examination of the functional properties of L-, M-, S- and rod driven contributions to postreceptoral processing mechanisms. Therefore, we believe these stimulus parameters could be used in investigation of various retinal diseases like Hereditary macular dystrophies, Glaucoma, Congenital stationary night blindness, Retinitis Pigmentosa, Age related macular degeneration. This work could possibly lead to the development of faster, efficient and time-effective testing protocols and allow understanding of how effective the treatment strategies are on individual class of photoreceptors.

References

Adler, R., Curcio, C., Hicks, D., Price, D. and Wong, F., 1999. Cell death in age-related macular degeneration. *Mol Vis*, *5*(31), p.31.

Aguirre, G.K., Komáromy, A.M., Cideciyan, A.V., Brainard, D.H., Aleman, T.S., Roman, A.J., Avants, B.B., Gee, J.C., Korczykowski, M., Hauswirth, W.W. and Acland, G.M., 2007. Canine and human visual cortex intact and responsive despite early retinal blindness from RPE65 mutation. *PLoS medicine*, *4*(6), p.e230.

Ahnelt, P. and Kolb, H., 1994a. Horizontal cells and cone photoreceptors in human retina: A Golgi-electron microscopic study of spectral connectivity. *Journal of comparative Neurology*, *343*(3), pp.406-427.

Ahnelt, P. and Kolb, H., 1994b. Horizontal cells and cone photoreceptors in primate retina: A Golgi-light microscopic study of spectral connectivity.*Journal of Comparative Neurology*, *343*(3), pp.387-405.

Ahnelt, P.K., Kolb, H. and Pflug, R., 1987. Identification of a subtype of cone photoreceptor, likely to be blue sensitive, in the human retina. *Journal of Comparative Neurology*, *255*(1), pp.18-34.

Albrecht, J., Jägle, H., Hood, D.C. and Sharpe, L.T., 2002. The multifocal electroretinogram (mfERG) and cone isolating stimuli: variation in L-and M-cone driven signals across the retina. *Journal of Vision*, *2*(8), pp.2-2.

Alexander, K.R., Levine, M.W. and Super, B.J., 2005. Characteristics of period doubling in the human cone flicker electroretinogram. *Visual neuroscience*, *22*(6), pp.817-824.

An, J., Guo, Q., Li, L. and Zhang, Z., 2012. Properties of Flicker ERGs in Rat Models with Retinal Degeneration. *ISRN ophthalmology*, *2012*.

Andréasson, S. and Ghosh, F., 2014. Cone implicit time as a predictor of visual outcome in macular hole surgery. *Graefe's Archive for Clinical and Experimental Ophthalmology*, *252*(12), pp.1903-1909.

Andreasson, S., Kjellstrom, S., Barth, H. and Ghosh, F., 2013. Cone implicit time as a predictor for visual outcome in Macular Hole Surgery. *Investigative Ophthalmology & Visual Science*, *54*(15), pp.5784-5784.

Arden, G.B. and Brown, K.T., 1965. Some properties of components of the cat electroretinogram revealed by local recording under oil. *The Journal of physiology*, *176*(3), pp.429-461.

Asenjo, A.B., Rim, J. and Oprian, D.D., 1994. Molecular determinants of human red/green color discrimination. *Neuron*, *12*(5), pp.1131-1138.

Asi, H. and Perlman, I., 1992. Relationships between the electroretinogram a-wave, b-wave and oscillatory potentials and their application to clinical diagnosis. *Documenta ophthalmologica*, *79*(2), pp.125-139.

Awatramani, G., Wang, J. And Slaughter, M.M., 2001. Amacrine and ganglion cell contributions to the electroretinogram in amphibian retina.*Visual neuroscience*, *18*(01), pp.147-156.

Baker, C.L., Hess, R.R., Olsen, B.T. and Zrenner, E., 1988. Current source density analysis of linear and non-linear components of the primate electroretinogram. *The Journal of physiology*, *407*(1), pp.155-176.

Barbur, J.L. and Spang, K., 2008. Colour constancy and conscious perception of changes of illuminant. *Neuropsychologia*, *46*(3), pp.853-863.

Bartels, A. and Zeki, S., 2000. The architecture of the colour centre in the human visual brain: new results and a review. *European Journal of Neuroscience*, *12*(1), pp.172-193.

Bartley, S.H., 1937. Some observations on the organization of the retinal response. *American Journal of Physiology--Legacy Content*, *120*(1), pp.184-189.

Baylor D.A., Lamb T.D., and Yau K.W. (1979) *Responses of retinal rods to single photons.* Journal of Physiology.288:613–34.

Baylor, D.A., 1987. Photoreceptor signals and vision. Proctor lecture.

Baylor, D.A., Fuortes, M.G.F. and O'bryan, P.M., 1971. Receptive fields of cones in the retina of the turtle. *The Journal of Physiology*, *214*(2), pp.265-294.

Baylor, D.A., Nunn, B.J. and Schnapf, J.L., 1987. Spectral sensitivity of cones of the monkey Macaca fascicularis. *The Journal of Physiology*, *390*(1), pp.145-160.

Biersdorf, W.R., 1968. Rod and cone contributions to the off-effect of the human ERG. *Investigative Ophthalmology & Visual Science*, *7*(4), pp.371-377.

Birch, D.G., Hood, D.C., Nusinowitz, S. and Pepperberg, D.R., 1995. Abnormal activation and inactivation mechanisms of rod transduction in patients with autosomal dominant retinitis pigmentosa and the pro-23-his mutation. *Investigative ophthalmology & visual science*, *36*(8), pp.1603-1614.

Birch, J., 1993. Diagnosis of defective colour vision. Oxford: Butterworth-Heinemann.

Birch, J., 2001. *Diagnosis of defective colour vision*. Elsevier Health Sciences.

Blaner, W.S., Das, S.R., Gouras, P. and Flood, M.T., 1987. Hydrolysis of 11-cis- and all-trans-retinyl palmitate by homogenates of human retinal epithelial cells. *Journal of Biological Chemistry*, *262*(1), pp.53-58.

Bloomfield, S.A. and Dowling, J.E., 1985a. Roles of aspartate and glutamate in synaptic transmission in rabbit retina. I. Outer plexiform layer. *Journal of neurophysiology*, *53*(3), pp.699-713.

Bloomfield, S.A. and Dowling, J.E., 1985b. Roles of aspartate and glutamate in synaptic transmission in rabbit retina. II. Inner plexiform layer. *Journal of neurophysiology*, *53*(3), pp.714-725.

Bonaventure, N., Roussel, G. and Wioland, N., 1981. Effects of DL-α-amino adipic acid on Müller cells in frog and chicken retinae in vivo: relation to ERG b wave, ganglion cell discharge and tectal evoked potentials. *Neuroscience letters*, *27*(1), pp.81-87.

Bone, R.A., Landrum, J.T., Fernandez, L. and Tarsis, S.L., 1988. Analysis of the macular pigment by HPLC: retinal distribution and age study. *Investigative ophthalmology & visual science*, *29*(6), pp.843-849.

Borwein, B, 1981. The retinal receptor: A description, in: Vertebrate Photoreceptor Optics (Enoc, J.M., and Tobey, F. L. eds) 11-81. Springer Verlag, Berlin.

Bowmaker, J.K. and Dartnall, H., 1980. Visual pigments of rods and cones in a human retina. *The Journal of physiology*, *298*(1), pp.501-511.

Bowmaker, J.K., Parry, J.W.L. and Mollon, J.D., 2003. The arrangement of L and M cones in human and a primate retina. *Normal and defective colour vision*, pp.39-50.

Boycott, B.B. and Wässle, H., 1974. The morphological types of ganglion cells of the domestic cat's retina. *The Journal of Physiology*, *240*(2), pp.397-419.

Boycott, B.B. and Wässle, H., 1991. Morphological classification of bipolar cells of the primate retina. *European Journal of Neuroscience*, *3*(11), pp.1069-1088.

Brainard, D.H., Pelli, D.G. and Robson, T., 2002. Display characterization. *Encyclopedia of imaging science and technology*.

Brainard, D.H., Roorda, A., Yamauchi, Y., Calderone, J.B., Metha, A., Neitz, M., Neitz, J., Williams, D.R. and Jacobs, G.H., 2000. Functional consequences of the relative numbers of L and M cones. *JOSA A*, *17*(3), pp.607-614.

Bramão, I., Faísca, L., Forkstam, C., Reis, A. and Petersson, K.M., 2010. Cortical brain regions associated with color processing: An FMRI study. *The open neuroimaging journal*, *4*(1).

Bresnick, G.H. and Palta, M., 1987. Oscillatory potential amplitudes: relation to severity of diabetic retinopathy. *Archives of Ophthalmology*, *105*(7), pp.929-933.

Bresnick, G.H., Korth, K., Groo, A. and Palta, M., 1984. Electroretinographic oscillatory potentials predict progression of diabetic retinopathy: preliminary report. *Archives of ophthalmology*, *102*(9), pp.1307-1311.

Breuninger, T., Puller, C., Haverkamp, S. and Euler, T., 2011. Chromatic bipolar cell pathways in the mouse retina. *Journal of Neuroscience*, *31*(17), pp.6504-6517.

Brindley, G.S., 1954. The summation areas of human colour-receptive mechanisms at increment threshold. *The Journal of physiology*, *124*(2), pp.400-408.

Brindley, G.S., Du Croz, J.J. and Rushton, W.A.H., 1966. The flicker fusion frequency of the blue-sensitive mechanism of colour vision. *The Journal of physiology*, *183*(2), pp.497-500.

Brown, K.T. and Murakami, M., 1964. A new receptor potential of the monkey retina with no detectable latency.

Brown, K.T. and Wiesel, T.N., 1961a. Localization of origins of electroretinogram components by intraretinal recording in the intact cat eye.*The Journal of physiology*, *158*(2), p.257.

Brown, K.T. and Wiesel, T.N., 1961b. Analysis of the intraretinal electroretinogram in the intact cat eye. *The Journal of physiology*, *158*(2), p.229.

Brown, K.T., 1968. The electroretinogram: its components and their origins. *Vision research*, *8*(6), pp.633IN1-677IN6.

Brown, K.T., Watanabe, K. and Murakami, M., 1965, January. The early and late receptor potentials of monkey cones and rods. In *Cold Spring Harbor symposia on quantitative biology* (Vol. 30, pp. 457-482). Cold Spring Harbor Laboratory Press.

Buck, S.L., Knight, R.F. and Bechtold, J., 2000. Opponent-color models and the influence of rod signals on the loci of unique hues. *Vision research*, *40*(24), pp.3333-3344.

Bunt-Milam, A.H. and Saari, J.C., 1983. Immunocytochemical localization of two retinoid-binding proteins in vertebrate retina. *The Journal of cell biology*,*97*(3), pp.703-712.

Burns, M.E. and Arshavsky, V.Y., 2005. Beyond counting photons: trials and trends in vertebrate visual transduction. *Neuron*, *48*(3), pp.387-401.

Burns, S.A., Elsner, A.E. and Kreitz, M.R., 1992. Analysis of nonlinearities in the flicker ERG. *Optometry & Vision Science*, *69*(2), pp.95-105.

Bush, R.A. and Sieving, P.A., 1994. A proximal retinal component in the primate photopic ERG a-wave. *Investigative ophthalmology & visual science*, *35*(2), pp.635-645.

Bush, R.A. and Sieving, P.A., 1996. Inner retinal contributions to the primate photopic fast flicker electroretinogram. *JOSA A*, *13*(3), pp.557-565.

Bustamante, J.J., Ziari, S, Ramirez, R.D. and Tsin, A.T., 1995. Retinyl ester hydrolase and the visual cycle in the chicken eye. *American Journal of Physiology-Regulatory, Integrative and Comparative Physiology*,*269*(6), pp.R1346-R1350.

Calkins, D.J. and Sterling, P., 1999. Evidence that circuits for spatial and color vision segregate at the first retinal synapse. *Neuron*, *24*(2), pp.313-321.

Cao, D., Pokorny, J. and Smith, V.C., 2005. Matching rod percepts with cone stimuli. *Vision Research*, *45*(16), pp.2119-2128.

Cao, D., Pokorny, J., Smith, V.C. and Zele, A.J., 2008. Rod contributions to color perception: linear with rod contrast. *Vision research*, *48*(26), pp.2586-2592.

Carroll, J., Neitz, J. and Neitz, M., 2002. Estimates of L: M cone ratio from ERG flicker photometry and genetics. *Journal of Vision*, *2*(8), pp.1-1.

Challa, N.K., McKeefry, D., Parry, N.R.A., Kremers, J., Murray, I.J. and Panorgias, A., 2010. L-and M-cone input to 12Hz and 30Hz flicker ERGs across the human retina. *Ophthalmic and Physiological Optics*, *30*(5), pp.503-510.

Chan, T.L. and Grünert, U., 1998. Horizontal cell connections with short wavelength-sensitive cones in the retina: A comparison between New World and Old World primates. *Journal of Comparative Neurology*, *393*(2), pp.196-209.

Chao, L.L. and Martin, A., 1999. Cortical regions associated with perceiving, naming, and knowing about colors. *Journal of Cognitive Neuroscience*, *11*(1), pp.25-35.

Chen, J.G., Nakamura, T., Ebrey, T.G., Ok, H., Konno, K., Derguini, F., Nakanishi, K. and Honig, B., 1989. Wavelength regulation in iodopsin, a cone pigment. *Biophysical journal*, *55*(4), pp.725-729.

Chen, C., Wu, L., Wu, D., Huang, S., Wen, F., Luo, G. and Long, S., 2004. The local cone and rod system function in early age-related macular degeneration. *Documenta ophthalmologica*, *109*(1), pp.1-8.

Cho, N.C., Poulsen, G.L., Ver Hoeve, J.N. and Nork, T.M., 2000. Selective loss of S-cones in diabetic retinopathy. *Archives of ophthalmology*, *118*(10), pp.1393-1400.

Cideciyan, A.V. and Jacobson, S.G., 1993. Negative electroretinograms in retinitis pigmentosa. *Investigative ophthalmology & visual science*, *34*(12), pp.3253-3263.

CIE (1932). *Commission internationale de l'Eclairage proceedings, 1931*. Cambridge: Cambridge University Press.

Conley, M. and Fitzpatrick, D., 1989. Morphology of retinogeniculate axons in the macaque. *Visual neuroscience*, *2*(03), pp.287-296.

Conner, J.D. and MacLeod, D.I., 1977. Rod photoreceptors detect rapid flicker. *Science*, *195*(4279), pp.698-699.

Conner, J.D., 1982. The temporal properties of rod vision. *The Journal of physiology*, *332*, p.139.

Conway, B.R. and Livingstone, M.S., 2006. Spatial and temporal properties of cone signals in alert macaque primary visual cortex. *The Journal of neuroscience*, *26*(42), pp.10826-10846.

Cornwall, M.C., Matthews, H.R., Crouch, R.K. and Fain, G.L., 1995. Bleached pigment activates transduction in salamander cones. *The Journal of general physiology*, *106*(3), pp.543-557.

Creel, D.J., 2015. The electroretinogram and electro-oculogram: clinical applications. *Webvision: The Organization of the Retina and Visual System. Salt Lake City (UT): University of Utah Health Sciences Center*.

Crevier, D.W. and Meister, M., 1998. Synchronous period-doubling in flicker vision of salamander and man. *Journal of neurophysiology*, *79*(4), pp.1869-1878

Crook, J.D., Manookin, M.B., Packer, O.S. and Dacey, D.M., 2011. Horizontal cell feedback without cone type-selective inhibition mediates “red–green” color opponency in midget ganglion cells of the primate retina. *The Journal of Neuroscience*, *31*(5), pp.1762-1772.

Crouch, R.K., Chader, G.J., Wiggert, B. and Pepperberg, D.R., 1996. Retinoids and the visual process. *Photochemistry and photobiology*, *64*(4), pp.613-621.

Curcio, C.A., Allen, K.A., Sloan, K.R., Lerea, C.L., Hurley, J.B., Klock, I.B. and Milam, A.H., 1991. Distribution and morphology of human cone photoreceptors stained with anti-blue opsin. *Journal of Comparative Neurology*, *312*(4), pp.610-624.

Curcio, C.A., Medeiros, N.E. and Millican, C.L., 1996. Photoreceptor loss in age-related macular degeneration. *Investigative ophthalmology & visual science*, *37*(7), pp.1236-1249.

Curcio, C.A., Owsley, C. and Jackson, G.R., 2000. Spare the rods, save the cones in aging and age-related maculopathy. *Investigative ophthalmology & visual science*, *41*(8), pp.2015-2018.

Curcio, C.A., Sloan, K.R., Kalina, R.E. and Hendrickson, A.E., 1990. Human photoreceptor topography. *Journal of Comparative Neurology*, *292*(4), pp.497-523.

Dacey, D.M. and Lee, B.B., 1994. The'blue-on'opponent pathway in primate retina originates from a distinct bistratified ganglion cell type. *Nature*,*367*(6465), pp.731-735.

Dacey, D.M. and Packer, O.S., 2003. Colour coding in the primate retina: diverse cell types and cone-specific circuitry. *Current opinion in neurobiology*,*13*(4), pp.421-427.

Dacey, D.M. and Petersen, M.R., 1992. Dendritic field size and morphology of midget and parasol ganglion cells of the human retina. *Proceedings of the National Academy of sciences*, *89*(20), pp.9666-9670.

Dacey, D.M., 1989. Axon-bearing amacrine cells of the macaque monkey retina. *Journal of Comparative Neurology*, *284*(2), pp.275-293.

Dacey, D.M., 1993. Morphology of a small-field bistratified ganglion cell type in the macaque and human retina. *Visual neuroscience*, *10*(06), pp.1081-1098.

Dacey, D.M., 1996. Circuitry for color coding in the primate retina.*Proceedings of the National Academy of Sciences*, *93*(2), pp.582-588.

Dacey, D.M., 1999. Primate retina: cell types, circuits and color opponency.*Progress in retinal and eye research*, *18*(6), pp.737-763.

Dacey, D.M., 2000. Parallel pathways for spectral coding in primate retina. *Annual review of neuroscience*, *23*(1), pp.743-775.

Dacey, D.M., Lee, B.B., Stafford, D.K., Pokorny, J. and Smith, V.C., 1996. Horizontal cells of the primate retina: cone specificity without spectral opponency. *Science*, *271*(5249), p.656.

Dacheux, R.F. and Raviola, E., 1986. The rod pathway in the rabbit retina: a depolarizing bipolar and amacrine cell. *Journal of Neuroscience*, *6*(2), pp.331-345.

Das, S.R., Bhardwaj, N., Kjeldbye, H. and Gouras, P., 1992. Muller cells of chicken retina synthesize 11-cis-retinol. *Biochemical Journal*, *285*(3), pp.907-913.

de Lange Dzn, H., 1958. Research into the dynamic nature of the human fovea→ cortex systems with intermittent and modulated light. II. Phase shift in brightness and delay in color perception. *JOSA*, *48*(11), pp.784-789.

De Monasterio, F.M. and Gouras, P., 1975. Functional properties of ganglion cells of the rhesus monkey retina. *The Journal of physiology*, *251*(1), p.167.

De Monasterio, F.M., Gouras, P. and Tolhurst, D.J., 1975. Trichromatic colour opponency in ganglion cells of the rhesus monkey retina. *The Journal of Physiology*, *251*(1), pp.197-216.

De Monasterio, F.M., Schein, S.J. and McCrane, E.P., 1981. Staining of blue-sensitive cones of the macaque retina by a fluorescentdye. *Science*, *213*(4513), pp.1278-1281.

De Valois, R.L., Cottaris, N.P., Elfar, S.D., Mahon, L.E. and Wilson, J.A., 2000. Some transformations of color information from lateral geniculate nucleus to striate cortex. *Proceedings of the National Academy of Sciences*,*97*(9), pp.4997-5002.

De Valois, R.L., Smith, C.J., Kitai, S.T. and Karoly, A.J., 1958. Response of single cells in monkey lateral geniculate nucleus to monochromatic light.*Science*.

Demb, J.B. and Singer, J.H., 2012. Intrinsic properties and functional circuitry of the AII amacrine cell. *Visual neuroscience*, *29*(01), pp.51-60.

Derrington, A.M. and Lennie, P., 1984. Spatial and temporal contrast sensitivities of neurones in lateral geniculate nucleus of macaque. *The Journal of physiology*, *357*(1), pp.219-240.

Derrington, A.M., Krauskopf, J. and Lennie, P., 1984. Chromatic mechanisms in lateral geniculate nucleus of macaque. *The Journal of physiology*, *357*(1), pp.241-265.

Dewar, J. and McKendrick, J.G., 1873. On the Physiological Action of Light: No. I. *Journal of anatomy and physiology*, *7*(Pt 2), p.275.

DeYoe, E.A. and Van Essen, D.C., 1985. Segregation of efferent connections and receptive field properties in visual area V 2 of the macaque. *Nature*,*317*(6032), pp.58-61.

Diller, L., Packer, O.S., Verweij, J., McMahon, M.J., Williams, D.R. and Dacey, D.M., 2004. L and M cone contributions to the midget and parasol ganglion cell receptive fields of macaque monkey retina. *The Journal of neuroscience*, *24*(5), pp.1079-1088.

Dobkins, K.R., Thiele, A. and Albright, T.D., 2000. Comparison of red–green equiluminance points in humans and macaques: evidence for different L: M cone ratios between species. *JOSA A*, *17*(3), pp.545-556.

Dong, C.J. and Hare, W.A., 2000. Contribution to the kinetics and amplitude of the electroretinogram b-wave by third-order retinal neurons in the rabbit retina. *Vision research*, *40*(6), pp.579-590.

Donner, K.O. and Rushton, W.A.H., 1959. Retinal stimulation by light substitution. *The Journal of physiology*, *149*(2), p.288.

Dornonville de la Cour, M. (1993). Ion transport in the retinal pigment epithelium. A study with double barrelled ion-selective microelectrodes. Acta Ophthalmologica Supplement. 209:1-32.

Dowling, J.E. (1987). The Retina: An Approachable Part of the Brain. Cambridge:Belknap Press.

Dowling, J.E. and Ripps, H., 1972. Adaptation in skate photoreceptors. *The Journal of general physiology*, *60*(6), pp.698-719.

Dreher, B., Fukada, Y. and Rodieck, R.W., 1976. Identification, classification and anatomical segregation of cells with X-like and Y-like properties in the lateral geniculate nucleus of old-world primates. *The Journal of Physiology*, *258*(2), pp.433-452.

Drum, B.A., 1977. Cone interactions at high flicker frequencies: Evidence for cone latency differences?. *JOSA*, *67*(11), pp.1601-1603.

Drummond-Borg, M., Deeb, S.S. and Motulsky, A.G., 1989. Molecular patterns of X chromosome-linked color vision genes among 134 men of European ancestry. *Proceedings of the National Academy of Sciences*, *86*(3), pp.983-987.

Eisenfeld, A.J., Bunt-Milam, A.H. and Saari, J.C., 1985. Localization of retinoid-binding proteins in developing rat retina. *Experimental eye research*,*41*(3), pp.299-304.

Eisner, A. and MacLeod, D.I., 1981. Flicker photometric study of chromatic adaptation: selective suppression of cone inputs by colored backgrounds.*JOSA*, *71*(6), pp.705-718.

ErikÖz, B., Jusuf, P.R., Percival, K.A. and GrÜnert, U., 2008. Distribution of bipolar input to midget and parasol ganglion cells in marmoset retina. *Visual neuroscience*, *25*(1), pp.67-76.

Estevez, O. and Spekreijse, H., 1982. The “silent substitution” method in visual research. *Vision research*, *22*(6), pp.681-691.

Evers, H.U. and Gouras, P., 1986. Three cone mechanisms in the primate electroretinogram: two with, one without off-center bipolar responses. *Vision Research*, *26*(2), pp.245-254.

Faber, D.S., *Analysis of the slow transretinal potentials, in response to light. Buffalo, NY: State University of New York, 1969* (Doctoral dissertation, Thesis).

Fairman, H.S., Brill, M.H. and Hemmendinger, H., 1997. How the CIE 1931 color-matching functions were derived from Wright-Guild data. *Color Research & Application*, *22*(1), pp.11-23.

Falsini, B., Iarossi, G., Fadda, A., Porrello, G., Valentini, P., Piccardi, M. and Scullica, L., 1999. The fundamental and second harmonic of the photopic flicker electroretinogram: temporal frequency-dependent abnormalities in retinitis pigmentosa. *Clinical neurophysiology*, *110*(9), pp.1554-1562.

Famiglietti Jr, E.V. and Kolb, H., 1975. A bistratified amacrine cell and synaptic circuitry in the inner plexiform layer of the retina. *Brain research*, *84*(2), pp.293-300.

Famiglietti, E.V. and Kolb, H., 1976. Structural basis for ON-and OFF-center responses in retinal ganglion cells. *Science*, *194*(4261), pp.193-195.

Famiglietti, E.V., 1981. Functional architecture of cone bipolar cells in mammalian retina. *Vision research*, *21*(11), pp.1559-1563.

Famiglietti, E.V., 1991. Synaptic organization of starburst amacrine cells in rabbit retina: analysis of serial thin sections by electron microscopy and graphic reconstruction. *Journal of Comparative Neurology*, *309*(1), pp.40-70

Feigl, B., Cao, D., Morris, C.P. and Zele, A.J., 2011. Persons with age-related maculopathy risk genotypes and clinically normal eyes have reduced mesopic vision. *Investigative ophthalmology & visual science*, *52*(2), pp.1145-1150.

Fein, A. & Szuts, E. Z. *Photoreceptors: Their Role in Vision* (Cambridge University Press, 1982).

Field, G.D., Greschner, M., Gauthier, J.L., Rangel, C., Shlens, J., Sher, A., Marshak, D.W., Litke, A.M. and Chichilnisky, E.J., 2009. High-sensitivity rod photoreceptor input to the blue-yellow color opponent pathway in macaque retina. *Nature neuroscience*, *12*(9), pp.1159-1164.

Fishman,G.A., 1985. Basic principles of clinical electroretinography.*Retina*, *5*(2), pp.123-126.

Fishman, G.A., Alexander, K.R. and Anderson, R.J., 1985. Autosomal dominant retinitis pigmentosa: a method of classification. *Archives of Ophthalmology*, *103*(3), pp.366-374.

Foster, D. H., (2010) Chromatic Function of the Cones. Elsevier Ltd. 266-274.

Francis, P. J. (2006). Genetics of inherited retinal disease. Journal of the Royal Society of Medicine, 99(4): 189-191.

Frishman, L.J. and Wang, M.H., 2011. Electroretinogram of Human. *Adler's Physiology of the Eye*, p.480.

Frishman, L.J., 2006. Origins of the electroretinogram. *Principles and practice of clinical electrophysiology of vision*, *2*, pp.139-183.

Frishman, L.J., Robson, J.G. and Reddy, M.G., 1996. Effects of background light on the human dark-adapted electroretinogram and psychophysical threshold. *JOSA A*, *13*(3), pp.601-612.

Fu, Y. and Yau, K.W., 2007. Phototransduction in mouse rods and cones.*Pflügers Archiv-European Journal of Physiology*, *454*(5), pp.805-819.

Furukawa, T and Hanawa, I., 1955. Effects of some common cations on electroretinogram of the toad. *The Japanese journal of physiology*, *5*, pp.289-300.

Gamgee A. Kühne's researches on photo-chemical processes in the retina. Nature. 1877;15:296.

Gegenfurtner K. R., and Kiper D.C (2003). Color Vision. Annual Review of Neuroscience, 26: 181-206.

Golczak, M., Maeda, A., Bereta, G., Maeda, T., Kiser, P.D., Hunzelmann, S., von Lintig, J., Blaner, W.S. and Palczewski, K., 2008. Metabolic basis of visual cycle inhibition by retinoid and nonretinoid compounds in the vertebrate retina. *Journal of Biological Chemistry*, *283*(15), pp.9543-9554.

Goldstein, E.B. and Wolf, B.M., 1973. Regeneration of the green-rod pigment in the isolated frog retina. *Vision research*, *13*(3), pp.527-534.

Gollapalli, D.R. and Rando, R.R., 2003. All-trans-retinyl esters are the substrates for isomerization in the vertebrate visual cycle. *Biochemistry*,*42*(19), pp.5809-5818.

Gollapalli, D.R., Maiti, P. and Rando, R.R., 2003. RPE65 operates in the vertebrate visual cycle by stereospecifically binding all-trans-retinyl esters.*Biochemistry*, *42*(40), pp.11824-11830.

Goodchild, A.K., Chan, T.L. and Grünert, U., 1996. Horizontal cell connections with short-wavelength-sensitive cones in macaque monkey retina. *Visual neuroscience*, *13*(05), pp.833-845.

Gouras, P. and Gunkel, R.D., 1964. The frequency response of normal, rod achromat and nyctalope ERGs to sinusoidal monochromatic light stimulation. *Documenta Ophthalmologica*, *18*(1), pp.137-150.

Gouras, P. and Zrenner, E., 1981. Color coding in primate retina. *Vision Research*, *21*(11), pp.1591-1598.

Grunert, U. and Martin, P.R., 1991. Rod bipolar cells in the macaque monkey retina: immunoreactivity and connectivity. *The journal of neuroscience*, *11*(9), pp.2742-2758.

Gu, S.M., Thompson, D.A., Srikumari, C.S., Lorenz, B., Finckh, U., Nicoletti, A., Murthy, K.R., Rathmann, M., Kumaramanickavel, G., Denton, M.J. and Gal, A., 1997. Mutations in RPE65 cause autosomal recessive childhood–onset severe retinal dystrophy. *Nature genetics*, *17*(2), pp.194-197.

Guild, J., 1932. The colorimetric properties of the spectrum. *Philosophical Transactions of the Royal Society of London. Series A, Containing Papers of a Mathematical or Physical Character*, *230*, pp.149-187.

Gurevich, L. and Slaughter, M.M., 1993. Comparison of the waveforms of the ON bipolar neuron and the b-wave of the electroretinogram. *Vision research*, *33*(17), pp.2431-2435.

Hagins, W.A., Penn, R.D. and Yoshikami, S., 1970. Dark current and photocurrent in retinal rods. *Biophysical journal*, *10*(5), p.380.

Hamel, C.P., 2007. Cone rod dystrophies. *Orphanet Journal of Rare Diseases*, *2*(1), p.1.

Hárosi, F.I., 1975. Absorption spectra and linear dichroism of some amphibian photoreceptors. *The Journal of General Physiology*, *66*(3), pp.357-382.

Hébert, M. and Lachapelle, P., 1999. Reproducibility of ERG responses obtained with the DTL electrode. *Vision research*, *39*(6), pp.1069-1070.

Hébert, M., Dumont, M. and Lachapelle, P., 2002. Electrophysiological evidence suggesting a seasonal modulation of retinal sensitivity in subsyndromal winter depression. *Journal of affective disorders*, *68*(2), pp.191-202.

Hébert, M., Gagné, A.M., Paradis, M.E., Jomphe, V., Roy, M.A., Mérette, C. and Maziade, M., 2010. Retinal response to light in young nonaffected offspring at high genetic risk of neuropsychiatric brain disorders. *Biological psychiatry*, *67*(3), pp.270-274.

Héberta, M., Vaeganb. & Lachapellec, P., 1999. Reproducibility of ERG responses obtained with the DTL electrode. *Vision Research,* 39(6): 1069–1070.

Hecht, S., Haig, C. and Chase, A.M., 1937. The influence of light adaptation on subsequent dark adaptation of the eye. *The Journal of general physiology*, *20*(6), pp.831-850.

Heynen, H. and Van Norren, D., 1985a. Origin of the electroretinogram in the intact macaque eye—I: Principal component analysis. *Vision research*,*25*(5), pp.697-707.

Heynen, H. and Van Norren, D., 1985b. Origin of the electroretinogram in the intact macaque eye—II: Current source-density analysis. *Vision research*,*25*(5), pp.709-715.

Hicks, T.P., Lee, B.B. and Vidyasagar, T.R., 1983. The responses of cells in macaque lateral geniculate nucleus to sinusoidal gratings. *The Journal of physiology*, *337*(1), pp.183-200.

Hofer, H., Carroll, J., Neitz, J., Neitz, M. and Williams, D.R., 2005. Organization of the human trichromatic cone mosaic. *The Journal of Neuroscience*, *25*(42), pp.9669-9679.

Holmgren, F., 1865. Method att objectivera effecten av ljusintryck pa retina.*Upsala Lakareforenings Forhandlingar*, *1*, pp.177-191.

Hood, D.C. and Birch, D.G., 1990a. A quantitative measure of the electrical activity of human rod photoreceptors using electroretinography. *Visual neuroscience*, *5*(04), pp.379-387.

Hood, D.C. and Birch, D.G., 1990b. The A-wave of the human electroretinogram and rod receptor function. *Investigative ophthalmology & visual science*, *31*(10), pp.2070-2081.

Hood, D.C. and Birch, D.G., 1996. Assessing abnormal rod photoreceptor activity with the a-wave of the electroretinogram: applications and methods. *Documenta ophthalmologica*, *92*(4), pp.253-267.

Hornstein, E.P., Verweij, J., Li, P.H. and Schnapf, J.L., 2005. Gap-junctional coupling and absolute sensitivity of photoreceptors in macaque retina. *Journal of Neuroscience*, *25*(48), pp.11201-11209.

Howard, R.J., Barnes, J., McKeefry, D., Ha, Y., Woodruff, P.W., Bullmore, E.T., Simmons, A., Williams, S.C., David, A.S. and Brammer, M., 1998. The functional anatomy of imagining and perceiving colour. *Neuroreport*, *9*(6), pp.1019-1023.

Howarth,C.I.,1961.On-off interaction in the human electroretinogram.

JOSA, *51*(3), pp.345-352.

Huang, J., Possin, D.E. and Saari, J.C., 2009. Localizations of visual cycle components in retinal pigment epithelium.

Hubel, D.H. and Livingstone, M.S., 1987b. Segregation of form, color, and stereopsis in primate area 18. *The Journal of Neuroscience*, *7*(11), pp.3378-3415.

Hubel, D.H. and Wiesel, T.N., 1966. Effects of varying stimulus size and color on single lateral geniculate cells in Rhesus monkeys. *Proceedings of the National Academy of Sciences of the United States of America*, *55*(6), pp.1345-1346.

Hubel, D.H. and Wiesel, T.N., 1972. Laminar and columnar distribution of geniculo-cortical fibers in the macaque monkey. *Journal of Comparative Neurology*, *146*(4), pp.421-450.

Imai, H., Kefalov, V., Sakurai, K., Chisaka, O., Ueda, Y., Onishi, A., Morizumi, T., Fu, Y., Ichikawa, K., Nakatani, K. and Honda, Y., 2007. Molecular properties of rhodopsin and rod function. *Journal of Biological Chemistry*, *282*(9), pp.6677-6684.

Investigative ophthalmology & visual science, *28*(1), pp.34-49.

Ives, H.E., 1922. Critical frequency relations in scotopic vision. *JOSA*, *6*(3), pp.254-268.

J. Kremers, M. W. Stepien, H. P. N. Scholl, and C. A. Saito, “Cone selective adaptation influences L- and M-cone driven signals in electroretinography and psychophysics,” J. Vis. 3(2):3, 146–160 (2003).

Jacobs, G.H. and Deegan, J.F., 1997. Spectral sensitivity of macaque monkeys measured with ERG flicker photometry. *Visual neuroscience*, *14*(5), pp.921-928.

Jacobs, G.H., Neitz, M., Deegan, J.F. and Neitz, J., 1996. Trichromatic colour vision in New World monkeys. *Nature*, *382*(6587), p.156.

Jacob, M.M., Pangeni, G., Gomes, B.D., Souza, G.S., da Silva Filho, M., Silveira, L.C.L., Maguire, J., Parry, N.R., McKeefry, D.J. and Kremers, J., 2015. The spatial properties of L-and M-cone inputs to electroretinograms that reflect different types of post-receptoral processing. *PloS one*, *10*(3), p.e0121218.

Jacobson, S.G., Aleman, T.S., Cideciyan, A.V., Sumaroka, A., Schwartz, S.B., Windsor, E.A., Traboulsi, E.I., Heon, E., Pittler, S.J., Milam, A.H. and Maguire, A.M., 2005. Identifying photoreceptors in blind eyes caused by RPE65 mutations: prerequisite for human gene therapy success. *Proceedings of the National Academy of Sciences*, *102*(17), pp.6177-6182.

Jang, G.F., McBee, J.K., Alekseev, A.M., Haeseleer, F. and Palczewski, K., 2000. Stereoisomeric specificity of the retinoid cycle in the vertebrate retina.*Journal of Biological Chemistry*, *275*(36), pp.28128-28138.

Jin, M., Li, S., Nusinowitz, S., Lloyd, M., Hu, J., Radu, R.A., Bok, D. and Travis, G.H., 2009. The role of interphotoreceptor retinoid-binding protein on the translocation of visual retinoids and function of cone photoreceptors. *The Journal of neuroscience*, *29*(5), pp.1486-1495.

Joselevitch, C., 2008. Human retinal circuitry and physiology. *Psychology & Neuroscience*, *1*(2), pp.141-165.

Juen, S. and Kieselbach, G.F., 1990. Electrophysiological changes in juvenile diabetics without retinopathy. *Archives of ophthalmology*, *108*(3), pp.372-375.

Julius, D., and Nathans, J. (2012). Signalling by sensory receptors. Cold Spring Harbor Perspectives in Biology. 4(1): a005991.

Kahn and Lowenstein (1924).-Graefe's Archive., Vol. XIV, p. 324.

Kaiser, P. K., B. B. Lee, P. R. Martin, and A. Valberg. "The physiological basis of the minimally distinct border demonstrated in the ganglion cells of the macaque retina." *The Journal of Physiology* 422, no. 1 (1990): 153-183.

Kaneko, A. and Saito, T., 1983. Ionic mechanisms underlying the responses of off-center bipolar cells in the carp retina. II. Studies on responses evoked by transretinal current stimulation. *The Journal of general physiology*, *81*(4), pp.603-612

Kaylor, J.J., Cook, J.D., Makshanoff, J., Bischoff, N., Yong, J. and Travis, G.H., 2014. Identification of the 11-cis-specific retinyl-ester synthase in retinal Müller cells as multifunctional O-acyltransferase (MFAT). *Proceedings of the National Academy of Sciences*, *111*(20), pp.7302-7307

Kefalov, V. J. (2012). Rod and cone visual pigments and phototransduction through pharmacological, genetic, and physiological approaches. The Journal of Biological Chemistry. 287(3):1635-41.

Kellenbach, M.L., Brett, M. and Patterson, K., 2001. Large, colorful, or noisy? Attribute-and modality-specific activations during retrieval of perceptual attribute knowledge. *Cognitive, Affective, & Behavioral Neuroscience*, *1*(3), pp.207-221.

Kelly, D.H., 1974. Spatio-temporal frequency characteristics of color-vision mechanisms. *JOSA*, *64*(7), pp.983-990.

Kendell, K.R., Quigley, H.A., Kerrigan, L.A., Pease, M.E. and Quigley, E.N., 1995. Primary open-angle glaucoma is not associated with photoreceptor loss. *Investigative ophthalmology & visual science*, *36*(1), pp.200-205.

Kennedy, M.J., Lee, K.A., Niemi, G.A., Craven, K.B., Garwin, G.G., Saari, J.C. and Hurley, J.B., 2001. Multiple phosphorylation of rhodopsin and the in vivo chemistry underlying rod photoreceptor dark adaptation. *Neuron*, *31*(1), pp.87-101.

Kizawa, J., Machida, S., Kobayashi, T., Gotoh, Y. and Kurosaka, D., 2006. Changes of oscillatory potentials and photopic negative response in patients with early diabetic retinopathy. *Japanese journal of ophthalmology*, *50*(4), pp.367-373.

Knapp, A.G. and Schiller, P.H., 1984. The contribution of on-bipolar cells to the electroretinogram of rabbits and monkeys: a study using 2-amino-4-phosphonobutyrate (APB). *Vision research*, *24*(12), pp.1841-1846.

Kolb, H. and Famigilietti, E.V., 1974. Rod and cone pathways in the inner plexiform layer of cat retina. *Science*, *186*(4158), pp.47-49.

Kolb, H. and Marshak, D., 2003. The midget pathways of the primate retina.*Documenta Ophthalmologica*, *106*(1), pp.67-81.

Kolb, H. and Nelson, R., 1981. Amacrine cells of the cat retina. *Vision research*, *21*(11), pp.1625-1633.

Kolb, H., 1970. Organization of the outer plexiform layer of the primate retina: electron microscopy of Golgi-impregnated cells. *Philosophical Transactions of the Royal Society of London B: Biological Sciences*, *258*(823), pp.261-283.

Kolb, H., 1974. The connections between horizontal cells and photoreceptors in the retina of the cat: electron microscopy of Golgi preparations. *Journal of Comparative Neurology*, *155*(1), pp.1-14.

Kolb, H., 1997. Amacrine cells of the mammalian retina: neurocircuitry and functional roles. *Eye-London-Ophthalmological Society Of The United Kingdom Then Royal College Of Ophthalmologists-*, *11*, pp.904-923.

Kolb, H., Ahnelt, P., Fisher, S.K., Linberg, K.A. and Keri, C., 1989. Chromatic connectivity of the three horizontal cell types in the human retina. *Invest Ophthalmol Vis Sci*, *30*(Suppl 3), p.348.

Kolb, H., Fernandez, E., Schouten, J., Ahnelt, P., Linberg, K.A. and Fisher, S.K., 1994. Are there three types of horizontal cell in the human retina?.*Journal of Comparative Neurology*, *343*(3), pp.370-386.

Kolb, H., Nelson, R. and Mariani, A., 1981. Amacrine cells, bipolar cells and ganglion cells of the cat retina: a Golgi study. *Vision research*, *21*(7), pp.1081-1114.

Kolesnikov, A.V., Golobokova, E.Y. and Govardovskii, V.I., 2003. The identity of metarhodopsin III. *Visual neuroscience*, *20*(03), pp.249-265.

Kondo, M. and Sieving, P.A., 2001. Primate photopic sine-wave flicker ERG: vector modeling analysis of component origins using glutamate analogs. *Investigative ophthalmology & visual science*, *42*(1), pp.305-312.

Konig, A. and Dieterici, C., 1886. The Modern Development of Thomas Young's Theory of Colour-Vision. *Rep. Brit. Ass. Advanc. Sci*, *56*, pp.431-439.

Kosower, E.M., 1988. Assignment of groups responsible for the" opsin shift" and light absorptions of rhodopsin and red, green, and blue iodopsins (cone pigments). *Proceedings of the National Academy of Sciences*, *85*(4), pp.1076-1080.

Kouyama, N. and Marshak, D.W., 1992. Bipolar cells specific for blue cones in the macaque retina. *The Journal of Neuroscience*, *12*(4), pp.1233-1252.

Kremers, J. and Link, B., 2008. Electroretinographic responses that may reflect activity of parvo-and magnocellular post-receptoral visual pathways. *Journal of Vision*, *8*(15), pp.11-11.

Kremers, J. and Pangeni, G., 2012. Electroretinographic responses to photoreceptor specific sine wave modulation. *JOSA A*, *29*(2), pp.A306-A313.

Kremers, J., 2003. The assessment of L-and M-cone specific electroretinographical signals in the normal and abnormal human retina.*Progress in retinal and eye research*, *22*(5), pp.579-605.

Kremers, J., 2011. Signal Pathways in the Electroretinogram. INTECH Open Access Publisher.

Kremers, J., Stepien, M.W., Scholl, H.P. and Saito, C., 2003. Cone selective adaptation influences L-and M-cone driven signals in electroretinography and psychophysics, by Kremers, Stepien, Scholl & Saito. *Journal of Vision*, *3*(2), pp.3-3.

Kremers, J., Usui, T., Scholl, H.P. and Sharpe, L.T., 1999. Cone signal contributions to electroretinograms [correction of electrograms] in dichromats and trichromats. *Investigative ophthalmology & visual science*, *40*(5), pp.920-930.

Krishna, V.R., Alexander, K.R. and Peachey, N.S., 2002. Temporal properties of the mouse cone electroretinogram. *Journal of Neurophysiology*, *87*(1), pp.42-48.

Kühn, H. and Wilden, U., 1987. Deactivation of photoactivated rhodopsin by rhodopsin-kinase and arrestin. *Journal of receptor research*, *7*(1-4), pp.283-298.

Kuhne, W. *On the Photochemistry of the Retina and on Visual Purple*. Ed. Michael Foster. Macmillan and Company, 1878.

Lai, Y.L., Wiggert, B., Liu, Y.P. and Chader, G.J., 1982. Interphotoreceptor retinol-binding proteins: possible transport vehicles between compartments of the retina. *Nature*, *298*(5877), pp.848-849.

Lam, R.W., Beattie, C.W., Buchanan, A. and Mador, J.A., 1992. Electroretinography in seasonal affective disorder. *Psychiatry research*,*43*(1), pp.55-63.

Lamb, T.D. and Pugh, E.N., 1992. A quantitative account of the activation steps involved in phototransduction in amphibian photoreceptors. *The Journal of Physiology*, *449*(1), pp.719-758.

Lamb, T.D. and Pugh, E.N., 2004. Dark adaptation and the retinoid cycle of vision. *Progress in retinal and eye research*, *23*(3), pp.307-380.

Lamb, T.D. and Pugh, E.N., 2006. Phototransduction, dark adaptation, and rhodopsin regeneration the proctor lecture. *Investigative ophthalmology & visual science*, *47*(12), pp.5138-5152.

Larsson, J. and Andréasson, S., 2001. Photopic 30 Hz flicker ERG as a predictor for rubeosis in central retinal vein occlusion. *British journal of ophthalmology*, *85*(6), pp.683-685.

Lavoie, J., Illiano, P., Sotnikova, T.D., Gainetdinov, R.R., Beaulieu, J.M. and Hébert, M., 2014a. The electroretinogram as a biomarker of central dopamine and serotonin: potential relevance to psychiatric disorders. *Biological psychiatry*, *75*(6), pp.479-486.

Lavoie, J., Maziade, M. and Hébert, M., 2014b. The brain through the retina: the flash electroretinogram as a tool to investigate psychiatric disorders.*Progress in Neuro-Psychopharmacology and Biological Psychiatry*, *48*, pp.129-134.

Lavoie, M.P., Lam, R.W., Bouchard, G., Sasseville, A., Charron, M.C., Gagné, A.M., Tremblay, P., Filteau, M.J. and Hébert, M., 2009. Evidence of a biological effect of light therapy on the retina of patients with seasonal affective disorder. *Biological psychiatry*, *66*(3), pp.253-258.

Lee, B. B., Martin, P. R., & Grünert, U. (2010). Retinal connectivity and primate vision. *Progress in Retinal and Eye Research*, *29*(6), 622–639.

Lee, B.B., 1997. Parallel pathways in primate retina. *John Dalton's colour vision legacy*, pp.24-25.

Lee, B.B., 2011. Visual pathways and psychophysical channels in the primate. *The Journal of Physiology*, *589*(1), pp.41-47.

Lee, B.B., Dacey, D.M., Smith, V.C. and Pokorny, J., 1999. Horizontal cells reveal cone type-specific adaptation in primate retina. *Proceedings of the National Academy of Sciences*, *96*(25), pp.14611-14616.

Lee, B.B., Martin, P.R. and Valberg, A., 1988. The physiological basis of heterochromatic flicker photometry demonstrated in the ganglion cells of the macaque retina. *The Journal of physiology*, *404*(1), pp.323-347.

Lee, B.B., Pokorny, J., Smith, V.C., Martin, P.R. and Valbergt, A., 1990. Luminance and chromatic modulation sensitivity of macaque ganglion cells and human observers. *JOSA A*, *7*(12), pp.2223-2236.

Lee, B.B., Smith, V.C., Pokorny, J. and Sun, H., 2008. Chromatic adaptation in red–green cone-opponent retinal ganglion cells of the macaque. *Vision research*, *48*(26), pp.2625-2632.

Leventhal, A.G., Rodieck, R.W. and Dreher, B., 1981. Retinal ganglion cell classes in the Old World monkey: morphology and central projections.*Science*, *213*(4512), pp.1139-1142.

Li, W. and DeVries, S.H., 2006. Bipolar cell pathways for color and luminance vision in a dichromatic mammalian retina. *Nature neuroscience*, *9*(5), p.669.

Liou, G.I., Bridges, C.D.B., Fong, S.L., Alvarez, R.A. and Gonzalez-Fernandez, F., 1982. Vitamin A transport between retina and pigment epithelium—an interstitial protein carrying endogenous retinol (interstitial retinol-binding protein). *Vision research*, *22*(12), pp.1457-1467.

Livingstone, M. and Hubel, D., 1988. Segregation of form, color, movement, and depth: anatomy, physiology, and perception.

Livingstone, M.S. and Hubel, D.H., 1987a. Psychophysical evidence for separate channels for the perception of form, color, movement, and depth.*The Journal of Neuroscience*, *7*(11), pp.3416-3468.

Logothetis, N.K., 2006. Vision: a window into consciousness. *Scientific American*, *16*, pp.4-11.

Lueck, C.J., Zeki, S., Friston, K.J., Deiber, M.P., Cope, P., Cunningham, V.J., Lammertsma, A.A., Kennard, C. and Frackowiak, R.S.J., 1989. The colour centre in the cerebral cortex of man.

Macke, J.P. and Nathans, J., 1997. Individual variation in size of the human red and green visual pigment gene array. *Investigative ophthalmology & visual science*, *38*(5), pp.1040-1043.

Marc, R.E. and Sperling, H.G., 1977. Chromatic organization of primate cones. *Science*, *196*(4288), pp.454-456

Marks, L.E. and Bornstein, M.H., 1973. Spectral sensitivity by constant CFF: effect of chromatic adaptation. *JOSA*, *63*(2), pp.220-226.

Marmor, M.F. and Zrenner, E. 1999. Standard for clinical electroretinography (1999 update). International Society for Clinical Electrophysiology of Vision. Doc Ophthalmol, 97(2): 143-156.

Marmor, M.F. and Zrenner, E., 1998. Standard for clinical electroretinography (1999 update). *Documenta Ophthalmologica*, *97*(2), pp.143-156.

Marmor, M.F., Fulton, A.B., Holder, G.E., Miyake, Y., Brigell, M., Bach, M.I.S.C.E.V. and International Society for Clinical Electrophysiology of Vision, 2009. ISCEV Standard for full-field clinical electroretinography (2008 update). *Documenta Ophthalmologica*, *118*(1), pp.69-77.

Marmor, M.F., Holder, G.E., Seeliger, M.W. and Yamamoto, S., 2004. Standard for clinical electroretinography (2004 update). *Documenta ophthalmologica*, *108*(2), pp.107-114.

Marré, M., 1973. The investigation of acquired colour vision deficiencies. *" Colour 73" 2nd Congr.*, pp.99-135.

Marrs, J.A., Andersson-Fisone, C., Jeong, M.C., Cohen-Gould, L., Zurzolo, C., Nabi, I.R., Rodriguez-Boulan, E. and Nelson, W.J., 1995. Plasticity in epithelial cell phenotype: Modulation by expression of different cadherin cell adhesion molecules. *The Journal of Cell Biology*, *129*(2), pp.507-519.

Martin, A., Haxby, J.V., Lalonde, F.M., Wiggs, C.L. and Ungerleider, L.G., 1995. Discrete cortical regions associated with knowledge of color and knowledge of action. *Science*, *270*(5233), p.102.

Martin, P.R., Blessing, E.M., Buzás, P., Szmajda, B.A. and Forte, J.D., 2011. Transmission of colour and acuity signals by parvocellular cells in marmoset monkeys. *The Journal of physiology*, *589*(11), pp.2795-2812.

Masland, R.H., 2012. The tasks of amacrine cells. *Visual neuroscience*,*29*(01), pp.3-9.

Massey, S.C., Redburn, D.A. and Crawford, M.L.J., 1983. The effects of 2-amino-4-phosphonobutyric acid (APB) on the ERG and ganglion cell discharge of rabbit retina. *Vision research*, *23*(12), pp.1607-1613.

Mata, N.L. and Tsin, A.T., 1998. Distribution of 11-cis LRAT, 11-cis RD and 11-cis REH in bovine retinal pigment epithelium membranes. *Biochimica et Biophysica Acta (BBA)-Lipids and Lipid Metabolism*, *1394*(1), pp.16-22.

Mata, N.L., Radu, R.A., Clemmons, R.S. and Travis, G.H., 2002. Isomerization and oxidation of vitamin a in cone-dominant retinas: a novel pathway for visual-pigment regeneration in daylight. *Neuron*, *36*(1), pp.69-80.

McBee, J.K., Palczewski, K., Baehr, W. and Pepperberg, D.R., 2001. Confronting complexity: the interlink of phototransduction and retinoid metabolism in the vertebrate retina. *Progress in retinal and eye research*,*20*(4), pp.469-529.

McCulloch, D. L., Van Boemel, G. B. & Borchert, M. S., 1998. Comparisons of contact lens, foil, fiber and skin electrodes for patterns electroretinograms. *Documenta Ophthalmologica,* 94(4): 327-340.

McCulloch, D.L., Marmor, M.F., Brigell, M.G., Hamilton, R., Holder, G.E., Tzekov, R. and Bach, M., 2015. ISCEV Standard for full-field clinical electroretinography (2015 update). *Documenta ophthalmologica*, *130*(1), pp.1-12.

McKeefry, D.J. and Zeki, S., 1997. The position and topography of the human colour centre as revealed by functional magnetic resonance imaging. *Brain*,*120*(12), pp.2229-2242.

Merbs, S.L. and Nathans, J., 1992. Absorption spectra of the hybrid pigments responsible for anomalous color vision. *Science*, *258*(5081), pp.464-466.

Miller, R.F. and Dowling, J.E., 1970. Intracellular responses of the Müller (glial) cells of mudpuppy retina: their relation to b-wave of the electroretinogram. *Journal of Neurophysiology*, *33*(3), pp.323-341.

Miyake, Y., Horiguchi, M., Ota, I. and Shiroyama, N., 1987. Characteristic ERG-flicker anomaly in incomplete congenital stationary night blindness. *Investigative ophthalmology & visual science*, *28*(11), pp.1816-1823.

Molday, L.L., Rabin, A.R. and Molday, R.S., 2000. ABCR expression in foveal cone photoreceptors and its role in Stargardt macular dystrophy. *Nature genetics*, *25*(3), p.257.

Mollon, J.D., 1982. A taxonomy of tritanopias. *Documenta Ophthalmologica Proceedings Series*, *33*, pp.87-101.

Mondal, M.S., Ruiz, A., Bok, D. and Rando, R.R., 2000. Lecithin retinol acyltransferase contains cysteine residues essential for catalysis.*Biochemistry*, *39*(17), pp.5215-5220.

Morimura, H., Fishman, G.A., Grover, S.A., Fulton, A.B., Berson, E.L. and Dryja, T.P., 1998. Mutations in the RPE65 gene in patients with autosomal recessive retinitis pigmentosa or leber congenital amaurosis. *Proceedings of the National Academy of Sciences*, *95*(6), pp.3088-3093.

Morrone, C., Fiorentini, A., Bisti, S., Porciatti, V. and Burr, D.C., 1994. Pattern-reversal electroretinogram in response to chromatic stimuli: II Monkey. *Visual Neuroscience*, *11*(5), pp.873-884.

Muniz, A., Villazana-Espinoza, E.T., Thackeray, B. and Tsin, A.T., 2006. 11-cis-Acyl-CoA: retinol O-acyltransferase activity in the primary culture of chicken Muller cells. *Biochemistry*, *45*(40), pp.12265-12273.

Murray, I.J., Kremers, J. and Parry, N.R., 2008. L-and M-Cone isolating ergs: LED versus CRT stimulation. *Visual neuroscience*, *25*(03), pp.327-331.

Noa, N.O.Y., 2000. Retinoid-binding proteins: mediators of retinoid action. *Biochemical Journal*, *348*(3), pp.481-495.

Nathans J, Thomas D, Hogness DS. Molecular genetics of human color vision: the genes encoding blue, green, and red pigments. Science. 1986b;232:193–202.

Nathans, J., Piantanida, T.P., Eddy, R.L., Shows, T.B. and Hogness, D.S., 1986a. Molecular genetics of inherited variation in human color vision.*Science*, *232*(4747), pp.203-210.

Neitz, M., Neitz, J. and Jacobs, G.H., 1995. Genetic basis of photopigment variations in human dichromats. *Vision research*, *35*(15), pp.2095-2103.

Neitz, M. and Neitz, J., 1995. Numbers and ratios of visual pigment genes for normal red-green color vision. *Science*, *267*(5200), pp.1013-1016.

Neitz, J. and Neitz, M., 2011. The genetics of normal and defective color vision. *Vision research*, *51*(7), pp.633-651

Neitz, J., Carroll, J., Yamauchi, Y., Neitz, M. and Williams, D.R., 2002. Color perception is mediated by a plastic neural mechanism that is adjustable in adults. *Neuron*, *35*(4), pp.783-792.

Nelson R, Famiglietti EV, Kolb H. Intracellular staining reveals different levels of stratification for on- and off-center ganglion cells in cat retina. J Neurophysiol. 1978;41:472–483.

Nelson, R. and Kolb, H., 1985. A17: a broad-field amacrine cell in the rod system of the cat retina. *Journal of neurophysiology*, *54*(3), pp.592-614.

Noell, W.K., 1954. The origin of the electroretinogram. *American journal of ophthalmology*, *38*(1), pp.78-90.

Noma, H., Funatsu, H. and Mimura, T., 2012. Association of electroretinographic parameters and inflammatory factors in branch retinal vein occlusion with macular oedema. *British Journal of Ophthalmology*,*96*(12), pp.1489-1493.

Nork, T.M., Ver Hoeve, J.N., Poulsen, G.L., Nickells, R.W., Davis, M.D., Weber, A.J., Sarks, S.H., Lemley, H.L. and Millecchia, L.L., 2000. Swelling and loss of photoreceptors in chronic human and experimental glaucomas. *Archives of ophthalmology*, *118*(2), pp.235-245.

Norren, D.V. and Padmos, P., 1973. Human and macaque blue cones studied with electroretinography. *Vision research*, *13*(7), pp.1241-1254.

Norren, D.V., 1972. Macaque lens absorption in vivo. *Invest. Ophthalmol*, *11*, pp.177-181.

Odom, J.V., Reits, D., Burgers, N. and Riemslag, F.C., 1992. Flicker electroretinograms: a systems analytic approach. *Optometry & Vision Science*, *69*(2), pp.106-116.

Okajima, T.I.L., Pepperberg, D.R., Ripps, H., Wiggert, B. and Chader, G.J., 1989. Interphotoreceptor retinoid-binding protein: role in delivery of retinol to the pigment epithelium. *Experimental eye research*, *49*(4), pp.629-644.

Osram Sylvania Corporation Lumens and mesopic vision Application Note FAQ0016-0297 (2000).

Osterberg, G.A., 1935. Topography of the layer of the rods and cones in the human retima. *Acta ophthalmol*, *13*(6), pp.1-102.

Ostwald, T.J., and Steinberg, R. H. (1980). Localization of frog retinal pigment epithelium NA^{+}-K^{+} ATPase. Experimental Eye Research. 31(3):351-60.

Owsley, C., Jackson, G.R., Cideciyan, A.V., Huang, Y., Fine, S.L., Ho, A.C., Maguire, M.G., Lolley, V. and Jacobson, S.G., 2000. Psychophysical evidence for rod vulnerability in age-related macular degeneration. *Investigative ophthalmology & visual science*, *41*(1), pp.267-273.

Oyster, C. W. (1999). The human eye: structure and function. Sinauer Associates.

Pacheco-Cutillas, M., Edgar, D.F. and Sahraie, A., 1999. Acquired colour vision defects in glaucoma—their detection and clinical significance. *British journal of ophthalmology*, *83*(12), pp.1396-1402.

Pacione, L.R., Szego, M.J., Ikeda, S., Nishina, P.M. and McInnes, R.R., 2003. Progress toward understanding the genetic and biochemical mechanisms of inherited photoreceptor degenerations. *Annual review of neuroscience*, *26*(1), pp.657-700.

Packer, O.S., Verweij, J., Li, P.H., Schnapf, J.L. and Dacey, D.M., 2010. Blue-yellow opponency in primate S cone photoreceptors. *The Journal of Neuroscience*, *30*(2), pp.568-572.

Padmos, P. and Van Norren, D., 1971. Cone spectral sensitivity and chromatic adaptation as revealed by human flicker-electroretinography.*Vision research*, *11*(1), pp.27-42.

Pang, J.J., Gao, F. and Wu, S.M., 2002. Relative contributions of bipolar cell and amacrine cell inputs to light responses of ON, OFF and ON–OFF retinal ganglion cells. *Vision research*, *42*(1), pp.19-27.

Pardue, M.T., McCall, M.A., LaVail, M.M., Gregg, R.G. and Peachey, N.S., 1998. A naturally occurring mouse model of X-linked congenital stationary night blindness. *Investigative ophthalmology & visual science*, *39*(12), pp.2443-2449.

Parker, R.O., Fan, J., Nickerson, J.M., Liou, G.I. and Crouch, R.K., 2009. Normal cone function requires the interphotoreceptor retinoid binding protein.*The Journal of Neuroscience*, *29*(14), pp.4616-4621.

Parry, N.R., Murray, I.J., Panorgias, A., McKeefry, D.J., Lee, B.B. and Kremers, J., 2012. Simultaneous chromatic and luminance human electroretinogram responses. *The Journal of physiology*, *590*(13), pp.3141-3154.

Paskowitz, D.M., LaVail, M.M. and Duncan, J.L., 2006. Light and inherited retinal degeneration. *British journal of ophthalmology*, *90*(8), pp.1060-1066.

Paulus, W. and KrÖger-Paulus, A., 1983. A new concept of retinal colour coding. *Vision research*, *23*(5), pp.529-540.

Pease, P.L., Adams, A.J. and Nuccio, E., 1987. Optical density of human macular pigment. *Vision research*, *27*(5), pp.705-710.

Penn, R.D. and Hagins, W.A., 1969. Signal transmission along retinal rods and the origin of the electroretinographic a-wave.

Penn, R.D. and Hagins, W.A., 1972. Kinetics of the photocurrent of retinal rods. *Biophysical Journal*, *12*(8), p.1073.

Pepperberg, D.R. and Clack, J.W., 1984. Rhodopsin photoproducts and the visual response of vertebrate rods. *Vision research*, *24*(11), pp.1481-1486.

Pepperberg, D.R., Birch, D.G. and Hood, D.C., 1997. Photoresponses of human rods in vivo derived from paired-flash electroretinograms. *Visual neuroscience*, *14*(01), pp.73-82.

Pepperberg, D.R., Brown, P.K., Lurie, M.A.R.K. and Dowling, J.E., 1978. Visual pigment and photoreceptor sensitivity in the isolated skate retina. *The Journal of general physiology*, *71*(4), pp.369-396.

Perlman, I., 2015. The Electroretinogram: ERG by Ido Perlman. *Webvision: The Organization of the Retina and Visual System*.

Perry, V.H., Oehler, R. and Cowey, A., 1984. Retinal ganglion cells that project to the dorsal lateral geniculate nucleus in the macaque monkey.*Neuroscience*, *12*(4), pp.1101-1123.

Phipps, J.A., Fletcher, E.L. and Vingrys, A.J., 2004. Paired-flash identification of rod and cone dysfunction in the diabetic rat. *Investigative ophthalmology & visual science*, *45*(12), pp.4592-4600.

Pokorny, J., Smith, V.C. and Lutze, M., 1987. Aging of the human lens.*Applied optics*, *26*(8), pp.1437-1440.

Pokorny, J., Smith, V.C. and Wesner, M.F., 1991. Variability in cone populations and implications. In *From pigments to perception* (pp. 23-34). Springer, Boston, MA.

Pokorny, J., Smithson, H., & Quinlan, J. 2004. Photostimulator allowing independent control of rods and the three cone types. *Visual Neuroscience,* 21: 263-267.

Polyak, S.L., 1941. The retina: the anatomy and the histology of the retina in man, ape, and monkey, including the consideration of visual functions, the history of physiological optics, and the histological laboratory technique.

Pourcho, R.G. and Goebel, D.J., 1983. Neuronal subpopulations in cat retina which accumulate the GABA agonist,(3H) muscimol: a combined Golgi and autoradiographic study. *Journal of Comparative Neurology*, *219*(1), pp.25-35.

Pourcho, R.G., 1982. Dopaminergic amacrine cells in the cat retina. *Brain research*, *252*(1), pp.101-109.

Pugh, E.N. and Lamb, T.D., 2000. Phototransduction in vertebrate rods and cones: molecular mechanisms of amplification, recovery and light adaptation. *Handbook of biological physics*, *3*, pp.183-255.

Puller, C. and Haverkamp, S., 2011. Bipolar cell pathways for color vision in non-primate dichromats. *Visual neuroscience*, *28*(1), pp.51-60.

Purves D, Augustine GJ, Fitzpatrick D, et al., editors. Neuroscience. 2nd edition. Sunderland (MA): Sinauer Associates; 2001. Phototransduction.

Purves D, Augustine GJ, Fitzpatrick D, et al., editors. Neuroscience. 2nd edition. Sunderland (MA): Sinauer Associates; 2001. Anatomical Distribution of Rods and Cones.

Qian, H., Alexander, K.R. and Ripps, H., 2010. Harmonic analysis of the cone flicker ERG of rabbit. *Experimental eye research*, *91*(6), pp.811-817.

Qian, H., Shah, M.R., Alexander, K.R. and Ripps, H., 2008. Two distinct processes are evident in rat cone flicker ERG responses at low and high temporal frequencies. *Experimental eye research*, *87*(1), pp.71-75.

Rattner, A., Smallwood, P.M. and Nathans, J., 2000. Identification and characterization of all-trans-retinol dehydrogenase from photoreceptor outer segments, the visual cycle enzyme that reduces all-trans-retinal to all-trans-retinol. *Journal of Biological Chemistry*, *275*(15), pp.11034-11043.

Raviola, E. and Gilula, N.B., 1973. Gap junctions between photoreceptor cells in the vertebrate retina. *Proceedings of the National Academy of Sciences*, *70*(6), pp.1677-1681.

Redmond, T.M., Yu, S., Lee, E., Bok, D., Hamasaki, D., Chen, N., Goletz, P., Ma, J.X., Crouch, R.K. and Pfeifer, K., 1998. Rpe65 is necessary for production of 11-cis-vitamin A in the retinal visual cycle. *Nature genetics*,*20*(4), pp.344-351.

Regan, D., 1966. Some characteristics of average steady-state and transient responses evoked by modulated light. *Electroencephalography and clinical neurophysiology*, *20*(3), pp.238-248.

Reid, R.C. and Shapley, R.M., 1992. Spatial structure of cone inputs to receptive fields in primate lateral geniculate nucleus. *Nature*, *356*(6371), pp.716-718.

Rieke, F., 2000. [12] Mechanisms of single-photon detection in Rod photoreceptors. In *Methods in enzymology* (Vol. 316, pp. 186-202). Academic Press.

Robson, J.G. and Frishman, L.J., 1995. Response linearity and kinetics of the cat retina: the bipolar cell component of the dark-adapted electroretinogram. *Visual neuroscience*, *12*(05), pp.837-850.

Robson, J.G. and Frishman, L.J., 1996. Photoreceptor and bipolar-cell contributions to the cat electroretinogram: a kinetic model for the early part of the flash response. *JOSA A*, *13*(3), pp.613-622.

Robson, J.G., Maeda, H., Saszik, S.M. and Frishman, L.J., 2004. In vivo studies of signaling in rod pathways of the mouse using the electroretinogram. *Vision research*, *44*(28), pp.3253-3268.

Robson, J.G., Saszik, S.M., Ahmed, J. and Frishman, L.J., 2003. Rod and cone contributions to the a-wave of the electroretinogram of the macaque.*The Journal of physiology*, *547*(2), pp.509-530.

Rodieck, R.W., 1998. *The first steps in seeing* (Vol. 1). Sunderland, MA: Sinauer Associates.

Roe, A.W. and Ts'o, D.Y., 1995. Visual topography in primate V2: multiple representation across functional stripes. *The Journal of Neuroscience*, *15*(5), pp.3689-3715.

Roorda, A. and Williams, D.R., 1999. The arrangement of the three cone classes in the living human eye. *Nature*, *397*(6719), pp.520-522.

Roorda, A., Metha, A.B., Lennie, P. and Williams, D.R., 2001. Packing arrangement of the three cone classes in primate retina. *Vision research*, *41*(10-11), pp.1291-1306.

Ruiz, A., Winston, A., Lim, Y.H., Gilbert, B.A., Rando, R.R. and Bok, D., 1999. Molecular and biochemical characterization of lecithin retinol acyltransferase. *Journal of Biological Chemistry*, *274*(6), pp.3834-3841.

Rushton, W.A.H. and Baker, H.D., 1964. Red/green sensitivity in normal vision. *Vision research*, *4*(1-2), pp.75-85.

Saari, J.C., 2000. Biochemistry of Visual Pigment Regeneration The Friedenwald Lecture. *Investigative Ophthalmology & Visual Science*, *41*(2), pp.337-348.

Saari, J.C., Bredberg, D.L. and Farrell, D.F., 1993. Retinol esterification in bovine retinal pigment epithelium: reversibility of lecithin: retinol acyltransferase. *Biochemical Journal*, *291*(3), pp.697-700.

Saari, J.C., Nawrot, M., Liu, T., Teller, D.C. and Crabb, J.W., 2004. Interactions of CRALBP and EBP50/NHERF–1. *Investigative Ophthalmology & Visual Science*, *45*(13), pp.1262-1262.

Saito, T. and Kaneko, A., 1983. Ionic mechanisms underlying the responses of off-center bipolar cells in the carp retina. I. Studies on responses evoked by light. *The Journal of general physiology*, *81*(4), pp.589-601.

Sawusch, M., Pokorny, J. and Smith, V.C., 1987. Clinical electroretinography for short wavelength sensitive cones. *Investigative ophthalmology & visual science*, *28*(6), pp.966-974.

Schiefer, U., Wilhelm, H. and Hart, W. eds., 2007. *Clinical neuro-ophthalmology: a practical guide*. Springer Science & Business Media.

Schiller, P.H., Logothetis, N.K. and Charles, E.R., 1990. Role of the color-opponent and broad-band channels in vision. *Visual neuroscience*, *5*(4), pp.321-346.

Schnapf JL, Kraft TW, Baylor DA. Spectral sensitivity of human cone photoreceptors. Nature. 1987;325:439–441.

Seeliger, M.W., Brombas, A., Weiler, R., Humphries, P., Knop, G., Tanimoto, N. and Müller, F., 2011. Modulation of rod photoreceptor output by HCN1 channels is essential for regular mesopic cone vision. *Nature communications*, *2*, p.532.

Seiple, W.H., Siegel, I.M., Carr, R.E. and Mayron, C., 1986. Evaluating macular function using the focal ERG. *Investigative ophthalmology & visual science*, *27*(7), pp.1123-1130.

Shapiro, A. G. & Pokorny, J. &. S. V. C., 1996. Cone-rod receptor spaces, with illustrations that use CRT phosphor and light-emitting-diode spectra. *Journal of the Optical Society of America A,* 13(12): 2319-2328.

Shapley, R. and Perry, V.H., 1986. Cat and monkey retinal ganglion cells and their visual functional roles. *Trends in Neurosciences*, *9*, pp.229-235.

Sharpe, L.T., Stockman, A., Jägle, H., Knau, H., Klausen, G., Reitner, A. and Nathans, J., 1998. Red, green, and red-green hybrid pigments in the human retina: correlations between deduced protein sequences and psychophysically measured spectral sensitivities. *Journal of Neuroscience*, *18*(23), pp.10053-10069.

Sharpe, L.T., Stockman, A., Jägle, H. and Nathans, J., 1999. Opsin genes, cone photopigments, color vision, and color blindness. *Color vision: From genes to perception*, pp.3-51.

Sher, A. and DeVries, S.H., 2012. A non-canonical pathway for mammalian blue-green color vision. *Nature neuroscience*, *15*(7), pp.952-953.

Shimazaki, H.and Oakley, B. 1984. Reaccumulation of [K+] o in the toad retina during maintained illumination. *The Journal of general physiology*, *84*(3), pp.475-504.

Sieving, P.A., Murayama, K. and Naarendorp, F., 1994. Push–pull model of the primate photopic electroretinogram: a role for hyperpolarizing neurons in shaping the b-wave. *Visual neuroscience*, *11*(03), pp.519-532.

Sillman, A.J., Ito, H. and Tomita, T., 1969. Studies on the mass receptor potential of the isolated frog retina: I. General properties of the response.*Vision research*, *9*(12), pp.1435-1442.

Silveira, L.C.L., Saito, C.A., Lee, B.B., Kremers, J., da Silva Filho, M., Kilavik, B.E., Yamada, E.S. and Perry, V.H., 2004. Morphology and physiology of primate M-and P-cells. *Progress in brain research*, *144*, pp.21-46.

Silveira, L.C.L., Yamada, E.S. and Picanço-Diniz, C.W., 1989. Displaced horizontal cells and biplexiform horizontal cells in the mammalian retina.*Visual neuroscience*, *3*(05), pp.483-488.

Simmons, W.K., Ramjee, V., Beauchamp, M.S., McRae, K., Martin, A. and Barsalou, L.W., 2007. A common neural substrate for perceiving and knowing about color. *Neuropsychologia*, *45*(12), pp.2802-2810.

Smith, V.C. and Pokorny, J., 1975. Spectral sensitivity of the foveal cone photopigments between 400 and 500 nm. *Vision research*, *15*(2), pp.161-171.

Smith, V.C., Lee, B.B., Pokorny, J., Martin, P.R. and Valberg, A., 1992. Responses of macaque ganglion cells to the relative phase of heterochromatically modulated lights. *The Journal of Physiology*, *458*(1), pp.191-221.

Smith, V.C., Pokorny, J., Davis, M. and Yeh, T., 1995. Mechanisms subserving temporal modulation sensitivity in silent-cone substitution. *JOSA A*, *12*(2), pp.241-249.

Solomon, S.G. and Lennie, P., 2007. The machinery of colour vision. *Nature Reviews Neuroscience*, *8*(4), p.276.

Stabell, U. and Stabell, B., 1977. Wavelength discrimination of peripheral cones and its change with rod intrusion. *Vision Research*, *17*(3), pp.423-426.

Steinberg, R.H., 1985. Interactions between the retinal pigment epithelium and the neural retina. *Documenta Ophthalmologica*, *60*(4), pp.327-346.

Steward, J.M. and Cole, B.L., 1989. What do color vision defectives say about everyday tasks?. *Optometry & Vision Science*, *66*(5), pp.288-295.

Stiles, W.S. and Burch, J.M., 1955. Interim report to the Commission Internationale de l'Eclairage, Zurich, 1955, on the National Physical Laboratory's investigation of colour-matching (1955). *Journal of Modern Optics*, *2*(4), pp.168-181.

Stiles, W.S., 1949. Increment thresholds & the mechanisms of colour vision. *Documenta Ophthalmologica*, *3*(1), pp.138-165.

Stockman, A. and Sharpe, L.T., 2000. The spectral sensitivities of the middle-and long-wavelength-sensitive cones derived from measurements in observers of known genotype. *Vision research*, *40*(13), pp.1711-1737.

Stockman, A. and Sharpe, L.T., 2000. Tritanopic color matches and the middle- and long-wavelength-sensitive cone spectral sensitivities. *Vision research*, *40*(13), pp.1739-1750.

Stockman, A. and Sharpe, L.T., 2006. Into the twilight zone: the complexities of mesopic vision and luminous efficiency. *Ophthalmic and physiological optics*, *26*(3), pp.225-239.

Stockman, A., and Sharpe, L. T., 1998. Human cone spectral sensitivities: a progress report. Vision Research, 38, 3193-3206.

Stockman, A., and Sharpe, L., 2000. The spectral sensitivities of the middle- and long-wavelength-sensitive cones derived from measurements in observers of known genotype. *Vision Research*, 40(13): 1711-1737.

Stockman, A., MacLeod, D.I. and DePriest, D.D., 1991. The temporal properties of the human short-wave photoreceptors and their associated pathways. *Vision research*, *31*(2), pp.189-208.

Stockman, A., MacLeod, D.I. and Johnson, N.E., 1993. Spectral sensitivities of the human cones. *JOSA A*, *10*(12), pp.2491-2521.

Stockman, A., Sharpe, L.T. and Fach, C., 1999. The spectral sensitivity of the human short-wavelength sensitive cones derived from thresholds and color matches. *Vision research*, *39*(17), pp.2901-2927.

Stockman, A., Sharpe, L.T., Merbs, S. and Nathans, J., 2000. [42] Spectral sensitivities of human cone visual pigments determined in vivo and in vitro.*Methods in enzymology*, *316*, pp.626-650.

Stockman, A., Sharpe, L.T., Zrenner, E. and Nordby, K., 1991. Slow and fast pathways in the human rod visual system: electrophysiology and psychophysics. *JOSA A*, *8*(10), pp.1657-1665.

Stockton, R.A. and Slaughter, M.M., 1989. B-wave of the electroretinogram. A reflection of ON bipolar cell activity. *The Journal of general physiology*, *93*(1), pp.101-122.

Sun, H., Pokorny, J. and Smith, V.C., 2001. Control of the modulation of human photoreceptors. *Color Research and Application*, *26*, pp.S69-S75.

Swanson, W.H., Ueno, T., Smith, V.C. and Pokorny, J., 1987. Temporal modulation sensitivity and pulse-detection thresholds for chromatic and luminance perturbations. *JOSA A*, *4*(10), pp.1992-2005.

Szikra, T. and Witkovsky, P., 2001. Contributions of AMPA-and kainate-sensitive receptors to the photopic electroretinogram of the Xenopus retina.*Visual neuroscience*, *18*(2), pp.187-196.

Tagarelli, A., Piro, A., Tagarelli, G., Lantieri, P.B., Risso, D. and Olivieri, R.L., 2004. Colour blindness in everyday life and car driving. *Acta Ophthalmologica Scandinavica*, *82*(4), pp.436-442.

Thompson DA, Gal A. Genetic defects in vitamin A metabolism of the retinal pigment epithelium. Developments in ophthalmology. 2003;37:141–154.

Travis, G.H., Golczak, M., Moise, A.R. and Palczewski, K., 2007. Diseases caused by defects in the visual cycle: retinoids as potential therapeutic agents. *Annu. Rev. Pharmacol. Toxicol.*, *47*, pp.469-512.

Travis, G.H., Radu, R.A., Lee, J. and Mata, N.L., 2002. Identification of a new pathway for retinol isomerization in cone-dominant ground squirrel and chicken retinas. *Investigative Ophthalmology & Visual Science*, *43*(13), pp.3608-3608.

Ueyama, H., Hayashi, S., Tanabe, S., Tanaka, Y., Hayashi, T., Deeb, S.S., Yamade, S. and Ohkubo, I., 2001. Number and arrangement of the red and green visual pigment genes in color-normal Japanese males. *Color Research & Application: Endorsed by Inter-Society Color Council, The Colour Group (Great Britain), Canadian Society for Color, Color Science Association of Japan, Dutch Society for the Study of Color, The Swedish*

Colour Centre Foundation, Colour Society of Australia, Centre Français de la Couleur, *26*(S1), pp.S84-S88.

Usui, T., Kremers, J., Sharpe, L.T. and Zrenner, E., 1998. Flicker cone electroretinogram in dichromats and trichromats. *Vision research*, *38*(21), pp.3391-3396.

Vaegan 1996. Electrode standards in electroretinography. Doc Ophthalmol, 92(3): 243- 245.

Valberg, A., Lee, B.B. and Tryti, J., 1987. Simulation of responses of spectrally-opponent neurones in the macaque lateral geniculate nucleus to chromatic and achromatic light stimuli. *Vision Research*, *27*(6), pp.867-882.

Van der Tweel, L.H. and Lunel, H.V., 1965. Human visual responses to sinusoidally modulated light. *Electroencephalography and clinical neurophysiology*, *18*(6), pp.587-598.

Vaney, D.I., 1990. The mosaic of amacrine cells in the mammalian retina.*Progress in retinal research*, *9*, pp.49-100

Veleri, S., Lazar, C. H., Chang, B., Sieving, P. A., Banin, E., & Swaroop, A. (2015). Biology and therapy of inherited retinal degenerative disease: insights from mouse models. *Disease Models & Mechanisms*, *8*(2), 109–129.

Verweij, J., Dacey, D.M., Peterson, B.B. and Buck, S.L., 1999. Sensitivity and dynamics of rod signals in H1 horizontal cells of the macaque monkey retina.*Vision research*, *39*(22), pp.3662-3672.

Verweij, J., Hornstein, E.P. and Schnapf, J.L., 2003. Surround antagonism in macaque cone photoreceptors. *Journal of Neuroscience*, *23*(32), pp.10249-10257.

Vishnivetskiy, S.A., Schubert, C., Climaco, G.C., Gurevich, Y.V., Velez, M.G. and Gurevich, V.V., 2000. An additional phosphate-binding element in arrestin molecule Implications for the mechanism of arrestin activation.*Journal of Biological Chemistry*, *275*(52), pp.41049-41057.

Viswanathan, S., Frishman, L.J. and Robson, J.G., 2002. Inner-retinal contributions to the photopic sinusoidal flicker electroretinogram of macaques. *Documenta Ophthalmologica*, *105*(2), pp.223-242.

Vollrath, D., Nathans, J. and Davis, R.W., 1988. Tandem array of human visual pigment genes at Xq28. *Science*, *240*(4859), pp.1669-1672.

Von Lintig, J., Kiser, P.D., Golczak, M. and Palczewski, K., 2010. The biochemical and structural basis for trans-to-cis isomerization of retinoids in the chemistry of vision. *Trends in biochemical sciences*, *35*(7), pp.400-410.

Vos, J.J. and Walraven, P.L., 1971. On the derivation of the foveal receptor primaries. *Vision Research*, *11*(8), pp.799-818.

Wachtmeister, L., 1998. Oscillatory potentials in the retina: what do they reveal. *Progress in retinal and eye research*, *17*(4), pp.485-521.

Waessle, H, Dacey, D.M., Haun, T., Haverkamp, S., Gruenert, U. and Boycott, B.B., 2000. The mosaic of horizontal cells in the macaque monkey retina: with a comment on biplexiform ganglion cells. *Visual neuroscience*, *17*(04), pp.591-608.

Wald, G.,1968.The molecular basis of visual excitation. *Nature*, *219*, p.800-807.

Wald, G., 1935. Carotenoids and the visual cycle. *The Journal of general physiology*, *19*(2), pp.351-371.

Walraven, P.L. and Leebeek, H.J., 1964. Phase shift of sinusoidally alternating colored stimuli. *JOSA*, *54*(1), pp.78-82.

Wang, J.S. and Kefalov, V.J., 2009. An alternative pathway mediates the mouse and human cone visual cycle. *Current Biology*, *19*(19), pp.1665-1669.

Wang, J.S. and Kefalov, V.J., 2011. The cone-specific visual cycle.*Progress in retinal and eye research*, *30*(2), pp.115-128.

Wassle, H. and Boycott, B.B., 1991. Functional architecture of the mammalian retina. Physiological reviews, 71(2), pp.447-480.

Wässle, H., Boycott, B.B. and Röhrenbeck, J., 1989. Horizontal cells in the monkey retina: cone connections and dendritic network. *European Journal of Neuroscience*, *1*(5), pp.421-435.

Wässle, H., Grünert, U., Röhrenbeck, J. and Boycott, B.B., 1990. Retinal ganglion cell density and cortical magnification factor in the primate. *Vision research*, *30*(11), pp.1897-1911.

Wässle, H., Peichl, L. and Boycott, B.B., 1981. Dendritic territories of cat retinal ganglion cells. *Nature*, *292*(5821), p.344.

Weinstein, G.W., Hobson, R.R. and Dowling, J.E., 1967. Light and dark adaptation in the isolated rat retina. *Nature*, *215*, pp.134-138.

Werblin, F.S. and Dowling, J.E., 1969. Organization of the retina of the mudpuppy, Necturus maculosus. II. Intracellular recording. *Journal of neurophysiology*, *32*(3), pp.339-355.

Whitlock, G.G. and Lamb, T.D., 1999. Variability in the time course of single photon responses from toad rods: termination of rhodopsin's activity. *Neuron*,*23*(2), pp.337-351.

Wiesel, T.N. and Hubel, D.H., 1966. Spatial and chromatic interactions in the lateral geniculate body of the rhesus monkey. *Journal of neurophysiology*, *29*(6), pp.1115-1156.

Wild, H.M., Butler, S.R., Carden, D. and Kulikowski, J.J., 1985. Primate cortical area V4 important for colour constancy but not wavelength discrimination.

Williams, D.R., MacLeod, D.I. and Hayhoe, M.M., 1981. Punctate sensitivity of the blue-sensitive mechanism. *Vision res*, *21*(9), pp.1357-75.

Wisowaty, J.J. and Boynton, R.M., 1980. Temporal modulation sensitivity of the blue mechanism: measurements made without chromatic adaptation. *Vision research*, *20*(11), pp.895-909.

Wright, W.D., 1929. A re-determination of the trichromatic coefficients of the spectral colours. *Transactions of the Optical Society*, *30*(4), p.141.

Wyszecki, G. and Stiles, W.S., 1982. *Color science* (Vol. 8). New York: Wiley.

Wyszecki, G., & Stiles, W. S. (1967). *Color Science: concepts and methods, quantitative data and formulae*. (1st ed.). New York: Wiley.

Xu, J., Dodd, R.L., Makino, C.L., Simon, M.I., Baylor, D.A. and Chen, J., 1997. Prolonged photoresponses in transgenic mouse rods lacking arrestin.*Nature*, *389*(6650), pp.505-509.

Yanagida, T., Koshimizu, M., Kawasaki, K. and Yonemura, D., 1987. Microelectrode depth study of the electroretinographic oscillatory potentials in the frog retina. *Documenta ophthalmologica*, *67*(4), pp.355-361.

Yau, K.W. and Hardie, R.C., 2009. Phototransduction motifs and variations.*Cell*, *139*(2), pp.246-264.

Yin, H. and Pardue, M.T., 2004. Performance of the DTL electrode compared to the jet contact lens electrode in clinical testing. *Documenta ophthalmologica*, *108*(1), pp.77-86.

Yonemura, D and Kawasaki, K 1967. The early receptor potential in the human electroretinogram. *The Japanese journal of physiology*, *17*(3), pp.235-244.

Yoshida, K., Watanabe, D., Ishikane, H., Tachibana, M., Pastan, I. and Nakanishi, S., 2001. A key role of starburst amacrine cells in originating retinal directional selectivity and optokinetic eye movement. *Neuron*, *30*(3), pp.771-780.

Zahiruddin, K., Banu, S., Dharmarajan, R., Kulothungan, V., Vijayan, D., Raman, R and Sharma, T*., 2010.* Effect of Illumination on Colour Vision Testing with Farnsworth-Munsell 100 Hue Test: Customized Colour Vision Booth versus Room Illumination*. Korean Journal of Ophthalmology*, 24(3): 159–162.

Zeki, S. and Marini, L., 1998. Three cortical stages of colour processing in the human brain. *Brain*, *121*(9), pp.1669-1685.

Zele, A.J. and Cao, D., 2015. Vision under mesopic and scotopic illumination. *Frontiers in psychology*, *5*, p.1594.

Zrenner, E., 1982. Electrophysiological characteristics of the blue sensitive mechanism: Test of a model of cone interaction under physiological and pathological conditions. *Documenta Ophthalmologica Proceedings Series*.

Zrenner,E.,1990.The physiological basis of the pattern electroretinogram. *Progress in retinal research*, *9*, pp.427-464.

Zrenner, E., Nelson, R. and Mariani, A., 1983. Intracellular recordings from a biplexiform ganglion cell in macaque retina, stained with horseradish peroxidase. *Brain research*, *262*(2), pp.181-185.

Presentations and Publications

Talks

- Temporal characteristics of L and M-cone isolated steady-state ERGs Deepika Kommanapalli , Declan Mckeefry, Ian Murray , Jan Kremers and Neil Parry ***(Ophthalmic & Physiological Optics, British Congress of Optometry and Vision Science, Glasgow, 2013)***

- Cracking eye's colour code: 3 minute thesis presentation ***(University of Bradford, 2015)***

- Can Rod ERGs be recorded in the light adapted human eye? ***(L V Prasad Eye Institute, Hyderabad, India, 2016)***

Poster presentations

- Temporal characteristics of L and M-cone isolated steady-state ERGs. Deepika Kommanapalli , Declan Mckeefry, Ian Murray , Jan Kremers and Neil Parry ***(International Colour Vision Society Symposium, 2013 (Poster #2))***

Publications

- Kommanapalli, D., Murray, I.J., Kremers, J., Parry, N.R. and McKeefry, D.J., 2014. Temporal characteristics of L-and M-cone isolating steady-state electroretinograms. ***JOSA A, 31(4), pp.A113-A120.***

- McKeefry, D., Kremers, J., Kommanapalli, D., Challa, N.K., Murray, I.J., Maguire, J. and Parry, N.R., 2014. Incremental and decremental L-and M-cone-driven ERG responses: I. Square-wave pulse stimulation. ***JOSA A*****, *31*****(4)*****, *pp.A159-A169.***

- Maguire, J., Parry, N.R., Kremers, J., Kommanapalli, D., Murray, I.J. and McKeefry, D.J., 2016. Rod electroretinograms elicited by silent substitution stimuli from the light-adapted human eye. ***Translational vision science & technology, 5(4), pp.13-13.***

APPENDIX

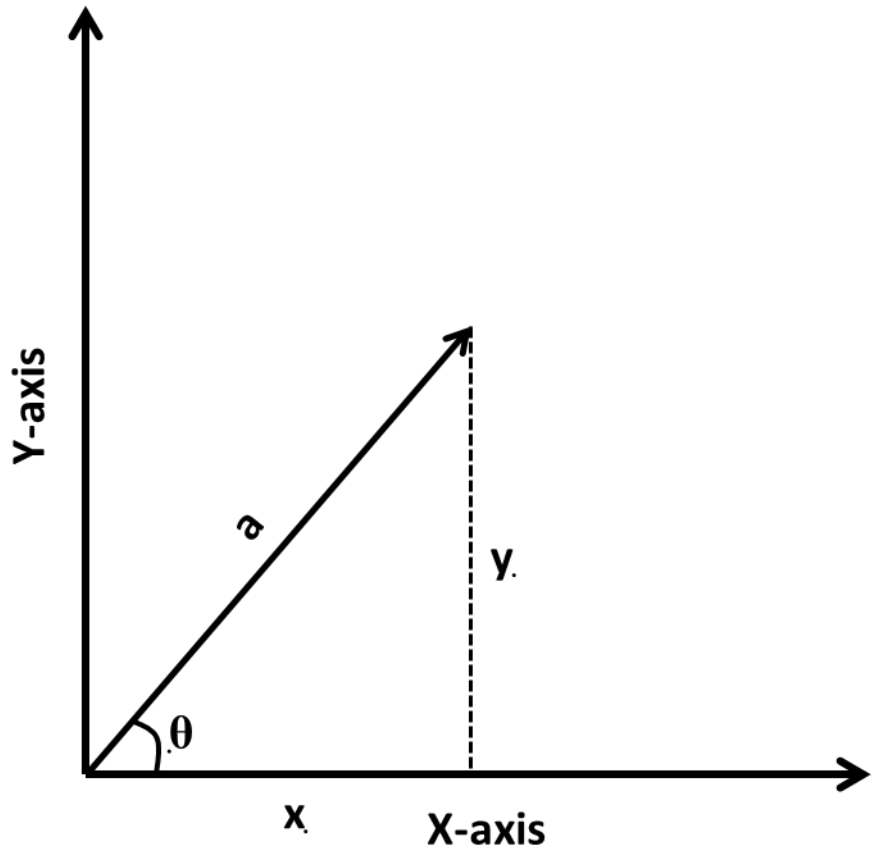

Graph showing an example of amplitude (a) and phase (θ) measured in microvolts and radians on the X-Y space with x & y depicting the adjacent and opposite sides on a right angled triangle.

The amplitude (a) and phase (θ) of a fundamental and second harmonic components of ERGs derived at a given frequency assuming retinal illuminance and a cone contrast is constant are averaged to understand the net effect of these responses as a function of temporal frequency.

To derive the mean amplitude and mean phase, firstly, we calculated x and y co-ordinates using amplitude and phase data at each temporal frequency. Before calculating the x/y co-ordinates for the data obtained at each frequency, we considered the phase value in radians for ease of computation in Microsoft Excel by using the formula

Radian (θ) = Degree(d) x Pi/180

where the phase values obtained after Fourier analysis were in degrees.

Using amplitude(a) and radian(θ) we then derived x/y co-ordinates as

y = a * Sin θ and

x = a * Cos θ (see figure above)

So for data acquired at each frequency, we derived different x and y coordinates (x1,x2,x3….,y1,y2,y3….). We then derived average x: co-ordinate (X) as mean of all x co-ordinates i.e X = (x1+x2+….xn)/n and average y co-ordinate(Y) = (y1+y2+….yn)/n.

Using these mean x and y co-ordinates, we then derived the mean amplitude (A)

A = (X^2+Y^2)^1/2.

To calculate average phase (P) we used the inverse trigonometric transformation

P(rad) = atan(Y/X) radians

To convert radians to degrees we used the formula P(deg) = Degrees(Prad)

For a given x- and y- coordinates, to derive a phase value , we used the following conditions in Microscoft Excel

If Y>0 and X>0, P(deg) = degrees(atan(Y/X))

If Y>0 and X<0, P(deg) = 180 - degrees(atan(Y/X))

If Y<0 and X<0, P(deg) = 180 + degrees(atan(Y/X))

If Y<0 and X>0, P(deg) = 360 - degrees(atan(Y/X))

The vector averaged Mean Amplitudes and Phase were then plotted as a function of temporal frequency.